RDH10 is Necessary for Initial Vagal Neural Crest Cell Contribution to Embryonic Gastrointestinal Tract Development

BY

Naomi Elaine Butler Tjaden

Submitted to the graduate degree program in Anatomy and Cell Biology and to the Graduate Faculty of The University of Kansas Medical Center in partial fulfillment of the requirements for the degree of Doctor of Philosophy.

Paul Trainor, Co-Chairperson

Brenda Rongish, Co-Chairperson

Timothy Fields

Dale Abrahamson

Osama Almadhoun

Paul Cheney

Date Defended: May 1, 2015

The Dissertation Committee for Naomi Elaine Butler Tjaden Certifies that this is the approved version of the following dissertation:

RDH10 is Necessary for Initial Vagal Neural Crest Cell Contribution to Embryonic Gastrointestinal Tract Development

Paul Trainor, Co-Chairperson

Brenda Rongish, Co-Chairperson

Date approved: May 5, 2015

Abstract

Retinol dehydrogenase 10 (RDH10) catalyzes the first oxidative step in the metabolism of vitamin A to its active form retinoic acid (RA). Insufficient or excess RA can result in various congenital abnormalities, such as Hirschsprung disease (HSCR). In HSCR, neurons are absent from variable lengths of the gastrointestinal tract due to a failure of neural crest cell (NCC) colonization or development, leading to megacolon and/or the failure to pass meconium. Enteric neurons are derived from neural crest cells (NCC); hence HSCR is associated with incomplete NCC development or colonization of the GI tract. We investigated our hypothesis that RDH10 is necessary for proper NCC contribution to the enteric nervous system (ENS). The mouse point mutant *Rdh10*$^{trex/trex}$ exhibits decreased retinoid signaling and colonic aganglionosis. Organ explant culture and *in utero* retinal supplementation experiments define a temporal requirement for RA in ENS development between E7.5-E9.5. Tamoxifen-inducible temporal deletion of RDH10 at E6.5-E7.5 confirms this early retinal role, while later RDH10 deletion suggests retinal independence for continued enteric NCC colonization. Removing RDH10 from NCCs shows no gross or ENS-specific neuronal defects, suggesting that RDH10 is not intrinsically required in enteric NCCs for proper colonization of the gut, but rather is necessary as a paracrine signal in the vagal NCC microenvironment. We investigated signaling cascades that are known to play a role in gut microenvironment maintenance that may be altered in these RDH10 mutants using both a targeted expression analysis approach as well as RNA-sequencing. Candidates include GDNF and its signaling family members such as RET and GFRα1, as well as extracellular matrix proteins. Novel models of HSCR, such as *Rdh10*$^{trex/trex}$ will improve our understanding of RA contribution to intestinal development and may lead to innovative non-surgical treatment approaches to reduce the morbidity and mortality of this common congenital disease.

Acknowledgements

I would like to thank Paul for being an incredible mentor. I am so lucky to have such an understanding, supportive and fun person to call my boss, I am so happy you gave me a chance to learn and grow in your lab for the last four years. I am so thankful for your approach of "raising" graduate students, for teaching me to think for myself, yet for pulling me back in when my ideas make no sense, and of course, for letting me work on such a fun project relating to my favorite pastime.

To my committee members, Tim, Brenda, Osama, Dale and Uncle Paul, thank you for being such wonderful role models and for helping me become the best student I could be. And to the MD/PhD program, especially to Janice, Tim, Brenda and Dr. B., you have supported me from the day I came to Kansas City, and gave me a chance to pursue my dream as a physician-scientist, and I will forever be grateful.

Thank you for everything you have taught me, Lisa. I hope to one day be able to think as clearly and critically as you do every day. Your words of encouragement, your advice on presentations, and your overall hip lifestyle have made such a big impact on the type of scientist and person I want to become. I am so happy you took the time to take me under your tiny trex wing and mentor me in the lab.

To the Trainor lab members: for your insights, constructive (and not constructive) comments throughout my time in the lab, and importantly, for the amazing environment and comradery, thank you. To my "work wife," Aude, je te remercie. For the thousands of coffee breaks we have taken over the last four years, the almost daily shared lunches, for all of our trips near and far, the hundreds of grams of calissons you have brought me from Paris, and for always being a patient friend and good listener when I need to vent. I know we will be life-long friends, even though you are Parisian. To Shachi, I am so grateful for your willingness to help me when I needed it most, even at the expense of your sleep. Your opinion means so much to me, and your dedication to your friends and colleagues is such an admirable trait, and I hope to be there for you, should you ever need me. Thank you, Annita and Jason (and Artemis!) for being such good friends in the lab,

medical school and in real life. I have really loved our time together, not just because of the amazing food you both make, but because you both make me strive to be a better person. Kristin, I'm so happy we got to go through this process together, and thankful that you were always there to help double-check my calculations. You are such a hardworking person, a great scientist and I know you will be an excellent mother. And William, thank you for having more house problems than me, so my problems seem smaller. Melissa, my work would not be what it is without you. Thank you for doing such an amazing job with the mice, and for being a great travel buddy outside of work. I would also like to thank the Trainor lab alumni: Raul, for keeping us all entertained; for Kaz and his endless knowledge of experimental techniques and willingness to help; to Liang for the last 加油 which gave me my final boost; to Daisuke for introducing me to the amazing Japanese baymate culture; to Mama Kim for the heartfelt conversations and experimental help; and to Hiroshi, the most efficient, friendly, tolerant baymate I could have ever wished for. I am not sure what you did to Paul for him to punish you with such a loud, messy baymate for 3 years, but I am happy you did it.

To the people at Stowers who have made this such a wonderful environment, which made coming to work every day fun, thank you. Robin, my work mom, thank you. You have supported me so much by just being yourself and keeping an eye out for me and helping to keep me out of trouble. You always manage to brighten my day every time I see you. To Carolyn and Shelly, THANK YOU x 1000! You both do so many things behind the scenes with no expectation of being thanked. If you two were not around, I think the Institute would collapse. To the histology ladies and back computer room guys, thank you for helping me with my incredible amount of problems! S-Bhatt, Marina and William, thank you for the last minute corrections and comment on this thesis, I know it was rough and I appreciate it! And thank you, Agne, for becoming such a supportive friend in the last year and for keeping my ego at bay when you crush me on the courts.

Thank you, Jen (jpoo). You were an amazing lab manager, and I am so happy we became such good friends. You are truly a friend that puts others' needs before her own, and I know I can always call on you when I need a hand, whether it is a chore around the

house or yard, a ride to the airport, to watch the pups or just to chat about life. I am so lucky to have someone like you in my life.

To my best childhood, college, and med school friends: Betny, Hooly, Vkwan, Tiny Baby Lindsay Allan, and Allison, thank you for the fun times, and the rational (and sometimes irrational) advice. I appreciate what you have to say, and when you bring me out of the grad school blur and back into the world. I am so lucky to have you as friends.

To my fellow Volkerites: Alan, Erin and John, April, Mary, Assassin Mike, Joe, Connor and Sarah, Elena and Travis and Nora and Alfie, Lynsi and Janete, Jackie and Emily, thank you for being such amazing neighbors, for tolerating my seemingly endless house construction and loud noises, for the borrowed cups of sugar, and for helping with Binker, Mateo, Cotton and Bruce at the drop of a hat.

To the Tjaden family: Aunt Heidi and Mr. Bruce, you have taken me in as one of your own, and I am so lucky to have such wonderful and supportive in-laws, which I do not take for granted, although I do not tell you, “thank you,” enough. To Anne, I have been so blessed by watching you grow as a woman, scientist, and caregiver, and recently as one of my dearest friends. I know you will be successful in everything that you do (it’s not too late to choose MD/PhD!). And to Amanda, my long-lost sister, you have been there for me in more ways that anyone can ever know. Without you, I would be a total mess (both physically and emotionally). Thank you for keeping me sane and making sure my nails always look good.

To my mom and dad, who have been my biggest advocates through every step of my existence. I am so happy to have such amazing, quirky, selfless people to call my parents, and importantly, my friends. It is so amazing to have parents who pursue their passions and constantly strive to be content with what you have. You remind me to always keep my head up and to live simply, and when I fail, you are there to pick me up.

Last but not least, I would like to thank Bruce. You are the most devoted person I know, even when you are pulled in so many directions from work and family. I am lucky to have had my Broo by my side for these last 9 years, and I am excited for where we will go from here.

Dedication

To my parents who have instilled in me the desire and freedom to do what I love, and to love what I do. And to Bruce, for being my more rational and empathetic better half.

Table of Contents

List of Figures

List of Tables

I. INTRODUCTION

This section describes the gastrointestinal tract, which is controlled by the enteric nervous system (ENS). The ENS is the peripheral nervous system of the gut, formed by a cell population termed neural crest cells (NCC). A failure of these cells to migrate, proliferate, differentiate, or survive may result in a devastating congenital disease, called Hirschsprung Disease (HSCR). This section will also introduce Vitamin A metabolism and deficiency, as well as the effects this deficiency may play in the development of the gastrointestinal tract.

Much of the introduction of Gastrointestinal Tract Development, Hirschsprung Disease, Neural Crest Cells, and Vitamin A metabolism has been edited and published in *Translational Research* as an invited review (Butler Tjaden and Trainor, 2013).

Gastrointestinal Tract

The gastrointestinal (GI) tract is an endoderm derived organ system that begins at the mouth and terminates at the anus. During fetal life, the GI tract is divided into three segments based on vascular supply. The foregut, supplied by the celiac artery, consists of the esophagus, stomach, part of duodenum, and biliary apparatus. The midgut, supplied by the superior mesenteric artery, contains the rest of small and large bowel up to the splenic flexure. Lastly, the hindgut consists of the remainder of the large bowel to the superior part of anal canal, and is supplied by the inferior mesenteric artery.

This organ system functions to digest and process foods and liquids taken in through the mouth via two types of digestion: mechanical, such as chewing and gut peristalsis, and chemical, such as enzymatic breakdown. The GI tract also plays a role as a major part of the immune system via the recognition of and response to introduced pathogens.

GASTROINTESTINAL TRACT DEVELOPMENT AND INNERVATION BY ENTERIC NERVOUS SYSTEM

There are two salient features of gut development, which make it unique in comparison to the rest of the developing embryo. The gut tube itself grows faster than the abdominal cavity. As a result, in a human fetus at 6 weeks of gestation, the midgut lies outside the cavity together with the umbilicus. It then undergoes significant elongation and a 270° counterclockwise rotation before returning to the fetal abdominal cavity at around 10 weeks gestation, with an intestinal anatomy reminiscent of familiar adult structures. Additionally, this organ system is controlled by a "second brain," the enteric nervous system, which functions almost independently of the central nervous system (Gershon, 1997).

REGULATION OF GI TRACT FUNCTION BY THE ENTERIC NERVOUS SYSTEM

The ability of the GI tract to respond to the state of the lumen and gut wall by activating peristalsis, controlling blood flow and secretions and thus maintain proper physiological balance depends on the enteric nervous system (ENS) (Heanue and Pachnis, 2007). The ENS is the largest part of the peripheral nervous system and is in direct control of the GI tract (Karaosmanoglu, 1996). ENS neurons and glia are organized into ganglia that are interconnected to form two plexi extending along the length of the bowel. The outer myenteric (Auerbach) plexus develops first during embryogenesis, runs the full length of the gut and regulates gut motility, while the inner submucosal (Meissner) plexus develops later, is found only in the small and large intestine and is responsible for regulating blood flow and the transport of ions across the intestinal epithelium. All of the neurons and glia of the ENS are derived from a cell population called the enteric neural crest cells (ENCC), whose proper development, differentiation, and survival is crucial for formation of a functional ENS.

Neural Crest Cells (NCCs)

NCCs are a multipotent, migratory cell population that gives rise to many cell lineages in vertebrate development, including the craniofacial skeleton, smooth muscle, melanocytes, and most of the peripheral nervous system. In mammals, NCCs are formed during neurulation at the border between neural and non-neural ectoderm. After induction, they undergo an epithelial to mesenchymal transition and subsequently delaminate to migrate to the periphery where they differentiate into various cell types. The fate of NCCs varies along the anterior-posterior axis of an embryo. Depending on the axial level of neural crest induction, NCCs are divided into four main territories, cranial neural crests which contributes to most of the craniofacial bone and cartilage and cranial nervous system, cardiac neural crest, which regulates the septation of the cardiac outflow tract into aorta and pulmonary tract, vagal and sacral neural crests which gives rise to the ENS, and the trunk neural crest, which forms all of the peripheral nervous system of the trunk and also forms the chromaffin cells within the adrenal gland.

ENTERIC NEURAL CREST CELLS (ENCCS)

Enteric Neural Crest cells (ENCCs) is the name given to all the NCCs that populate the developing gut and form the ENS. This includes vagal neural crest cells, (originating at the vagal (somites 1-7) regions of the embryonic axis) and sacral neural crest cells (originating at the sacral (caudal to somite 24) regions of the embryonic axis). The vagal and sacral neural crest cells contribute to the ENS at different gut regions (Burns et al., 2000; Durbec et al., 1996; Wallace and Burns, 2005; Young and Newgreen, 2001). Vagal NCCs migrate in a rostral to caudal direction and sequentially contribute to the foregut and midgut and proximal portion of the hindgut (Durbec et al., 1996; Gershon, 1997; Young et al., 1998). In contrast, sacral NCCs contribute to the distal hindgut (Burns and Le Douarin, 1998; Kapur, 2000).

In mice, ENCCs take about six days to colonize the gut. Vagal NCCs enter the foregut around embryonic day E8.5/E9.0 and gut colonization is complete around E14.5 (Figure II-1) (Newgreen and Young, 2002; Young and Newgreen, 2001), with typical mouse gestation ranging from 18-21 days. In humans, this process takes about three weeks (Anderson et al., 2006b), beginning around week 4 and ending by week 7 (Druckenbrod and Epstein, 2005; Fu et al., 2003).

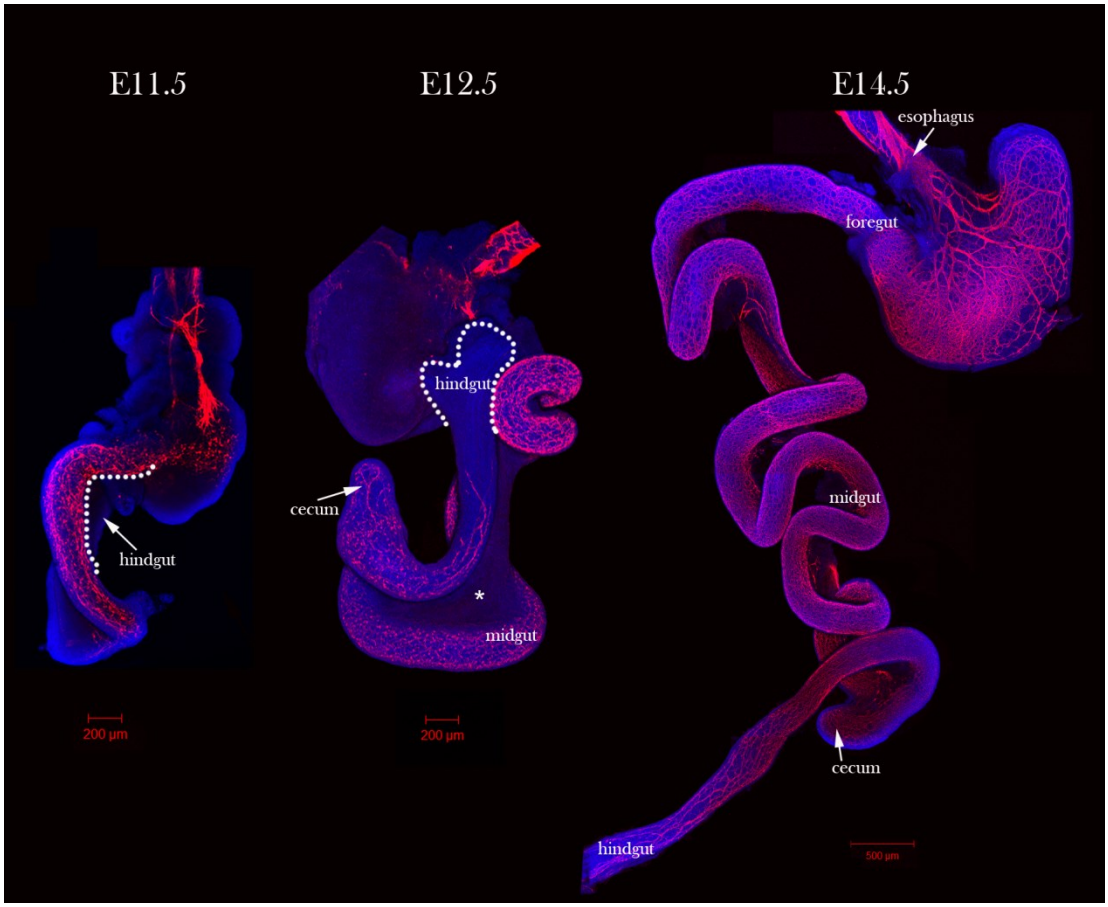

Figure I-1: Enteric neuron (Tuj1) immunostaining in wild-type embryonic guts. Tuj1 (red) immunostaining of E11.5 to E14.5 whole guts show the extent of colonization at the particular embryonic stage. At E11.5, the embryonic gut is in a hairpin formation and neurons are present to the cecum. At E12.5 the gut has grown, and the neurons have reached the proximal hindgut. At E14.5 neurons have reached the distal hindgut and grown significantly and the hairpin formation is no longer present. Nuclei are counterstained with 4',6-diamidino-2-phenylindole (DAPI) (blue). (Figure 1 from (Butler Tjaden and Trainor, 2013)).

ENTERIC NEURAL CREST CELL MIGRATION

ENCCs migrate through the gut tube as chains of interconnected cells. The cells at the leading edge of the migrating ENCC population are referred to as the wavefront, while the cells behind the wavefront are referred to as the trailing cells (Druckenbrod and

Epstein, 2005, 2007; Young et al., 2004). The migratory behavior of the leading and trailing cells is different, suggesting a role for the micro-environment and cell-cell interactions during the process of ENCC migration (Druckenbrod and Epstein, 2007). For example, it has been shown that the leading wavefront cells display significant caudal expansion, while the trailing cells exhibit limited expansion. Thus, it is the wavefront ENCCs that are responsible for the colonization of the hindgut (Nishiyama et al., 2012).

It had been previously proposed that migration of ENCCs through the cecum (circumflex ENCCs: cfENCCs) was important for hindgut colonization (Barlow et al., 2003; Coventry et al., 1994; Kruger et al., 2003). However, recent real-time imaging experiments have shown that, between E10.5-11.5, ENCCs destined for the hindgut traverse the mesentery (trans-mesenteric ENCCs: tmENCCs) as solitary cells. At this stage, the gut is in a hairpin formation and the midgut and hindgut are positioned opposite to each other in parallel, which allows for this trans-mesenteric migration of ENCCs. These tmENCCs, which were previously thought to be sacral neural crest cells (Young et al., 2004), are the major source of the ENS in the hindgut (Figure I-2) (Nishiyama et al., 2012).

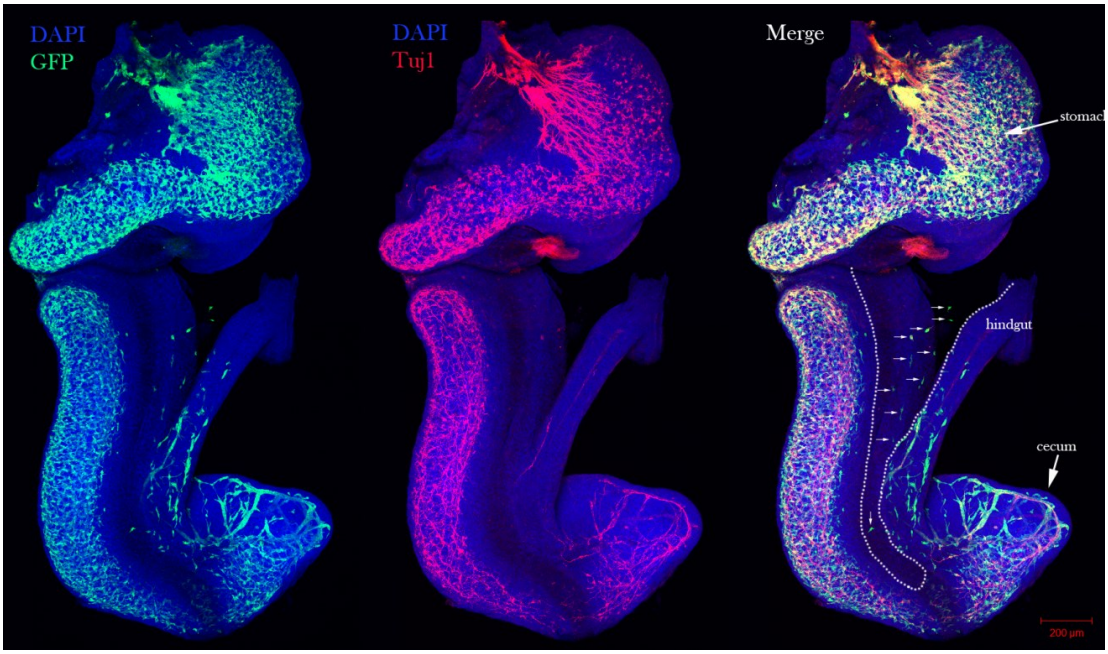

Figure I-2: Trans-mesenteric enteric neural crest cells migrate through the mesentery of E11.75 guts. Whole-mount co-immunostain of GFP and Tuj1 staining of E11.75 gut from a *RosaeYFP; Wnt1Cre* embryo. White arrows depict tmENCCs in the mesentery between the midgut and hindgut. Mesentery is located between dotted lines. Neural crest cells are stained with GFP and mature neurons are stained with Tuj1 (red). Nuclei are counterstained with 4',6-diamidino-2-phenylindole (DAPI) (blue). (Figure 2 from (Butler Tjaden and Trainor, 2013)).

Since the midgut and hindgut are juxtaposed only during E10.5-11.5, and tmENCCs are the primary cell population contributing to the hindgut ENS, these cells have only a limited period of time to reach the hindgut. Should these tmENCCs experience delayed migration through the mesentery, the result will be impaired colonization of the hindgut (Nishiyama et al., 2012). Whether there is a strict time window for ENCCs to colonize the hindgut is still debatable. ENCC grafting experiments done by Druckenbrod et al. showed that the age of the recipient, not the donor, determined whether the colon could be colonized, suggesting that the hindgut microenvironment changes at E14.5, indicated by increased laminin levels, and these

changes are no longer permissive to ENCC migration (Druckenbrod and Epstein, 2009). In contrast, using another mouse model that has delayed ENCC migration, Barlow et al has shown that colonization can be completed after E14.5, suggesting that there may not be a strict permissive window for hindgut colonization (Barlow et al., 2012).

A completely colonized gut with a functioning ENS is necessary for peristaltic activity of the gut wall and proper gut function. Defects in ENCC survival, migration, proliferation, or differentiation result in their failure to colonize the entire gut (Clavel, 1988; Gaillard, 1982; Hoehner et al., 1996; Langer, 1994; Tosney et al., 1986; Webster, 1973) and present as a devastating neurocristopathy, Hirschsprung disease (HSCR).

Hirschsprung Disease (HSCR)

Hirschsprung Disease (HSCR) is a devastating neurocristopathy that affects 1/5000 live births and usually presents with the inability to pass meconium, together with abdominal distension and discomfort. Most HSCR cases are limited to the rectum and sigmoid colon, but cases of total intestinal aganglionosis are possible, occurring in 3-8% of HSCR patients (N-Fékété, 1986). Patients with HSCR typically present with sustained contraction of the aganglionic bowel segment, leading to intestinal obstruction and distension of proximal segments (megacolon) and subsequently, the inability to pass stool. Currently, the only treatment available is surgical removal of the aganglionic bowel (Parisi, 2006).

CLINICAL PRESENTATION

Histologically, aganglionosis is pathognomonic for HSCR. In 80-85% of HSCR cases, this aganglionosis is limited to the rectum and sigmoid (short-segment disease). Long segment disease occurs in up to 20% of cases, where the aganglionosis extends proximal to the sigmoid colon. Total aganglionosis is more rare, occurring in 3-8% of

patients with HSCR (N-Fékété, 1986). Another rare variant is ultra-short segment disease, affecting only the distal rectum below the pelvic floor and anus (Neilson and Yazbeck, 1990). Hypoganglionosis and aganglionosis of the terminal gut can be caused by a reduction in enteric progenitor cells (Gianino et al., 2003; Stanchina et al., 2006). The portion of the bowel with reduced enteric neuron density is termed the transition zone, and it is always cranial to the aganglionic region (Kapur, 2009). The zone of aganglionosis results in tonic contraction of the affected bowel, leading to obstructive symptoms. Most often, patients are diagnosed in the neonatal period (Singh et al., 2003), presenting with a distended abdomen, the delayed passage of meconium (>24 hours), and vomiting. When patients are diagnosed later in childhood, they often have short-segment aganglionosis and present with chronic constipation and distension, vomiting, and failure to thrive (Parc, 1984). In 10% of HSCR cases, patients can present with enterocolitis, fever, and even septicemia.

HSCR occurs in 1/5000 live births and has an overall 4:1 male predominance (Spouge, 1985). However, for short segment disease there is a 4.2-4.4 male: female predominance and for long-segment disease there is a 1.2-1.9 male: female predominance (J A Badner, 1990). Furthermore, the risk of an HSCR sibling recurrence is 200 times higher than in the general population (4% versus 0.02%) (Bodian and Carter, 1963; J A Badner, 1990). Up to 30% of patients with HSCR also exhibit other abnormalities (Passarge, 1967; Spouge, 1985), such as velocardiofacial defects (Kerstjens-Frederikse et al., 1999), congenital heart defects (Ryan et al., 1992), gastrointestinal tract malformations, CNS abnormalities, genitourinary problems, craniofacial malformations and spina bifida (Amiel and Lyonnet, 2001; J A Badner, 1990; Parisi and Kapur, 2000; Ryan et al., 1992; Sarioglu, 1997). In addition, 2-15% of HSCR cases are also associated with Down's syndrome (Amiel and Lyonnet, 2001; Fu et al., 2003).

DIAGNOSIS

The diagnosis of HSCR can be made by a variety of methods. However, the preferred first diagnostic procedure is a contrast enema. In about 70-90% of the cases, this contrast enema will show the transition zone between normal (dilated) bowel and the narrow aganglionic bowel (Rosenfield, 1984; Smith and Cass, 1991). The rectosigmoid ratio is used to evaluate the transition zone, with a ratio greater than 1 being considered 'normal.' A stool-filled proximal bowel will decrease the rectum to sigmoid ratio. Plain radiographs showing dilated bowel loops, and anorectal manometry may also help with the diagnosis. When using anorectal manometry, clinicians note an absent rectoanal inhibitory reflex (Tobon et al., 1968). This absence of internal sphincter relaxation (Emir et al., 1999) is a reliable test after neonatal day 12, when the rectoenteric reflex is present (Lopez Alonso, 1992).

The gold standard for an HSCR diagnosis is a rectal biopsy, and it is possible to obtain a submucosal rectal suction biopsy without anesthesia (R J Andrassy, 1981). A positive diagnosis for HSCR includes confirming the absence of ganglionic cells in the myenteric and submucosal plexi, and presence of hypertrophic nerve trunks. Clinicians must be careful to biopsy proximal to the pectinate (dentate) line, which is normally physiologically hypoganglionotic, and caudal enough to detect even very short segment aganglionosis (Kapur, 2006). The biopsy specimen can also be stained for increased acetylcholinesterase activity, which contributes to a positive diagnosis (Kurer et al., 1986). If a suction biopsy does not provide an accurate diagnosis, a full-thickness biopsy is indicated.

TREATMENT

Currently, the only treatment for HSCR is surgery. Failure to surgically treat HSCR can be fatal due to malnutrition or sepsis following bowel perforation. Although

surgery is the routine therapy for HSCR patients, surgical outcomes can vary widely, with a range of long term consequences, such as constipation, fecal incontinence and enterocolitis (Baillie et al., 1999; Menezes et al., 2006). The surgical treatments aim to remove the aganglionic bowel and anastomose the normal bowel with the anus while preserving sphincter function. The main techniques used currently include the total transanal endorectal pull-through (TERPT) (Albanese et al., 1999; De la Torre-Mondragón and Ortega-Salgado, 1998; Langer et al., 1999) and the laparoscopic assisted pull-through (Georgeson et al., 1995; Jona, 1998) procedures.

Compared to traditional transabdominal open surgery, TERPT and laparoscopic assisted pull-through facilitate faster recoveries, shorter hospital stays, improved cosmetic appearance, and fewer perioperative complications (Fujiwara et al., 2007; Georgeson, 1999). The TERPT is useful for aganglionosis confined to the rectosigmoid area (De la Torre and Ortega, 2000), as it minimizes intraabdominal contamination, adhesion formation, and the risk of damage to pelvic structures. The laparoscopic assisted pull-through has the added benefit of collecting seromuscular biopsies for the identification of normal colon, better mobilization and dissection of the aganglionic colon, and minimized dilation of the anal canal (Georgeson, 1999; Georgeson et al., 1995).

Although the TERPT and laparoscopic assisted pull-through procedures have better outcomes than traditional open surgery, there are risks and complications. Common post-surgical problems include long-term obstructive symptoms and soiling. Milder obstructive symptoms can be treated by dietary changes, laxatives, enemas or botulinum toxin injections every 3-4 months (Minkes and Langer, 2000; Patrus et al., 2011). Patients who are responsive to botulinum toxin injections but are unable to undergo repeated injections can have a myectomy procedure (Wildhaber et al., 2004).

Although a repeat pull-through procedure can be done if there is residual or acquired aganglionosis, strictures or dysfunctional, dilated proximal bowel, it is very difficult due to the scarring from the previous procedure (Langer, 1999; Teitelbaum and Coran, 2003).

PATHOGENESIS

Proper neural crest cell migration, proliferation, differentiation, survival and apoptosis all contribute to a functional ENS. Perturbation in any of these processes can lead to a Hirschsprung disease phenotype. Many genes which play a critical functional role in neural crest cell development have been implicated in HSCR, including the proto-oncogene *RET*, endothelin signaling genes, and transcription factors (Parisi and Kapur, 2000). Although over a dozen genes have been identified that contribute to the etiology of HSCR, these pathways only account for about half of the known cases (Table I-1).

Table I-1: Hirschsprung disease genes and contribution to neural crest cell migration, proliferation, differentiation and survival. (Adapted from Table 1 from (Butler Tjaden and Trainor, 2013)).

Gene	Migration	Proliferation	Differentiation	Survival/Cell Death
RET	Attracted to GDNF	Promote proliferation	Promote neuronal differentiation	Promote ENCC and enteric neuron survival, Inhibit non-apoptotic cell death
GDNF	Gradient to attract RET+ and GFRα1+ ENCCs	Promote proliferation	Promote neuronal differentiation	Promote survival
GFRa-1	Attracted to GDNF, necessary to cross mesentery			Promote enteric neuron survival
EDNRB	Necessary for normal migration	Maintain proliferative state		
EDN3/ET3	Necessary for normal migration, may maintain permissive environment		Inhibit neuronal differentiation	
ZFHX1B	Neural specification, Epithelial-to-mesenchymal transition			
PHOX2B	Expressed in migrating ENCCs			
BMPs	Regulation of ENCC migration		Required for normal ganglion formation	
PAX3			Required for normal ganglion formation	
SHH	Oppose GDNF, reduce migration	Promote proliferation	Inhibit neuronal differentiation by affecting responsiveness to GDNF	
CXCR4	Indirect support of trans-mesenteric migration by regulating vascular development			
SOX10		Maintain ENS progenitor state		
NRTN/NTN		Promote proliferation	Promote neuronal differentiation	Promote survival

For the sake of simplification, I have classified the HSCR phenotype causing gene mutations into two categories: (1) affecting ENCC migration and (2) affecting ENCC survival, proliferation and differentiation.

ENCC MIGRATION

Many genes contribute to normal enteric neural crest cell migration to form a functional enteric nervous system, and mutations in any of these genes may cause an HSCR phenotype (Table I-1).

GDNF and RET regulate neural crest cell migration

Mutations in receptor tyrosine kinase (*Ret*) and glial cell line-derived neurotrophic factor (*Gdnf*) family members are the major contributors for HSCR cases caused due to failed ENCC migration. Mutations in the *Ret* receptor tyrosine kinase pathway account for 15-35% of patients with sporadic HSCR (HSCR in a single family member) and 50% of familial cases (Brooks et al., 2005). Patients with heterozygous mutations in *Gdnf* have also been diagnosed with HSCR. GDNF is a secreted ligand protein that binds glycosylphosphatidylinositol-linked receptor (GFRα1), expressed on ENCCs. Together, the GDNF- GFRα1 complex then binds and activates RET, a transmembrane protein also expressed on ENCCs. RET then auto-phosphorylates and activates downstream pathways (Tansey et al., 2000) that influence ENCC survival and apoptosis, proliferation, migration and differentiation. (Figure I-3) (Eng, 1999; Mulligan, 2014).

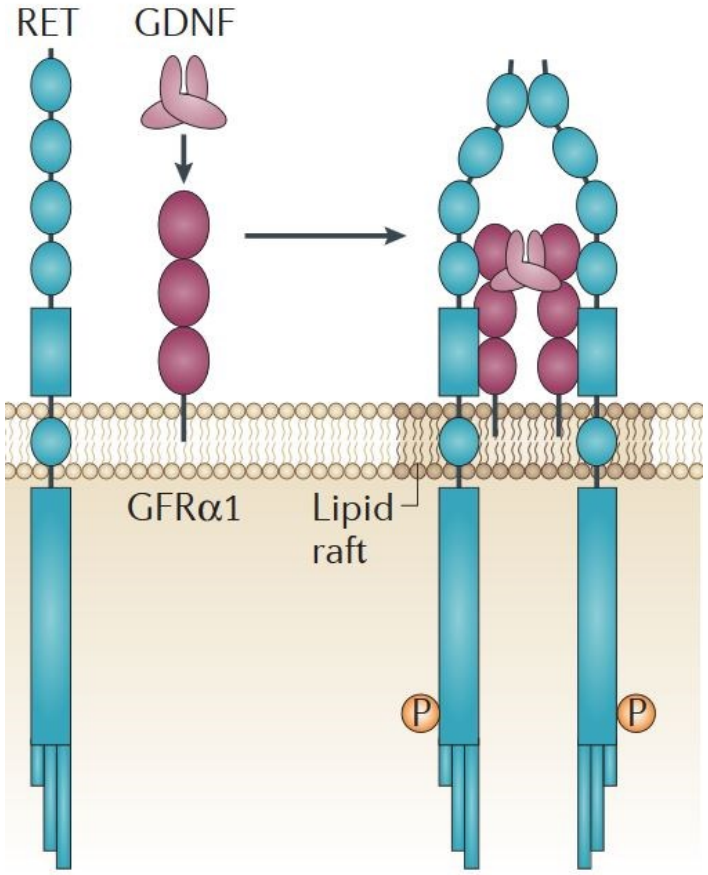

Figure I-3: GDNF and RET are expressed on enteric neural crest cells. GNDF is expressed in the gut mesoderm. GNDF forms a complex with GFRα1, which bind and activate RET to influence ENCC survival, proliferation, migration and differentiation. Figure 1B from (Mulligan, 2014).

GDNF expression in the gut mesoderm is the primary chemoattractant for the ENCC wavefront (Figure I-4). Prior to the entry of ENCCs into the foregut, GDNF is expressed in the gut mesoderm (Natarajan et al., 2002). During ENCC entry into the gut, RET and GFRα1 are expressed on the ENCCs (Tomac et al., 1999). When the ENCC wave front reaches the esophagus, GDNF is expressed in the stomach, and as the ENCCs approach the distal small intestine GDNF expression is again elevated in the cecum, suggesting GDNF acts to attract RET and GFRα1 expressing ENCCs to the proper

location (Natarajan et al., 2002; Young et al., 2001). This GDNF- GFRα1-RET pathway is also important for the tmENCC migration through the mesentery between the midgut and hindgut (Figure I-4). Without GFRα1, tmENCCs are unable to leave the midgut (Nishiyama et al., 2012). Defects in the formation of the GDNF-RET-GFRα1 complex result in an aganglionosis phenotype, irrespective of whether the mutation is in *RET*, *GDNF* or *GFRα1* (Cacalano et al., 1998; Eketjäll and Ibáñez, 2002; Moore et al., 1996; Nishiyama et al., 2012; Pichel et al., 1996; Sanchez et al., 1996; Schuchardt et al., 1994; Shepherd et al., 2004).

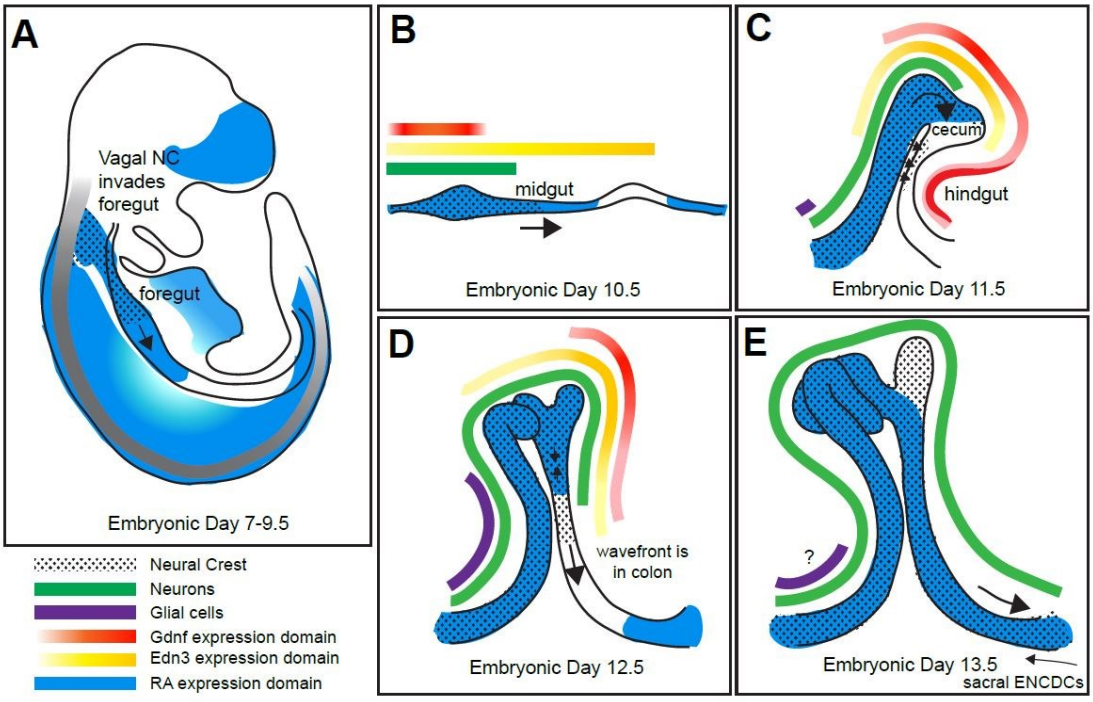

Figure I-4: Enteric neural crest cell colonization of mouse GI tract. GDNF (red) expression acts to attract RET+ /GFRα1+ ENCCs (black dots) throughout gut development. Yellow shows where Edn3 expression is present, and blue shows where retinoic acid signaling is present. Neural crest cells must differentiate into neurons (green) and glia (purple) during their migratory phase. Adapted from Figure 1 from (Lake and Heuckeroth, 2013), modified by Joaquin Navajas Acedo.

Patients with long and short segment disease have been identified with mutations in *RET* (Edery et al., 1994; Romeo et al., 1994). However, penetrance is estimated between 50-70% (Bolk et al., 2000). The "gene dosage" necessary for normal ENS development differs between mice and humans. For example, a heterozygous mutation of RET in humans can lead to HSCR, but $RET^{+/-}$ only exhibit hypoganglionosis in mice (Carniti et al., 2006). In contrast, $RET^{-/-}$ mice have complete intestinal aganglionosis (Schuchardt et al., 1994). To mimic the aganglionic phenotype, mice need to lose at least 60-70% of RET expression (Uesaka et al., 2008). RET has two isoforms: RET9 and RET51, both of which are conserved between humans and mice (Carter, 2001). Deletion of *Ret51* ($Ret^{9/9}$), does not affect colonization of distal colon in mice. In contrast, point mutations and complete deletion of *Ret9* result in failure of distal colon colonization suggesting that unlike RET51, RET9 is necessary and sufficient for normal ENS development (Asai et al., 2006; Carniti et al., 2006; de Graaff et al., 2001; Nishiyama et al., 2012).

Interestingly, Ret+ intestinal ENS progenitor cell transplantation from wild-type E11.5 embryos to the E8.5 vagal region of recipient control and $Ret^{-/-}$ embryos resulted in colonize of the entire length of the control intestine by transplanted cells, but only the proximal foregut in the $Ret^{-/-}$ embryos, suggesting a non-cell autonomous *Ret* effect on *early* gut colonization and ENS development (Bogni et al., 2008). Combined with previous transplantation experiments (Natarajan et al., 1999), which transplanted Ret+ cells directly into the gut wall of $Ret^{-/-}$ embryos, and resulted in full colonization of the gut, this vagal transplantation study emphasizes the capacity of Ret+ cells to colonize the gut, but the extent of colonization relies on the transplantation location and timing, and number of transplanted progenitors.

Endothelin Pathway regulation of neural crest cell migration

Endothelin signaling is another pathway necessary for normal ENCC migration and helps maintain a permissive NCC environment. Endothelin 3 (EDN3 or ET3) is a peptide secreted by gut mesenchyme (Figure I-4) (Nataf et al., 1998), that binds to the G-protein coupled receptor ENDRB, which is expressed on migrating ENCCs. Endothelin converting enzyme 1 (ECE1) post-translationally modifies the immature form of EDN3 into its active form (Baynash et al., 1994; Xu et al., 1994). The EDN3-EDNRB signaling pathway is involved in regulating the normal migration of ENCCs, and maintains enteric progenitors in a proliferative state (Barlow et al., 2003; Bondurand et al., 2006). Thus, END3 inhibits ENCC differentiation (Bondurand et al., 2006; Hearn et al., 1998; Nagy and Goldstein, 2006; Wu et al., 1999).

Patients with heterozygous mutations in the *EDN3-EDNRB* pathway account for 5% of HSCR cases (Amiel and Lyonnet, 2001), including one case caused by a mutation in *ECE1* (Hofstra et al., 1999). *EDN3* and *EDNRB* mutations are associated with both syndromic (Waardenburg Shah) and non-syndromic forms of Hirschsprung disease (Amiel and Lyonnet, 2001; Brooks et al., 2005). Patients with Waardenburg Shah Syndrome have colonic aganglionosis, pigmentation defects and sensorineural deafness. The inheritance of this syndrome can be either recessive (which is the case for patients with mutations in *EDNRB* and *EDN3* cases) or dominant (Amiel and Lyonnet, 2001; Brooks et al., 2005). Patients with *EDNRB* Hirschsprung disease are associated with a large Mennonite population (Mulligan et al., 1993). Carriers of the EDNRB Tryp276Cys mutation display incomplete penetrance, with heterozygous mutations leading to HSCR in 21% of the affected patients, and 74% in patients with homozygous mutations (Puffenberger et al., 1994). As with RET mutations, the human ENS is more sensitive to reduced ENDRB signaling than in mice (Wallace and Anderson, 2011).

Mouse models with mutations in *Edn3*, *Ednrb* or *Ece1* display various aganglionosis and pigmentation defects (Baynash et al., 1994; Hosoda et al., 1994; Yanagisawa et al., 1998). *Lethal spotted* mice have a mutation in the EDN3 ligand (*Edn3*$^{ls/ls}$), and *piebald lethal* have an EDNRB mutation (*Ednrb*$^{sl/sl}$). Both these mutants exhibit ENCC migration defects (delayed number of ENCCs in small intestine), and lack enteric neurons in the distal bowel, and display piebaldism (Barlow et al., 2003; Baynash et al., 1994; Hosoda et al., 1994; Lee et al., 2003; Ro et al., 2006). Conditional deletion studies suggest that the critical time window where EDN3-EDNRB signaling is necessary is between E10.5-12.5 (Shin et al., 1999). Interestingly, beginning at E10.0, *Edn3* mRNA is detected ahead of migrating ENCCs (Barlow et al., 2003). It has been suggested that because aganglionosis in *Ednrb*- and *Edn3*-deficient mice is restricted to the distal colon, the EDN3-EDNRB signaling pathway is required for hindgut colonization (Leibl et al., 1999).

Homozygous deletion of *Ednrb* results in a 24 hour delay in ENCC advancement. By E14.5, wild-type guts are fully occupied by ENCCs, but in mutant guts, ENCCs have altered trajectories and reduced speed. Grafting experiments suggest that donor invasion is restricted by the age of the recipient tissue, not genotype. It has been previously hypothesized that at E14.5 the gut microenvironment changes to become non-permissive to ENCC migration and that if ENCCs have not finished migration by E14.5, the embryos will present a HSCR phenotype (Druckenbrod and Epstein, 2009). However, recent experiments in *Tcof1* haploinsufficient mice, a mouse model for reduced NCC formation, challenge this hypothesis. In spite of delayed ENCC migration between E10.5-E14.5, *Tcof* haplosufficient embryos display continued colonization from E14.5-E18.5 and form a complete ENS, suggesting that the balance between NCC proliferation in concert with

differentiation and extrinsic gut microenvironmental influences can overcome pathogenic migration and decreased cell numbers (Barlow et al., 2012).

Additional genes regulating neural crest cell migration

The zinc finger homeobox 1b, SMAL interacting protein, or ZFHX1B/SIP1/SMADIP1, is expressed in premigratory and migratory vagal neural crest cells. This transcription factor is involved in neural specification and the epithelial to mesenchymal transition that occurs during early NCC development. A human mutation in ZFHX1B is associated with Mowat-Wilson syndrome, of which HSCR is a component (Yamada et al., 2001). *Zfxh1b*$^{-/-}$ embryos exhibit a complete absence of vagal NCC precursors, and die around E9.5 due to cardiovascular and neural defects (Van de Putte et al., 2003). Analysis of neural crest cell-specific *Zfx1b* mutants suggests that ZFHX1B may be required for anterior vagal NCCs differentiation for the colonization of the GI tract (Van de Putte et al., 2007).

Paired-like homeobox2b (PHOX2b) is a transcription factor expressed in migrating ENCCs, enteric neurons and glial cells (Corpening et al., 2008). This transcription factor is required for RET expression in ENCCs. Mouse and zebrafish models lacking *Phox2b* have total intestinal aganglionosis due to a failure of ENCCs to colonize the gut properly (Elworthy et al., 2005; Pattyn et al., 1999). *Phox2b* mutant mice lack a PNS, and die at birth (Pattyn et al., 1999). Human mutations in *PHOX2b* have recently been described in association with HSCR, particularly with congenital central hypoventilation syndrome (CCHS) and neuroblastoma (NB), referred to as CCHS-HSCR-NB. (Amiel et al., 2003; Nagashimada et al., 2012; Trochet et al., 2005).

Bone morphogenetic proteins (BMPs) also play a role in the regulation of NCC migration and ENS enteric ganglion formation (Faure et al., 2007; Goldstein et al., 2005). Targeted inhibition of intestinal BMP activity using noggin leads to delayed ENCC

migration by interfering with the migratory effects of GDNF signals. Therefore, appropriate BMP and GDNF interactions are necessary for the proper formation of a complete ENS (Goldstein et al., 2005).

Sonic Hedgehog (SHH) is another key regulator of ENCCs migration (Fu et al., 2004) and ENS plexus formation (Ramalho-Santos et al., 2000). SHH and GDNF have opposing effects on ENCC migration. ENCCs migrate in the presence of GDNF, but addition of SHH reduces this migration by affecting the responsiveness of ENCCs towards GDNF signaling or by regulating proliferation and differentiation of ENCCs in the gut (Fu et al., 2004). Thus, a balance between GDNF and SHH may be important for the proper positioning of the ENS plexus.

CXCR4 is a cell surface receptor for the CXC chemokine PBSF/SDF-1 (pre-B-cell growth-stimulating factor/stromal-cell derived factor). This factor is expressed in developing vascular endothelial cells. *Cxcr4* null mice display a failure to properly form the large vessels that supply the GI tract (Tachibana et al., 1998). These mice also exhibit fewer tmENCCs at E11.5 and impaired hindgut colonization of ENCCs by E14.5 compared to wild-type littermates (Nishiyama et al., 2012). This implies that tmENCC migration is partially dependent on vascular-derived signals, as CXCR4 indirectly supports trans-mesenteric migration by regulating vascular development.

ENCC PROLIFERATION, SURVIVAL AND DIFFERENTIATION

Proliferation rates in the developing GI system are equivalent throughout the ENS. Active ENCC proliferation at the wavefront is necessary to colonize the gut, while that behind the wavefront is necessary to fully populate the expanding intestine (Young et al., 2005). Millions of enteric neurons and glia are present in the adult intestine (Gianino et al., 2003), and a balance between proliferation and differentiation ensures maintenance of a sufficient progenitor pool of cells necessary for complete ENS colonization (Heanue

and Pachnis, 2007; Laranjeira and Pachnis, 2009; Stanchina et al., 2006). Many of the genes discussed above, such as RET, GDNF, GFRα1 and another GDNF family member, NRTN, also function to maintain ENCCs and post-mitotic enteric neuron survival in the gastrointestinal tract.

Ret, *Gdnf*, and *Gfrα1* are necessary for early ENCC survival (Taraviras and Pachnis, 1999). *Gfrα1* and *Ret* are essential for survival of colonic enteric neurons. GDNF and RET promote proliferation of ENS progenitors and their differentiation into neurons and glia (Heuckeroth et al., 1998; Taraviras et al., 1999), whereas GDNF determines the rate of ENS progenitor proliferation (Gianino et al., 2003). Additionally, enteric neuron survival is sensitive to *Ret* dosage (Uesaka et al., 2007; Uesaka et al., 2008). Low *Ret* dosage leads to delayed migration and increased non-apoptotic cell death in ENCCs (Uesaka et al., 2008). Inhibiting cell death in *Ret* hypomorphic embryos results in formation of a normal ENS, suggesting that cell death, not a migratory delay of ENCCs, is a principle cause of isolated HSCR (Uesaka and Enomoto, 2010).

The EDN3-EDNRB signaling pathway is not only involved with regulating ENCC migration, but also plays a role in maintaining enteric progenitors in a proliferative state (Barlow et al., 2003; Bondurand et al., 2006). By keeping progenitors in a self-renewing state, the presence of Edn3 inhibits ENCC differentiation (Bondurand et al., 2006; Hearn et al., 1998; Nagy and Goldstein, 2006; Wu et al., 1999).

Neurturin (NRTN or NTN) is a ligand in the GDNF family, which binds to GFRα2 to activate RET and promote the projection and branching of some enteric neuron axons. This trophic factor is important for the maintenance of neuronal projections, as neuturin-deficient mice have reduced nerve fiber density in the ENS, smaller enteric neuron cell bodies and abnormal GI motility, as well as abnormal gut neurotransmitter release and motility (Gianino et al., 2003; Heuckeroth et al., 1999).

NRTN promotes the proliferation of ENS precursors and neuronal differentiation to increase the number of neurons and glia (Heuckeroth et al., 1998). Homozygous mice with null mutations in *Nrtn* and *Gfrα2* have reduced excitatory fibers present in the ENS and decreased gut motility along the entire GI tract (Gianino et al., 2003; Heuckeroth et al., 1999; Rossi et al., 2003). Myenteric ganglion cells were also smaller in $Nrtn^{-/-}$ adult mice compared to wild-type mice, suggesting that NRTN plays a supportive role for neurons and cell size maintenance (Heuckeroth et al., 1999), and promotes survival of enteric NCCs as well as the maintenance of enteric neurons and glia. In addition, *Ret*+ cells from embryonic rat guts were cultured and failed to survive in the absence of GDNF or NRTN (Taraviras et al., 1999). Thus, it has been shown both *in vivo* and *in vitro* that NRTN promotes survival of enteric NCCs as well as the maintenance of enteric neurons and glia.

SOX10 (SRY-related high mobility group-box transcription factor) is expressed in NCCs as they emigrate from the neural tube. *Sox10*+ cells are used as a marker of ENS progenitors as it is expressed during NCC migration, and maintains the ENS progenitor state (Bondurand et al., 2006; Bondurand et al., 2003). This transcription factor regulates key genes required for ENS, melanocyte and glial development (Kelsh, 2006), such as *Ednrb* and *Ret* in ENCCs (Lang et al., 2000; Lang and Epstein, 2003; Zhu et al., 2004). In humans, *SOX10* mutations account for less than 5% of both syndromic and nonsyndromic forms of HSCR. In patients, *SOX10* mutations are associated with the dominant inheritance of HSCR in Waardenburg Syndrome (Pingault et al., 1998), and some patients have additional neurologic phenotypes (Inoue et al., 1999; Southard-Smith et al., 1999; Touraine et al., 2000), which is attributed to dysmyelination of their central and peripheral nervous systems (Touraine et al., 2000). Homozygous $Sox10^{lacZ}$ mice display total intestinal aganglionosis and die perinatally (Britsch et al., 2001). Zebrafish *sox10*

homozygous mutants display abnormal ENS and melanocyte phenotypes. *Sox10*^{Dom} mice have a single base pair insertion leading to a spontaneous dominant negative mutation. This truncates Sox10 downstream of its DNA binding domain (Southard-Smith et al., 1998). These mice display a smaller pool of ENS progenitors, compared to wild-type mice (Britsch et al., 2001; Paratore et al., 2002), and lack enteric neurons through the entire GI tract (Kapur, 1999; Southard-Smith et al., 1998). *Sox10* homozygous mutant mice die at birth, and exhibit total intestinal aganglionosis, as the vagal NCC die prior to their entry into the gut (Britsch et al., 2001; Kapur, 1999). Up to 20% of the heterozygous mice have colonic aganglionosis, but the incidence is background-dependent (Cantrell et al., 2004; Maka et al., 2005; Southard-Smith et al., 1998; Stanchina et al., 2006).

GENETIC INTERACTIONS BETWEEN INVOLVED IN ENCC DEVELOPMENT AND HSCR PHENOTYPE

Noncoding mutations in RET have been shown to increase susceptibility to other HSCR mutations (Brooks et al., 2005; Emison et al., 2005; Griseri et al., 2007). These noncoding mutations may be involved with regulatory elements and cellular mechanisms, such as transcription, translation, location or level of gene expression, or may be associated with linked susceptible loci. For example, the 9q31 locus segregates with the HSCR phenotype in families with noncoding *RET* mutations, suggesting that a combination of these specific loci may cause a HSCR phenotype (Brooks et al., 2005). Additionally, a genome-wide association study on a Mennonite population (with a ten-fold increase in HSCR compared to the general population), identified a HSCR-associated, non-coding *RET* mutation in the transcriptional enhancer of intron 1, which associates with *EDNRB* mutations (Carrasquillo et al., 2002). It was later found that this same *RET* Mennonite haplotype makes a 20-fold greater contribution to HSCR risk than

the rarer protein-coding HSCR mutations (Emison et al., 2005). However, not all *RET* variants increase susceptibility to HSCR. A common variant in the 3'UTR of the *RET* gene has been shown to slow mRNA transcript decay (Griseri et al., 2007). The increasing number of identified non-coding susceptibility *RET* mutations is a reminder that although noncoding mutations may have low penetrance (Emison et al., 2005), they are capable of acting synergistically with other mutations to affect a disease phenotype.

As noted above, mutations may act synergistically resulting in a more severe phenotype. Numerous models which typically cause distal colonic aganglionosis when crossed to an endothelin pathway mutant, resulting in total colonic aganglionosis, which is indicative of genetic interactions. For example, $RET^{51/51}$*; Edn3*$^{ls/ls}$ double mutants (Barlow et al., 2003), *Sox10*$^{Dom/+}$*; Edn3*$^{ls/ls}$ double mutants (Stanchina et al., 2006) and *Sox10*$^{Dom/+}$*; Ednrb*$^{sl/sl}$ double mutants (Cantrell et al., 2004) all exhibit total intestinal aganglionosis, suggesting genetic interactions that increase the penetrance and severity of the HSCR phenotype.

Gdnf also has a synergistic effect with Edn3 to enhance this proliferative effect, but inhibits neuronal differentiation to maintain the precursor cell population (Hearn et al., 1998; Nagy and Goldstein, 2006).

PAX3 (Paired box 3) is also required for normal enteric ganglion formation, and does so by acting through RET. Pax3 and Sox10 bind to the RET enhancer, and thus activate RET transcription and expression (Lang et al., 2000). Furthermore, neither *Pax3*$^{+/-}$ nor *Tcof1*$^{+/-}$ mice exhibit colonic aganglionosis, but the compound *Tcof1*$^{+/-}$; *Pax3*$^{+/-}$ animals have distal colonic aganglionosis at E18.5, suggesting that Pax3 acts a modifier of the *Tcof1*$^{+/-}$ phenotype by increasing the apoptosis of ENCCs, reducing the number of NCCs that can migrate into the foregut (Barlow et al., 2013).

A reciprocal interaction between Sox10 and Phox2b is illustrated using a model for CCHS-HSCR-NB, created by a introducing a nonpolyalanine repeat expansion mutation in PHOX2B in the *Phox2b* mouse locus. These mouse mutants have persistent *Sox10* expression, leading to reduced proliferation and biased glial differentiation (Nagashimada et al., 2012). Therefore, the interaction between Sox10 and Phox2b is necessary to maintain appropriate differentiation of neurons and glia in the ENS.

Rare human cases have been documented with NTN mutations, and of those cases, a mutation was found in *RET* or another HSCR gene, suggesting a modifier effect (Angrist et al., 1996; Doray, 1998; Eketjäll and Ibáñez, 2002; Hofstra et al., 1996; Ivanchuk et al., 1996; Parisi and Kapur, 2000; Salomon et al., 1996).

DISCUSSION: PROMISING MOUSE TRANSPLANTATION RESCUE EXPERIMENTS

Currently the only treatment available for patients with HSCR is surgical removal of the aganglionic bowel. However, recently it has been suggested that stem cell therapy may be a viable option to treat patients with aganglionosis. Studies have been conducted in both embryonic and postnatal intestines to further elucidate the role and microenvironmental requirements of ENS progenitors, as well as to investigate a potential rescue during postnatal development of the HSCR phenotype.

There have been numerous studies showing the potential of progenitor and stem cells to give rise to neurons of the embryonic ENS (Bondurand et al., 2003; Lindley et al., 2008; Mosher et al., 2007; Natarajan et al., 1999), but until recently it was unclear whether this could be a viable treatment option for humans born and diagnosed with HSCR. Recently, in a very promising study, transplanted fetal and postnatal intestinal NCC-derived neurospheres into the colons of postnatal mice revealed that the cells derived from the neurosphere transplantations were able to migrate, proliferate and generate neurons and glia in the recipient colons (Hotta et al., 2013). This study

emphasizes the importance to treat disease such as HSCR in the postnatal period, as the diagnosis is definitively made after birth.

DISCUSSION: NEED TO CONTINUE TO ELUCIDATE GENES THAT CONTRIBUTE TO HSCR

Many genes that contribute to the pathogenesis of HSCR have been identified, however, mutations in these genes only account for about half of the known human cases. Other genes may contribute to the etiology of HSCR by acting as modifiers or contributing to critical ENCC developmental processes, such as migration, proliferation, differentiation and survival (Butler Tjaden and Trainor, 2013). There needs to be a continued effort in finding genes that are responsible for or associated with HSCR, not only through mouse models but also by identifying mutations in affected individuals. Whole exome and whole genome sequencing of patient samples would be an ideal way to identify these genes and mutations.

With new genetic models of HSCR and new tools to examine them, new modes of pathogenesis may be proposed. For example, recent time lapse imaging using a photoconvertible mouse mutant showed that ENCCs reach the hindgut by migrating through the mesentery between the midgut and hindgut, as opposed to a sequential migration from midgut to cecum to hindgut (Nishiyama et al., 2012). Even this single deviation from the previous model of ENCC migration necessitates that mutants with migratory dysfunction be revisited to examine the possible changes in tmENCC and cfENCC behaviors (Nishiyama et al., 2012), and the effects those changes may have on the progression of colonic aganglionosis.

Hirschsprung disease is a highly complex and non-Mendelian disease, with wide phenotypic variability and incomplete penetrance. Additionally, the same phenotype (HSCR) is associated with mutations of multiple distinct genes (multigenic disease). These characteristics suggest the involvement of modifier genes or environmental

influences (Angrist et al., 1996; Bolk et al., 2000; Parisi and Kapur, 2000; Salomon et al., 1996). For example, rare human cases have been documented with NTN mutations, and many of these cases had a concomitant mutation in RET or another known HSCR gene, suggesting a modifier effect (Doray, 1998).

Thus, great strides are being made to better understand HSCR, but much is still unknown. Although the most promising transplantation rescue experiments have emphasized treating patients postnatally, after a definitive HSCR diagnosis (Hotta et al., 2013), the continuation to find new animal models and more associated human genes along with new techniques to study these genetic disruptions are necessary, in the hopes that patients can be routinely screened, and newer potential treatments can be administered before clinical symptoms arise.

Recently, mouse and chick studies have revealed important roles for the Vitamin A-derived molecule, retinoic acid, during ENS development (Fu et al., 2010; Niederreither et al., 2003; Sato and Heuckeroth, 2008; Simkin et al., 2013). These models will be discussed in the following section, and a new genetic model for RA-deficiency-induced-HSCR is presented as the bulk of this thesis work.

Vitamin A

Vitamin A is an essential nutrient that plays major roles in embryonic development, gene transcription, bone growth and metabolism, skin and mucous membrane health, vision, hematopoiesis, and immune system maintenance (NAP, 2001). In food, vitamin A is found in two major forms: Retinol and carotenoids, of which beta-carotene is the most important. Retinol is the highly bio-available form, found in animal liver, eggs, and milk products. Because this form of vitamin A is fat-soluble, it can build up in the body and become toxic. Beta-carotene, a “pro-vitamin A,” is a vitamin A

precursor that must be converted in the body to become a usable retinoid. This anti-oxidant is found in deeply colored fruits and vegetables, and is most well-known for giving orange color to carrots. Although a diet high in fruits and vegetables may provide vitamin A and other necessary nutrients, relying totally on this source of vitamin A through beta-carotene can lead to deficiencies, as the conversion of carotenoids to retinol is low (12:1) (NAP, 2001). Furthermore, this conversion takes place mainly in the small intestine during absorption (Bendich and Langseth, 1989), and is tightly regulated to avoid excessive vitamin A absorption (Underwood, 1985).

The recommended daily allowance of retinol varies from 400-600µg/day in infants to 600-1700µg/day in adults, and 750-2800µg/day in lactating or pregnant women. Too little vitamin A can result in infectious disease and vision problems, and too much vitamin A in the form of retinol can be toxic. Too much beta-carotene can make skin turn yellow or orange. Hypervitaminosis A (vitamin A excess) is a minor epidemiological problem compared with vitamin A deficiency, but typically happens acutely by ingesting high doses over a short period of time (by eating the liver of a carnivore or by overuse of supplements), or chronically by continually ingesting high doses. Some symptoms may include headache, nausea, vomiting, fever, vertigo and visual disruptions (Bendich and Langseth, 1989). Serious teratogenic defects can result from excess retinoids during pregnancy, targeting all major organ systems (Zile, 1998).

VITAMIN A DEFICIENCY (VAD)

Vitamin A also plays a role in embryonic development. In both adults and embryos, vitamin A functions through its active form, retinoic acid (RA). RA is an important signaling molecule in embryonic development, crucial for patterning, morphogenesis and organogenesis. Congenital abnormalities and fetal death can result from excess or insufficient RA. Major organ systems affected by vitamin A (and retinoid)

deficiency include the craniofacial, cardiovascular and ocular tissues, circulatory, respiratory (Antipatis et al., 1998) and urogenital (Moreau et al., 1998) systems (Zile, 1998).

Vitamin A deficiency (VAD) is a major preventable cause of nyctalopia (night blindness), a large contributor to morbidity and mortality due to infections leading to diarrhea and respiratory diseases, particularly in children and pregnant and lactating women, especially in lower income countries (WHO, 2009). VAD is predominantly a nutritional concern, brought on by a consistent diet insufficient in vitamin A. This vitamin deficiency is one of the most serious and common nutritional disorders worldwide (Barber et al., 2014). A chronic poor diet can lead to decreased vitamin A stores in the body, which then results in VAD-associated pathology such as xerophthalmia (dry eyes), anemia, hyperkeratosis, and decreased immunity (WHO, 2009, 2015). Xerophthalmia is the leading cause of preventable childhood blindness. A chronic poor diet often coexists in countries with frequent infections (including those that cause diarrhea), leading to further reduced vitamin A intake due to appetite suppression, increased metabolism and increased excretion of retinol (Alvarez et al., 1995). This results in a cycle of depleted retinol stores in the body, and leads to further susceptibility to severe infection (especially measles and diarrheal diseases) (WHO, 2009, 2015).

Numerous studies of various organ systems have implicated Vitamin A Deficiency Diseases (VADD) with alterations of ECM expression, such as increased collagen levels, decreased MMP activity and decreased laminins (Esteban-Pretel et al., 2013; Marin et al., 2005), which often leads to organ fibrosis and dysfunction (Barber et al., 2014). NCCs use proteases ADAM10, and matrix metalloproteases 2 and 9 (MMP2 and MMP9) to break down portions of the ECM as they migrate through it (Taneyhill and Padmanabhan, 2014).

In 1995, WHO estimated that 60 countries are afflicted with severe endemic VAD based on the level of xerophthalmia and low serum retinol concentration (<0.35μM/L). In 2005 it was estimated that 122 countries have VAD based on night blindness and serum retinol concentrations of <0.70μM/L in pre-school children (WHO, 2009). In 2015, the WHO declared VAD a public health problem in more than half of all countries (WHO, 2015).

Various studies have shown a reduction in maternal and infant death associated with severe VAD by supplementing pregnant mothers and infants with vitamin A (reviewed in (WHO, 2009)). The three major ways to improve vitamin A status in communities that are highly affected with VAD is to encourage dietary diversification, fortification of staple foods, and to deliver high-potency supplements (WHO, 2009). Specifically, children at risk can be given high dose vitamin A capsules, which provide supplementation for 4-6 months, and lactating mothers can be given high dose supplementation tablets while being encouraged to breast feed their infant, as breast milk is a natural source of vitamin A (WHO, 2009, 2015).

VITAMIN A METABOLISM TO RETINOIC ACID

Vitamin A functions through its active form, retinoic acid (RA). RA acts predominantly in a paracrine fashion (Duester, 2008), as a ligand for nuclear RA receptors (RARs) and retinoid X receptors (RXRs) to regulate transcriptional activity of target genes (Niederreither and Dolle, 2008). Vitamin A (retinol) is stored primarily in the hepatic stellate cells and is transported by retinol binding protein 4 (RBP4) to the cell surface RBP receptor Stra6 (stimulated by retinoic acid gene 6). Once inside the cell, retinol is bound by cellular retinol binding proteins (CRBP) and undergoes two consecutive oxidation reactions to become retinoic acid. In the first reaction, retinol is oxidized to all-trans-retinal (also called retinaldehyde) by microsomal retinol

dehydrogenase 10 (RDH10) or cytosolic alcohol dehydrogenases (ADH). Although studies initially indicated that members of the ADH family catalyzed this reaction ubiquitously throughout the embryo (Molotkov et al., 2002), more recent loss of function studies have revealed primarily postnatal importance for ADH oxidation (Kumar et al., 2011), whereas a homozygous mouse mutation in RDH10 (Sandell et al., 2007) indicated that RDH10 is the critical enzyme necessary for the regulation of this first oxidation step during embryonic development (Cammas et al., 2007).

All-trans retinal is then oxidized by retinaldehyde dehydrogenases RALDH1, RALDH2 and RALDH3 to retinoic acid. RA can also be produced by an alternative route through beta carotene. Beta-carotene is cleaved by beta, beta-carotene 15/15'-monooxygenase 1 (BCMO1/BCOX) to retinaldehyde. RALDH expression patterns are highly correlated with RA signaling, as shown using RA response element (RARE) reporter mice (Methods: Mouse lines, pg 37) (Haskell and LaMantia, 2005; Rossant et al., 1991). RALDH2, the first retinaldehyde dehydrogenase to be expressed, is induced in the primitive streak and mesoderm during gastrulation, and is later restricted to the posterior embryonic region. This enzyme is responsible for almost all retinaldehyde to RA conversion during early embryogenesis. A deficiency in RALDH2 affects the forebrain, hindbrain, heart, forelimbs and somites (Mic et al., 2002; Mic et al., 2004; Niederreither et al., 2001; Niederreither et al., 2000; Niederreither et al., 2002; Ribes et al., 2006; Sirbu and Duester, 2006; Vermot and Pourquie, 2005). Newly formed RA is bound by cellular retinoic acid binding proteins (CRABPs). All-trans RA will then bind to the in vivo RAR ligand, and the 9-cis RA to the RXR ligand (in vitro) (reviewed in (Niederreither and Dolle, 2008), Figure I-5).

In addition to controlling the level of RA via production through vitamin A metabolism, and the distribution of the retinoid receptors, the levels and spatiotemporal

distribution of this biologically active morphogen is also regulated by catabolism and RA feedback mechanisms.

Cytochrome P450 26B1 is also expressed in embryonic tissues at the sites of RA production and it catalyzes the conversion of retinol to retinaldehyde and RA (Chambers et al., 2007). When necessary, RA can be transformed to 4-hydoxy-RA for metabolism and elimination by cytochrome P450 26A1, B1, and C1 (Cyp26) enzymes. Just as the oxidation enzymes that convert vitamin A to RA are important, so are the enzymes that prevent excess RA by reducing RA back to retinol. Dehydrogenase/reductase superfamily member 3 (DHRS3) catalyzes the reduction of retinal to retinol, and when this reductase is absent in mice, *Dhrs3*$^{-/-}$ embryos exhibit excess retinal activity, leading to several developmental abnormalities, and late embryonic and perinatal lethality (Billings et al., 2013), indicating that reduction of retinal by DHRS3 is critical for maintaining the delicate balance of RA production. Collectively, the balance between retinoic acid synthesis and catabolism is critical to regulate the precise spatiotemporal domains of retinoid signaling during embryogenesis.

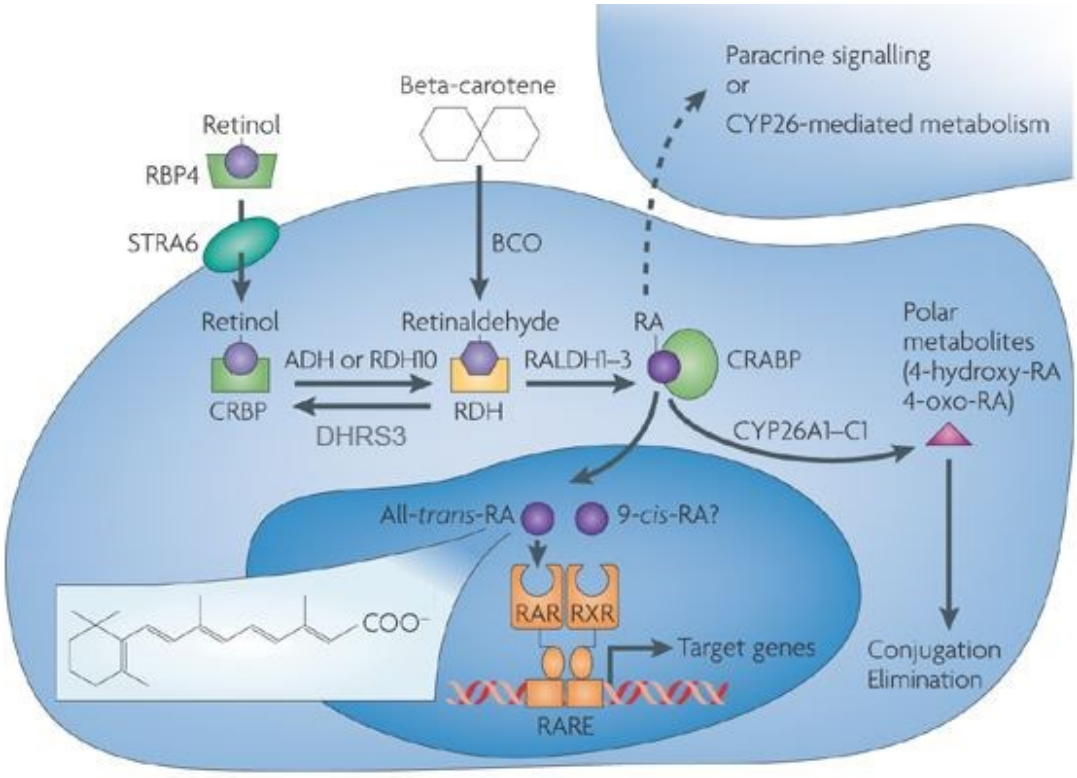

Figure I-5: Retinoid signaling and metabolism from retinol and beta-carotene, as well as catabolism via CYP26A1-C1 (Modified from Figure 1 from (Niederreither and Dolle, 2008)).

RETINOID DEFICIENT HSCR MOUSE MODELS

Currently, more than 50% of HSCR cases have an identified gene and mechanism of pathogenesis, but many affected individuals' mutations remain unaccounted for, leaving an important task to identify novel genes and pathways that may cause or potentiate HSCR. Recently, a role for retinoid signaling in ENS development and the pathogenesis of colonic aganglionosis has been suggested (Fu et al., 2010; Niederreither et al., 2003).

As evidenced by numerous mouse knock-out studies, RA is necessary in the development of various organ systems, such as the eye, brain, liver, kidneys, lungs,

spleen, heart, face, and limbs (reviewed in (Cunningham and Duester, 2015; Zile, 1998)), and now, the enteric nervous system of the gastrointestinal tract (Fu et al., 2010; Niederreither et al., 2003). Currently, there are two mouse models of depleted retinoid signaling that display evidence of colonic aganglionosis, *Rbp4* $^{-/-}$ and *Raldh2*$^{-/-}$ (Fu et al., 2010; Niederreither et al., 2003). However, these mouse models of depleted retinoid signaling rely on dietary modifications (vitamin A restriction or RA supplementation) to visualize and evaluate their ENS phenotypes.

The first study depicting the role for Vitamin A deficiency as a non-genetic risk factor for HSCR penetrance and severity was done in *Rbp4*$^{-/-}$ mice (Fu et al., 2010). *Rbp4*$^{-/-}$ mice are unable to store retinol in their livers. When subjected to a vitamin A deficient diet during embryogenesis (starting at E7.5), these mice become fully depleted of Vitamin A and its active form, RA, and exhibit distal bowel aganglionosis due to increased phosphatase and tensin homolog (Pten) accumulation-mediated slowed ENCC migration. The migrating ENCCs in *Rbp4*$^{-/-}$mice display a defect in maintaining lamellipodia formation, suggesting a requirement of RA in maintaining signals for ENCC migration.

The studies done in *Raldh2*$^{-/-}$ mouse model, also deficient in RA signaling, further suggest a role for RA in ENCC colonization of the gut. Although these mice typically die by E9.5, prior to ENS development, maternal RA supplementation between E7.5-E8.5 rescues the animals long enough to observe deficiency in vagal NCC and agenesis of the enteric ganglia (Niederreither et al., 2003). Compound *Raldh1*$^{-/-}$*; Raldh2*$^{+/-}$; *Raldh3*$^{+/-}$ mutant mice also demonstrate reduced myenteric and submucosal neuron density in adult mouse colons, suggesting that all three enzymes, RALDH 1, 2 and 3, contribute to ENS development (Wright-Jin et al., 2013).

Although these studies suggest a role for retinoid signaling in the pathogenesis of colonic aganglionosis, they require a dietary intervention to elucidate this, creating a somewhat artificial situation (Butler Tjaden and Trainor, 2013). The phenotype in *Rbp4*$^{-/-}$ mutants is only observed in response to a vitamin A deficient diet. Similarly, without providing RA rescue, *Raldh2*$^{-/-}$ mutants die before a colonic aganglionosis phenotype can be examined. These partially-rescued mice develop with a range of physical anomalies, so the precise role of RA remains to be completely characterized. Thus, additional experiments are necessary to reveal the true contribution of retinoic acid on gastrointestinal tract development. Furthermore, the effects of RA on NCC formation, migration proliferation and differentiation are not completely understood. A mouse model without the need for dietary control or partial RA rescue would be ideal to further investigate the role of RA in ENS development, as exogenous RA is known to cause developmental malformations (Quemelo et al., 2007). Human studies are also needed to complement these animal models. Collectively, this could validate the importance of retinoid signaling in the etiology and pathogenesis of HSCR.

II. METHODS

This chapter will describe mouse lines, experimental laboratory methodology, imaging techniques, as well as RNA sequencing and qPCR protocols.

Mouse Lines

Mice were housed in the Laboratory Animal Services Facility at the Stowers Institute for Medical Research according to IACUC animal welfare guidelines. Control mice described in experiments using *Rdh10*^{trex} were either wild-type or heterozygous littermates. Control mice described in experiments using *Rdh10*$^{flox/flox}$ x Cre lines were either *Rdh10*$^{fx/+}$ or *Rdh10*$^{flox/flox}$ littermates.

RDH10 MOUSE LINES

The hypomorphic *Rdh10*$^{trex/trex}$ mice were derived from an ENU screen and have previously been described in detail (Cunningham et al., 2011; Farjo et al., 2011; Sandell et al., 2011; Sandell et al., 2012; Sandell et al., 2007), and the allelic deletions of RDH10 (*Rdh10*$^{\beta geo}$, *Rdh10*$^{flox/flox}$ and *Rdh10*$^{\Delta/\Delta}$) were created using Rdh10_D08 embryonic stem cells from the Knockout Mouse Project (KOMP) consortium. The resulting KOMP mouse line (C57BL/6N-Rdh10$^{tm1a(KOMP)Wtsi}$) and derivative lines have been previously described (Sandell et al., 2012), but are also summarized here for convenience to the reader.

ENU Screen

Our lab conducted an unbiased three-generation forward genetic screen using *N*-ethyl-*N*-nitrosurea (ENU) in an effort to phenotypically identify early craniofacial mutants (Sandell et al., 2011). 8-12 week old male C57BL/6 mice were intraperitoneally injected once a week for three weeks with 100mg/kg of ENU (Sandell et al., 2011). ENU is a known alkylating agent that induces approximately 1 mutation every 800 base pairs

when given in this fractionated dose regimen (Justice et al., 2000). This mutagen specifically targets spermatogonial stem cells, where it induces point mutations. After 90 days, the injected male mice (G0) were bred to wild-type FVB/NJ female mice. The resultant heterozygous males generated from this cross are termed founder males (F1). These founder males (F1) were then outcrossed to FVB/NJ females to create Generation 2 (G2) animals. G2 females were then backcrossed to their fathers (F1) and embryos were examined at E9.5-10 for reproducible craniofacial defects. From the 50 founder males, 10 new recessive mouse mutant lines were generated.

Mapping the mutation to Rdh10

These lines were maintained by crossing to FVB/NJ, which allowed for chromosomal positional mapping of regions of the C57BL/6 genome that co-segregated with the mutant phenotype. Using a panel of 140 polymorphic microsatellite markers between C57BL/6 and FVB/NJ strains, ear biopsies of both parents as well as the yolk sac for each mutant (and control) were screened to determine the region of the C57BL/6 genome that was linked to the mutant phenotype. Once the phenotype was mapped to the single chromosomal location, the region was narrowed via single nucleotide polymorphisms (SNP), and candidate genes were sequenced to find the causative mutation (Sandell et al., 2011).

Of the 10 new mouse mutants created, one mutant displayed a small forelimb phenotype, and was named "*trex*," after the dinosaur *T. rex* (Sandell et al., 2011). This mutation mapped to the proximal portion of chromosome 1 using microsatellite markers. This region was narrowed using single nucleotide polymorphisms and subsequent candidate gene sequencing. SNP analysis and sequencing revealed a T to C pyrimidine transition at position 251 of the *retinol dehydrogenase 10* (*Rdh10*) gene, causing a cysteine to arginine substitution in the RDH10 protein (Figure II-1), leading to

destabilization of the protein (Figure II-2 A)(Sandell et al., 2007). The first four generations following the ENU mutagenesis screen are shown in Figure II-2 D.

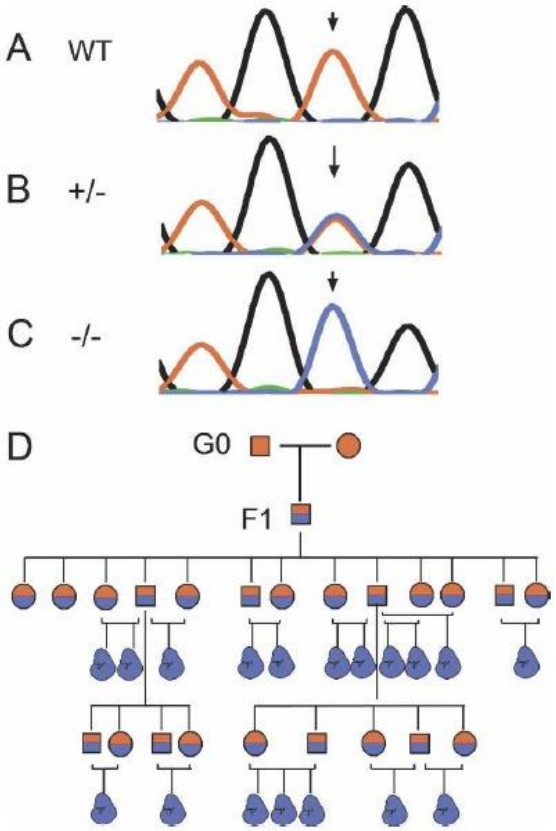

Figure II-1: Sequence electropherograms for wild-type, heterozygous and homozygous mutant *Rdh10*$^{trex/trex}$ animals. This sequencing revealed a T to C pyrimidine transition at position 251 of the *retinol dehydrogenase 10* (*Rdh10*) gene, causing a cysteine to arginine substitution in the RDH10 protein. (D) Pedigree for first four generations following ENU mutagenesis. Squares represent adult males, circles are adult females, blue embryo icons are mutant embryos, and red/blue split indicates heterozygous animals. Wild-type (A), heterozygous (B) and homozygous mutant *Rdh10*$^{trex/trex}$ animals (C). Figure 2 from (Sandell et al., 2007).

The RDH10 protein model revealed that the substituted amino acid in *Rdh10*$^{trex/trex}$ mutant is located in the core of the RDH10 protein, which would cause steric clashes and destabilize the protein structure (Figure II-2 A). Western blot analysis using wild-type and mutant RDH10 protein expressed in tissue culture suggest that mutant RDH10 is less stable than the wild-type version (Figure II-2 B). Furthermore, RDH10 enzymatic assays using wild-type and mutant RDH10 protein revealed that the mutated RDH10 has significantly less enzymatic activity than wild-type RDH10 (Figure II-2 C).

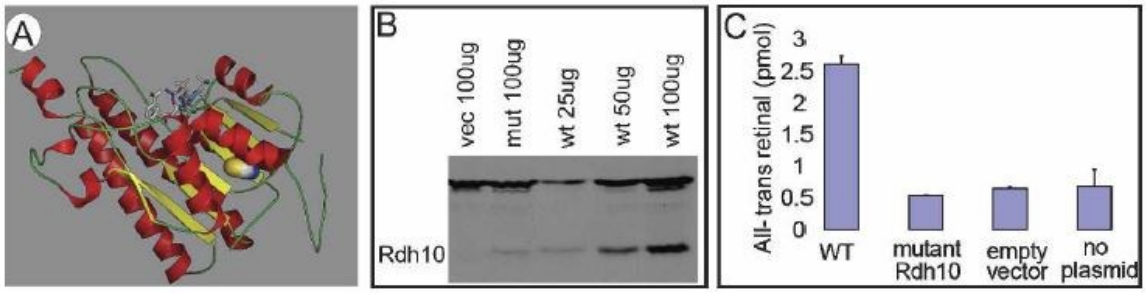

Figure II-2: Mutation in *Rdh10*$^{trex/trex}$ disrupts protein stability and function of RDH10 enzyme. (A) RDH10 protein model. The substituted amino acid in the *Rdh10*$^{trex/trex}$ mutant is located in the core of the RDH10 protein, which would cause steric clashes and destabilize the protein structure. (B) Western blot with wild-type and mutant RDH10 protein expressed in tissue culture. Results suggest that mutant RDH10 is less stable than the wild-type version (C) RDH10 enzymatic assays using wild-type and mutant RDH10 protein. Mutated RDH10 has significantly less enzymatic activity than wild-type RDH10. Figure 4A-C from (Sandell et al., 2007).

Phenotypic Description

Along with the obvious forelimb defect, which gives this mouse mutant its name, the *Rdh10*$^{trex/trex}$ mutant has other developmental malformations, which have previously been described (Figure II-3, Figure II-4) (Cunningham et al., 2011; Farjo et al., 2011; Sandell et al., 2011; Sandell et al., 2012; Sandell et al., 2007). In the craniofacial region, the *Rdh10*$^{trex/trex}$ mutant has an obvious orofacial cleft (Figure II-4: L), absent pharyngeal

arches 3-6 (Figure II-3 D), deformed eye (Figure II-4: J), and duplicated otic vesicles (Figure II-3 B). There is deficient arterial remodeling in the pharyngeal arches, as well as vasculogenesis anomalies (Sandell et al., 2011). Along with a reduced forelimb, this mutant also has a reduction in the cartilage condensations of the limb (Figure II-4: B; H; R). In addition, there are organ defects, such as hypoplastic lungs (Figure II-4: N) and liver (Figure II-4: P), as well as severe cardiac defects. The mutant *Rdh10*$^{trex/trex}$ heart fails to septate, and maintains a single outflow tract (Figure II-5). These mutants also exhibit peripheral nervous system defects, such as total colonic aganglionosis, which is described extensively in this manuscript. These embryos die during mid-gestation, around embryonic day E13.5 (Figure II-4: E, F), possibly due to severe cardiac hemorrhaging.

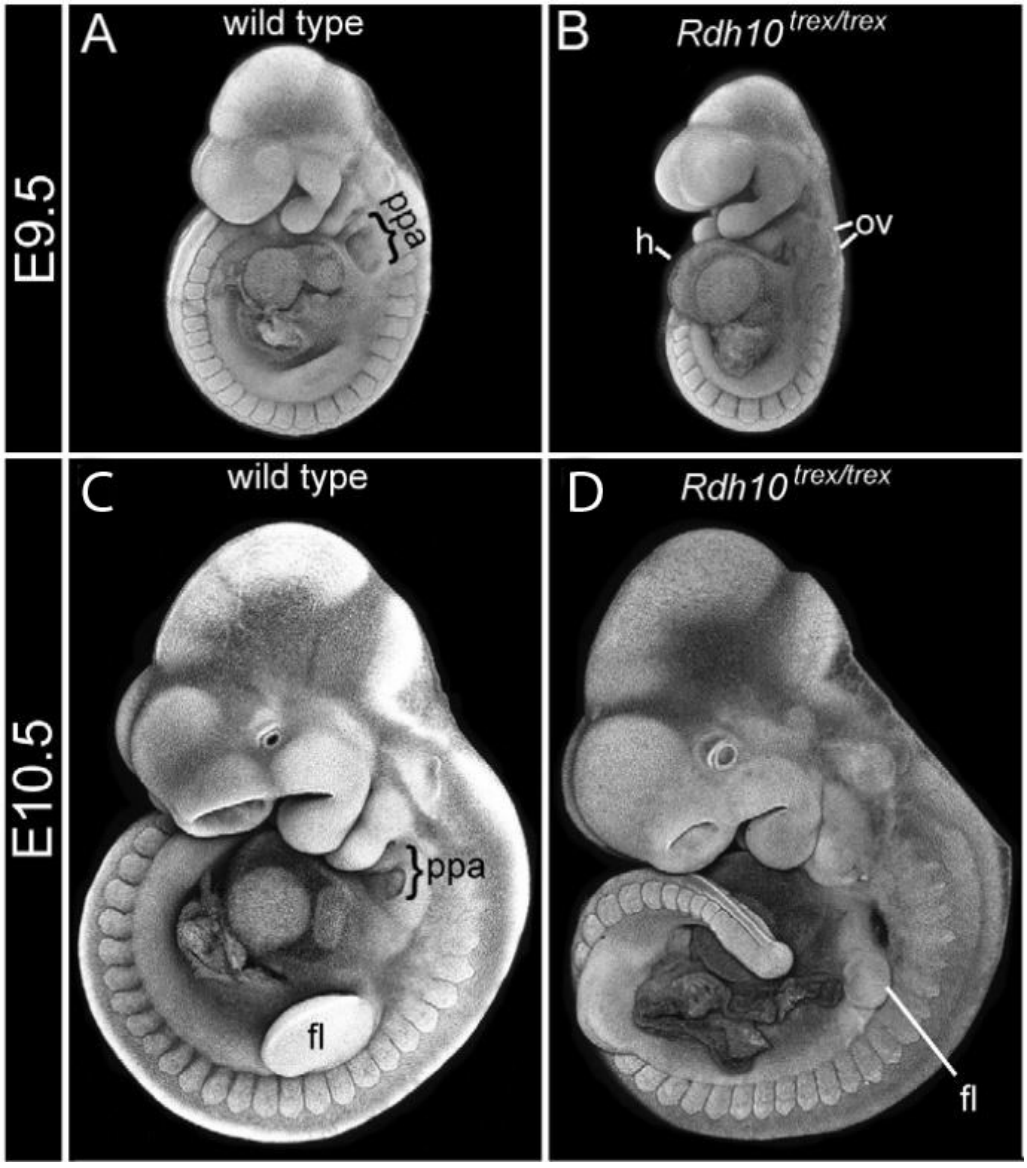

Figure II-3: E9.5 and E10.5 wild-type and mutant embryos. Wild-type (A,C) and mutant (B,D) embryos were stained with DAPI and confocal imaged as a Z-stack and processed into a maximum intensity projection. *Rdh10*$^{trex/trex}$ mutants display duplicated otic vesicles (B), and absent posterior pharyngeal arches 3-6 (D). Adapted from (Sandell et al., 2012).

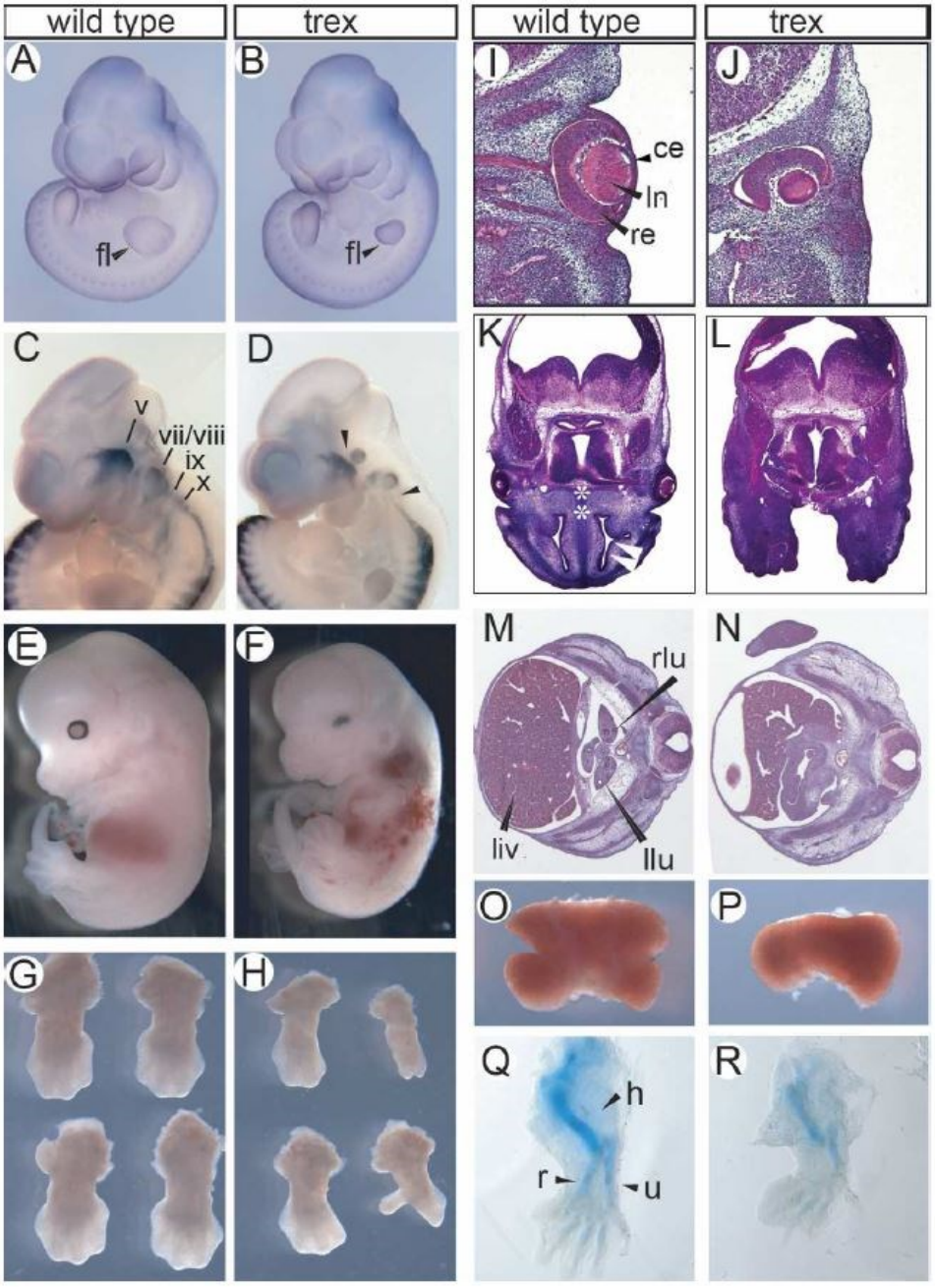

Figure II-4: E10.5 to E13.5 *RDH10*$^{trex/trex}$ embryos have numerous developmental defects.Mutant embryos display various physical deformities, including smaller forelimbs (A,B; G,H); reduced cranial ganglia (C,D); hemorrhaging just prior to mid-gestational lethality (E,F); eye malformations (I,J); orofacial clefting (K,L); reduced liver and lung sizes (M,N; O,P) and reduction of limb cartilage condensations (Q,R). Figure 1 from (Sandell et al., 2007).

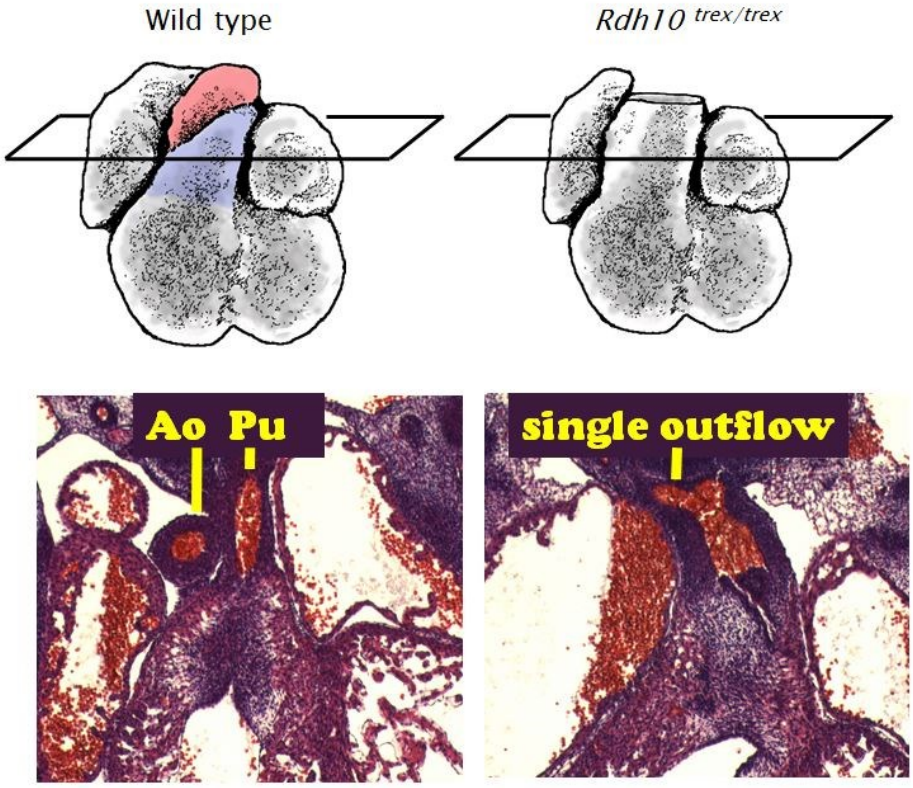

Figure II-5: Cardiac models of wild-type and mutant *Rdh10*$^{trex/trex}$ embryos. H & E section at the level of the outflow tract reveals an unseptated, single outflow tract in the *Rdh10*$^{trex/trex}$ heart. Image courtesy of Lisa Sandell, PhD.

Rdh10$^{\beta geo}$

A splice acceptor lacZ gene trap cassette (flanked by FRT sites) was knocked into the *Rdh10* gene between the first and second exons, creating the null allele *Rdh10*$^{\beta geo}$ mice (Figure II-6 B). Additionally, *Rdh10*$^{\beta geo}$ mice have loxP sites flanking the second exon. The gene trap insertion creates a *lacZ* fusion transcript that disrupts endogenous *Rdh10* transcript production. *Rdh10*$^{\beta geo}$ heterozygous animals appear similar to wild-type animals. When these heterozygous animals are stained for β-galactosidase activity, staining revealed the gene trap transcript in the same pattern as *Rdh10* RNA expression (Sandell et al., 2012). Homozygous *Rdh10*$^{\beta geo/\beta geo}$ animals are functionally null. When

Rdh10$^{\beta geo}$ mice are crossed to an FLP-recombinase line, the "β geo" gene trap is excised, leaving a phenotypically wild-type animal with a conditional allele (with the second exon of *Rdh10* flanked by loxP sites), termed *Rdh10*^{flox} (Figure II-6 C).

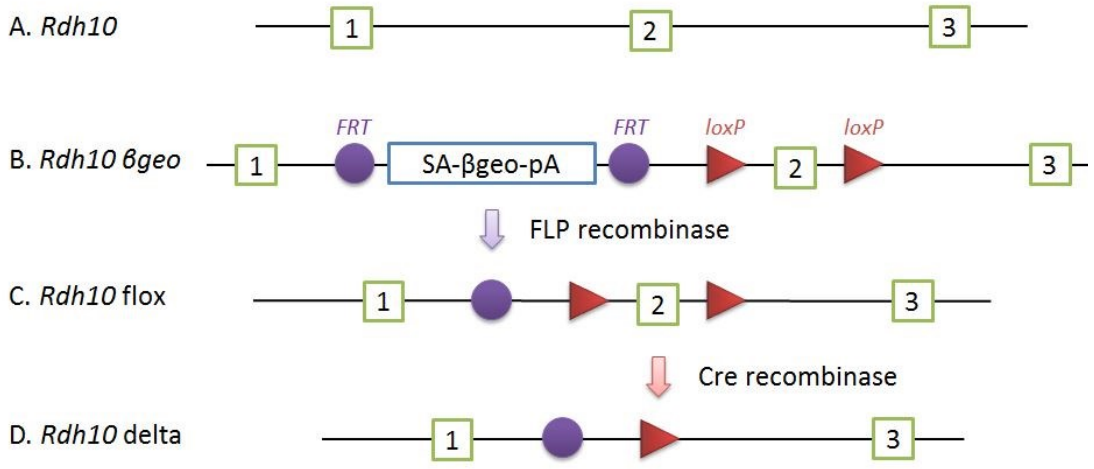

Figure II-6: Schematic map of Rdh10 allelic deletion animals. (A) Wild-type Rdh10 (B) *Rdh10*$^{\beta geo}$ has a splice acceptor lacZ gene trap cassette (flanked by FRT sites) knocked into the Rdh10 gene between the first and second exons. When crossed to a FLP recombinase, the "β geo" gene trap is excised, leaving a phenotypically wild-type animal with a conditional allele, termed *Rdh10*^{flox} (C). When *Rdh10*^{flox} is crossed to a Cre recombinase, the second exon is excised, creating *Rdh10*^{delta} mice, which have a premature stop codon, resulting in a null mutation. Adaption of Figure 2 from (Sandell et al., 2012).

Rdh10^{flox} *(Rdh10*^{fx}*)*

Rdh10^{flox} mice are a result of *Rdh10*$^{\beta geo}$ mice crossed to an FLP-recombinase line (in this case, FLPeR in the Rosa26 locus, official name: B6.129S4-*Gt(ROSA)26Sor*$^{tm1(FLP1)Dym}$/RainJ; Jax stock #009086), leaving the second exon of *Rdh10* flanked by loxP sites ("floxed"). This floxed exon is the conditional line (Figure II-6 C) (Sandell et al., 2012). This can then be crossed to various Cre recombinase lines to excise the second exon in specific tissues (Figure II-6 D), such as the oocyte specific

ZP3Cre (official name: C57BL/6-TgN(Zp3-Cre)93Knw; Jax stock #003651), neural crest cell specific *Wnt1Cre,* or the ubiquitous tamoxifen inducible $ER^{T2}Cre$ lines. Heterozygous and homozygous $Rdh10^{flox}$ mice are functionally wild-type.

***Rdh10*^{delta} (*Rdh10*$^{\Delta}$)**

$Rdh10^{delta}$ mice are produced by crossing $Rdh10^{flox/flox}$ mice to the oocyte specific *ZP3Cre*, which caused excision of exon 2, flanked by loxP sites (Figure II-6 D) (Sandell et al., 2012), resulting in a null stop codon mutation. Heterozygous $Rdh10^{delta/+}$ mice display a wild-type phenotype and homozygous $Rdh10^{delta/delta}$ mice are embryonic lethal at E10.5 and have a defects consistent with other severe retinoid deficiency models. Quantitative RT-PCR was used to determine the transcript levels of $Rdh10^{delta}$ mice. Mutant $Rdh10^{delta/delta}$ mice had only ~50% transcript level as compared to their wild-type littermates, suggesting nonsense mediated decay (Figure II-7) (Sandell et al., 2012).

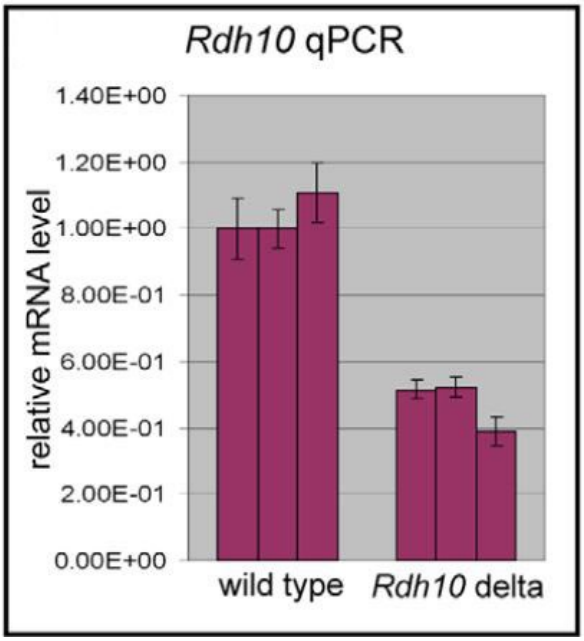

Figure II-7: Histogram showing relative levels of Rdh10 mRNA by qPCR analysis. Rdh10delta animals have significantly reduced mRNA levels. Figure 4F from (Sandell et al., 2012).

CRE RECOMBINASE LINES

Two Cre recombinase lines were used extensively to conditionally remove the second exon of *Rdh10*. *Wnt1Cre* is used in a tissue specific manner, by excising *Rdh10* from dorsal neural tube cells. *ER^{T2}Cre* is a tamoxifen-inducible Cre line used in a temporal manner removing RDH10 ubiquitously when tamoxifen is administered to pregnant dam.

Wnt1Cre

Wnt1Cre mice were obtained from the Jackson Laboratories (official name: Tg(Wnt1-cre)11Rth Tg(Wnt1-GAL4)11Rth/J; stock #003829). This transgene was created by inserting a Cre recombinase cDNA sequence in a polylinker site between the mouse *Wnt1* promotor and enhancer elements. When *Wnt1Cre* mice are crossed to floxed animals (ie *Rdh10^{flox}*), cre-mediated recombination results in the deletion of the floxed DNA sequence in a *Wnt1* pattern of expression, in the midbrain and neural tube, beginning at E8.5. *Rdh10$^{flox/flox}$; Wnt1Cre* embryos will have the second exon of Rdh10 excised from dorsal neural tube cells which encompass neural crest cell progenitors.

ER^{T2}Cre

ER^{T2}Cre mice were obtained from the Jackson Laboratories (official name: B6.129-*Gt(ROSA)26Sor$^{tm1(cre/ERT2)Tyj}$*/J; Jax stock #008463). This mouse line has a conditional Cre recombinase fused to the estrogen receptor T2 cassette inserted into the Rosa 26 locus (Ventura et al., 2007). Without tamoxifen available, the Cre-ER^{T2} fusion protein is retained in the cytoplasm bound to the heatshock protein 90 (HSP90). When tamoxifen is administered (in our case, by maternal oral gavage), the tamoxifen binds to the ER^{T2} domain, releasing the inhibition by HSP90, allowing the translocation of the Cre-ER^{T2} into the nucleus where it mediates recombination using *loxP* flanked DNA sites

(Figure II-8), such as in *Rdh10*^{flox} (Figure II-6 C), leading to excision of the floxed exon (Figure II-6 D).

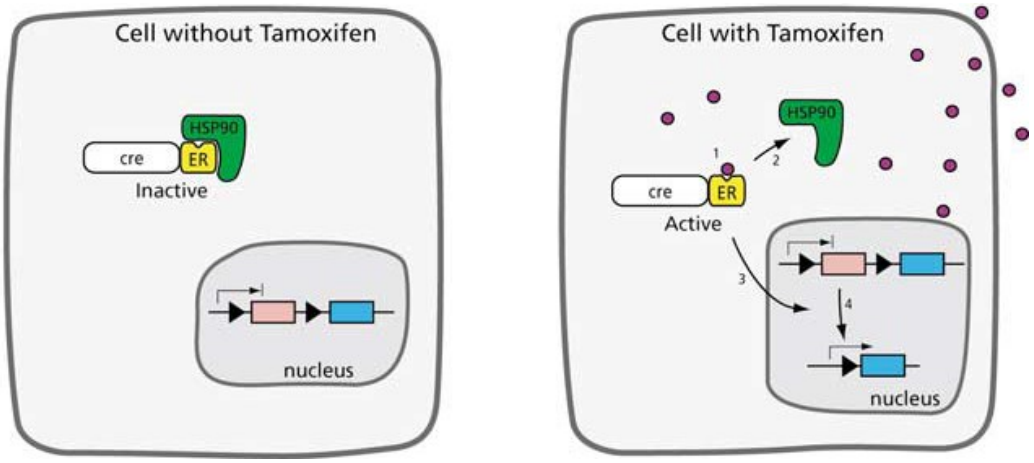

Figure II-8: Schematic of tamoxifen-inducible cre recombinase. In the absence of Tamoxifen, the Cre-ER^{T2} fusion protein is retained in the cytoplasm bound to the heatshock protein 90 (HSP90). When tamoxifen is administered, (1) the drug binds to the ER^{T2} domain, (2) releasing the inhibition by HSP90, (3) allowing the translocation of the Cre-ER^{T2} into the nucleus where it (4) mediates recombination using *loxP* flanked DNA sites. Figure 1 B from (Leone et al., 2003).

Previous studies using a similar tamoxifen-inducible cre-recombinase line (*EsrCre*, Official Name: B6.Cg-Tg(cre/Esr1)5Amc/J, Stock # 004682) have shown ~50% recombination after 24 hours and ~90% recombination after 48 hours, with similar levels of recombination when using between 2mg and 6mg of tamoxifen (Hayashi and McMahon, 2002). This study used intraperitoneal injection (IP) as a method of tamoxifen and progesterone delivery.

Using *EsrCre* as a guide, we have empirically determined an appropriate tamoxifen dosage of 5mg of tamoxifen and 1mg progesterone, and demonstrated efficient tamoxifen-induced Cre-recombination by crossing to a cre-responsive β-galactosidase reporter strain, Rosa R26R (Figure II-9). Unlike in the *EsrCre* model, IP injection of

tamoxifen did not result in reliable recombination in the *ER^{T2}Cre* line. Instead, we used maternal gavage with doses of tamoxifen dissolved in corn oil. In an effort to minimize fetal abortions in female mice, progesterone was co-administered.

ER^{T2}Cre mice were crossed to the *Rosa R26R* reporter line and pregnant mothers were treated with either 2.5mg Tamoxifen and 1mg Progesterone (Figure II-9 A,C) or 5mg Tamoxifen and 1mg Progesterone (Figure II-9 B,D). Mothers were gavaged at E8.5 and embryos were harvested at E11.5 to determine the appropriate dosage needed for full cre excision. This three day post-gavage period allows for sufficient recombination. *R26R; ER^{T2}Cre^{+}* embryos stain blue with β-galactosidase (Figure II-9 C,D). It is evident that 2.5mg of Tamoxifen gavage is not sufficient for total cre excision (Figure II-9 C), whereas 5mg of Tamoxifen is sufficient for total cre excision (Figure II-9 D).

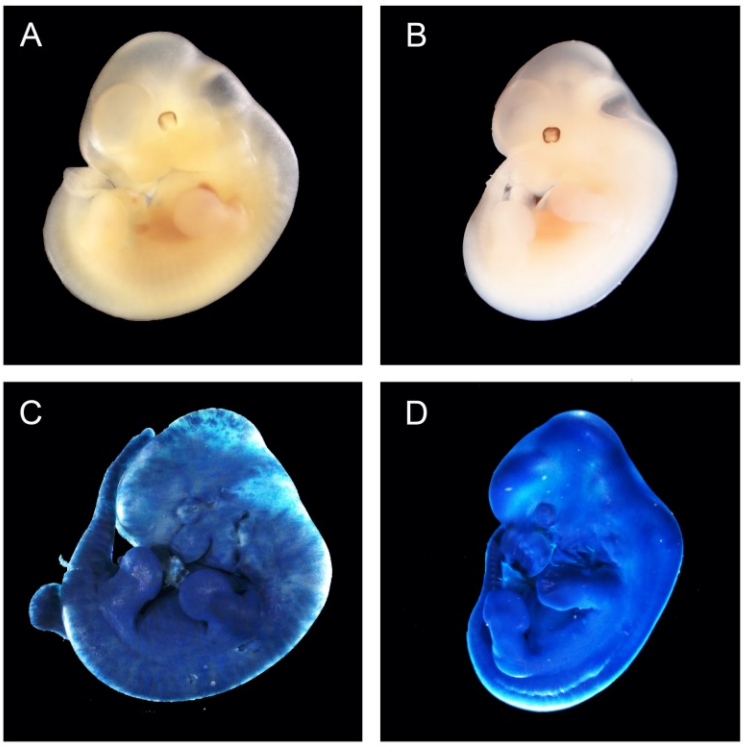

Figure II-9: *ER^{T2}Cre* mice were crossed to the *Rosa R26R* reporter line Pregnant mothers were treated with either 2.5mg Tamoxifen and 1mg Progesterone (A,C) or 5mg Tamoxifen and 1mg Progesterone (B,D) at E8.5 to determine the appropriate dosage needed for full cre excision. *R26R; ER^{T2}Cre^{+}* embryos stain blue with β galactosidase (C,D). It is evident that 2.5mg of Tamoxifen gavage is not sufficient for total cre excision (C), whereas 5mg of Tamoxifen is sufficient for total cre excision (D). Images A and C courtesy of Shachi Bhatt, PhD.

REPORTER LINES

Various reporter lines have been used for visualizing retinoid signaling (*RARElacZ*), cell lineage tracing (*RosaEYFP* and *Rosa R26R*), tamoxifen-inducible efficiency (*Rosa R26R*) and neural crest cell lineage tracing (*F10N*). These lines are detailed in this section.

RARElacZ

RARElacZ mice were a generous gift from J Rossant (Rossant et al., 1991) and are available through the Jackson Laboratory (Official name: Tg(Rare-Hspa1b/lacZ)12Jrt/J, Stock # 008477). In these mice, 3 copies of the RARE sequence lie upstream of the heat shock protein 1B (*Hspa1b*) promotor and the β galactosidase gene (Figure 1B in (Rossant et al., 1991)). This mouse line is used as a retinoid acid signaling reporter strain, and can be crossed to mutant mouse lines, such as $Rdh10^{trex}$, and stained with β galactosidase to visualize where retinoid signaling is present in these mutants.

RosaEYFP

RosaEYFP animals are used extensively in cell lineage tracing (Official name: B6.129X1-$Gt(ROSA)26Sor^{tm1(EYFP)Cos}$/J; Stock # 006148). These animals have a *loxP*-flanked STOP sequence followed by the Enhanced Yellow Fluorescent Protein gene (EYFP) inserted into the *Gt(ROSA)26Sor* locus. When these mice are crossed to mice expressing a Cre recombinase, the STOP sequence is removed and EYFP expression is observed in the *cre*-expressing tissues of interest. This reporter line was particularly useful in the studies in this thesis for neural crest cell lineage tracing experiments when crossed to *Wnt1Cre* animals.

Rosa R26R

Rosa R26R animals (Official name: FVB.129S4(B6)-$Gt(ROSA)26Sor^{tm1Sor}$/J; Jax stock #009427) are useful as a cre-reporter strain when stained with β-galactosidase. It can be used both for testing tissue expression patterns as well as for testing the efficiency of the drug inducible cre lines, such as $ER^{T2}Cre$. Similar to RosaEFYP animals, when Rosa R26R mice are crossed to a cre recombinase line, the STOP sequence is deleted and *lacZ* is expressed in the *cre*-expressing tissues of interest and their derivatives (Friedrich and Soriano, 1991; Soriano, 1999).

***Mef2c-F10N*, referred to as "*F10N*"**

Our lab has created a new transgenic mouse line in which the *F10N* enhancer of the *Mef2c* gene was fused to *lacZ*. A full description of the *F10N* (*Mef2c-F10N-lacZ*) has been described (Aoto et al., 2015). The *F10N* line expresses β galactosidase in all migrating NCC that have delaminated from the neural tube, and maintains expression in subsequent NCC derivatives. Early in development, this line has a very similar expression pattern to *Wnt1Cre;R26R* mice (Figure II-10).

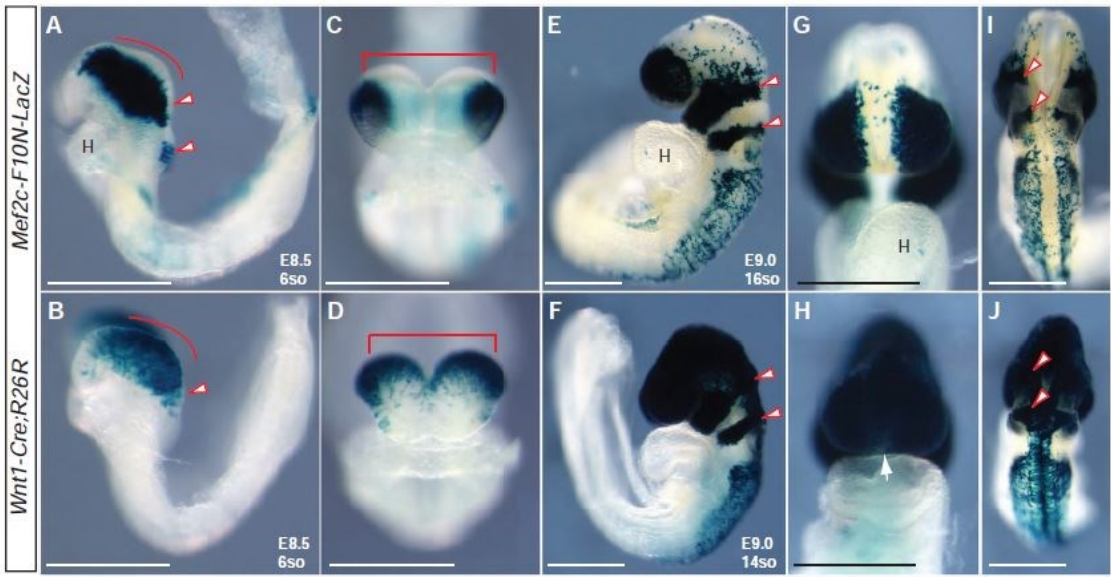

Figure II-10: Comparison of *F10N* and *Wnt1Cre;R26R* expression from E8.5 to E9.0. Figure 5 of (Aoto et al., 2015).

Analyses of *Mef2c* cis regulatory elements in transient transgenic animals by the Black laboratory have revealed the *F10N* enhancer element transiently marked migrating NCC in E9.5 embryos (De Val et al., 2008). The *Mef2c-F10N* plasmid provided by Brian Black, PhD was cloned into the *Hsp68-LacZ* reporter plasmid to create the *Mef2c-F10N-lacZ* plasmid (Figure II-11 A), which was then injected into the pronucleus of CBA: B10 F1 hybrid embryos to create stable transgenic lines. Expression of this plasmid is

examined via *lacZ* staining of whole and sectioned embryos at various stages (Figure II-11 B-M).

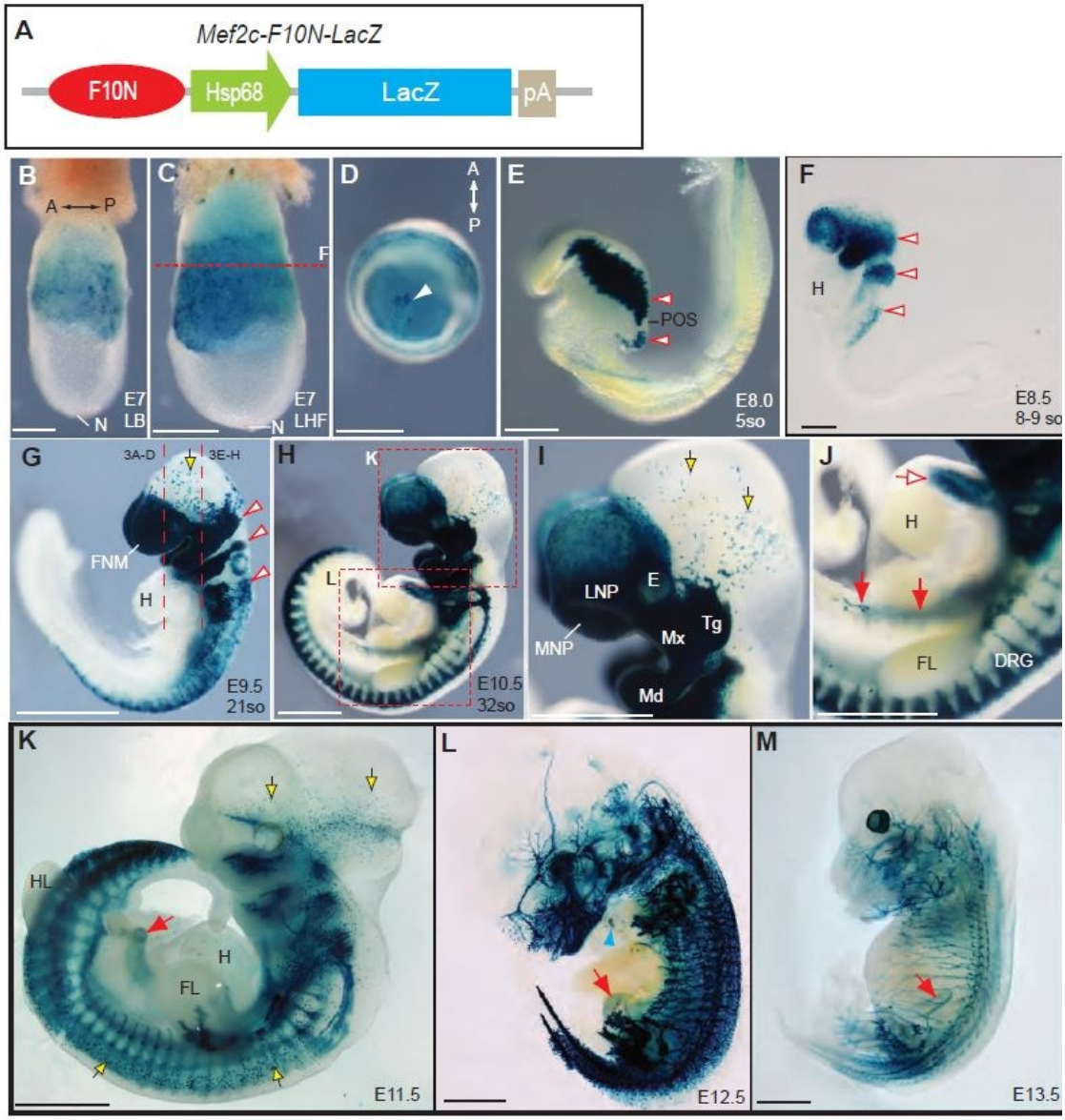

Figure II-11: *Mef2c-F10N-lacZ* plasmid construct and expression from E7 to E13.5. This construct was injected into the pronucleus of CBA: B10 F1 hybrid embryos to create a stable transgenic line. (B-M) *lacZ* expression from E7 to E13.5. (K-M) Embryos from E11.5-E13.5 have been cleared using Sca*l*eA2. Adapted from Figure 1 of (Aoto et al., 2015).

Of particular interest for this project, *F10N* mice express β-galactosidase in gut neurons and glia (Figure II-12). This can been seen with triple stained immunohistochemistry for β-galactosidase which co-localizes in the enteric nervous system with differentiated neuronal marker Tuj1, and autonomic neuronal marker Phox2B, which mark the enteric nervous system neurons (Figure II-12 A, B). Additionally, β galactosidase co-localizes in the enteric nervous system glial markers SOX10 and neurofilament (NF) (Figure II-12 C, D).

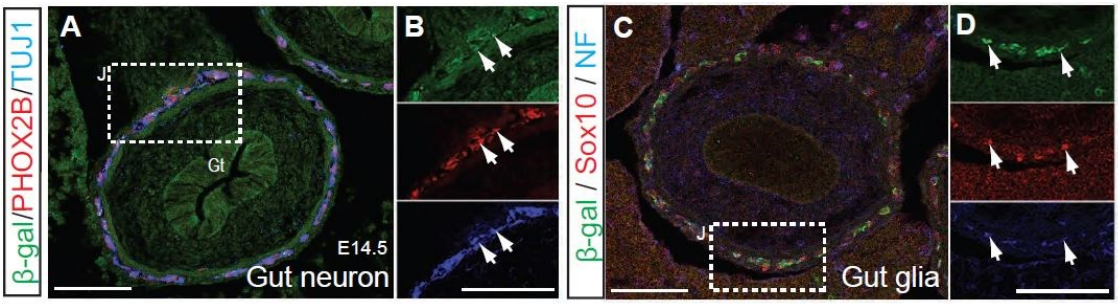

Figure II-12: *F10N* mice express β galactosidase in gut neurons and glia. (A, B) β galactosidase co-localizes in the enteric nervous system with differentiated neuronal marker Tuj1, autonomic neuronal marker Phox2B, as well as (C,D) the glial marker SOX10 and neurofilament (NF). Figure Adapted from Figure 10 I-L of (Aoto et al., 2015).

The plasmid used to create this new *F10N* line has also been adapted into a *Mef2c-F10N-Cre* line for *cre*-mediated excision of neural crest cells (Aoto et al., 2015).

Gut Organ Culture

E11.5 embryos were dissected from the uterus and placed on ice cold PBS. The gut (esophagus, stomach, small and large intestines with accompanying mesentery) were dissected in clean PBS and placed in L15 Leibowitz medium (Sigma). The gut was then transferred to a Millicell 0.4μm cell culture insert (Millipore) in a 6-well tissue culture dish (Millipore). The L15 medium was replaced with 400μL OptiMEM (Invitrogen) with 1mM L-Glutamine (Life Technologies Glutamax) and Penicillin/Streptomycin

(Invitrogen). The explants were cultured in a 37°C incubator with 5% CO_2 and media was changed every 2 days. This protocol was adapted from (Natarajan et al., 1999). For retinoid-supplemented cultures, guts were prepared as described above, and 1μM all-trans-retinoic acid (Sigma R2625) or 1μM all-trans-retinal (Sigma R2500) was added to the culture media (a 10^{-6} M concentration of RA produces morphological changes in 50% of cultured guts (Pitera et al., 2001)).

Whole gut immunohistochemistry

Embryos (E11.5, 15.5, 18.5) were dissected from the uterus and placed in ice cold PBS. Whole embryonic guts (E11.5 cultured, E11.5, E15.5 and E18.5) were fixed in 4% paraformaldehyde in PBS (PFA) overnight at 4°C. Guts were washed 3 x 5 minutes in PBS with 0.1% TritonX100 (PBT) at room temperature. Blocking and antibody hybridization was performed in 10% heat-inactivated lamb serum in PBT. Non-specific antibody binding was blocked by 20 minute incubation with blocking solution, and primary antibody was applied overnight at 4°C in the same solution. Guts were then washed 5 x 1 hour in PBT at room temperature. Secondary antibody hybridization was performed in blocking solution overnight at 4°C. Secondary antibody was removed by 3 x 20 minute washes in PBT at room temperature. TUNEL staining was performed as follows: guts were incubated at a slant with nutation for 2 hours at 37°C in 100μL TUNEL reaction (*in situ* Cell Death Detection Kit) (Roche), and then washed 2 x 30 minutes in PBT at room temperature. Guts were then stained with DAPI dilactate, 10 μg/ml in PBT, 10 minutes or longer at room temperature. Specimens were then placed into Vectashield with DAPI (Vector Laboratories) for storage and imaging.

In situ hybridization

Embryos (E8.5, 9.5, 10.5, 11.5) were dissected from the uterus and placed in ice cold DEPC-PBS. They were then fixed in 4% paraformaldehyde (PFA) in phosphate buffered solution (PBS) overnight at 4ºC. Embryos were washed 3 x 5 minutes in DEPC-PBS-1% Tween (PBS-Tw), and then treated with 10μg/mL Proteinase K in PBS-Tw without shaking. Proteinase K treatment time varied based on the age of the embryos.

Embryos were washed 5 minutes in 2mg/mL glycine in PBS-Tw, and then washed 2 x 5 minutes in PBS-Tw. Embryos were re-fixed in 4% paraformaldehyde/0.2% glutaraldehyde solution in PBS for 20 minutes. Embryos were washed 3 x 5 minutes in PBS-Tw and rinsed in 65°C pre-warmed hybridization solution (for hybridization solution, MABT and NTMT recipes, see (Nagy A, 2003)), then placed in fresh pre-warmed hybridization solution for 2 hours at 65°C. Probe was added to fresh hybridization solution and placed on the embryos at 65°C overnight. Embryos were washed in pre-warmed hybridization solution 2 x 30 minutes, then 3 x 30 minutes at 65°C with Formamide Wash Solution (50% formamide, 1xSSC, pH4.5, 0.1% Tween). Next, embryos were washed 30 minutes in a 1:1 formamide wash solution: MABT, then 3 x 5 minutes MABT. Embryos were blocked in MABT + 2% *Boehringer Blocking Reagent* (BBR) for 1 hour at room temperature, then an additional 1-2 hours in MABT + 2% BBR +20% heat-treated goat serum. Embryos were incubated overnight at 4°C in 1:1000 anti-DIG in MABT + 2% BBR + 20% heat-treated goat serum. Embryos were rinsed, and then washed 2 x 15 minutes in MABT, then 5-7 x 1.5 hour in MABT, followed by an overnight RT MABT wash. For antibody detection, embryos were washed 3 x 10 minutes in NTMT, then incubated in the dark in NBT/BCIP reaction mix (3.375 µl/mL of 100mg/mL NBT and 3.5µL/mL of 50mg/mL BCIP per 1mL reaction mix) until the reaction was deemed complete. Finally, embryos were washed with PBS-Tw and fixed with 4% PFA/0.1% glutaraldehyde.

Whole mount immunohistochemistry

E11.5 embryos were dissected from the uterus and placed in ice cold PBS. Embryos were fixed in 4% PFA overnight at 4°C, then washed in PBS and transferred through a graded series into 100% methanol. Tissues and embryos to be immunostained were permeabilized in Dent's bleach (MeOH:DMSO:30%H_2O_2, 4:1:1) for 2 hours at room temperature, then washed with 100% methanol and transferred (through a graded series) into PBS. Blocking and antibody hybridization was performed in 0.1M Tris pH7.5/0.15M NaCl buffer. Non-specific antibody binding was blocked by two hour

incubation in Tris/NaCl buffer with 3% Bovine Serum Albumen with gentle rocking. Primary antibody hybridization was performed in same blocking buffer overnight at 4°C. Following primary antibody hybridization specimens were washed 5 x 1 hour in PBS at room temperature. Secondary antibody hybridization was performed in blocking buffer overnight at 4°C. Secondary antibody was removed by 3 X 20 minutes washes in PBS at room temperature. Specimens were stained with DAPI dilactate, 10 µg/ml in PBS, 10 minutes or longer at room temperature or overnight at 4°C. Prior to imaging, immunostained specimens were cleared with Scale*A*2 for at least 5 days (Hama et al., 2011), or *Clear*^{T2} for at least 2 days (Kuwajima et al., 2013). Glass imaging wells were prepared by coating a Teflon O-ring with vacuum grease and affixing the ring to a glass depression slide. Scale*A*2 or *Clear*^{T2} cleared specimens were placed into the well and the well filled with Scale*A*2 or *Clear*^{T2}. A coverslip was then adhered to the vacuum grease coated O-ring.

PRIMARY ANTIBODIES

βIII neuronal tubulin antibody (TUJ1), 1/1000, (MMS-435P or MRB-435P, Covance); GFP antibody, 1/500, (A6455 Invitrogen/Molecular Probes); p75 antibody, 1/300, (G323a Promega).

SECONDARY ANTIBODIES

Alexa Fluor 488, 1/500, (A21206 Invitrogen/Molecular Probes); Alexa Fluor 546, 1/500, (A11030 Invitrogen/Molecular Probes).

β-galactosidase staining

Rdh10^{trex} mice were mated to *F10N* or *RARElacZ* (Rossant et al., 1991) mice and embryos/embryonic tissues were collected at E9.5, 10.5, 11.5 and 12.5. Embryos were fixed with 2% Paraformaldehyde + 0.25% Glutaraldehyde, and then stained using the β-galactosidase staining solution kit (Chemicon/Millipore) according to manufacturer's instructions.

Mouse Gavage Administration

RETINAL GAVAGE

For retinal supplementation experiments, pregnant mothers were gavaged with 312.5µg of all-trans-retinal (Sigma R2500) in 100µL corn oil (3.125mg/mL) on mornings and/or nights of E6.5, E7.5, 8.5, 9.5, 10.5 and/or 11.5 (Farjo et al., 2011).

TAMOXIFEN AND PROGESTERONE GAVAGE

5 mg of tamoxifen (Sigma T5648) was administered via maternal gavage at varying embryonic days (E) in 100µL corn oil (50mg/mL). To prevent pregnancy loss, 1mg of progesterone (Sigma P3972) was also co-administered via 100µL corn oil gavage (10mg/mL). To dissolve tamoxifen, 500mg of tamoxifen was initially dissolved in 1mL of ethanol, and 9mL of corn oil was added and warmed to 37^{o}C until all tamoxifen went into solution (approximately 8 hours).

Imaging

CONFOCAL IMAGING

Confocal images were captured on an upright Zeiss LSM510 or LSM700 Pascal equipped with a 405 nm laser. For each specimen, a z-stack of images was collected and processed as a maximum intensity projection.

BRIGHT FIELD IMAGING

Stacks of light microscope images were taken on a Leica MZ9.5 stereomicroscope and assembled in Helicon Focus.

ZEISS SLIDE SCANNER IMAGING

6µm sections of *Rdh10*$^{trex/trex}$ and control embryos were stained with Hematoxylin and Eosin (H&E) and 10µm sections of *Rdh10*$^{trex/trex}$*; F10N* and control embryos were stained with LacZ and Eosin. These sections of control and mutant embryos were placed

on glass slides and were scanned at 20x in a Zeiss Axio Scan.Z1 slide scanner. Images were detected using the "tissue detection wizard" and optimized for each batch of slides.

qPCR

500 ng of mouse RNA harvested from the otic vesicle to the seventh somite region of E9.5 embryos was used as a template in 40µl total volume reaction of Superscript III (Life Technologies) reverse transcription kit utilizing random hexamer primers. The 40ul reaction was diluted 10 times and 2µl of cDNA was used in 10ul total qPCR reactions prepared with PerfeCTa SYBR Green FastMix, ROX (Quanta Biosciences) and cycled on an ABI 7900HT according to Quanta Biosciences standard protocol. Analysis of the fluorescence curves was done using Life Technologies SDS2.4 software. All curves that showed errors as determined by the SDS2.4 software or that were above 35 Ct were thrown out. The remaining Ct values were exported and analyzed using the Biogazelle qBase plus version 2.4. Three appropriate endogenous controls (M-value < .5) for each sample set were selected from a panel of five primer sets using geNorm in qBase plus. All primer sets (Table II-1) used were experimentally determined to be within 10% of ideal efficiency. Individual gene results are graphed with standard error bars, and relative expression (of all genes) results are graphed with 95% confidence intervals.

Table II-1: qPCR primers

Target	Primer Sequence	Product Size (bp)
Gapdh	F – TGGCCAAGGTCATCCATGA R – CAGTCTTCTGGGTGGCAGTGA	84
Canx	F – CCAGACCCTGATGCAGAGAAG R – CCTCCCATTCTCCGTCCATA	61
Atp5b	F – TTGACAACATCTTCCGCTTTACC R – AAGGGATTCTGCCCAATAAGG	66
Gdnf	F – CTAAAGGAAAGGGTCAGGAG R – TTGCTGCTCAGATGGATAG	106
Ret	F – GCACAATTACAAGCTGATTCT R – GAAATGGAGGACGAGGATAC	130
Gfrα1	F – GACTCCTGCAAGACAAATTAC R – ACTGTGCCAATCAGTCC	146
Col1a1	F – CTAGACATGTTCAGCTTTGTG R – GACTTCAGGGATGTCTTCTT	93
Col1a2	F – CTGGACCAATGGGTTTAATG R – AGCAGGTCCTTGGAAAC	83
Lamc3	F – TCCTACCTCACAGACTTCC R – ATCTCATAGGCCTTCCCTAA	125
Gata3	F – CGATCCAGCACAGAAGG R – GGCATTGCAAAGGTAGTG	96
TnC	F – CAGGGTTGCCACCTATTT R – CTAGAGGATCCCACTCTACTT	89
Fn1	F – TGTACCTCCAGAAACAGATG R – TTTCCTCGGTTGTCCTTC	89

RNA Sequencing

Two rounds of RNA Sequencing were performed on *Rdh10*^{trex} embryos at E9.5. In RNA Seq1, we used a portion of the embryo from below the otic vesicle to the base of the tail (Figure II-13 A). In the RNA Seq2, we used a portion of the embryo from just posterior to the otic vesicle to the seventh somite, and removed the heart (Figure II-13 B).

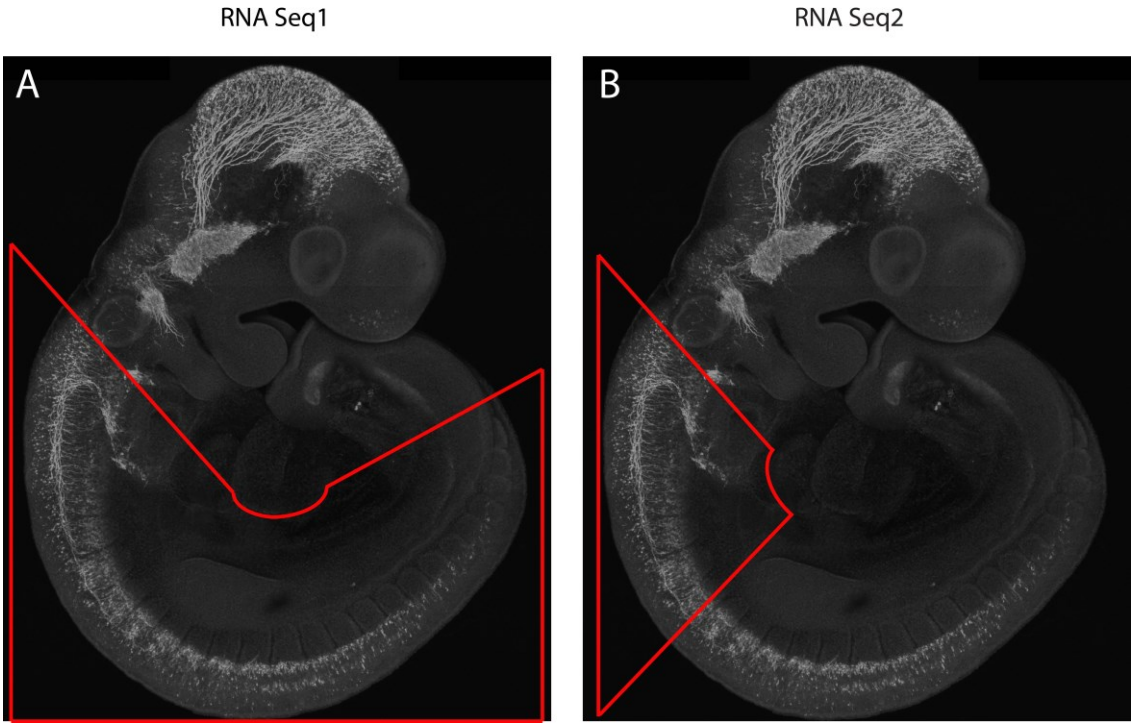

Figure II-13: Portion of E9.5 embryo used for RNA Sequencing experiments. Tissue portion used for RNA Seq is outlined in red on this black and white Tuj1 pseudo-SEM embryo. (A) RNA Seq1 included posterior to the otic vesicle to the base of the tail. (B) RNA Seq2 included posterior to the otic vesicle to the 7th somite, just anterior to the forelimb bud.

Total RNA was extracted using a Qiagen RNEasy kit according to the manufacturer's protocol. Samples were run on the Agilent 2100 BioAnalyzer and subsequently used to create polyA strand-specific libraries. Samples were sequenced on

the Illumina HiSeq 2500 platform. Sequences for each RNA sample were aligned using TopHat (v2.0.10). The reference genome and annotation files used for the alignment were from the UCSC mm10 genome and the ensembl build 73 for RNA Seq1 and ensembl 77 for RNA Seq2. Gene expression levels for genes were calculated using R and Bioconductor. TopHat aligned reads were tabulated using the GenomicFeatures library, and differential expression was assessed using edgeR (Robinson et al., 2010). RNA sequencing analysis was performed by Chris Seidel, PhD.

RNA Seq1 analysis was performed on a single time point of tissue taken from the torso of mouse embryos at developmental time E9.5. The experiment was performed in triplicate on 3 mutants and 3 wild-type littermates. Data was collected by counting read mappings to 39017 genes. However after filtering for genes with a sum total of at least 1 count per million (cpm) across all six samples, the final analyzed data set contains 19205 genes.

RNA Seq2 analysis was performed on a single time point of tissue taken from the area of the first seven somites of mouse embryos at developmental time E9.5. The experiment was performed in triplicate on 4 mutant and 4 wild-type littermates. Data was collected by counting read mappings to 39017 genes. However after filtering for genes with a sum total of at least 1 count per million (cpm) across all eight samples, the final analyzed data set contains 22674 genes.

III. HYPOTHESIS AND SPECIFIC AIMS

The overall project hypothesis and specific aims have previously been proposed in the National Institutes of Health (NIH) Ruth L. Kirschstein National Research Service Award (NRSA) Individual Predoctoral MD/PhD fellowship (Parent F30). The revised application F30DK096842-01A1 was successfully funded. The proposed studies investigate the role of vitamin A metabolism in NCC and GI tract development using new animal models of retinoid deficiency.

HYPOTHESIS

RDH10 has a significant impact on RA synthesis and is necessary for organogenesis, specifically via a role in NCC proliferation, differentiation or migration during formation of the enteric nervous system (ENS).

SPECIFIC AIMS

The proposed study investigates the role of vitamin A metabolism on neural crest cells (NCC) and gastrointestinal (GI) tract development using new mouse models of retinoid deficiency. Understanding the mechanisms that govern NCC formation, migration and differentiation is important for understanding the etiology and pathogenesis of neurocristopathies such as Hirschsprung disease (HSCR), which arise as a consequence of defects in NCC development. We identify RDH10 as a novel regulator of vitamin A metabolism and embryonic RA synthesis, and note digestive system defects in our RA deficient mouse line, $Rdh10^{trex/trex}$, similar to those seen in human cases of total intestinal aganglionosis. RA is an important signaling molecule, crucial for patterning, morphogenesis and organogenesis during embryonic development. Our newly generated tamoxifen inducible RDH10 conditional knock out allele, $Rdh10^{flox/flox};ER^{T2}Cre$, allows for selective temporal disruption of RA signaling.

As evidenced with previous retinoid deficient mouse models, the effects of RA, and specifically RDH10, on NCC formation, migration proliferation and differentiation have not been well understood, and until now, we have not had the necessary mouse models to investigate spatially and temporally the precise cellular and molecular mechanisms of RDH10 and RA during ENS development without any dietary modification. Because vitamin A deficiency is so widespread throughout the world, and metabolism of this nutrient results in an important developmental morphogen, it is important to continue to understand when RA is spatiotemporally required, and how it may contribute to the etiology and pathogenesis of disease such as HSCR.

The following studies address the effects of retinoid deficiency on gut and ENS development, as well as investigate the cause and potential rescue of the HSCR phenotype in mutant *Rdh10* embryos. To further understand mechanisms by which RA directs ENS development, we have examined the following specific aims.

Aim 1: Retinoic acid signaling is spatiotemporally required for proper ENS formation and gut development

Although there have been a few studies examining the role of retinoids on ENS development, there has not yet been an in-depth spatiotemporal examination of the role of vitamin A metabolism (specifically the contribution of RDH10) in the formation and development of the enteric nervous system (ENS) and GI tract.

The phenotypes observed in $Rdh10^{trex/trex}$ mice together with mid-gestational lethality of these mutants, reiterate the importance of RA signaling during embryonic development. It is therefore critical to understand the temporal and spatial dynamics of this small signaling molecule. The goal of this aim is to elucidate the spatiotemporal requirements of retinoic acid signaling for appropriate NCC colonization of the ENS to occur. This is relevant as nutritional anomalies can occur prior to and during pregnancy,

hence it is extremely beneficial to understand when and in what cells RA signaling is required, for formation of ENS during embryogenesis.

Using the *RARElacZ* reporter line, gut cultures supplemented with retinoids, *in utero* retinal gavage supplementation experiments in pregnant $Rdh10^{trex/+}$ females, and a tamoxifen inducible $Rdh10^{flox/flox};ER^{T2}Cre$ mouse line, we have defined the precise temporal requirements for retinoid signaling for proper NCC colonization of the gut and complete ENS formation. Supplementing pregnant mothers with retinal during specific gestational time points allows us to determine the range of development in which retinoic acid is crucial to forming a complete ENS. The tamoxifen inducible RDH10 conditional knock out confirmed both the RA temporal requirement range, as well as provided a clean genetic model for retinoic activity disruption.

Using an RDH10 NCC-specific knockout line, $Rdh10^{flox/flox};Wnt1Cre$, we were able to determine if RDH10 is intrinsically required in ENCCs or if RDH10 plays a more important role in maintaining a permissive microenvironment. Additional experiments examining cell death in the RDH10 expressing mesenchyme surrounding the foregut have provided further support for this spatial requirement of RDH10.

These results clarify the spatiotemporal importance of RA signaling throughout embryonic development as well as in the pathogenesis of HSCR, and have acted as a springboard for research into understanding the cellular and molecular mechanisms responsible for the HSCR phenotype in the $Rdh10^{trex/trex}$ mutant embryos.

Aim 2: RDH10 is required for migration and entry of vagal neural crest cells into the foregut during enteric nervous system and gastrointestinal development.

Previous experiments have shown that normal gut colonization relies on a combination of survival, proliferation, migration and differentiation of the NCC population (Amiel et al., 2008; Anderson et al., 2006a; Bogni et al., 2008; Heanue and

Pachnis, 2007). To understand the pathogenesis of HSCR and design novel treatment options for such neurocristopathies, it is necessary to first understand the cellular and molecular mechanisms that govern normal NCC formation, migration and differentiation during ENS formation in the gut.

We have investigated the cellular and molecular mechanisms underlying defective ENS development in *Rdh10*$^{trex/trex}$ mutants, including interactions with known genes that contribute to overall ENCC development, by investigating genes known to play important roles in NCC migration, proliferation, differentiation and survival during ENS development. Specifically, we examined the genes that when mutated, cause a devastating total intestinal aganglionosis phenotype, similar to *Rdh10*$^{trex/trex}$ mutants, such as *Ret* (Eng, 1999; Natarajan et al., 2002; Uesaka et al., 2008), *Gdnf* (Gianino et al., 2003; Young et al., 2001), *Gfrα1* (Nishiyama et al., 2012; Tansey et al., 2000), *Ednrb* (Barlow et al., 2003), *Edn3* (Bondurand et al., 2006; Nagy and Goldstein, 2006; Wu et al., 1999), *Phox2b* (Corpening et al., 2008; Pattyn et al., 1999), *Pax3* (Lang et al., 2000), and *Sox10* (Bondurand et al., 2006; Kelsh, 2006). Analysis of expression of these markers will allow us to further investigate potential RA signaling pathway interactions that are critical for NCC migration and colonization of the gut.

Additionally, in an effort to identify novel genes and potential pathways that may be regulated by RDH10, we have employed RNA-sequencing to determine transcriptome differences between *Rdh10*$^{trex/trex}$ mutants and control littermates at E9.5. Consequently, we have identified numerous genes that are up- and downregulated in *Rdh10*$^{trex/trex}$ embryos that may mediate the effects of deficient RA signaling.

CONCLUDING STATEMENTS

In summary, these studies offer a new model for investigating the role of vitamin A and its active form, retinoic acid, in the ENS development. This work provides

information regarding the spatiotemporal requirements for RA during embryonic intestinal development, pathogenic cellular mechanisms of RDH10 deficient animals, as well as the interactions of RA with pathways that regulate normal NCC colonization and ENS formation. Our hope is that these data may lead to novel non-surgical therapeutic options in human HSCR cases. These studies will have a significant impact on our understanding of the pathogenesis of RA-deficient intestinal aganglionosis and may lead to improved treatments and preventive measures to reduce the morbidity and mortality associated with Hirschsprung disease.

IV. RESULTS

This section will discuss results from *pertinent* experiments that contribute to understanding whether RDH10 has a significant impact on the RA synthesis necessary for organogenesis, specifically on NCC proliferation, differentiation or migration during formation of the enteric nervous system (ENS).

Establishing vitamin A metabolism defects as a cause of Hirschsprung Disease

This initial portion of this study provides a temporal analysis of the importance of retinoic acid signaling to emphasize that this small molecule is dynamically active throughout gut development. Additionally, we show that *Rdh10*$^{trex/trex}$*; RARElacZ* mutants have a significant retinoid signaling deficiency as compared to wild-type embryos, both in the context of the whole animal at E9.5 and more specifically in the gastrointestinal tract at E12.5.

These retinoid deficient animals have peripheral and enteric nervous system defects, as evidenced by Tuj1 immunohistochemical staining. This mimics the early pathogenesis of Hirschsprung disease and suggests retinoid signaling is essential for proper formation of a complete enteric nervous system.

RETINOIC ACID IS EXPRESSED DYNAMICALLY THROUGHOUT DEVELOPMENT

RARElacZ reporter mice were used to visualize the spatiotemporal domains of active retinoid signaling using beta-galactosidase (X-gal) staining during gastrointestinal tract development (Figure IV-1) (Rossant et al., 1991). At E10.5, the small intestines and distal colon have active RA signaling, whereas the hindgut does not have active RA signaling at this time. In the next 24 hours (E11.5), the GI tract has grown almost twice as long and the expression domain of retinoid signaling remains in the anterior foregut and

continues distally ¾ of the way down towards the cecum. The most distal colonic retinoid activity becomes diminished from E11.5 to E12.5. At E12.5, the entire foregut and midgut are active with retinoid signaling, whereas the cecum and beginning of the hindgut are devoid of RA. It is at this stage that the lower esophagus and anterior stomach become active with retinoid signaling. E14.5 is the stage at which the entire small and large intestines display active retinoid signaling, although the esophagus is now devoid of retinoid signaling, and the stomach continues to have a more restricted retinoid signaling domain. Although the cecum displays less active retinoid cells than the more distal colonic structures, it now is weakly active with retinoids.

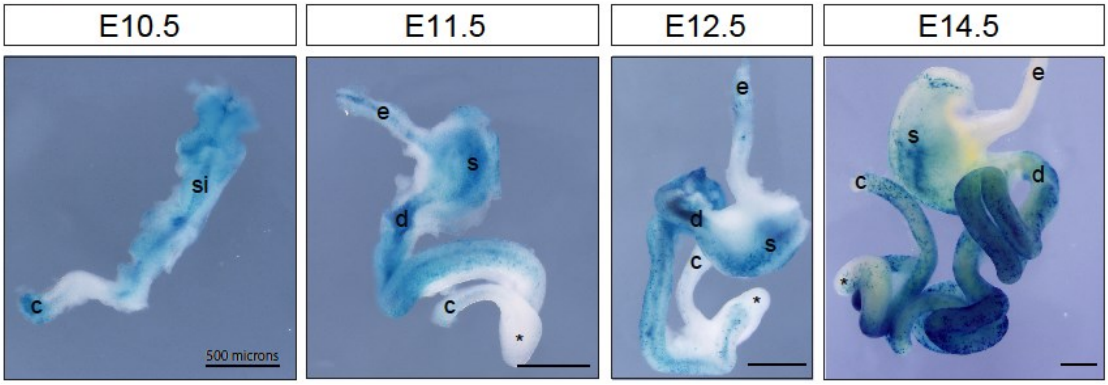

Figure IV-1: Timeline of *RARElacZ* expression in E10.5 to E14.5 dissected guts. This expression timeline highlights the dynamic changes of retinoid signaling during gut development. Scale bars are 500µm.

RDH10$^{TREX/TREX}$ MICE DISPLAY RETINOIC ACID SIGNALING DEFECTS

Rdh10$^{trex/trex}$ point mutant embryos are deficient in the enzyme RDH10, which contributes to the oxidation of Vitamin A to retinoic acid. These *Rdh10*$^{trex/trex}$ point mutants have several embryonic defects, many of which have been previously described both in Chapter II: Methods and in previous publications (Sandell et al., 2011; Sandell et al., 2012; Sandell et al., 2007). *Rdh10*^{trex} mice were crossed to *RARElacZ* to visualize the

localization of active retinoid signaling using beta-galactosidase (X-gal) staining (Rossant et al., 1991).

Rdh10$^{trex/trex}$ mice display severely reduced RA synthesis (Kumar et al., 2011; Sandell et al., 2007), evident in both whole embryo staining (Figure IV-2 A, C), as well as specifically in the gut (Figure IV-2 B, D). At E12.5, *Rdh10*$^{trex/trex}$; *RARElacZ* guts have less active retinoid signaling (Figure IV-2 D), and the active retinoid signaling domain is located only half-way to the cecum (Figure IV-2 C).

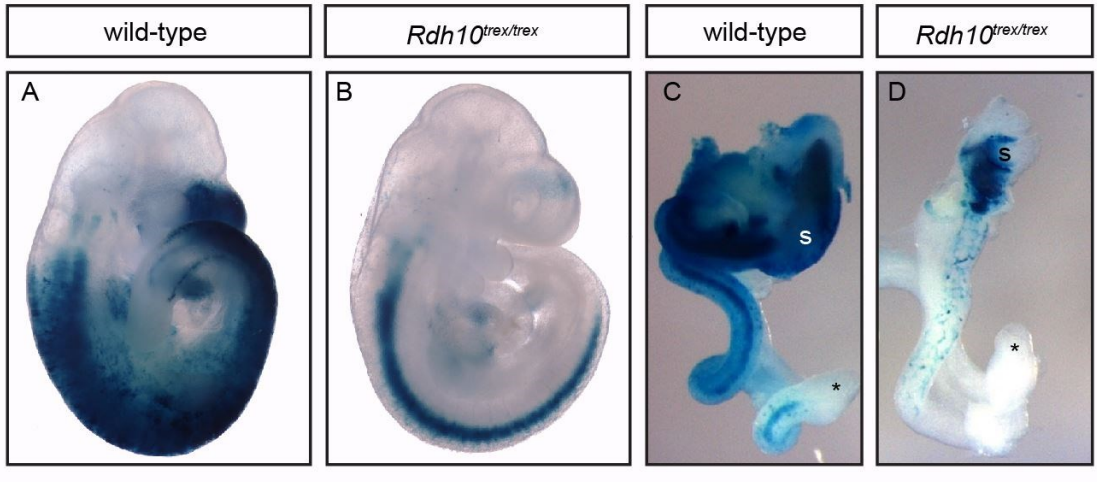

Figure IV-2: *Rdh10*$^{trex/trex}$; *RARElacZ* embryos and intestines were stained for β-galactosidase to visualize the extent of RA deficiency. This cross shows the RA signaling present in wild-type versus *Rdh10*$^{trex/trex}$ mutant embryos. The *RARElacZ* transgenic reporter is used to visualize where RA is active. An overall deficit in retinoic acid signaling (in blue) is observed in the whole mutant mouse at E9.5 (A, B), as well as specific lack of signaling in E12.5 intestines (C, D). In particular, a scarce amount of RA signaling is detected distal to the stomach. Images C and D courtesy of Lisa Sandell, PhD.

The dynamic expression of retinoic acid, shown in Figure IV-1, is important to development of a fully colonized gut, as the gut microenvironment changes with the growing gut (Druckenbrod and Epstein, 2009). Importantly, it has previously been shown that retinoid receptors are present in the developing gut as the ENCCs are migrating and

colonizing the distal gut (Sato and Heuckeroth, 2008), indicating the responsiveness of the gut mesenchyme to RA. In the case of *Rdh10*$^{trex/trex}$ mice, the severe deficiency of active retinoid signaling in the gut is indicative of an absence of this morphogen and its ability to participate in GI tract developmental processes.

Rdh10$^{TREX/TREX}$ MICE DISPLAY TOTAL INTESTINAL AGANGLIONOSIS

In addition to craniofacial, cardiac and limb deformities, *Rdh10*$^{trex/trex}$ embryos have a complete absence of enteric neurons in the developing GI tract. Mature enteric neuronal differentiation was assessed in *Rdh10*$^{trex/trex}$ embryos by immunohistochemical staining of β-tubulin III (Tuj1). The colonic aganglionosis phenotype is first evident in E9.5 whole embryo preparations (Figure IV-3 E). As the embryos grow, both the size difference and gut aganglionosis phenotype in *Rdh10*$^{trex/trex}$ embryos becomes even more pronounced (Figure IV-3). This total intestinal aganglionosis phenotype is reminiscent of severe Hirschsprung Disease (HSCR) in humans, leading us to propose that *Rdh10*$^{trex/trex}$ as a new genetic model for this devastating disease.

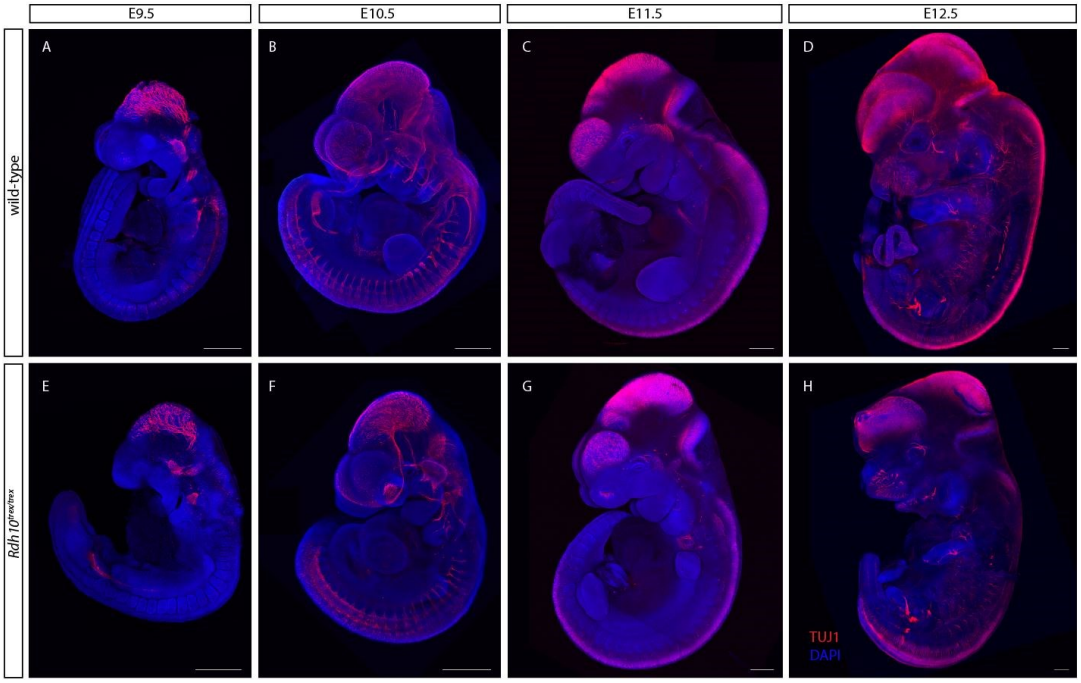

Figure IV-3: Timeline of βtubulin and DAPI immunostaining in *Rdh10*$^{trex/trex}$ embryo and wild-type littermates from E9.5 to E12.5. The lack of mature neurons developing to colonize the enteric nervous system is evident from E9.5 onwards. Scale bars are 500μm. Images B and F courtesy of Liang Liang, Ph.D.

The colonic aganglionosis phenotype caused by RDH10 deficiency is most evident in E10.5 embryos and E11.5 dissected gut preparations. In E10.5 *Rdh10*$^{trex/+}$ (control) embryos (Figure IV-4), enteric neural crest cells (ENCC) have begun differentiating (Tuj1+) into mature neurons throughout the GI tract (Figure IV-4 A), whereas *Rdh10*$^{trex/trex}$ (mutant) mice exhibit total intestinal aganglionosis (Figure IV-4 C). When embryonic guts are dissected from E11.5 embryos, just prior to embryonic lethality, and immunostained for Tuj1, it is evident that wild-type guts have mature neurons to the level of the cecum (Figure IV-4 B), whereas *Rdh10*$^{trex/trex}$ embryonic guts have no evidence of healthy, mature neuronal development, much less in the same reticular network as that seen in the wild-type littermates (Figure IV-4 D).

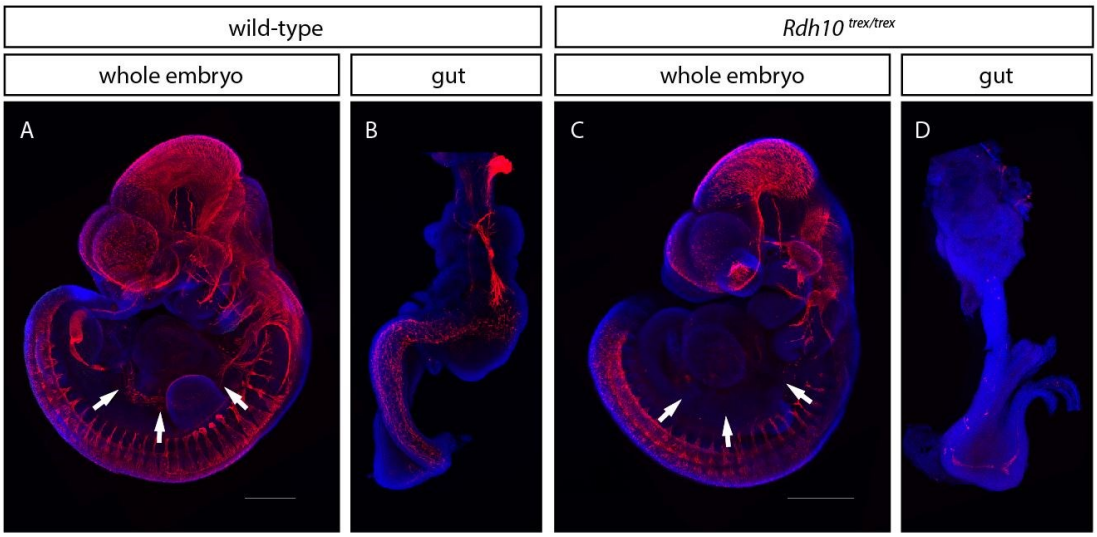

Figure IV-4: βtubulin and DAPI immunostaining in E10.5 whole embryos and E11.5 whole guts. Neurons in the body and in the digestive system (white arrows) in the *Rdh10*$^{trex/trex}$ embryo and wild-type littermates are stained with Tuj1, which is specific to βtubulin (labels differentiated neuronal populations). White arrows in the mutant embryo (C) indicate the absence of ENS neurons. Mature neurons in the E11.5 gut have reached the cecum in the wild-type (B) but have not colonized the gut in mutants (D). Scale bars are 500μm. Images A and C courtesy of Liang Liang, PhD.

RA is spatiotemporally required for proper ENS development

This portion of the study focuses on investigating the hypothesis that retinoic acid signaling is spatiotemporally required for the developing gastrointestinal system. To study the spatial and temporal contributions of RA, we utilize *Rdh10*$^{trex/trex}$ mice in a gut explant culture system, along with maternal retinal gavage rescue experiments.

RDH10$^{TREX/TREX}$ TOTAL INTESTINAL AGANGLIONOSIS CANNOT BE RESCUED IN GUT ORGAN CULTURE

Previous studies of HSCR in mouse models have implicated that a delay in ENCC migration may be the cause for an HSCR phenotype (Barlow et al., 2012; Wallace et al., 2011). In avian models, RA was implicated as a requirement for the initial and continued

migration of ENCCs into the developing gut (Simkin et al., 2013). Additionally, it was previously thought that the migration of ENCCs through the cecum (circumflex ENCCs) was important for hindgut colonization (Barlow et al., 2003; Coventry et al., 1994; Kruger et al., 2003), but recent photo-conversion real-time imaging experiments have shown that ENCCs destined for the hindgut traverse the mesentery (trans-mesenteric ENCSS: tmENCCs) as solitary cells when the midgut and hindgut are opposed in parallel (between E10.5-11.5), and these ENCCs are the major source of the ENS in the hindgut (Nishiyama et al., 2012). Because the midgut and hindgut are juxtaposed only during E10.5-11.5, and tmENCCs are the primary cell population contributing to the hindgut ENS, these cells have only a limited period of time to reach the hindgut. Should these tmENCCs experience delayed migration through the mesentery, the result should be impaired colonization of the hindgut by ENCCs (Nishiyama et al., 2012).

With that in mind, we investigated the hypothesis that providing more time or additional exogenous retinoids for these *Rdh10*$^{trex/trex}$ gut explants to complete colonization would rescue the total intestinal aganglionosis phenotype observed at the time of embryonic lethality. Using ENS formation as a surrogate for successful ENCC migration, we have assayed for Tuj1 in the subsequent experiments. We cultured E11.5 *Rdh10*$^{trex/trex}$ gut explants in RA-deficient media for up to ten days, or supplemented E11.5 *Rdh10*$^{trex/trex}$ gut explants with retinal or retinoic acid for up to four days to determine if retinoids were necessary for ENS development after E11.5.

Total intestinal aganglionosis phenotype in *Rdh10*$^{trex/trex}$ embryos is not simply due to delayed ENCC migration or differentiation in enteric neurons

Rdh10$^{trex/trex}$ embryos typically die around E12.5 due to cardiovascular failure and hemorrhaging, prior to complete NCC colonization of the gut. However, by culturing the intestines in vitro, we can bypass this embryonic lethality. To investigate the possibility

that delayed ENCC migration is a potential cause of colonic aganglionosis in retinoid signaling deficient mutants, the intestines of E11.5 *Rdh10*$^{trex/trex}$ embryos and their phenotypically wild-type littermates were removed and cultured in retinoid deficient media for 2, 4 or 10 days. At E11.5, wild-type intestines have mature neurons throughout the proximal gut up to the cecum between the midgut and hindgut. *Rdh10*$^{trex/trex}$ intestines do not have mature neurons at this time point (Figure IV-4 B, D).

After 2 days of culture, neurons in control intestines have reached the hindgut. At this time, these hindgut neurons have not yet formed the same pattern or density of neural network as is seen in the midgut. However, after 4 or 10 days of culture, the neurons in the hindgut have formed a thick, reticulated neural network. In contrast, after 2, 4, or 10 days of culture, *Rdh10*$^{trex/trex}$ intestines have little to no neuronal staining throughout (Figure IV-5). This gut culture experiment revealed that the gut phenotype observed in *Rdh10*$^{trex/trex}$ embryos is not simply due to a delay in ENCC migration and/or differentiation. However, it is still important to determine if the phenotype is due to a lack of ENCCs entering into the foregut at the time of gut harvest (E11.5). Additionally, we must determine whether retinoid requirements in the mouse gut echo that of the avian gut for initial and continued ENCC migration.

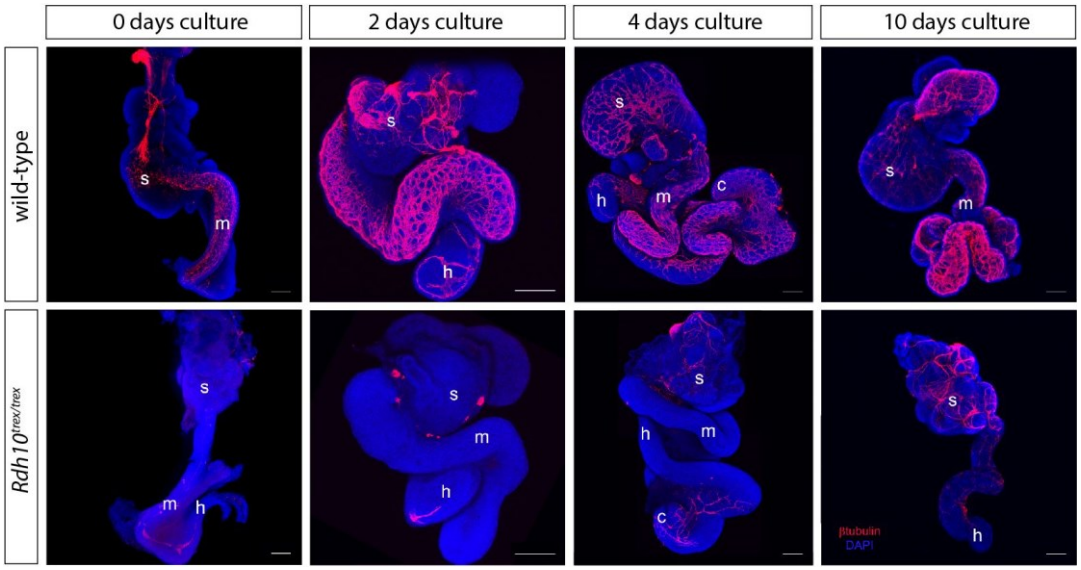

Figure IV-5: βtubulin and DAPI immunostaining at E11.5 0-day and 10-day cultured guts. E11.5 mutant guts were carefully dissected from the embryo in L15+glutamine media, and cultured in an RA-free environment. Cultured guts were then IHC stained with Tuj1 and DAPI to compare the ability to differentiate into ENS neurons (Tuj1). A severe deficit of ENS neurons is shown in the mutants (bottom row). Wild-type gut neurons continued to differentiate and colonize the remainder of the gut tube, while *Rdh10*$^{trex/trex}$ gut is colonized sporadically. Scale bars are 200μm. s, stomach; m, midgut; c, cecum; h, hindgut.

Addition of retinoids after E11.5 does not improve the total intestinal aganglionosis phenotype in *Rdh10*$^{trex/trex}$ intestines.

To investigate if retinoid supplementation would improve the migration and differentiation of ENCCs, and hence enteric neuron formation in *Rdh10*$^{trex/trex}$ gut explants, E11.5 intestines from control and *Rdh10*$^{trex/trex}$ embryos were cultured with retinoids (all-trans-retinoic acid or retinal) for 4 days (Figure IV-5). All-trans-RA is an active small molecule, and in an unregulated manner, supplemented RA has the potential to elicit teratogenic defects (Quemelo et al., 2007). Hence, we also supplemented our control and mutant gut explants with retinal. Supplemental retinal should only be

converted to RA in the presence of Raldh2, and thus was expected to elicit a spatiotemporally appropriate physiological response. Interestingly, even 0.3nM of retinal supplementation (Newton et al., 1980) results in changes of neuronal characteristics in the control gut. Instead of thick neural networks observed in Figure IV-5, and control untreated gut cultures in Figure IV-6, the neural network in retinal-treated gut cultures has fewer projections and is more disorganized (Figure IV-6). When control guts are cultured with 25nM of all-trans-RA, a sub-physiological, non-teratogenic dose (Cunningham et al., 2011), the neuronal cell population has an even more punctate appearance, with few, short axonal projections (Figure IV-6). Culturing *Rdh10*$^{trex/trex}$ intestines for 4 days with either retinal or RA display no neuronal improvement (Figure IV-6).

If retinoids were important only for continued ENCC migration and their differentiation into enteric neurons, we would have observed a restoration of neuronal staining within the retinoid-treated *Rdh10*$^{trex/trex}$ gut cultures. Lack of neuronal staining in retinoid-treated and RA-deficient gut cultures led us to hypothesize that *Rdh10*$^{trex/trex}$ guts might not have enough ENCCs, the ENS precursor cells, at the time of dissection, i.e. E11.5. Nevertheless, these experiments indicate to us that retinoids are specifically required prior to E11.5 for proper ENS development in mice embryos.

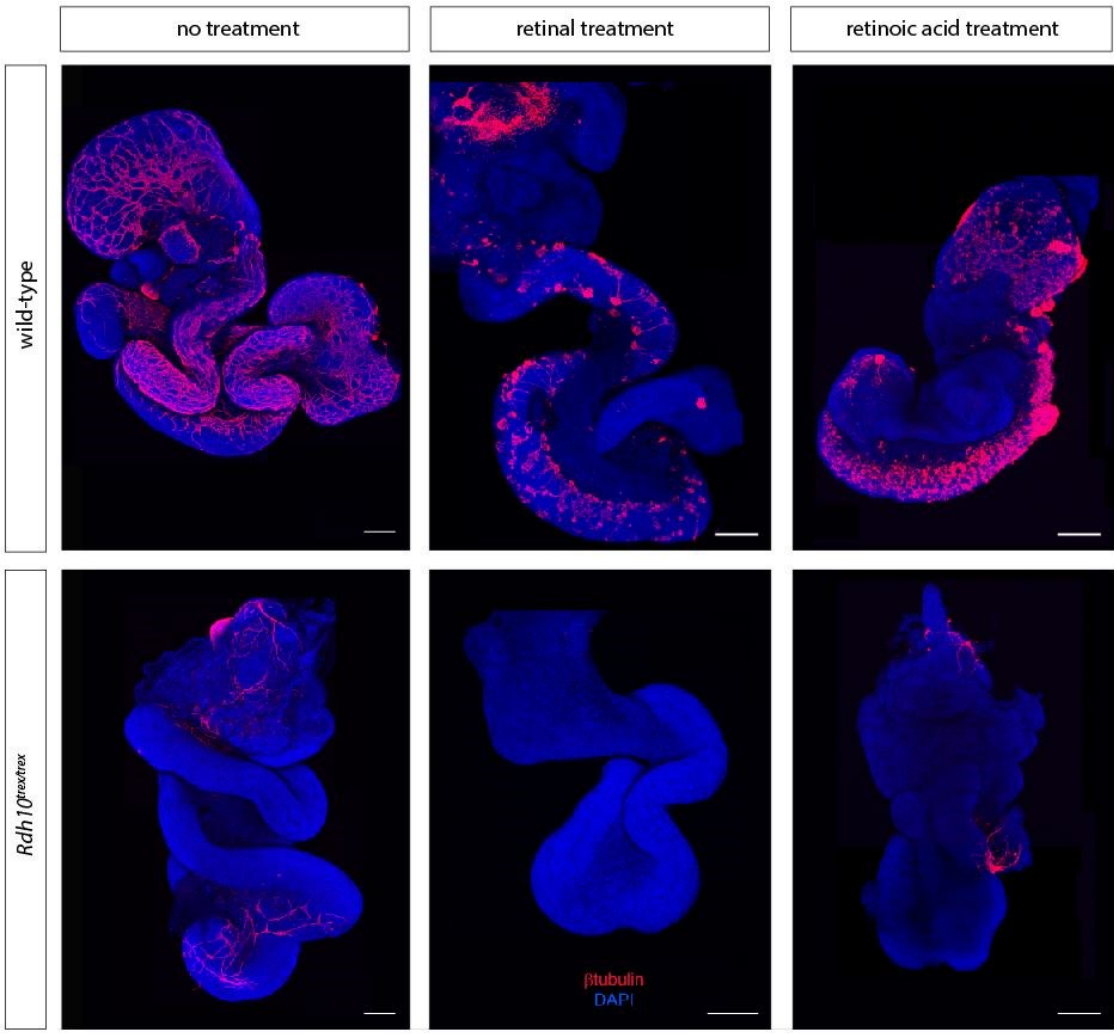

Figure IV-6: Four day gut explant culture with retinoid treatment. Gut preparations were cultured in L15+glutamine media, in an RA-free environment, or with the addition of 0.3nM of retinal or 25nM of all-trans-retinoic acid for the duration of the gut explant culture experiment. After four days of culture, guts were stained with Tuj1 and DAPI. Addition of retinoids after E11.5 development does not improve the ENCC colonization of *Rdh10*$^{trex/trex}$ mutant guts. Scale bars are 200μm.

RDH10$^{TREX/TREX}$ TOTAL INTESTINAL AGANGLIONOSIS CAN BE RESCUED WITH MATERNAL RETINAL GAVAGE BEGINNING AT E7.5

Our gut explant culture data suggests that RA may be necessary earlier than E11.5 for proper ENS formation. Recent photo-conversion real-time imaging experiments

(Nishiyama et al., 2012) and avian transplantation models (Simkin et al., 2013), combined with our gut explant culture data suggests that RA may be necessary to instruct ENCCs to initially colonize the foregut and/or cross the mesentery separating the midgut and hindgut at E10.5, and failure to do so during these time points may lead to the HSCR phenotype observed in *Rdh10*$^{trex/trex}$ embryos. Gut explants from younger embryos are not viable *in vitro*. Thus, to further narrow down the time window of retinoid requirement we shifted to *in vivo* supplementation of pregnant *Rdh10*$^{trex/+}$ mothers, carrying control and *Rdh10*$^{trex/trex}$ embryos, using all-trans-retinal (retinal).

Once per day retinal supplementation

Ex vivo gut organ culture experiments indicate that *Rdh10*$^{trex/trex}$ gut neural progenitors must require retinoid signaling prior to E11.5 for appropriate ENS development. To investigate this further, pregnant *Rdh10*$^{trex/+}$ mothers were supplemented with retinal prior to E11.5 to determine when retinoid signaling is necessary and if it can rescue the *Rdh10*$^{trex/trex}$ intestinal aganglionosis phenotype. The effective retinal gavage rescue dosage for *Rdh10*$^{trex/trex}$ embryos has previously been defined (Cunningham et al., 2011). Gavage supplementation overcomes the lethal cardiovascular defect in these mice, and allows us to empirically determine a temporal requirement for RA signaling during gut colonization and ENS formation. Retinal was used, as this bypasses the oxidation step requiring RDH10 and helps to ensure that retinal will only be converted to retinoic acid where RALDH enzymes are present. Thus, RA is synthesized in a relatively "normal" tissue distribution, limiting the teratogenicity associated with exogenous retinoic acid.

Various *in utero* oral gavage retinal supplementation time windows were assessed. *Rdh10*$^{trex/+}$ mothers were gavaged with retinal (12.5mg all-trans-retinal/kg maternal body weight) once per day for up to six consecutive days, starting at various

time points between E6.5 to E11.5, and guts were subsequently harvested at E11.5 (Figure IV-7, red arrows).

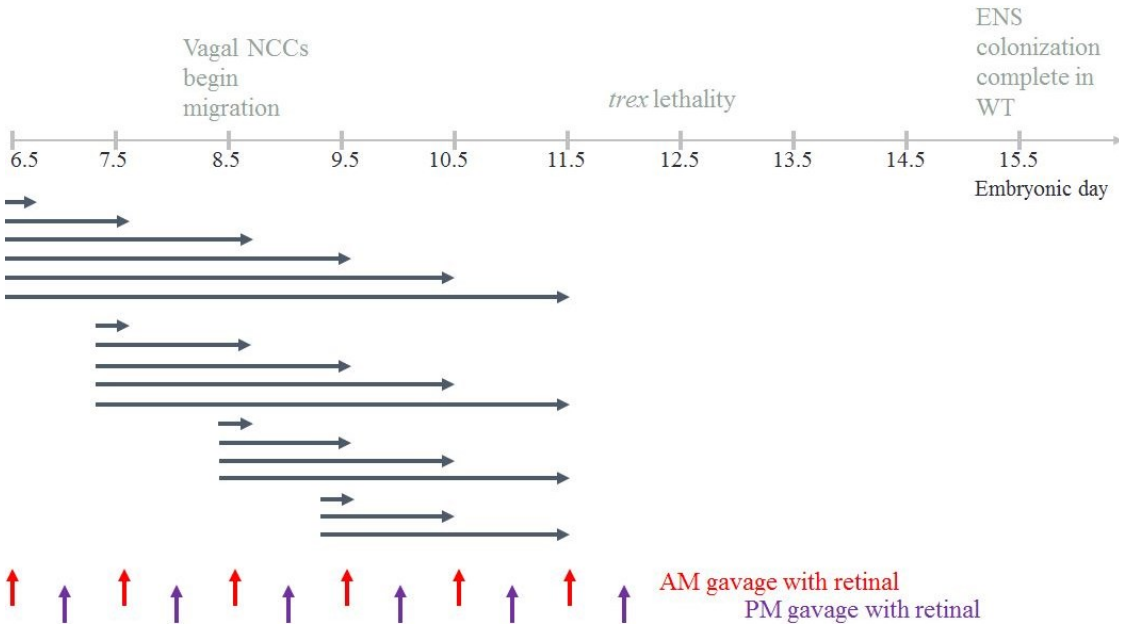

Figure IV-7: Gavage administration schedule. Pregnant *Rdh10*^{trex} mothers were gavaged with retinal on consecutive days ranging from E6.5-E11.5 (black lines represent individual pregnancies and the duration of retinal treatment). Red arrows indicate when retinal gavage was administered for once daily morning retinal treatment. Red and purple arrows indicate when retinal gavage was administered for twice daily morning and evening retinal treatments.

In supplementation trials, once per day retinal gavage from E7.5-11.5 revealed normal enteric neuron development in control littermates and a partial rescue of enteric neuronal differentiation in *Rdh10*$^{trex/trex}$ guts (Figure IV-8). Compared to other time points (with different starting and ending days, and length of gavage treatment), this treatment regime from E7.5-11.5 gave the best phenotypic rescue for single morning retinal gavage treatments. Unlike a typically aganglionic gut in *Rdh10*$^{trex/trex}$ embryos with no treatment, the treated *Rdh10*$^{trex/trex}$ guts had mature neurons present in the foregut, half-way to the cecum (Figure IV-8).

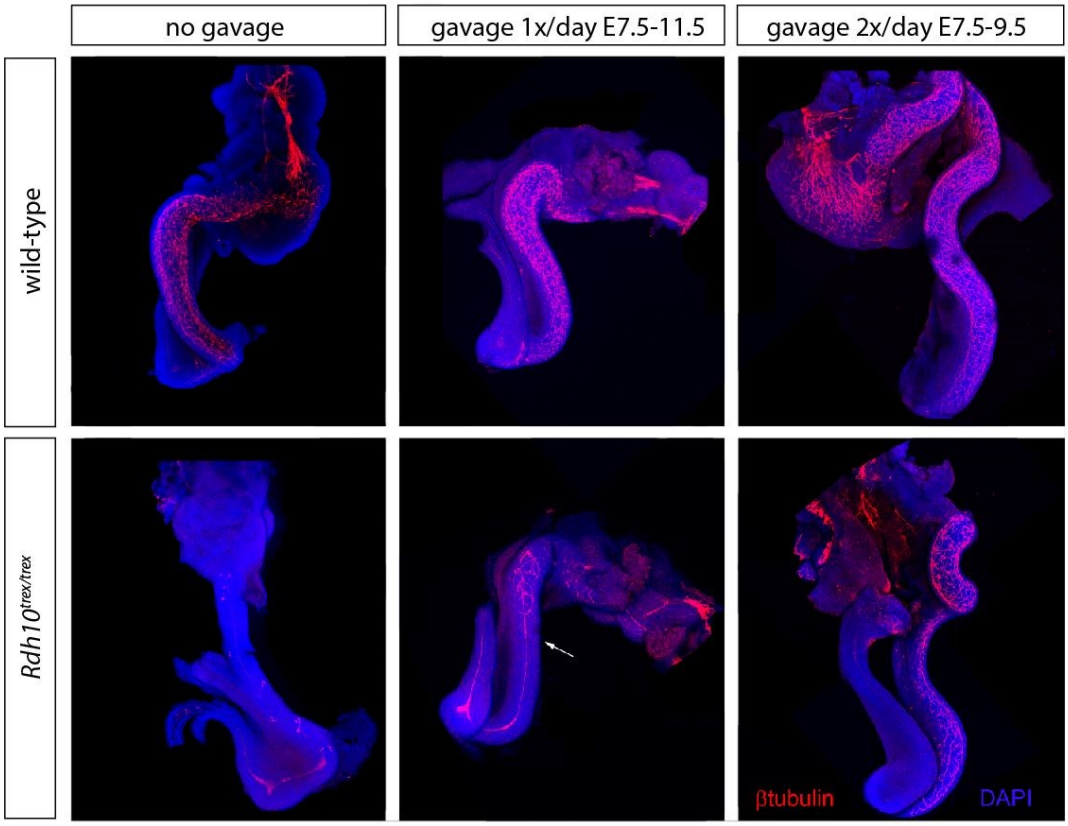

Figure IV-8: Retinal *in utero* gavage rescue beginning at E7.5. Pregnant mothers were gavaged once a day between E7.5-11.5, which partially rescues the *Rdh10*$^{trex/trex}$ gut (white arrow). Pregnant mothers gavaged twice a day between E7.5-9.5 rescues the *Rdh10*^{trex} gut wavefront to a comparable wild-type location.

Twice per day retinal supplementation

To increase retinal availability and potentially further improve the rescue, we tested twice-a-day supplementation of retinal, for consecutive days beginning at E6.5 (Figure IV-7 red + purple arrows). Embryos were subsequently harvested at E11.5, E15.5 and E18.5 (only E11.5 rescued guts are shown). Compared with once daily retinal gavage supplementation experiments (Figure IV-8), a shorter period of morning and evening supplementation, between E7.5-9.5, provided a significant phenotypic rescue of enteric

neuron formation in *Rdh10*$^{trex/trex}$ embryos. With this supplementation regimen, neuronal differentiation in *Rdh10*$^{trex/trex}$ guts appears comparable to treated and untreated wild-type guts, with mature neurons present to the cecum (Figure IV-8). When pregnant *Rdh10*$^{trex/+}$ mothers were gavaged twice a day between E6.5-E9.5, a similarly significant rescue was observed (data not shown). Rescues beginning at E6.5 or E7.5 and lasting at least 3 days resulted in complete ENS formation up to the distal gut by E15.5 (data not shown). Although earlier and longer gavage supplementation treatments may result in a rescue of the colonic aganglionosis phenotype, the minimal treatment for a full rescue is observed to be between E7.5 to E9.5, a time window that precedes vagal NCC invasion into the gut. These maternal gavage experiments suggest that active RA signaling is required prior to and during the vagal NCC invasion into the foregut during early embryonic development, and is not required for the maintenance of NCC migration or differentiation after the initial invasion into the foregut, or necessary to convey the ability to ENCCs to cross the mesentery separating the midgut and hindgut at E10.5. Perhaps the reason multiple days of retinal treatment (E7.5-9.5) is necessary, is to keep the tissues surrounding the foregut opening appropriately patterned until a sufficient number of NCCs have entered into the foregut.

TEMPORAL DELETION OF RDH10 IN *RDH10*$^{FLOX/FLOX}$*; ER*^{T2}*CRE* MICE CONFIRMS EARLY REQUIREMENT OF RETINOIDS DURING ENS DEVELOPMENT

As mentioned previously, there two major retinoid deficient mouse models that suggest RA as an important morphogen for ENS development. The first study demonstrating that RA deficiency may lead to a HSCR phenotype used *Raldh2*$^{-/-}$ mice partially rescued with RA (maternal RA supplementation from E7.5-E9.5 or E7.5-E11.5). These mice have deficient Ret signaling in the vagal domain, and the VNCC are unable to appropriately colonize the gastrointestinal tract (Niederreither et al., 2003). The second

major study, which first proposed Vitamin A deficiency as a non-genetic risk factor that increases HSCR penetrance and severity used *Rbp4*$^{-/-}$ mice, which are unable to store retinol in their livers. When these mice were subjected to a vitamin A deficient diet during embryogenesis via maternal restriction starting at E7.5, these mice became fully depleted of Vitamin A and RA, and had a distal bowel aganglionosis phenotype (Fu et al., 2010).

Although these studies provided initial evidence suggesting that RA is important for ENS development, these models, along with *Rdh10*$^{trex/trex}$, are all reliant on dietary modifications suggesting a retinoic acid effect on ENS precursor development (Fu et al., 2010; Niederreither et al., 2003; Sato and Heuckeroth, 2008). To investigate the true spatiotemporal requirement for RA signaling in ENS formation, we crossed *Rdh10*$^{flox/flox}$ to the tamoxifen inducible ubiquitous Cre line, *ER*^{T2}*Cre* (Ventura et al., 2007). The *Rdh10*$^{flox/flox}$; *ER*^{T2}*Cre* strain allowed us to selectively and temporally block RDH10, while simultaneously overcoming limitations of *Rdh10*$^{trex/trex}$ lethality and the need for retinoid supplementation in other models of retinoid deficiency.

A combination gavage of tamoxifen and progesterone (5mg tamoxifen + 1mg progesterone) was administered to pregnant mothers at E6.5, 7.5, 8.5, 9.5, 10.5, or 11.5. Progesterone is necessary to ensure pregnancy is not terminated. Using the *R26R; ER*^{T2}*Cre* reporter line, when gavaged with 5mg tamoxifen + 1mg progesterone dosage, cre recombination is complete within 24 hours of oral gavage administration. *Rdh10*$^{flox/flox}$*; ERT2Cre* embryos were harvested at E11.5, E15.5 and E18.5 to analyze the extent of NCC migration and ENS differentiation via immunohistochemistry (IHC). We hypothesized that conditionally deleting RDH10 at each of these times points would genetically define the precise temporal requirement for RA during ENS formation.

Temporal deletion of RDH10 at E6.5 in *Rdh10*$^{flox/flox}$; *ER*^{T2}*Cre* mice results in an intestinal hypoganglionosis phenotype, evident throughout the duodenum, cecum and distal colon (Figure IV-9). Very few neurons are present in various portions of the bowel (Figure IV-9 D, E, F). Tamoxifen-induced deletion of RDH10 at E7.5 results in normal enteric neuron differentiation in the duodenum and cecum, but displays distal colonic aganglionosis, reminiscent of a short-segment Hirschsprung disease phenotype (Figure IV-9 I, white arrow). Removal of RDH10 at later time points (E8.5, 9.5, 10.5, 11.5) does not induce a HSCR-like phenotype (Figure IV-9 J, K, L and data not shown). Normal ENS formation was observed in all treatment *Rdh10*$^{flox/+}$ littermates irrespective of the age of treatment (E10.5 gavage shown in Figure IV-9 A, B, C). These deletion studies confirm an early temporal requirement for retinoid signaling for proper ENS formation. Combined with the results from retinal-supplemented gut culture analyses and *in vivo* retinal supplementation of *Rdh10*$^{trex/trex}$ embryos, it seems that RA is required during the time window before and right when ENCCs are invading the foregut, but might not be necessary for the maintenance of NCC migration or differentiation after the initial invasion.

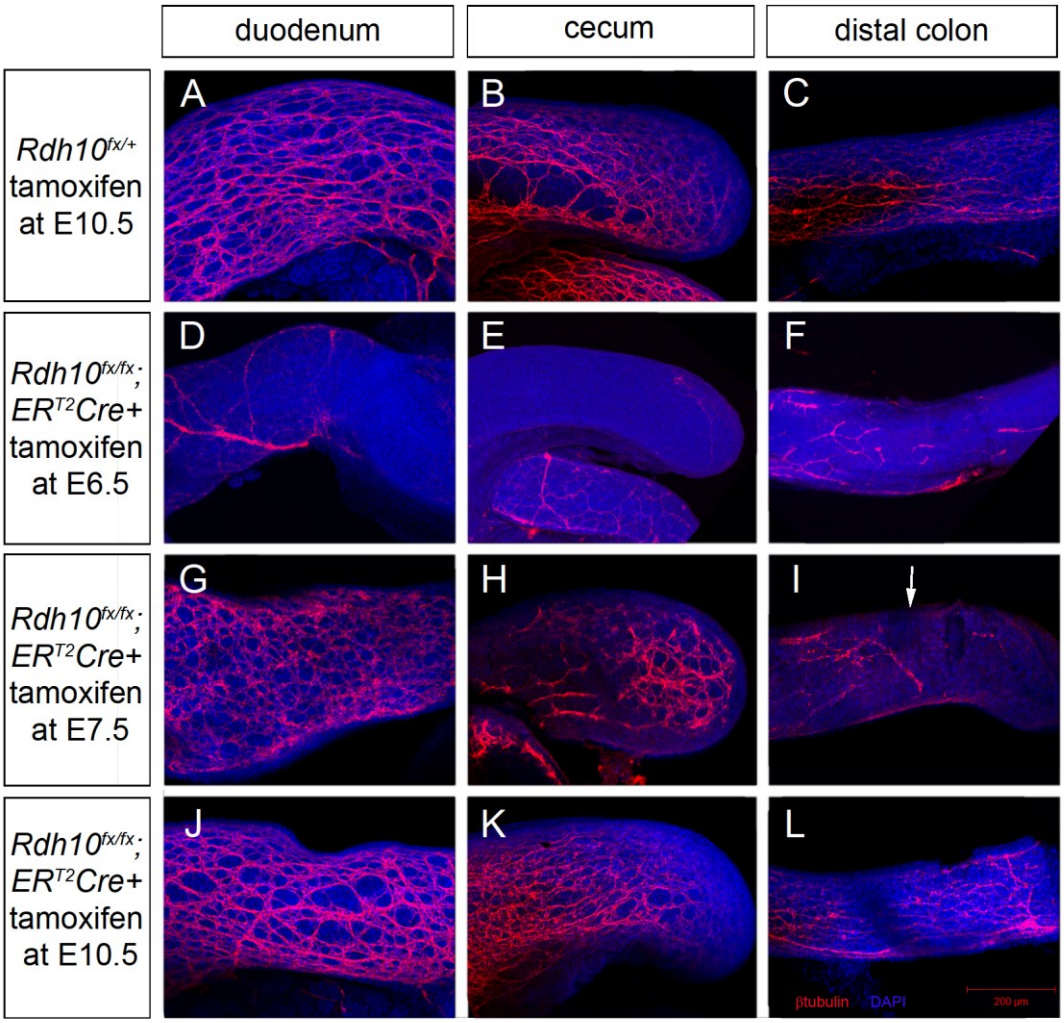

Figure IV-9: Temporal RDH10 excision in *Rdh10*$^{flox/flox}$; *ER*^{T2}*Cre*. *Rdh10*$^{flox/flox}$; *ER*^{T2}*Cre* mice were administered tamoxifen and progesterone gavage in utero at E6.5 (D, E, F), E7.5 (G, H, I) and E10.5 (J, K, L). Control littermates at each of these time points is represented by the *Rdh10*$^{flox/+}$ littermates given tamoxifen and progesterone gavage at E10.5 (A,B,C). Guts from embryos treated after E8.5 appears indistinguishable from controls A, B and C, with full colonization and neural reticulation. Temporal deletion of RDH10 at E6.5 in *Rdh10*$^{flox/flox}$; *ER*^{T2}*Cre* mice results in an total intestinal hypoganglionosis phenotype, whereas deletion one day later at E7.5 results in only distal colon aganglionosis (I, white arrow).

RDH10 is required in the gut microenvironment for proper ENS development

The early temporal requirement for RDH10 to form a complete enteric nervous system could indicate a role for RDH10 either intrinsically in ENCCs, or within the environment that interacts with ENCCs and through which the ENCCs traverse.

DORSAL NEURAL TUBE DELETION OF RDH10 IN *RDH10$^{FLOX/FLOX}$; WNT1CRE* MICE REVEALS NON-INTRINSIC ROLE OF RDH10 IN NCCS

To determine the tissue-specific requirement for RDH10, we used the *Wnt1Cre* line to conditionally delete RDH10 from the dorsal neural tube, the territory from which NCCs are derived. This helped test whether RDH10 and retinoid signaling are intrinsically required within the NCCs during ENS development. *Rdh10$^{flox/flox}$; Wnt1Cre* and *Rdh10$^{flox/flox}$* whole embryos stained with Tuj1 and DAPI at E9.5 showed normal peripheral nervous system development (Figure IV-10). At this stage, the vagal nerve is clearly extending towards the future enteric nervous system.

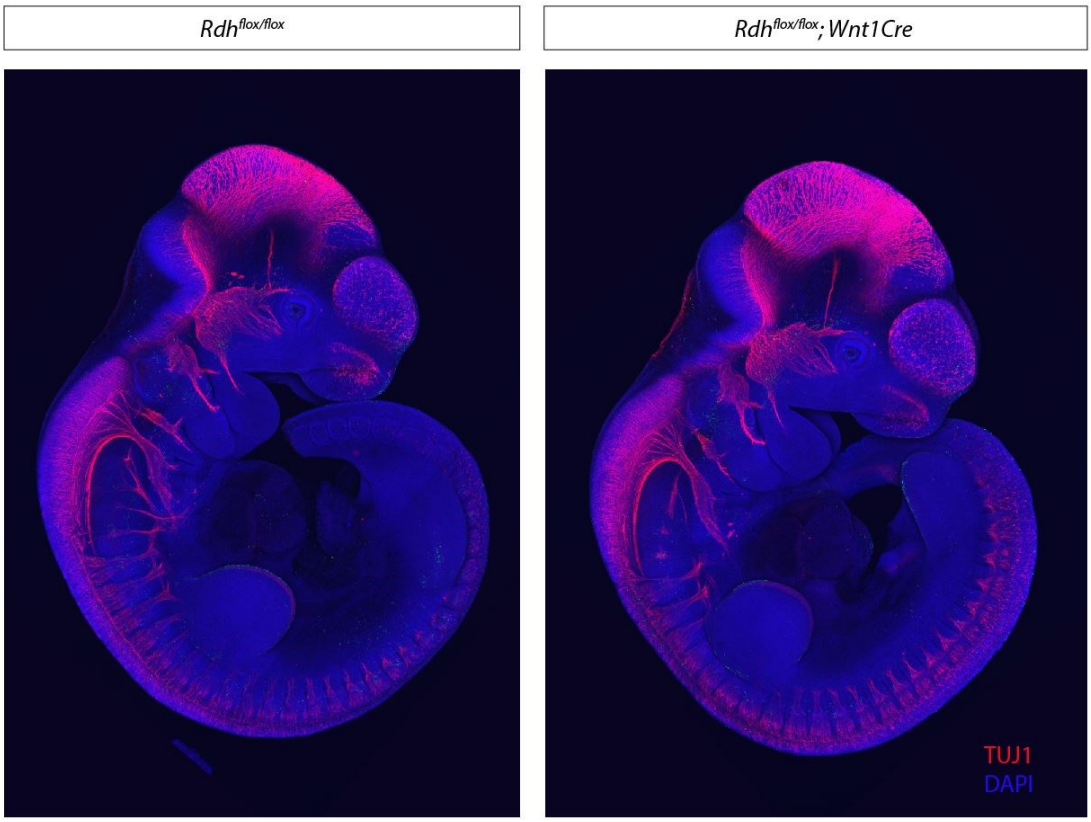

Figure IV-10: *Rdh*$^{flox/flox}$*;Wnt1Cre* embryos and wild-type littermates at E9.5 stained with Tuj1 and DAPI. When RDH10 is conditionally removed from the dorsal neural tube, the territory from which NCCs are derived, (as seen in *Rdh*$^{flox/flox}$*;Wnt1Cre*), the peripheral nervous system develops normally (as seen in *Rdh*$^{flox/flox}$).

Whole guts from E15.5 and E18.5 embryos had mature neurons present in the same pattern and density in the entire length of the gut in *Rdh10*$^{flox/flox}$ as well as *Rdh10*$^{flox/flox;}$ *Wnt1Cre* embryos (E18.5 guts shown in Figure IV-11), indicating that the vagal nerve development was not only normal at E9.5 (Figure IV-10), but the nerve was also able to extend into the enteric nervous system by E15.5. This experiment shows that removing RDH10 specifically from neural crest cells does not affect the ENS formation, indicating that RDH10 is not intrinsically required for NCCs to enter the gut and differentiate into the ENS.

Although RDH10 is not intrinsically required for neural crest cells to appropriately develop the peripheral and enteric nervous systems, it may instead be important in the microenvironment surrounding the developing foregut. Interestingly, by culturing ENS precursors *ex vivo*, Sato and Heuckeroth demonstrated that RA directly influences ENS precursor development, which can be independent of retinoid-induced changes in the gut mesenchyme or early neural crest development (Sato and Heuckeroth, 2008). However, these ENS precursors were collected from E12.5 mouse stomachs, small bowels and colons, which we have previously found is *after* the most important period of retinoid environment patterning. We think it is important to continue investigating the possibility that the *early* environment surrounding the ENCCs during their migration is reliant on appropriate retinoid signaling.

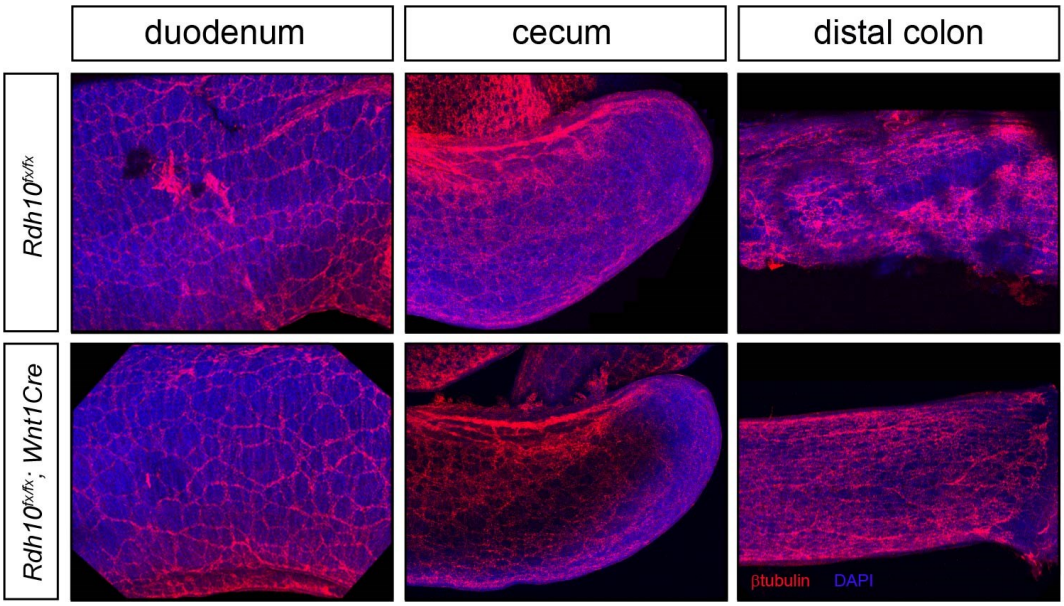

Figure IV-11: E18.5 guts of *Rdh10*$^{flox/flox;}$ *Wnt1Cre* and wild-type littermates stained with Tuj1 and DAPI. *Rdh10*$^{flox/flox;}$ *Wnt1Cre* guts have the same density and pattern of enteric neuron colonization as the control *Rdh10*$^{flox/flox}$ guts.

Rdh10$^{trex/trex}$ NCCs MIGRATE OUT OF THE NEURAL TUBE BUT DO NOT ENTER THE FOREGUT

Using the newly created *Mef2c-F10N-lacZ* mouse line to label neural crest cells and derivatives (Aoto et al., 2015), we were able to investigate any potential differences in NCC migration and differentiation between *Rdh10*$^{trex/trex}$ mice and their wild-type littermates via *LacZ* staining. Using this reporter line, it is clear that neural crest cells are specified but do not migrate to the appropriate location within the gastrointestinal tract (Figure IV-12, Figure IV-13). In E9.5 control embryos, both in wholemount and in section, it is clear that NCCs have already undergone appropriate ventrolateral migration towards the foregut (Figure IV-12). However, in mutant embryos, neural crest cells fail to migrate ventrally towards the foregut opening.

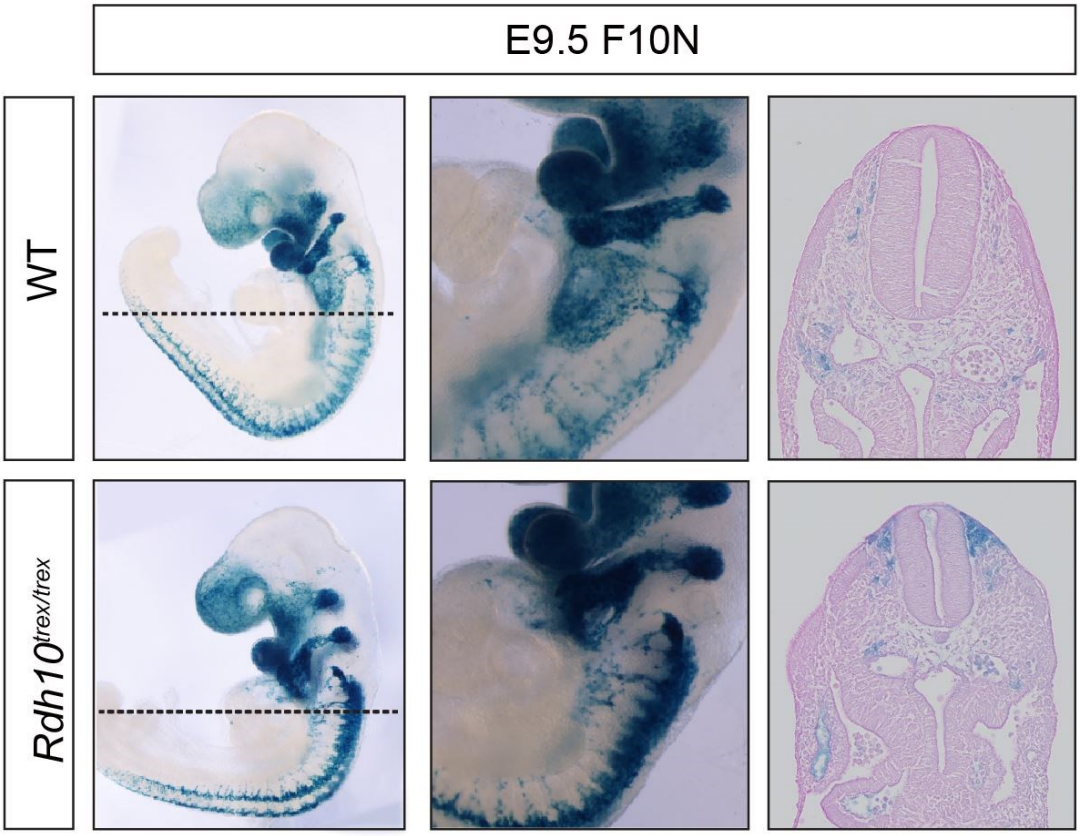

Figure IV-12: E9.5 *Rdh10^{trex}; F10N* mice stained and sectioned. LacZ labels neural crest cells and derivatives. Section at the dotted line emphasizes altered neural crest cell migratory pattern in mutants.

By E10.5, the differences in neural crest cell colonization are much more evident, with wild-type embryos exhibiting classic sympathetic ganglion colonization patterns as well as a clear vagal neural crest cell stream contributing to the ENS (Figure IV-13, Figure IV-12). However, in the mutant embryos, very few F10N+ neural crest cells migrate towards the entrance of the foregut. This abnormal pattern of neural crest cell migration is clearer in sections.

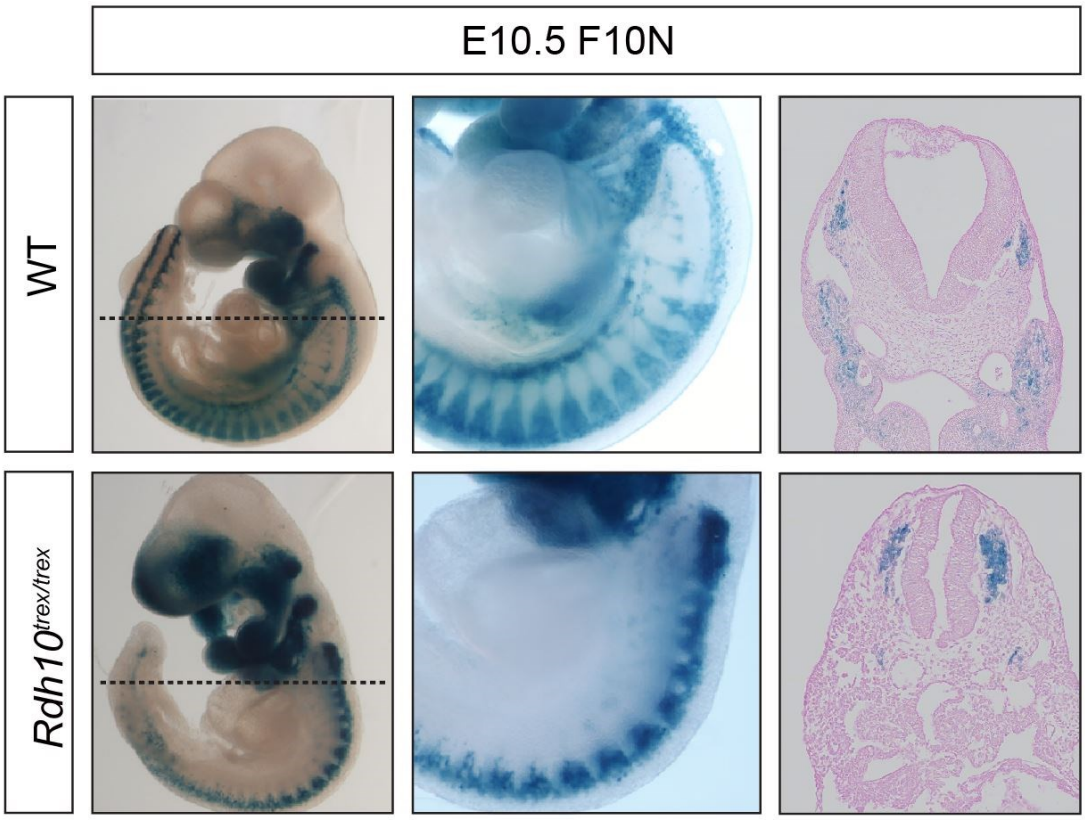

Figure IV-13: E10.5 *Rdh10^{trex}; F10N* mice stained and sectioned. *LacZ* labels neural crest cells and derivatives. In zoomed in vagal area of mutant embryos, it is obvious the vagal neural crest stream is missing. Section at the dotted line emphasizes altered neural crest cell migratory pattern in mutants.

RDH10$^{TREX/TREX}$ MICE HAVE INCREASED CELL DEATH BUT DEATH IS NOT RESTRICTED TO ENTERIC NEURAL CREST CELLS

The deficiency of neural crest cells in the gut at E10.5 of *Rdh10$^{trex/trex}$* embryos could be due to failed NCC survival. E9.5 cryosections were examined for the potential for NCC death. Sections of mutant embryos caudal to the otic vesicle near the opening of the foregut reveal fewer Ap2α+ neural crest cells near the entrance of the foregut, as well as an increase in caspase-3 mediated cell death (Figure IV-15). However, this cell death is not specific to neural crest cells, but rather is found in the cells immediately surrounding NCCs (Figure IV-14).

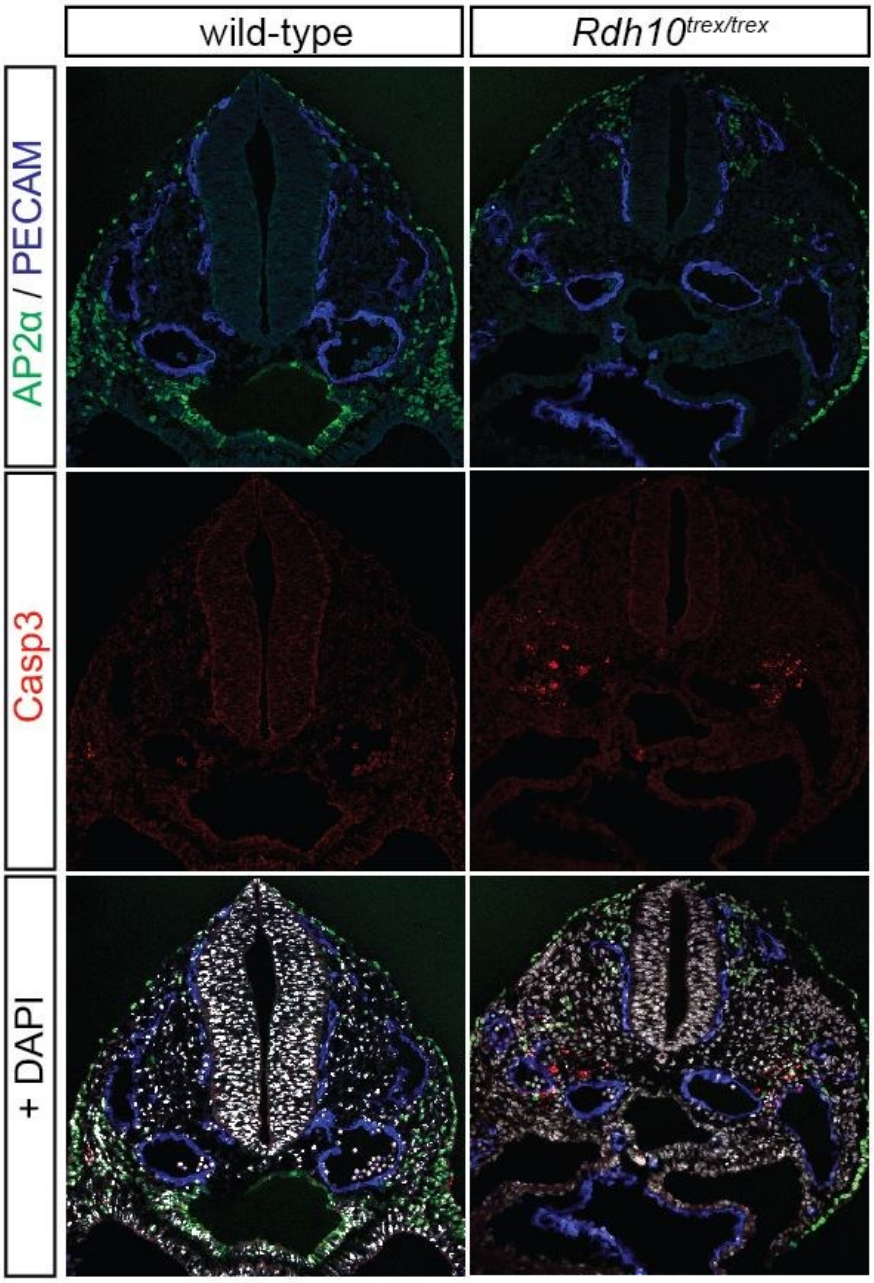

Figure IV-14: Cryosections taken at E9.5 in mutant and wild-type embryos. Less Ap2α+ neural crest cells are visualized near the entrance of the foregut, along with increased cell death in *Rdh10*$^{trex/trex}$. Images courtesy of Kazushi Aoto, Ph.D.

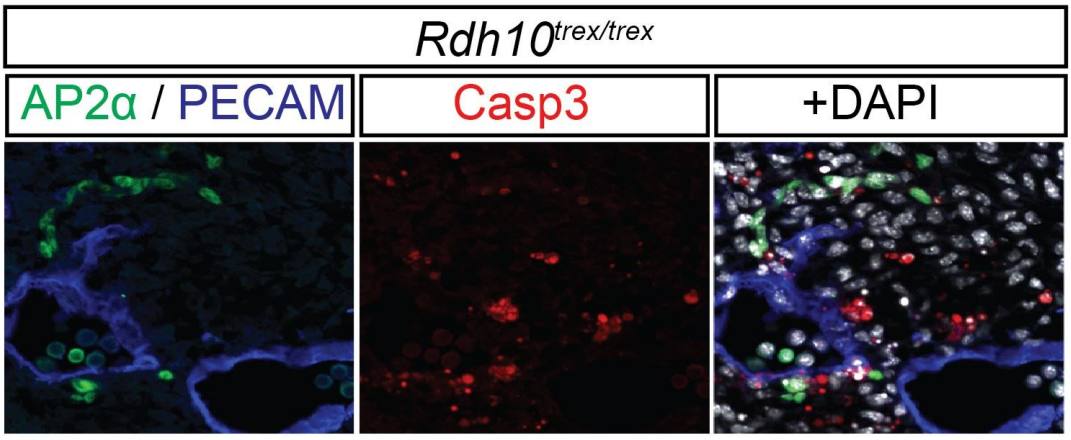

Figure IV-15: Zoom-in at the area of significantly increased cell death in *Rdh10*$^{trex/trex}$ mutants. Cell death does not co-localize with Ap2α+ neural crest cells. Images courtesy of Kazushi Aoto, Ph.D.

Rdh10 is expressed in the surrounding mesenchyme around the developing foregut

To investigate the significance of increased cell death in the mesenchyme surrounding the NCCs, we used in situ hybridization to visualize the *Rdh10* expression in the same areas. *Rdh10* is expressed in the mesenchyme surrounding the foregut at E9.0. (Figure IV-16). Interestingly, this is the area NCCs must traverse to enter into the foregut to colonize the ENS and where we observe increased cell death. These data, combined with a lack of aganglionosis phenotype in *Rdh10*$^{flox/flox}$; *Wnt1-Cre*, lead us to hypothesize a potential extrinsic, environmental role for RDH10 and RA signaling in facilitating NCC entry and migration into the foregut.

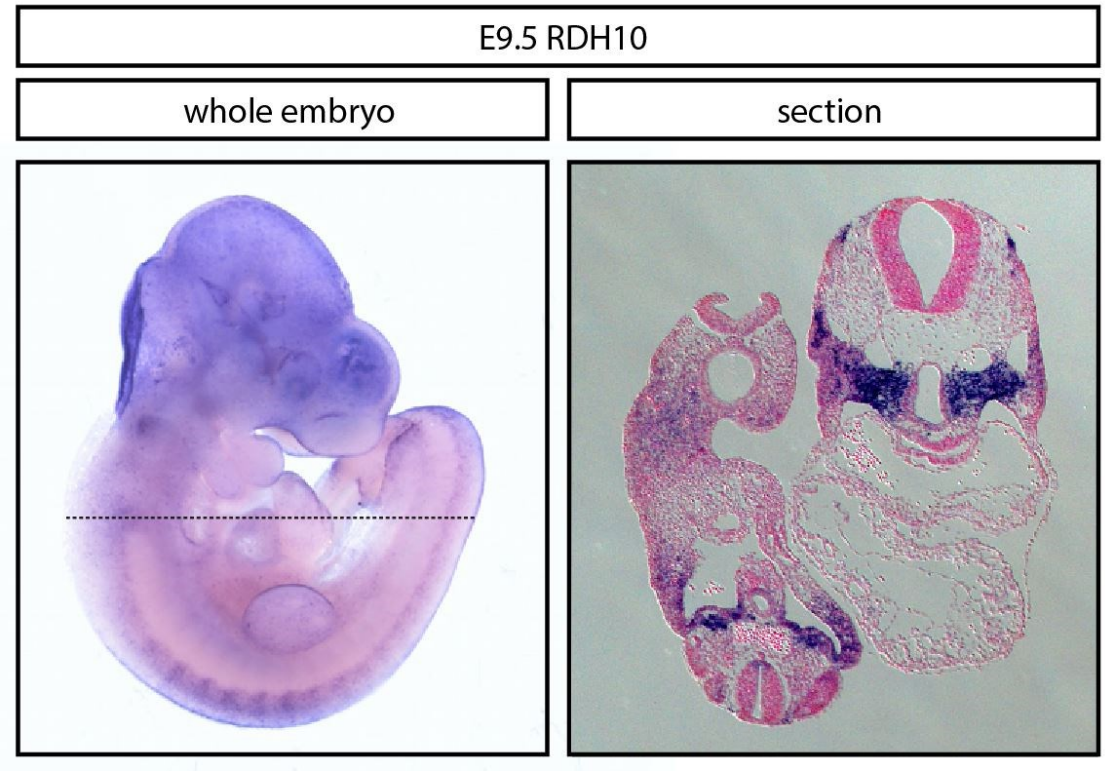

Figure IV-16: Whole embryo staining of *Rdh10* in E9.5 embryo shows high expression in foregut area. Dotted line shows level of section. Section *in situ* reveals high expression in mesenchyme surrounding the foregut. Section image courtesy of Lisa Sandell, Ph.D.

Genes that play a role in total intestinal aganglionosis phenotypes are altered in *RDH10*$^{trex/trex}$ embryos

Although many genes influencing vagal neural crest migration are known, the mechanisms controlling ENS migration into the developing gastrointestinal tract are not completely understood. We have shown that RDH10 is not intrinsically required in NCCs for their entry and colonization of the gut, so there must be another extrinsic explanation for why *Rdh10*$^{trex/trex}$ mutant embryos display this total colonic aganglionosis phenotype. Previous studies have shown that both ENCCs and the microenvironment surrounding

them can actively modify one another as ENCCs traverse through the environment (Akbareian et al., 2013; Simkin et al., 2013). Here we propose that RA is necessary for ENCC migration into the GI tract by either altering the expression of ENCC development genes, or by modifying the environment through which the ENCCs must traverse. Specifically, we are interested in the ENCC development genes that cause a similar total intestinal aganglionosis phenotype in a null mouse line, as the *Rdh10*$^{trex/trex}$ mutants, such as the *GDNF*, *RET*, *GFRa1*, *Sox10*, *Phox2b* and *Pax3*. If these genes are changed in *Rdh10*$^{trex/trex}$ mutants, the phenotypic changes may be attributed to genetic interactions between RA and these known ENCC development genes, or RA may act upstream or downstream of these genes. Additionally, we wanted to test whether RDH10 and RA signaling play a role in proper ENCC microenvironment factors, such as in maintaining a permissive extracellular matrix (ECM).

Using *in situ* hybridization, we investigated spatiotemporal changes in expression of key genes associated with aganglionosis phenotype between *Rdh10*$^{trex/trex}$ mutants and their wild-type littermates. In cases where *in situ* expression data were unavailable, we used qPCR or RNA Seq fold change values (For this section we used the data from "RNASeq2"). Tissue encompassing the first seven somites of E9.5 embryos was used for RNA Seq and qPCR experiments (Figure II-13).

GDNF, RET, AND GFRA1 ARE ALTERED IN *RDH10*$^{TREX/TREX}$ EMBRYOS

Gdnf, *Ret*, and *Gfrα1* homozygous mutants display a similar total intestinal aganglionosis phenotype as *Rdh10*$^{trex/trex}$ embryos. *Ret in situ* hybridization reveals no expression in developing *Rdh10*$^{trex/trex}$ guts (Figure IV-17). However, this lack of *Ret* does not prove causality. It is not certain whether there is no *Ret* signaling because RA is necessary for acquiring RET+ ENCCs (as in avian models), or if there is no *Ret*

expression simply because there are no ENCCs. Without further evidence, a conclusive statement cannot be made on the exact reason *Ret* is absent.

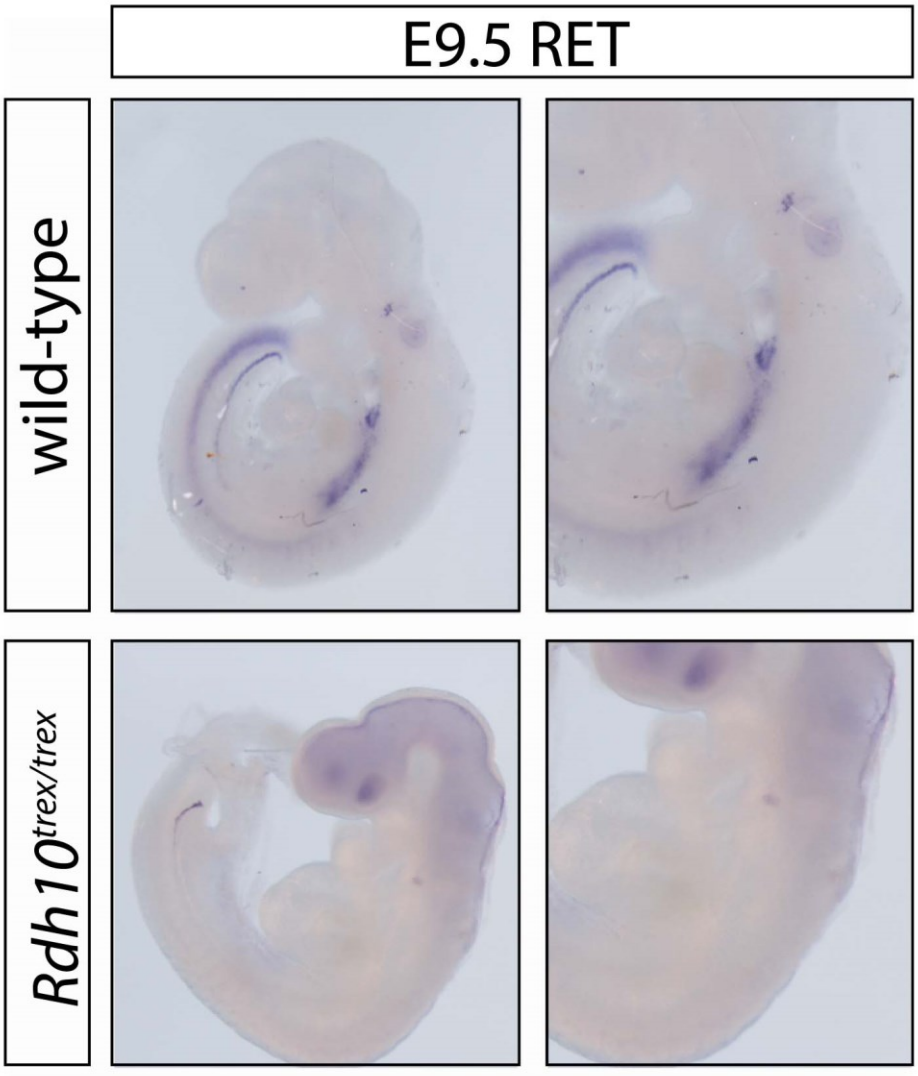

Figure IV-17: RET *in situ* hybridization of mutant and wild-type littermates at E9.5 reveals RET expression in developing gut, and no RET expression in mutant developing gut.

It is therefore expected that *Gfrα1* expression would also be absent in mutant animals. Other researchers have reported that when GDNF is absent, ENCCs are unable to locate and enter into the foregut. We hypothesized that because GDNF is such an

important ENCC chemoattractant, it is important for us to analyze the expression of *Gdnf* in *Rdh10*$^{trex/trex}$ embryos.

qPCR data for *Gdnf*, *Ret* and *Gfrα1* showed significantly reduced levels of mRNA for each of these genes in *Rdh10*$^{trex/trex}$ embryos compared to their wild-type littermates (Figure IV-18). Compared to wild-type littermates, *Gdnf*, *Ret* and *Gfrα1* had only 70%, 54% and 49% relative expression levels, respectively. Each of these three gene expression level differences showed significant p-values ($p<0.05$).

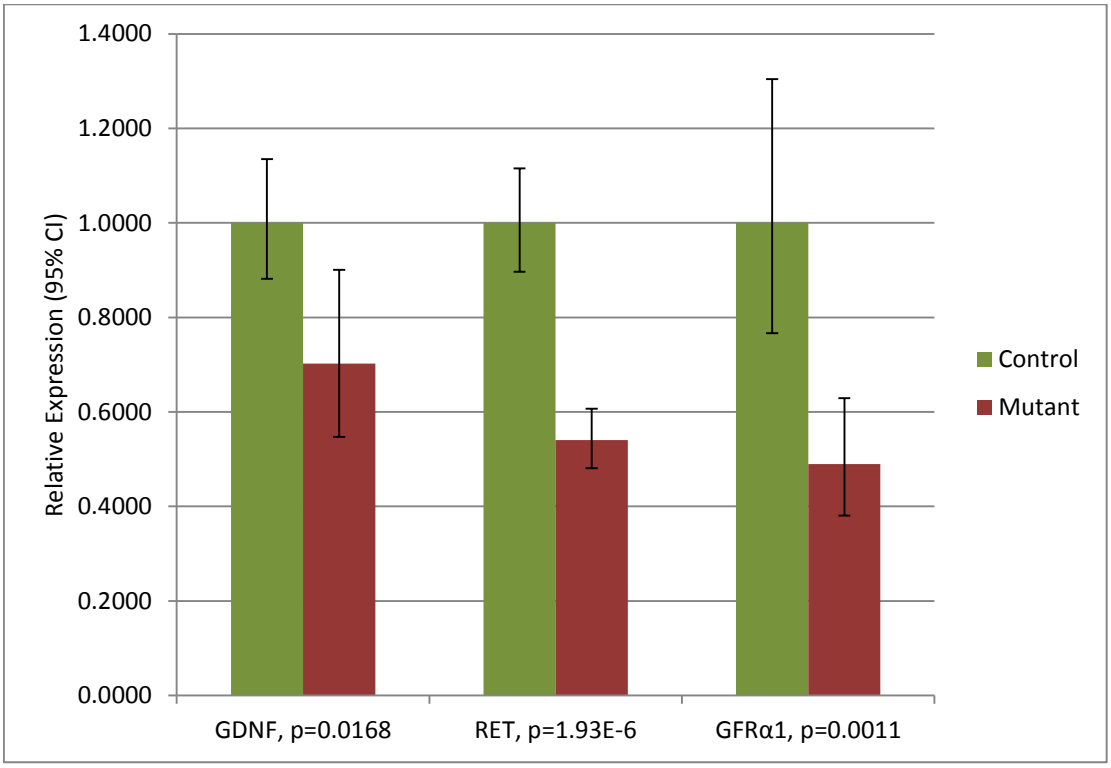

Figure IV-18: qPCR results comparing *Rdh10*$^{trex/trex}$ and wildtype littermates. There is a significantly reduced level of GDNF, RET and GFRα1 in *Rdh10*$^{trex/trex}$ embryos. Relative quantities (of each gene) are graphed with 95% confidence intervals. Each of these three gene expression level differences showed significant p-values ($p<0.05$).

Currently we do not know whether RA signaling is directly required for *Ret* or *Gdnf* expression. Interestingly, it has been proposed in avian models that vagal NCCs

experience RA secreted from the somites, and as they migrate through this field of RA, the vagal NCCs upregulate *Ret* expression, which then allows them to respond to the GDNF signal present in the gut mesenchyme (Simkin et al., 2013). We can speculate that the RA signaling deficient ENCCs in *Rdh10*$^{trex/trex}$ embryos are unable to regulate *Ret* expression, rendering them non-responsive to GDNF signal. A *Gdnf in situ* hybridization would help elucidate whether the ENCCs of *Rdh10*$^{trex/trex}$ embryos are experiencing the same phenomenon as seen in avian embryos. Nevertheless, the down-regulation of *Gdnf*, *Ret* and *GFRα1* transcripts in *Rdh10*$^{trex/trex}$ embryos suggests that RA signaling is somehow required for regulation of GDNF/RET signaling during ENCC migration and ENS formation.

SOX10 IS ALTERED IN *RDH10*$^{TREX/TREX}$ EMBRYOS

Homozygous *Sox10*$^{lacZ/lacZ}$ mice exhibit total intestinal aganglionosis (Britsch et al., 2001), resembling the phenotype found in *Rdh10*$^{trex/trex}$ embryos. When *Rdh10*$^{trex/trex}$ embryos are stained for *Sox10*, there is an obvious absence of *Sox10*+ cells in the foregut, unlike the control embryos, which have a *Sox10*+ labeled vagal NCC stream extending towards the foregut region of the embryo (Figure IV-19). The expression of *Sox10* is very similar to that of the *Rdh10*$^{trex/trex}$*; F10N* mice, indicative of the failure of vagal NCCs to migrate towards and enter the opening of the foregut. Interestingly, the mutant *Rdh10*$^{trex/trex}$ embryos have *Sox10* expression in the craniofacial region and along the dorsal portion of the embryo, and the major deficiency in *Sox10*+ NCCs is seen specifically in the vagal NCC population, further supporting the hypothesis that RA may play a role in modulating ENS developmental genes, as *Sox10* will play an important role in maintaining the ENS in a progenitor state.

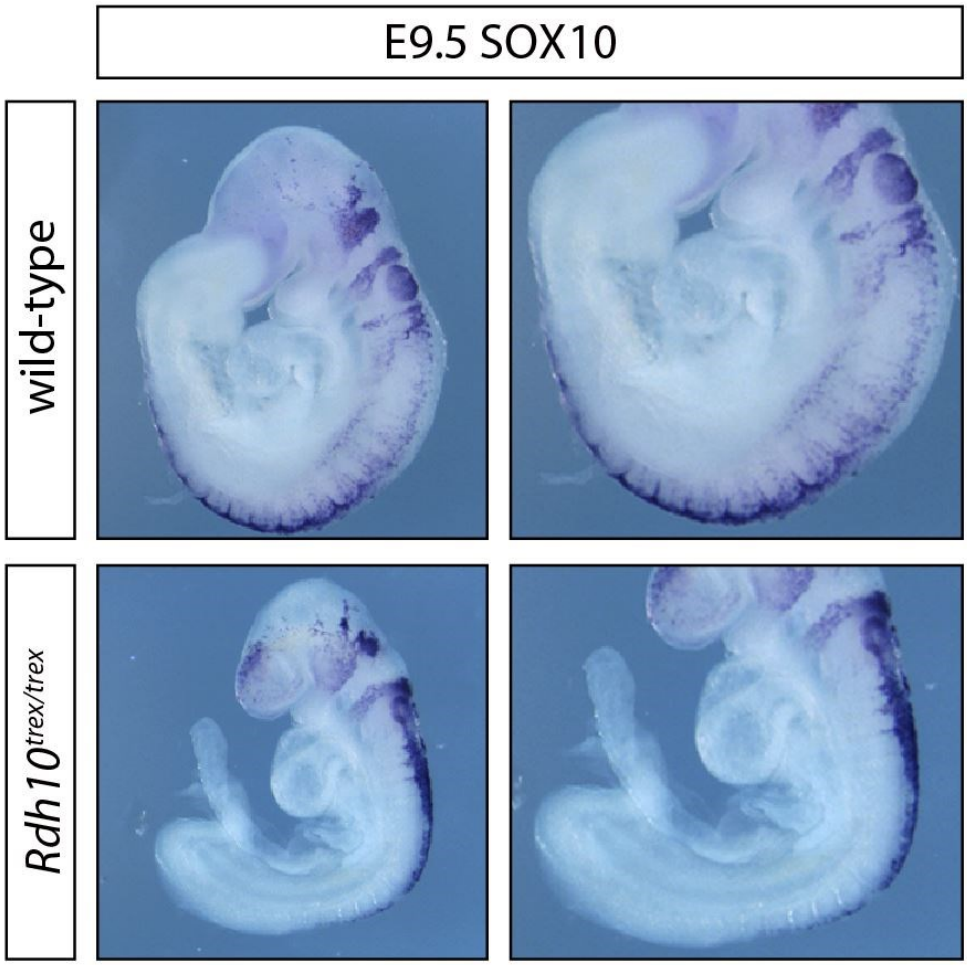

Figure IV-19: *Sox10 in situ* hybridization of mutant and wild-type littermates at E9.5*Sox10* staining reveals *Sox10* expression in the developing wild-type gut, and no *Sox10*+ NCCs in the mutant developing gut.

PHOX2B, PAX3 AND EDNRB ARE ALTERED IN *RDH10*$^{TREX/TREX}$ EMBRYOS

To conclude the investigation into genes in which mutations are associated with total intestinal aganglionosis, we used RNA Seq to compare relative expression levels of *Phox2b, Pax3* and *Ednrb* in *Rdh10*$^{trex/trex}$ mutant and wild-type embryos. PHOX2B and PAX3 are both required for normal ENS formation, and in mice, it has been shown that *Phox2b* and *Pax3* homozygous mice have total intestinal aganglionosis (Elworthy et al., 2005; Lang et al., 2000; Pattyn et al., 1999). The EDN3-EDNRB pathway is necessary

for normal ENCC migration, double knockout mice models of SOX10 and EDN3 or EDNRB3 show a worse aganglionosis phenotype that just one gene knockout alone, suggesting a genetic interaction between SOX10 and EDNR signaling that increases the penetrance and severity of the phenotype. Both the *Sox10*$^{Dom/+}$*; Edn3*$^{ls/ls}$ double mutants (Stanchina et al., 2006) and *Sox10*$^{Dom/+}$*; Ednrb*$^{sl/sl}$ double mutants (Cantrell et al., 2004) results in total intestinal aganglionosis. By RNA Seq analysis, we detected decreased relative expression levels of these genes in the *Rdh10*$^{trex/trex}$ embryos (Table IV-1). *Rdh10*$^{trex/trex}$ embryos have significantly less *Phox2b* expression (3.877 fold), and slightly less *Pax3* (1.255 fold) and *Ednrb* (1.751 fold) expression than wild-type littermates. Each of these three gene expression level differences showed significant p-values ($p<0.05$). *Rdh10*$^{trex/trex}$ embryos have a non-statistically significant minor decrease in *Edn3* expression.

Table IV-1: RNA sequencing fold changes for Phox2b, Pax3, Ednrb and Edn3.

Gene	Fold Change	P Value
Phox2b	-3.877	9.87E-26
Pax3	-1.255	3.55E-4
Ednrb	-1.751	8.99E-19
Edn3	-1.103	0.317725

GUT MICROENVIRONMENT COMPONENTS ARE ALTERED IN *RDH10*$^{TREX/TREX}$ EMBRYOS

Additionally, we have assayed for changes in gene expression of molecules that play a role in retinoic acid signaling within the gut microenvironment, such as L1CAM, a neuronal cell adhesion molecule, and CRABP1, a cellular RA-binding protein important for RA-mediated differentiation and proliferation processes. In the avian model which found that RA is necessary for continued ENCC migration (Simkin et al., 2013), it was noted that as ENCCs passed through the paraxial tissues surrounding the foregut, the

ENCCs became *Crabp1*+, rendering the cells able to respond to the RA in the surrounding environment (Simkin et al., 2013). *Crabp1* expression was analyzed in *Rdh10*$^{trex/trex}$ mutants and wild-type littermates at E9.5 and E10.5. *Rdh10*$^{trex/trex}$ mutants display an overall decrease in *Crabp1* expression, especially surrounding the developing gut, while wild-type embryos have *Crabp1*+ cells near the developing gut (Figure IV-20). Similar to the *Sox10* expression in mutant *Rdh10*$^{trex/trex}$ embryos (Figure IV-19), *Crabp1* expression is still present in the craniofacial region, forelimb, and dorsal neural tube, but specifically absent in the vagal NCC population, again supporting the hypothesis that RA may be specifically acting to regulate ENS developmental genes.

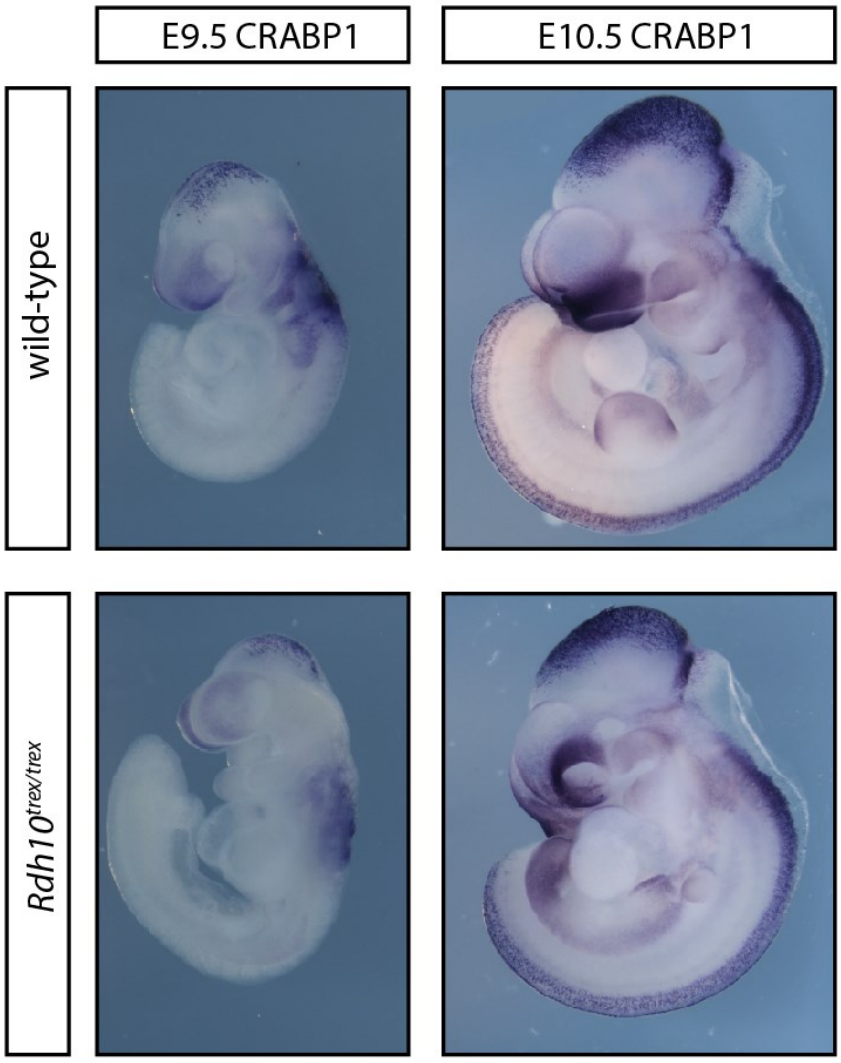

Figure IV-20: *Crabp1 in situ* hybridization of mutant and wild-type littermates at E9.5 and E10.5. *In situ* hybridization reveals *Crabp1* expression near developing wild-type gut, and no *Crabp1* expression surrounding mutant developing gut.

L1Cam is expressed by early migrating ENCCs, and has been proposed to contribute to the efficiency of ENCCs movement. Although *L1Cam* mutant mice have a functional ENS at birth, they do exhibit delayed colonization during development due to solitary migration instead of chain migration (Anderson et al., 2006c). The first reported human case in a neural cell adhesion molecule was in the L1CAM gene (Okamoto et al.,

1997), and it has since been suggested that mutations in this X-chromosomally located gene may contribute to the male predominance of HSCR (Hofstra et al., 2002).

In the RNA sequencing experiment (RNASeq2), *L1Cam* was significantly decreased, with a 1.52 fold change difference (Table IV-2). This is an interesting finding, as *L1Cam* also acts as a modifier gene in conjunction with *Sox10, Edn3,* and *Ednrb* to increase the incidence of aganglionosis (Wallace et al., 2010; Wallace et al., 2011). Again, this supports the notion that RA may allow for ENCC initial foregut migration by modulating the expression of genes such as *L1Cam*, which would then be able to act in conjunction with ENS development genes such as *Sox10, Edn3,* and *Ednrb.*

ECM COMPONENTS ARE ALTERED IN *RDH10*$^{TREX/TREX}$ EMBRYOS

In addition to our targeted gene approach to understand the pathogenesis of the *Rdh10*$^{trex/trex}$ mutant phenotype, our RNA Seq data provided an unbiased approach to understand additional microenvironment changes. Using the Signaling Pathway Impact Analysis (SPIA) algorithm (Tarca et al., 2009) to assess Kyoto Encyclopedia of Genes and Genomes (KEGG) pathway perturbations, we found the top two upregulated pathways in the *Rdh10*$^{trex/trex}$ mutants as compared to their wild-type littermates were altered extracellular matrix (ECM) composition and focal adhesion (FA) pathways.

Extracellular matrix proteins such as Fibronectin (FN), Tenascin-C (TnC), Laminin 1 and 8, Collagen types I, III, IV, and VI, Thrombospondin-1, ADAMs 10 and 13 and MMPs 2 and 9 are thought to play a permissive role in successful NCC migration (Anderson, 2010; Breau et al., 2009; Kerosuo and Bronner-Fraser, 2012; McCarthy and Hay, 1991; Monsonego-Ornan et al., 2012; Perris and Perissinotto, 2000; Theveneau and Mayor, 2014) (Akbareian et al., 2013). Non-permissive ECM components include Collagen type II, Perlecan, and Fibulin-1. Lastly, ECM components that inhibit NCC migration include Aggrecan, Versican, and Collagen IX (Perris and Perissinotto, 2000;

Sotoodehnejadnematalahi and Burke, 2013; Tsang et al., 2010). We hypothesized that in comparison to their wild-type littermates, *Rdh10*$^{trex/trex}$ mutants would exhibit an up-regulation of "non-permissive" and "inhibitory" ECM components and down-regulation of "permissive" components. We investigated this hypothesis using the RNA Seq RPKM values and fold changes for these genes (Table IV-2) and verified some of the findings using qPCR (Figure IV-21).

Using RNA Seq, Collagen 1A1 and Collagen 6A3 had greater than 2 fold differences, with significant p-values ($p<0.05$). Aggrecan, Fibronectin, Tenascin-C, and Collagen 6A4 had greater than 1.5-fold change differences, with all having significant p-values except Collagen 6A4. L1Cam had a decrease in expression fold change of greater than 1.5-fold, with a significant p-value ($p<0.05$). Comparison of relative gene expression in *Rdh10*$^{trex/trex}$ mutants and wild-type littermates by qPCR revealed that LAMC3 has a 53% reduction of relative expression levels, and COL1A1, COL1A2, TnC and FN1 have 172%, 136%, 122% and 120% relative expression levels, respectively (Figure IV-21). LAMC3, COL1A1 and COL1A2 gene expression level differences showed significant p-values ($p<0.05$). There is a slightly increased level of TnC and FN1, but these changes are not significant.

It is clear that the appropriate spatiotemporal distribution of ECM components has a profound effect on NCC migration. It has previously been postulated that abnormal ECM microenvironments may be responsible for, or are at least implicated in, the pathogenesis of enteric nervous system defects, such as Hirschsprung Disease (Alpy et al., 2005; Parikh et al., 1992). Our broad hypothesis that *Rdh10*$^{trex/trex}$ mutants would have upregulated "non-permissive" and "inhibitory" ECM components and downregulated "permissive" components, compared to wild-type littermates seems too simplified. A revised hypothesis needs to take into account which ECM components are specifically

necessary in the microenvironment directly surrounding the foregut and directly interacting with the NCCs invading the foregut. Subsequently, we would be able to analyze how these genes are modified in *Rdh10*$^{trex/trex}$ mutants.

Table IV-2: RNA sequencing fold changes for ECM and FA components. Permissive components are shown in green, non-permissive components are shown in orange, and inhibitory components are shown in red. FA components are shown in blue. Components that retinoid signaling is known to regulate is shown in blue.

Gene	Fold Change	P Value
Collagen 2A1	1.186	0.003019
Perlecan (HSPG2)	1.442	2.64E-08
Fibulin-1	1.245	8.41E-05
Aggrecan	1.829	0.032858
Versican	1.035	0.548477
Collagen 9A1	1.094	0.158002
Collagen 9A2	1.188	0.181727
Collagen 9A3	1.380	0.083503
Fibronectin	1.545	4.59E-09
Tenascin-C	1.99	1.05E-10
Laminin I (α1)	-1.063	0.33356
Laminin I (β1)	1.397	9.03E-06
Laminin I (γ1)	1.269	0.000174
Laminin 8 (α4)	1.186	0.061167
Collagen 1A1	2.761	8.60E-15
Collagen 1A2	1.443	3.03E-06
Collagen 3A1	1.430	1.92E-07
Collagen 4A1	1.061	0.284618
Collagen 4A2	1.154	0.009759
Collagen 4A3	-1.046	1
Collagen 4A4	-1.078	1
Collagen 4A5	1.162	0.127496
Collagen 4A6	1.442	0.000274
Collagen 6A1	-1.051	0.679077
Collagen 6A2	-1.037	0.773363
Collagen 6A3	2.172	6.58E-08
Collagen 6A4	1.595	0.109034
Collagen 6A5	-1.262	0.495553
Collagen 6A6	-1.119	0.342821
Thrombospondin-1	1.242	0.007336
ADAM 10	-1.064	0.270702
MMP2	1.158	0.005653512
MMP9	-1.297	0.196087539
L1cam	-1.520	0.003541816
N Cadherin	-1.005	0.934511
Elastin	1.110	0.619503
Entactin	1.050	0.425888
β1 Integrin	1.109	0.097041

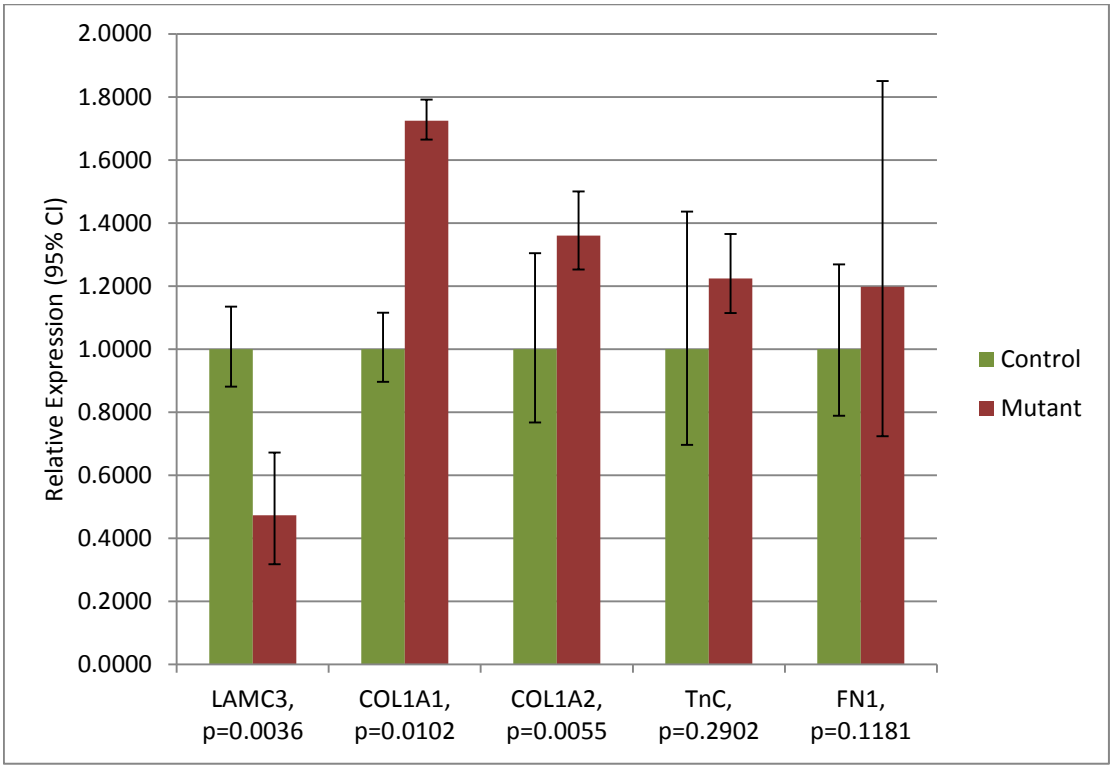

Figure IV-21: qPCR results comparing *Rdh10*$^{trex/trex}$ and wildtype littermates. There is a significantly reduced level of LAMC3, and significantly increased level of COL1A1 and COL1A2 in *Rdh10*$^{trex/trex}$ embryos. Relative quantities (of each gene) are graphed with 95% confidence intervals. Each of these three gene expression level differences has a significant p-value ($p<0.05$). There is a slightly increased level of TnC and FN1, but these changes are not significant.

RDH10 may act as a modifier gene

Finally, numerous studies have suggested the involvement of modifier genes or environmental influences in the etiology and pathogenesis of HSCR, both in mouse models, and in human patients (Angrist et al., 1996; Barlow et al., 2013; Bolk et al., 2000; Cantrell et al., 2004; Doray, 1998; Parisi and Kapur, 2000; Salomon et al., 1996; Stanchina et al., 2006; Wallace et al., 2010; Wallace et al., 2011). The modifier genes act by contributing to pathways that are critical for ENCC developmental processes, such as

migration, proliferation, differentiation and survival (Butler Tjaden and Trainor, 2013). Of particular interest, *L1cam* acts as a modifier gene in conjunction with *Sox10, Edn3,* and *Ednrb* to increase the incidence of aganglionosis (Wallace et al., 2010; Wallace et al., 2011) and *Pax3* and *Tcof* act through a p53 dependent apoptosis pathways to cause increased ENCC cell death, resulting in a decreased number of NCCs that can migrate into the foregut to complete colonization of the distal gut by E18.5. Compound $Pax3^{+/-}$; $Tcof1^{+/-}$ animals display distal colonic aganglionosis, although neither $Pax3^{+/-}$ nor $Tcof1^{+/-}$ mice exhibit colonic aganglionosis alone (Barlow et al., 2013).

As a preliminary study, we crossed RDH10 to mouse models we have in the lab that have been implicated in HSCR, or have a role in NCC migration. When $Rdh10^{trex/+}$ was crossed with $Pax3^{+/-}$, $Gcnf^{+/-}$ or $Tcof1^{+/-}$, no compound heterozygous embryos resulted in a distal colonic aganglionosis phenotype (Figure IV-22). Although GCNF has not previously been implicated in ENS development, $Gcnf^{-/-}$ mouse mutants have a decreased number of NCCs, and significantly reduced *Sox10* expression (data not shown). In each of these crosses, we see a colonized distal colon with similar density and pattern as the control $Rdh10^{+/-}$ gut.

These compound heterozygous crosses suggest that RDH10 likely does not act through the same ENCC developmental pathways as these genes, such as through the p53-dependent apoptosis ($Pax3^{+/-}$ and $Tcof1^{+/-}$), or by reducing the number of NCCs available for migration. These conclusions make sense in the broader context of this study, as we have already seen in our data (Figure IV-15) and others (Sato and Heuckeroth, 2008), that retinoid deficiency does not seem to change the level of NCC death. These data do not rule out the possibility that RDH10 may still be a modifier of other pathways that may result in colonic aganglionosis, but future investigations with other crosses are necessary to determine that potential role.

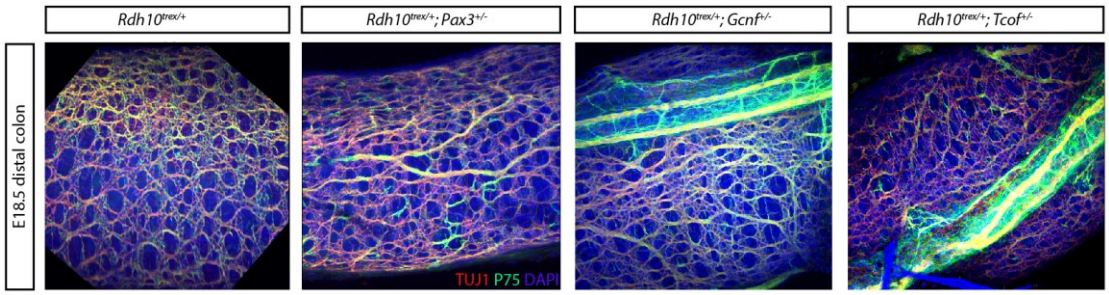

Figure IV-22: Analysis of RDH10 as a potential modifier. *Rdh10*$^{trex/+}$ was crossed to *Pax3*$^{+/-}$, *Gcnf*$^{+/-}$ and *Tcof1*$^{+/-}$, and intestines were stained with Tuj1 (mature neurons), P75 (neural crest cells) and DAPI to analyze ENS formation. None of these compound heterozygous animals resulted in a distal aganglionosis phenotype.

General Conclusion

These studies have established a new model for studying the total intestinal aganglionosis form of HSCR, provided information regarding the spatiotemporal requirements for RA during embryonic intestinal development and potential pathogenic cellular mechanisms of RDH10 deficient animals, as well as predicted potential interactions of RA with pathways that govern normal NCC formation of the ENS and ECM maintenance of the microenvironment.

V. DISCUSSION

Only half of the cases of Hirschsprung disease (HSCR) have been associated with a specific genetic mutation. Hence, it is important to continue the search for genetic and environmental factors that may contribute to the etiology of HSCR as independent mutations or as modifiers. To that end, our lab generated mouse embryos deficient in RDH10, which results in decreased retinoid signaling (Sandell et al., 2011) and exhibit total intestinal aganglionosis (Figure IV-4). This body of work establishes *Rdh10* deficiency as a model of genetically induced Hirschsprung disease, specifically total intestinal aganglionosis, and vitamin A deficiency as a potential environmental modifier.

This study investigated the spatial and temporal requirements of retinoic acid during gastrointestinal system development using $Rdh10^{trex/trex}$ mice (an ENU mutagenesis generated point mutant) and *Rdh10-conditional* knockout mice. We discovered a critical requirement for retinoic acid during early ENCC migration and in establishing a receptive microenvironment for ENCC entry into the foregut tissue. In contrast to what has been found in avian organisms (Simkin et al., 2013), we did not observe a requirement for retinoic acid in maintaining continued migration of ENCCs or their differentiation after ENCC entry into the foregut.

Retinoic Acid must be tightly regulated spatiotemporally, to allow for normal enteric nervous system development

Insufficient or excess dietary vitamin A can result in congenital anomalies and even fetal death (Ross et al., 2000), largely due to the important functions of retinoic acid, the active form of vitamin A, during embryonic development. When vitamin A deficiency occurs prior to or during pregnancy, it can affect NCC development, potentially resulting in neurocristopathies such as HSCR. Hence it is critical to

understand which stage of NCC development requires retinoid signaling during ENS formation and gut development. Although there have been a few studies examining the role of retinoids on ENS development, there has not yet been an in-depth spatiotemporal examination of the role of vitamin A metabolism (specifically the contribution of RDH10) in the formation and development of the enteric nervous system (ENS) and GI tract in mammalian embryos.

Currently, two mouse models implicate a role for retinoid signaling in the pathogenesis of colonic aganglionosis (*Rbp4*$^{-/-}$ and *Raldh2*$^{-/-}$) (Fu et al., 2010; Niederreither et al., 2003). Additionally, it has been suggested that RA is necessary for continued ENCC chain migration in avian models (Simkin et al., 2013). To understand the RDH10 mutant intestinal aganglionosis phenotype (Figure IV-4) in a vitamin A metabolism deficiency context, it was important to visualize retinoic acid signaling in the mutant embryos to determine if the gut phenotype was correlated with a decrease in retinoid signaling. Using a *RARElacZ* reporter mouse line that expresses lacZ under influence of retinoic acid signaling, we showed that *Rdh10*$^{trex/trex}$ embryos have significantly diminished retinoid signaling in the developing gut, suggesting that RA may play a role in ENS formation (Figure IV-2).

To determine whether the necessity of RA for continued ENCC migration is conserved between avian and murine models, we conducted gut explant culture experiments to determine what role RDH10 and retinoid signaling play in ENS development. Knowing that the etiology of previous models of HSCR in the mouse was due to delayed ENCC migration throughout the gut (Barlow et al., 2012), we investigated this as a potential cause of the aganglionosis phenotype seen in *Rdh10*$^{trex/trex}$ mutant embryos. To that effect, we cultured *Rdh10*$^{trex/trex}$ gut explants in RA-deficient media and

found that proper colonization of the gut by ENCCs and formation of a complete ENS only occurs when *Rdh10* is fully functional (Figure IV-5).

There are a few potential explanations for why the *Rdh10*$^{trex/trex}$ explants do not have a completely colonized GI tract: there could be an insufficient number of ENCCs (progenitor cells), RDH10 (and hence RA) might be required for the survival of ENCCs within the gut, or RDH10 might be required for differentiation of ENCCs into ENS neurons and glia. If RDH10 or RA is required for survival or differentiation of ENCCs within the gut, then supplementation with RA at time of culturing should rescue the aganglionosis phenotype in *Rdh10*$^{trex/trex}$ guts, which is not what we case observe (Figure IV-6). This indicates a clear requirement for RDH10-mediated conversion to RA prior to E11.5. Our results support the recent results shown in avian models, where RA has been implicated in the initial colonization of the gut, but we find that RDH10 is not necessary for continued ENCC chain migration (Simkin et al., 2013). Consistent with previous data (Sato and Heuckeroth, 2008), we do not observe increased cell death in *Rdh10*$^{trex/trex}$ guts (Figure IV-15), suggesting that RDH10 and RA are not required for the survival of ENCCs.

RETINOIDS ARE NECESSARY PRIOR TO INITIAL ENCC INTO THE FOREGUT

It is important to determine the critical time window during with retinoids are required for ENS development. Our culture experiments clearly suggest a role for retinoids in regulating gut colonization prior to E11.5. *In vitro* gut-culturing experiments prior to mid-gestation are technologically challenging. Instead, we approached this question through a maternal rescue experiment. We administered retinal to pregnant dams carrying control and *Rdh10*$^{trex/trex}$ embryos, using oral gavage. In our initial once per day gavages, we found that the retinal administration for five consecutive days, between E7.5 to E11.5, resulted in the best rescue of the neuronal colonization of the gut. When we

increased the gavage administrations to twice per day, we were able to narrow the critical time window of retinal requirement to E7.5 - E9.5 with a better rescue of gut colonization, where both mutant and control guts were colonized up to the cecum (Figure IV-8). During normal murine development, ENCCs do not enter the gut until E8.5-E9.0, suggesting that retinoids must be necessary in the embryo before or right as vagal neural crest cells begin invading into the anterior foregut. Given that retinal supplementation for this short time window is sufficient to allow mutant ENCC colonization of the gut equivalent to control guts, argues against the role for retinoids in continued migration and differentiation of ENS.

Although our preliminary studies support previous work done in the field (Fu et al., 2010; Niederreither et al., 2003), they still rely on dietary modifications (RA or retinal supplementation) to elucidate the role for RDH10 in ENS colonization, and we were concerned that our analyses might be influenced by teratogenic effects of excess exogenous RA (Quemelo et al., 2007). In order to obtain a cleaner genetic model system to investigate the role for RA and RDH10 in ENS development, we shifted to *Rdh10$^{flox/flox}$; ER^{T2}Cre* mouse line, where we used tamoxifen administration to temporally excise RDH10 ubiquitously throughout the animal. The results of these *in vivo* conditional *Rdh10* deletion experiments reiterate our retinal gavage rescue findings, that RA is necessary in early ENCC migration and their entry into the gut, but not for continued migration throughout the gut. *Rdh10* excision prior to vagal neural crest cell migration leads to either distal colonic aganglionosis (tamoxifen administration at E7.5) or total colonic hypoganglionosis (tamoxifen administration at E6.5), but *Rdh10* excision later than these time-points results in normal gut colonization, emphasizing the retinoid independence of ENCCs for continued colonization (Figure IV-9).

Thus far, we have utilized retinoid supplementation both in culture and via *in utero* gavage supplementation, along with conditional knockout mice to define the temporal requirement for RA signaling. Maternal gavage experiments providing retinal to RDH10 deficient mouse mutants revealed RA activity is critically required between E7.5-E9.5 only. These retinoid gut culture and retinal gavage data suggest that RA is not necessary for the maintenance of NCC migration, differentiation or proliferation after the initial NCC migratory period. Rather, retinoids are important for initiating vagal ENCC migration and entry into the gut. In combination with data from RDH10 conditional knockout mice, we showed that there is a critical requirement for retinoids prior to early ENCC migration, but are not necessary to maintain continued ENS migration or differentiation, indicating that retinoic acid signaling may be necessary to establish a receptive NCC environment near the anterior foregut.

Pathogenesis of *RDH10*$^{trex/trex}$ is attributed to ENCC extrinsic factors

Since the ENS is entirely derived from NCCs, we analyzed the status of NCCs in *Rdh10*$^{trex/trex}$ embryos using the newly developed *Mef2c-F10N-lacZ* reporter line (Aoto et al., 2015). In *Rdh10*$^{trex/trex}$ embryos, NCCs have failed to enter into the foregut region between E9.5 and E10.5 (Figure IV-12, Figure IV-13). Section analysis suggests that at both E9.5 and E10.5, only a few NCCs have migrated ventrally to the proximity of the foregut and with the majority still remaining near the neural tube. The failure of these *Rdh10*$^{trex/trex}$ ENCCs to migrate ventrally to the same extent as control embryos and to enter the GI tract could be due to an intrinsic requirement for RDH10 in ENCCs or an extrinsic requirement for RDH10 and RA in maintaining an appropriate ENCC microenvironment.

RDH10 IS NOT INTRINSICALLY REQUIRED FOR ENCC GUT COLONIZATION

To determine the tissue specific requirement for RDH10, we excised *Rdh10* specifically from neural crest cells using *Rdh10*$^{flox/flox}$*; Wnt1Cre* mice. As can be observed in E9.5 whole embryos (Figure IV-10) and E15.5 and E18.5 guts (Figure IV-11), *Rdh10*$^{flox/flox}$*; Wnt1Cre* embryos display normal neuronal differentiation and are indistinguishable from their wild-type littermates in the pattern and density of stained mature neurons, indicating that RDH10 is not intrinsically required within NCCs.

Consistent with previous results, section immunohistochemistry reveals neural crest cell migration abnormalities and that loss of *Rdh10* results in non-neural crest cell death in regions around the foregut (Figure IV-14), indicating that dying cells are not neural crest cells, but may be supporting cells in the microenvironment (Figure IV-15). Interestingly, this zone of cell death corresponds with the region of *Rdh10* expression (Figure IV-16).

In avian models, as ENCCs passed through the paraxial tissues surrounding the foregut, they became *Crabp1*+, rendering the cells able to respond to the RA in the surrounding environment (Simkin et al., 2013). *Rdh10*$^{trex/trex}$ mutants and wild-type littermates at E9.5 and E10.5 were stained for *Crabp1* expression, which revealed predominantly reduced signal around the developing mutant gut region (Figure IV-20). The lack of *Crapb1* expression can be interpreted as requiring either RDH10 or RA signaling to acquire CRABP1 on ENCCs, so the absence of RA resulted in an inability to migrate into the gut, or that the lack of *Crabp1* expression in *Rdh10*$^{trex/trex}$ embryos was simply a consequence of lacking ENCCs. Without further experimentation, we are unable to determine which interpretation is more likely, as CRABP1 is known to be responsive to RA, so one might infer ENCCs were unable to migrate into the foregut due to the lack

of *Crabp1* expression is due to the lack of RDH10 and RA, but there are Crabp1+ NCCs throughout the rest of this animal that seem unaffected by the retinoid deficiency.

Altogether, these data indicate a role for RDH10 and RA signaling in regulating ENCC entry into the foregut via extrinsic factors such as the ENCC microenvironment, and not in ENCCs themselves.

EXTRINSIC ENCC FACTORS INFLUENCE ENS DEVELOPMENT IN *RDH10*$^{TREX/TREX}$

As highlighted in the introduction various pathways have been implicated in ENS development through genetic analysis of HSCR patient samples and mouse models with aganglionosis. Unfortunately, the relations between these pathways are not well defined including how retinoid signaling affects and is affected by components extrinsic to ENCC development, particularly how RA may play a role in targeting known ENS signaling pathways, the gut microenvironment, and as a modifier of other HSCR models.

Retinoids play a role in the enteric nervous system signaling pathways that cause a similarly devastating total intestinal aganglionosis phenotype

Although great strides have been made in the HSCR field to identify genes influencing ENCC migration to form the ENS, there is still much to learn. To evaluate if RDH10 causes total intestinal aganglionosis via genetic interactions between RA and known ENCC developmental genes, we utilized *in situ* hybridization, qPCR and RNA Seq to assess the effects of retinoid deficiency on their spatiotemporal activity.

We analyzed the *Ret, Gdnf* and *Gfrα1* expression using *in situ* hybridization and qPCR. *Ret*, *Gdnf* and *Gfrα1* mutants display a similar total intestinal aganglionosis phenotype as *Rdh10*$^{trex/trex}$ embryos. Expression analysis via qPCR of all three of these genes was significantly decreased in *Rdh10*$^{trex/trex}$ embryos (Figure IV-18) suggesting that RDH10 and RA signaling may have a role in regulating GDNF-RET-GFRα1 signaling during ENS development. *In situ* hybridization reveals complete absence of *Ret*+ ENCCs

within the *Rdh10*$^{trex/trex}$ mutant guts (Figure IV-17). Given that few ENCCs migrate into the *Rdh10*$^{trex/trex}$ mutant guts (Figure IV-12, Figure IV-13), the lack of *Ret* expression can be interpreted as one of two things: either RDH10 and RA signaling are required for acquiring RET on ENCCs and absence of RET in *Rdh10*$^{trex/trex}$ ENCCs inhibits them from migrating into the gut or RDH10 and RA signaling have no direct role in regulation of *Ret* expression and lack of *Ret* expression is just a consequence of missing ENCCs in *Rdh10*$^{trex/trex}$ embryos. However, preliminary motif analysis suggests that *Gdnf* has a putative Retinoic acid receptor (RAR) binding site upstream of the coding region, implying a possibility that RA signaling may directly control *Gdnf* expression and therefore is required for the GDNF-RET-GFRα1 complex. It is important to visualize the expression pattern of *Gdnf* within the surrounding *Rdh10*$^{trex/trex}$ mutant gut paraxial mesenchyme to determine how the lack of RA signaling affects this important chemoattractant. Additionally, a role for RA signaling has already been suggested in avian models, as vagal NCCs respond to RA signaling from the environment by upregulating *Ret* expression and thus becoming GDNF-responsive (Simkin et al., 2013). Additionally, *Gdnf*$^{+/-}$ mutants have decreased *Ret* expression in the myenteric plexus (Shen et al., 2002), which suggests that *Gdnf* may be a regulator of *Ret*. Therefore, if RA has a role in directly regulating *Gdnf,* it may then indirectly regulate *Ret*.

Sox10, Phox2b, *Pax3* and *Ednrb* also play important roles in ENS development, as homozygous *Sox10*^{lacZ}, *Phox2b* and *Pax3*, as well as *Sox10*$^{Dom/+}$*; Edn3*$^{ls/ls}$ and *Sox10*$^{Dom/+}$*; Ednrb*$^{sl/sl}$ double mutants exhibit total intestinal aganglionosis. At E9.5, we note *Sox10* expression in the developing wild-type gut, and no *Sox10* expression in the mutant developing gut (Figure IV-19). This lack of Sox10+ ENCCs in the developing gut was not unexpected, as the lack of ENCCs was evidenced in previous experiments (Figure IV-12, Figure IV-13). This suggests an indirect effect of RA deficiency, because

ENCCs are unable to enter into the foregut, and thus there will be no Sox10+ ENCCs in the gut during development. Molecular analysis of *Phox2b*, *Pax3* and *Ednrb* in *Rdh10*$^{trex/trex}$ mutant and wild-type littermates at E9.5 revealed significantly decreased levels of expression (Table VII-5), indicating that RA may act in the same pathways as many of these important ENS developmental pathways.

Retinoids play a role in *Rdh10*$^{trex/trex}$ microenvironment maintenance

In addition to our targeted gene approach to understand the pathogenesis of the *Rdh10*$^{trex/trex}$ mutant phenotype, our RNA Seq data provided an unbiased approach to understand additional changes that contribute to the total intestinal aganglionosis phenotype in *Rdh10*$^{trex/trex}$ mutant. Here we discuss changes in ENS development genes that also play a role in the maintenance of the ENS microenvironment (*Gdnf, Edn3, L1cam*), as well as the numerous extracellular matrix (ECM) components identified via RNA Seq KEGG pathway analysis.

Gdnf is found in the surrounding gut microenvironment and acts as an ENCC chemoattractant. The potential role of RA signaling on *Gdnf* expression has previously been discussed. *Edn3* is another component found in the surrounding microenvironment that acts to maintain a permissive gut environment. Using RNA Seq data as a first pass of how changes in expression of pathways involved in ENS development are affected by RA deficiency, we observed a slight decrease in expression in *Rdh10*$^{trex/trex}$ mutants (Table IV-1). *L1Cam* has been associated with modulating ENCC migratory efficiency and neurite outgrowth, and has been suggested as an HSCR modifier. *L1Cam* RNA Seq expression data showed a significant ($p<0.05$) decrease in mRNA levels (Table IV-2), suggesting that RA may act in controlling the ENCC ability to enter into the foregut by acting through L1CAM.

Preliminary data from RNA Seq experiments revealed the extracellular matrix as the top changed KEGG pathway in the *Rdh10*$^{trex/trex}$ mutants as compared to their wild-type littermates. Unlike what we had initially hypothesized, the majority of the ECM differences were not seen as significant up-regulation of "non-permissive" and "inhibitory" ECM components or as downregulated "permissive" components in *Rdh10*$^{trex/trex}$ embryos, compared to wild-type littermates. However, the numerous small changes in multiple ECM components indicate that the overall composition of the ECM as a cohesive unit is disrupted. This potential role of RA in modulating the ECM resulting in total intestinal aganglionosis is particularly enticing, as it has been previously postulated that an abnormal ECM microenvironment is associated with HSCR (Alpy et al., 2005). The following subheadings gives a brief introduction to particularly interesting ECM components and how they important for NCCs, ENS development, VAD or *Rdh10*$^{trex/trex}$ RNA Seq results.

Introduction to the extracellular matrix (ECM)

The ECM provides a scaffold for cell attachment and provides signals to promote adequate cell function and behavior (Frantz et al., 2010). Characteristic components of the interstitial matrix include fibril-forming proteins (Barber et al., 2014), such as collagens, elastins, fibrillins, and fibronectins, whereas the basement membrane is a specialized sheet of cells containing laminin, collagen IV and heparan sulfate proteoglycans (Tsang et al., 2010). Cell adhesion molecules (CAM) are located on the surface of a cell and connect it to the extracellular matrix. There are several families of adhesion receptors, including integrins, immunoglobulins (such as L1CAM and N-CAM), and cadherins (Albelda and Buck, 1990). Proteases are particularly important for migrating NCCs, as they cleave cell adhesion molecules, allowing for easier migration (Taneyhill and Padmanabhan, 2014).

Relationship between Extracellular Matrix Proteins, Cell Adhesion Molecules and Neural Crest Cells

During development, cell movement is exquisitely orchestrated, partly through to the ability of cells to talk to one another and their surrounding environment. This intercellular movement is mediated by cell-cell interactions, spatiotemporal distribution of ECM proteins and CAMs, and chemotactic signals (Leckband and Prakasam, 2006; Theveneau and Mayor, 2012, 2014).

A notable example of this is when neural crest cells undergo an epithelial-to-mesenchymal transition (EMT). For neural crest cells to successfully emigrate from the neural tube, cells must temporarily lose their intercellular adhesion properties, yet maintain contact with a substrate on which to migrate, be free from physical obstacles, and acquire migratory potential (Duband and Thiery, 1982; Newgreen and Gibbins, 1982; Savagner, 2015; Sternberg and Kimber, 1986; Taneyhill and Padmanabhan, 2014). These requirements indicate that the basal lamina portion of the basement membrane must be broken down for cells to emigrate, and in NCC this is facilitated by various secreted proteases, including ADAM-10, and matrix metalloproteases 2 and 9 (MMP2 and MMP9) (Taneyhill and Padmanabhan, 2014).

Part of the process of NCC emigration requires the dynamic expression of ECM components, which continues to change throughout early development as NCCs continually interact with their microenvironment (Perris and Perissinotto, 2000). Prior to detachment from the neural tube, NCCs express E-cadherin but this is replaced with N-cadherin as NCCs delaminate and begin to migrate (Erickson and Perris, 1993; Lim and Thiery, 2012; Nakagawa and Takeichi, 1995; Taneyhill, 2008). During EMT, to increase their migratory potential while simultaneously reducing intercellular adhesion, it has been proposed that migrating neural crest cells bind to a fibronectin substratum using integrins, while reducing the level of N-cadherin intercellular adhesion during NCC migration

(Monier-Gavelle and Duband, 1997). As N-cadherin is downregulated to allow for NCC migration (Cheung et al., 2005), Cadherin 6 is upregulated, which has been shown to assist in cell motility by assisting in NCC detachment (Clay and Halloran, 2014; Nakagawa and Takeichi, 1995; Park and Gumbiner, 2010). This cadherin switching results in the down-regulation of cadherins, which normally maintain tight cell-cell contacts, thus allowing the cell to become free. Thus, decreased adhesion promotes cell motility (Perris and Perissinotto, 2000; Theveneau and Mayor, 2012).

After NCC have delaminated from the dorsal neural tube and begun to migrate through the embryo, further changes in the spatiotemporal expression of ECM proteins occurs, influencing the way NCC interact with their microenvironment (Perris and Perissinotto, 2000). The regulation of neural crest cell migration can be broadly broken down into being controlled by permissive, non-permissive, or inhibitory components. Permissive components support NCC movement, non-permissive ones promote weak cell-adhesion but do not aid in locomotion, and inhibitory components impede NCC migration (Perris and Perissinotto, 2000). Generally, ECM components are considered to play a permissive role (Theveneau and Mayor, 2012), but even within the family of ECM proteins, certain proteins are more permissive than others. It has been proposed that because NCC migration can be regulated by spatiotemporal changes in the ECM components, the ratio of permissive to non-permissive ECM components, and the level of inhibitory components are key to migratory success (Perris and Perissinotto, 2000). Additionally, individual ECM components have varying levels of permissiveness depending on the spatiotemporal location, which needs to be carefully considered when determining what relative gene expression changes may mean in the context of RDH10 and RA signaling on the development of the ENS. For example, laminins have been cited as NCC migration promoting elements near the neural tube during initial NCC migration

(Perris, 1997), while in the enteric nervous system, increased laminin in both mouse and humans in late ENS colonization has been associated with the inhibition of NCC migration and the pathogenesis of colonic aganglionosis (Alpy et al., 2005; Druckenbrod and Epstein, 2009; Parikh et al., 1992).

ECM-Modulated ENS Colonization

As indicated previously, spatiotemporal distribution of ECM components has a profound effect on NCC migration. And with the longest migratory path of NCCs being into the gastrointestinal tract, it is not surprising that ECM abnormalities may be responsible in the pathogenesis of HSCR (Alpy et al., 2005; Parikh et al., 1992). Numerous ECM components have been implicated in the proper development of ENCC and the formation of the ENS, such as laminin, *MMP2* and *MMP9*, *β1 integrin*, *L1Cam* and *N-Cam* (Alpy et al., 2005; Anderson, 2010; Anderson et al., 2006c; Breau et al., 2009; Breau et al., 2006; Druckenbrod and Epstein, 2009; Fu et al., 2006).

In a study examining human patient bowel specimens of distal aganglionic and proximal aganglionic segments, laminin was found to be highly expressed in the aganglionic zone of the colon, along with differences in laminin intensities in the inner and outer muscular layers (abnormal ECM distribution) and reorganization of the subepithelial basement membranes of the aganglionic versus ganglionic colon preparations (Alpy et al., 2005; Parikh et al., 1992). Consistent with this human study, data from mouse experiments suggest that a change in the gut microenvironment occurs at E14.5 when the gut is no longer permissive to migrating ENCCs, and that high laminin levels may play a role in this non-permissive environment (Druckenbrod and Epstein, 2009).

During ENCC migration, cells must be able to attach and detach to other cells and substrates to continue effective migration. Therefore, it is imperative that proteases are

functional to allow for adequate cell detachment (Anderson, 2010). MMP2 and MMP9 inhibition result in disrupted migration of ENCCs in mouse gut explants (Anderson, 2010). MMP2 is expressed within the developing gut environment and is necessary for the complexity of the NCC network (Anderson, 2010; Anderson et al., 2006c).

Integrins play an important role in normal development by interacting with matrix proteins (Tsang et al., 2010). β1 integrin depletion in ENCCs result in their failure to colonize the gut completely, leading to descending colon aganglionosis, along with an abnormal ganglia network organization (Breau et al., 2006). Interestingly, ENCCs in which β1 integrin are depleted, colonized low Fibronectin (FN) and Tenascin (TNC) environments. But in areas of high FN and TNC, such as the hindgut and cecum, *β1 integrin* mutants showed abnormally aggregated ENCCs and distal colonic aganglionosis. This suggests that β1 integrins are necessary to overcome TNC-mediated inhibition and enhance FN-dependent migration in the cecum and distal hindgut (Breau et al., 2009). These results highlight the delicate relationship of cellular adhesion between ENCC and their microenvironment to allow for normal migration through the gut (Barlow, 2014). Due to a similar phenotype induced by blocking MMPs, and the fact that integrins can act as MMP receptors, it has been postulated that β1 integrins and MMPs may interact in the developing gut (Anderson, 2010).

One cell adhesion molecule expressed by early migrating ENCCs which has a significant effect on ENS development is L1CAM by making ENCC movement more efficient. Although *L1Cam* mutant mice have a functional ENS at birth, they do exhibit delayed colonization during development, and gut explants cultured in the presence of L1Cam-function-blocking antibodies had more NCCs which broke away from the typical chain migration population to migrate independently, then subsequently become immobile (Anderson et al., 2006c). This adhesion molecule acts as a modifier for HSCR-

associated genes like *Sox10*, *Ednrb* and *Edn* (Anderson et al., 2006c; Wallace and Anderson, 2011; Wallace et al., 2010; Wallace et al., 2011).

Lastly, it has been shown that the addition of polysialic acid (PSA) to N-CAM alters cell-cell interactions. This PSA addition is modulated by bone morphogenic protein (BMP), and modulating BMP results in reduced ENCC migration into the distal bowel and reduction of enteric neuron ganglion formation by altering cell-cell interactions, suggesting that PSA-NCAM may influence HSCR penetrance (Fu et al., 2006).

Because these ECM components have been implicated in the pathogenesis of HSCR, it is important to investigate these components in the context of *Rdh10*$^{trex/trex}$ embryos as well as with other known HSCR genes, as they may act as modifiers to increase the penetrance or severity of the HSCR phenotype.

Vitamin A Deficiency and Extracellular Matrix

Vitamin A and its conversion to retinoic acid play significant roles in embryonic development and continued postnatal processes. The actions of vitamin A can be modulated through transcriptional and non-transcriptional regulation. RA signaling affects the synthesis of many ECM proteins (such as collagen, laminin, fibronectin, elastin and proteoglycans and entactin) and cellular membrane receptors (such as integrins), and may therefore have an effect on the many organ systems in which ECM components play a role (Aguilar et al., 2009; Axel et al., 2001; Barber et al., 2014; Lee and Jeong, 2012; Matsui, 1996). Of particular interest in this thesis work is whether vitamin A metabolism affects ECM components, which subsequently alters ENCC migration, and formation of the ENS, leading to a Hirschsprung Disease phenotype.

Modifying the structure and composition of ECM in Vitamin A Deficiency Diseases (VADD) can lead to pathological changes in affected organ systems (Barber et al., 2014). In most VADD organ phenotypes, excessive ECM deposition is a major

complication which often leads to fibrosis. A thicker BM may lead to organ dysfunction and eventually may lead to organ failure (Barber et al., 2014).

In VADD, the kidney has increased collagen IV, alongside a decrease in MMP 2 and 9 (Marin et al., 2005). The decrease in MMPs contributes to a thickened BM, as the BM degrading capacity is reduced with less MMP activity (Barber et al., 2014). In the lungs of rats subjected to a VAD diet, a thickened alveolar BM was observed alongside a similar increase in collagen IV and decrease in MMP 2 and 9 as seen in kidneys, but also experience increased collagen I, and lowered elastin and laminin proteins (Esteban-Pretel et al., 2013). Not unexpectedly, the liver also exhibits ECM changes when subjected to VAD. The liver is responsible for the storage of most of the body's vitamin A in the form of retinyl ester droplets in hepatic stellate cells (HSC). These HSCs are important for secreting the correct amount of ECM molecules, and MMPs (Geerts, 2001). When HSCs are compromised due to liver injury, the role of ECM secretion is also compromised and may lead to liver fibrosis (Geerts, 2001).

Importantly, other chronic diseases, such as alcoholism and diabetes, can further exacerbate VADD phenotypes (Clugston and Blaner, 2012). ECM components collagen IV, laminin 1 and fibronectin are increased in VAD (Aguilar et al., 2009). In the skin, RA promotes collagen production in the dermis, which is regulated by MMP and hyaluronidase (HAse) production. Too much MMP and HAse production leads to elevated collagen degradation and ineffectual skin maintenance. Type 1 diabetic mice and rats subjected to a VAD diet experienced increased MMP2 and HAse activity, indicating a possible relationship between diabetes and VAD deficiency-induced skin abnormalities (Takahashi and Takasu, 2011).

It is logical to conclude that if vitamin A deficiency can cause changes in ECM composition, then it may be possible to reverse any negative effects via vitamin A

supplementation. However, it is important to note that there are contradictory studies regarding the efficacy of retinoid or vitamin A supplementation (Barber et al., 2014; Zhou et al., 2012).

Thus, many studies have described changes in organs systems such as the kidneys, lungs, liver and skin due to VAD related ECM changes. Furthermore, it has been well established that appropriate levels of ECM components are important for neural crest cell migration. Therefore, it is not unreasonable to assume that VAD may cause additional ECM changes that affect GI tract development, and specifically affect the migration of vagal neural crest cells into the developing gut.

ECM component changes in* Rdh10$^{trex/trex}$ *mutants

It is well known that appropriate spatiotemporally expressed ECM components are vital for neural crest cell migration. Combined with RNA Seq data showing perturbations in numerous ECM components, this suggests that ECM changes in the gut microenvironment may play a significant role in the pathogenesis of total intestinal aganglionosis seen in *Rdh10$^{trex/trex}$* embryos.

Numerous ECM components were identified as being altered in *Rdh10$^{trex/trex}$* mutants. In general, we expected to find upregulated "non-permissive" and "inhibitory" ECM components and downregulated "permissive" components in *Rdh10$^{trex/trex}$* embryos, compared to wild-type littermates. Using RNA Seq to broadly examine the ECM components known to play a specific role in ENS formation, ENCC development, or that are regulated by retinoid signaling (Table IV-2), we found two genes (Collagen 1A1 and Collagen 6A3) with greater than two-fold difference with significant p-values ($p<0.05$), and surprisingly, these genes were previously reported as "permissive" components. Two more "permissive" components, Fibronectin, and Tenascin-C had greater than 1.5 expression fold increases with significant p-values ($p<0.05$), again opposing our

hypothesis. One gene that followed our hypothesis in fold change directionality was Aggrecan, an "inhibitory" component, with a 1.829 fold increase ($p<0.05$). In contrast to what we expected, none of the proteases (MMP2, MMP9, or ADAM10) were significantly altered in *Rdh10*$^{trex/trex}$ embryos. In an effort to validate RNA Seq data using qPCR, we compared *Rdh10*$^{trex/trex}$ mutants to wild-type littermates, and found that LAMC3 had a 53% reduction in relative expression level ($p<0.05$), and COL1A1, COL1A2, TnC and FN1 had a 172%, 136%, 122% and 120% relative increase in expression levels, respectively (Figure IV-21), with both COL1A1 and COL1A2 relative increases being significant ($p<0.05$). Surprisingly, of the known retinoid mediated ECM components, only relative expression levels of Laminin C3, Collagen 1A1, 1A2 and 6A3 were significantly changed ($p<0.05$). The reduction of LAMC3 was an interesting finding, as laminins are considered to be overall "permissive" components in NCC migration, but were found to be highly expressed in the distal aganglionic bowels of mice and humans. However, high laminin causality has not been established. It is not clear if the elevated level of laminin is the cause of the HSCR phenotype or a result of the failure of ENCCs to enter the distal bowel and remodel the ECM.

From the numerous studies investigating the ECM in regards to its role in NCC migration and in VADD, it is clear that appropriate spatiotemporal distributions of these important components have a profound effect normal development. To our surprise, we did not see an overt pattern of upregulated "non-permissive" and "inhibitory" ECM components or downregulated "permissive" components in *Rdh10*$^{trex/trex}$ mutants. Most of the ECM analysis reveals low fold change differences in individual components, but we suspect that the overall changes in the gestalt of the ECM play a larger role in comprehensively changing the permissiveness of the microenvironment that ENCCs must traverse. In the future it will be necessary to investigate which ECM components may

specifically be necessary in the microenvironment directly surrounding the developing foregut, which the ENCCs must traverse, and use immunohistochemistry to visualize how the ECM components are spatiotemporally modified in *Rdh10*$^{trex/trex}$ mutants.

RDH10 HAS NOT BEEN CONFIRMED NOR DENIED AS POTENTIAL HSCR MODIFIER GENE

Our preliminary investigations of crossing *Rdh10*$^{trex/+}$ to lines known to have defects in NCC or ENS development did not identify RDH10 as a modifier of HSCR through *Pax3*$^{+/-}$, *Gcnf*$^{+/-}$ or *Tcof1*$^{+/-}$. However, this just suggests that the development of the ENS in these compound heterozygous crosses suggest that RDH10 likely does not act through the same ENCC developmental pathways as these genes (such as p53 dependent apoptosis pathway (*Pax3* and *Tcof1*) or by modulating neural stem cell populations (*Gcnf*)), but does not rule out the possibility that RDH10 may act as a modifier of other important ENS development or microenvironmental genes.

General Conclusion

Results from these studies have established RDH10 and vitamin A deficiency as new models for studying HSCR, providing information regarding the spatiotemporal requirements for RA during embryonic intestinal development, the pathogenic cellular mechanisms of RDH10 deficient animals, as well as the interactions of RA with pathways that govern normal ENS NCC colonization and ECM maintenance.

Future Directions

Here I outline potential future experiments that would further improve our knowledge of how RA might act in relation to the formation of the ENS, normal development of the gastrointestinal system, and in the context of maintaining a NCC permissive ECM.

ANALYZE DIRECT BINDING OF RA TO IMPORTANT ENS DEVELOPMENT GENES

Using Motif Map (http://motifmap.ics.uci.edu/), we searched for putative retinoid X receptor binding motifs 1000bp upstream and downstream of ENS development genes and ECM components of interest that were altered in *Rdh10*$^{trex/trex}$ molecular expression assays. We identified a putative retinoid binding site upstream of *Gdnf* . To test if this putative RXR binding site is active in *Gdnf*, thus making *Gdnf* responsive to retinoid signaling, we would clone the *Gdnf* promotor including the putative RXR binding site then fuse it to a luciferase reporter. After transfecting these plasmids into a retinoid responsive cell line, we could test if RA induces increased transcription by measuring luciferase activity after the addition of RA to the media. If there is no difference with RA-deficient versus RA-supplemented media, we know that this putative binding site is not active. However, if we see that RA increases luciferase activity, we would need to determine if the putative RXR binding site is responsible for RA responsiveness. To do this, we would mutagenize the putative RXR binding site, and test if RA induces transcription of the mutagenized *Gdnf* promotor. If the addition of RA results in the same increase in luciferase as seen in the non-mutagenized version of the plasmid, we know the assumed RA responsiveness was not due to the putative RXR site. If the addition of RA does not result in an increase in luciferase activity, we can conclude that the RXR binding site is active and does induce transcription of *Gdnf*, and thus, *Gdnf* is directly responsive to RA.

EXAMINE ENS CELL POPULATION FOR PRESENCE OF GLIAL CELLS AND APPROPRIATE RATIO OF NEURONAL SUBTYPES

Enteric glial cells, also derived from neural crest cells, begin differentiating after neurons, around E11.5 (Young et al., 2003). These cells have been well characterized for their role as support cells of the enteric neurons, necessary for providing nourishment,

physical support and protection. However, this cell type is also important for regulating synaptic transmission, regulation of gut motility, gut secretion and absorption and immunological responses (reviewed briefly in (Boesmans et al., 2015)). Glial cells are frequently identified by immunohistochemistry, staining positively with GFAP and S100β, along with many overlapping antibodies that stain progenitor cells (such as SOX10 and p75) (Coelho-Aguiar et al., 2015).

Because the function of the ENS relies on both neurons and glia, it is important to stain the guts of rescued *Rdh10*$^{trex/trex}$ as well as the distal colons of RDH10 conditional lines, *RDH10*$^{flox/flox}$*; Wnt1Cre* and *RDH10*$^{flox/flox}$*; ER*^{T2}*Cre* to confirm the presence of this important cell type. We plan to use the GFAP and S100β antibodies. We do not expect to see a difference in the glial populations, as it has been suggested that although retinoids may enhance neuronal differentiation, they have not been found to block glial differentiation (Sato and Heuckeroth, 2008).

In addition to checking for unaltered glial populations, it would be interesting to examine if rescued *Rdh10*$^{trex/trex}$, and *RDH10*$^{flox/flox}$*; Wnt1Cre* intestines develop appropriate populations of neuronal subtypes, which can be a positive indicator that the ENS would function properly (as in (Hotta et al., 2013)). To do this, we would stain neurons for the major neuronal populations, choline acetyltransferase (ChAT) and nitric oxide synthase (NOS) neurons.

INVESTIGATE ECM COMPONENTS AND LEVEL OF PERMISSIVENESS SPECIFIC FOR ENCC MIGRATION

To further investigate how mutant NCCs respond to different ECM components and densities of the matrix, we can conduct *in vitro* assays culturing ENCCs harvested from the vagal stream of E8.5 *Wnt1Cre; R26YFP* embryos on various substrates. We could compare differences in migratory dynamics on different ECM coated plates,

varying the coating of the plate (collagen, fibronectin or laminin), and the collagen gel media conditioning treatments, by adding additional ECM components to the gel. ENCCs would be plated, and analyzed after growing overnight. We expect that when ENCCs are cultured with a denser ECM, the cells will not migrate as efficiently. Results from these experiments would allow us to perturb the migratory environment and determine how changes in ECM components affect the ability of these cells to migrate, and will also shed light onto which ECM components play the most important role for normal ENCC migration.

IDENTIFY NOVEL CAUSES OF HSCR USING NEXT-GENERATION SEQUENCING TECHNIQUES

As stated before, we only know the genetic cause of about half of the cases of HSCR, and it is important to continue to investigate potential causes of this devastating disease. We propose the use of next-generation sequencing techniques as a way to identify important new pathways.

Potential experiment: RNA sequencing to analyze difference of rescued and vehicle-treated *Rdh10*$^{trex/trex}$ microenvironmental changes

Another interesting experiment would be to analyze the differences in the microenvironment of retinal rescued and vehicle-treated *Rdh10*$^{trex/trex}$ tissues. In a model examining intestinal adaptation using vitamin A deficiency as a model, VAD resulted in changes in expression of ECM components, such as collagen IV (Swartz-Basile et al., 2003). Here, we propose using the same twice per day retinal gavage rescue between E8.5-E9.5 and harvest the embryos at late E9.5, and conduct an RNA sequencing experiment on the same tissues as RNASeq2 (Figure II-13). Using KEGG pathway analysis, it would be interesting to look at what pathways were "rescued" with retinal. We predict that the ECM components would not be as drastically different between the

Rdh10$^{trex/trex}$ tissues and their wild-type vehicle treated littermates. For adequate controls, we would also need to re-run untreated *Rdh10*$^{trex/trex}$ embryonic tissues as well.

Potential Experiment: Investigate RDH10 as a modifier gene by crossing *Rdh10*$^{trex/+}$ to other ENCC development genes

Only half of the HSCR cases are attributable to known genetic defects, and it is therefore necessary to explore other pathways and potential modifiers of this disease. It has been established that numerous genes may act as modifiers to the HSCR phenotype. Using mice readily available in the lab, we crossed *Rdh10*$^{trex/+}$ to different heterozygous mice that have previously shown a NCC phenotype when analyzed in homozygous mutants. Although there was no distal colonic aganglionosis phenotype when *Rdh10*$^{trex/+}$ was crossed with *Pax3*$^{+/-}$, *Gcnf*$^{+/-}$ or *Tcof1*$^{+/-}$, we will continue to investigate RDH10 and vitamin A deficiency as potential modifiers of the HSCR phenotype.

We speculate that *Rdh10*$^{trex/+}$ crossed to *L1cam*, *Gdnf*, *Ret*, *Sox10*, *Ednrb* or *Edn3* mutants may cause a distal colonic aganglionosis phenotype, as these genes are known to be modified by other genes, or the expression in our *Rdh10*$^{trex/trex}$ embryos was significantly reduced, suggesting that RDH10 may act through downstream pathways and could act to potentiate the mild HSCR phenotype. Additionally, after further analyzing changes in the ECM using cryosections of *Rdh10*$^{trex/trex}$ embryos, it would be interesting to cross *Rdh10*$^{trex/+}$ to animals with heterozygous mutations in those components, then analyze through which pathway RDH10 acts to modify the development of ENCCs, colonization of the gut, and formation of the ENS.

Potential Experiment: Whole exome and genome sequencing

In an effort to help discover genes that play a role in the pathogenesis of HSCR in human cases, we suggest whole exome and whole genome sequencing of patient samples as an ideal way to identify new causative mutations. This type of approach would be well

suited to finding new genes that play a role in HSCR, as well as modifier genes. With the decrease in whole exome sequencing costs, it is now faster and cheaper to sequence the whole exome rather than just targeting known mutations.

Currently, our idea is to collaborate with Children's Mercy Hospital and the University of Kansas Medical center, through a joint IRB that is already in place. Our point of contact would be Stephen Kingsmore. The first step in starting this sequencing project is to find ideal candidates with HSCR. Thus far, we have identified 3 potential candidates that have been treated at KUMC, and believe recruiting these families to this study would be well received, as knowing the potential inheritance of these mutations could help families with planning subsequent children.

If we are able to identify new mutations that contribute to the etiology of HSCR, we can begin making new mouse models of these mutations to begin the process of understanding the pathogenesis of those mutations.

INVESTIGATE VITAMIN A SUPPLEMENTATION AS A POTENTIAL RESCUE FOR ENVIRONMENTALLY-INDUCED VAD IN RODENTS AND HUMANS

Currently, all of the models of total intestinal aganglionosis are genetic, including this new *Rdh10*$^{trex/trex}$ model. However, the ability to modulate the phenotype through dietary modification brings up the interesting possibility that perhaps some cases of HSCR are modulated through a pathway such as RA, and vitamin A metabolism (i.e. RA as a modifier of HSCR). In addition to looking for genes that RDH10 and RA may modify, we would also like to investigate how VAD plays a role in HSCR in rodent models and eventually in humans.

Chronic diseases, such as alcoholism, can further exacerbate VADD phenotypes. Chronic alcoholism further aggravates VAD mediated liver damage, as chronic alcohol consumption is known to deplete retinol stores, by increasing the rate of catabolism of

retinol, leading to similar problems as those found in VADD (Clugston and Blaner, 2012). Numerous studies in rodent models have explored chronic alcohol consumption in association with decreased retinoid status (reviewed in (Clugston and Blaner, 2012)). It would be an interesting experiment to administer alcohol to an animal model where embryos exhibit distal colonic aganglionic, such as *Rdh10*$^{flox/flox;}$ *ERT2Cre* animals (given tamoxifen at E7.5), to evaluate if the decrease in retinol availability due to maternal chronic alcohol use exacerbates the phenotype. Additionally, mothers of retinal rescued *Rdh10*$^{trex/trex}$ embryos (with twice daily retinal gavages from E7.5-9.5) could also be a good model to examine if alcohol use inhibits the retinal rescue.

In the context of a greater (human) public health issue, if we note that HSCR incidence is higher in countries with VAD (currently data not available), we may be able to investigate the possibility that vitamin A fortification may lead to decreased incidence of HSCR, similar to how maternal ingestion of folic acid reduces the incidence of neural tube defects (Pitkin, 2007). Because we do not currently have that data, we can look at the United States, where VAD alone is an uncommon occurrence, except in the alcoholic population and women with low socioeconomic status (SES), as alcohol consumption has been associated with decreased liver stores of retinol (Clugston and Blaner, 2012). Retrospective chart review may help us determine if there is a link between alcohol consumption or low SES and the incidence of HSCR. We suspect that alcohol consumption will be associated with HSCR cases with *L1Cam* mutations, as ethanol has been shown to block L1-mediated cell adhesion (Greenberg, 2003).

According to the 2012 Substance Abuse and Mental Health Services Administration (SAMHSA), in 2012 in the United States, 87.6% of people 18 and up reported drinking alcohol in their lifetime, and approximated 17 million adults had an alcohol use disorder, which included 5.7 million women (SAMHSA, 2012). Apart from

the economic, social and family burden, and morbidity and mortality that alcohol use disorders present, there is also an alarming problem alcohol can pose on unwilling participants, such as fetuses. It is estimated that Fetal Alcohol Syndrome (FAS) occurs between 2-7 cases per 1000 (Stratton, 1996), and FAS spectrum disorders may be as high as 20-50 cases per 1000 (May et al., 2009).

First, it would be important to determine the vitamin A status of women of child-bearing age with a history of alcohol consumption. In 2002, it was estimated to cost $15 to measure retinol concentration of blood preserved on filter paper. This test is particularly convenient for collecting blood samples, as it only requires a finger prick of 10-12μL of blood soaked into a filter paper, as compared to a minimum of 200 μL with typical venipuncture which requires refrigeration when transported, and can be analyzed later, using high performance liquid chromatography system. However, a new technology to measure retinol binding protein (RBP) by antibody staining is estimated at $1, and an even newer method to semi-quantitatively assess RBP in whole blood is estimated at 25 cents (de Pee and Dary, 2002). Measuring RBP concentration is easier to analyze than serum retinol levels, and correlates well with serum retinol concentrations, and should be a good indicator of VAD status. With these retinol and RBP measuring capabilities and increasingly low cost, it should be financially feasible to analyze the vitamin A status of female alcohol consumers in the United States.

If differences in vitamin A status of female alcohol consumers versus females who abstain from alcohol use are found, women interested in becoming pregnant could be provided vitamin A supplementation to improve their retinol levels to a healthy level (>0.70 μmol/L). If successful, studies such as this may eventually lead to a reduction in the incidence of RA acting as a modifier to genetic disease such as HSCR.

VI. REFERENCES

Aguilar, R.P., Genta, S., Oliveros, L., Anzulovich, A., Gimenez, M.S., Sanchez, S.S., 2009. Vitamin A deficiency injures liver parenchyma and alters the expression of hepatic extracellular matrix. Journal of applied toxicology : JAT 29, 214-222.

Akbareian, S.E., Nagy, N., Steiger, C.E., Mably, J.D., Miller, S.A., Hotta, R., Molnar, D., Goldstein, A.M., 2013. Enteric neural crest-derived cells promote their migration by modifying their microenvironment through tenascin-C production. Developmental Biology 382, 446-456.

Albanese, C.T., Jennings, R.W., Smith, B., Bratton, B., Harrison, M.R., 1999. Perineal one-stage pull-through for Hirschsprung's disease. Journal of Pediatric Surgery 34, 377-380.

Albelda, S.M., Buck, C.A., 1990. Integrins and other cell adhesion molecules. The FASEB Journal 4, 2868-2880.

Alpy, F., Ritie, L., Jaubert, F., Becmeur, F., Mechine-Neuville, A., Lefebvre, O., Arnold, C., Sorokin, L., Kedinger, M., Simon-Assmann, P., 2005. The expression pattern of laminin isoforms in Hirschsprung disease reveals a distal peripheral nerve differentiation. Hum Pathol 36, 1055-1065.

Alvarez, J.O., Salazar-Lindo, E., Kohatsu, J., Miranda, P., Stephensen, C.B., 1995. Urinary excretion of retinol in children with acute diarrhea. The American journal of clinical nutrition 61, 1273-1276.

Amiel, J., Laudier, B., Attie-Bitach, T., Trang, H., de Pontual, L., Gener, B., Trochet, D., Etchevers, H., Ray, P., Simonneau, M., Vekemans, M., Munnich, A., Gaultier, C., Lyonnet, S., 2003. Polyalanine expansion and frameshift mutations of the paired-like homeobox gene PHOX2B in congenital central hypoventilation syndrome. Nature Genetics 33, 459-461.

Amiel, J., Lyonnet, S., 2001. Hirschsprung disease, associated syndromes, and genetics: a review. Journal of Medical Genetics 38, 729-739.

Amiel, J., Sproat-Emison, E., Garcia-Barcelo, M., Lantieri, F., Burzynski, G., Borrego, S., Pelet, A., Arnold, S., Miao, X., Griseri, P., Brooks, A.S., Antinolo, G., de Pontual, L., Clement-Ziza, M., Munnich, A., Kashuk, C., West, K., Wong, K.K.-Y., Lyonnet, S., Chakravarti, A., Tam, P.K.-H., Ceccherini, I., Hofstra, R.M.W., Fernandez, R., Consortium, f.t.H.D., 2008. Hirschsprung disease, associated syndromes and genetics: a review. Journal of Medical Genetics 45, 1-14.

Anderson, R., Newgreen, D., Young, H., 2006a. Neural Crest and the Development of the Enteric Nervous System, in: Saint-Jeannet, J.-P. (Ed.), Neural Crest Induction and Differentiation. Springer US, pp. 181-196.

Anderson, R., Stewart, A., Young, H., 2006b. Phenotypes of neural-crest-derived cells in vagal and sacral pathways. Cell and Tissue Research 323, 11-25.

Anderson, R.B., 2010. Matrix metalloproteinase-2 is involved in the migration and network formation of enteric neural crest-derived cells. Int J Dev Biol 54, 63-69.

Anderson, R.B., Turner, K.N., Nikonenko, A.G., Hemperly, J., Schachner, M., Young, H.M., 2006c. The Cell Adhesion Molecule L1 Is Required for Chain Migration of Neural Crest Cells in the Developing Mouse Gut. Gastroenterology 130, 1221-1232.

Angrist, M., Bolk, S., Halushka, M., Lapchak, P.A., Chakravarti, A., 1996. Germline mutations in glial cell line-derived neurotrophic factor (GDNF) and RET in a Hirschsprung disease patient. Nature Genetics 14, 341-344.

Antipatis, C., Ashworth, C.J., Grant, G., Lea, R.G., Hay, S.M., Rees, W.D., 1998. Effects of maternal vitamin A status on fetal heart and lung: changes in expression of key developmental genes. The American journal of physiology 275, L1184-1191.

Aoto, K., Sandell, L.L., Butler Tjaden, N.E., Yuen, K.C., Watt, K.E., Black, B.L., Durnin, M., Trainor, P.A., 2015. Mef2c-F10N enhancer driven beta-galactosidase (LacZ) and Cre recombinase mice facilitate analyses of gene function and lineage fate in neural crest cells. Dev Biol 402, 3-16.

Asai, N., Fukuda, T., Wu, Z., Enomoto, A., Pachnis, V., Takahashi, M., Costantini, F., 2006. Targeted mutation of serine 697 in the Ret tyrosine kinase causes migration defect of enteric neural crest cells. Development 133, 4507-4516.

Axel, D.I., Frigge, A., Dittmann, J., Runge, H., Spyridopoulos, I., Riessen, R., Viebahn, R., Karsch, K.R., 2001. All-trans retinoic acid regulates proliferation, migration, differentiation, and extracellular matrix turnover of human arterial smooth muscle cells. Cardiovascular research 49, 851-862.

Baillie, C.T., Kenny, S.E., Rintala, R.J., Booth, J.M., Lloyd, D.A., 1999. Long-term outcome and colonic motility after the Duhamel procedure for Hirschsprung's disease. Journal of Pediatric Surgery 34, 325-329.

Barber, T., Esteban-Pretel, G., Marin, M.P., Timoneda, J., 2014. Vitamin a deficiency and alterations in the extracellular matrix. Nutrients 6, 4984-5017.

Barlow, A., de Graaff, E., Pachnis, V., 2003. Enteric Nervous System Progenitors Are Coordinately Controlled by the G Protein-Coupled Receptor EDNRB and the Receptor Tyrosine Kinase RET. Neuron 40, 905-916.

Barlow, A.J., 2014. Chapter 12 - Neural Crest Cells in Enteric Nervous System Development and Disease, in: Trainor, P.A. (Ed.), Neural Crest Cells. Academic Press, Boston, pp. 231-253.

Barlow, A.J., Dixon, J., Dixon, M., Trainor, P.A., 2013. Tcof1 acts as a modifier of Pax3 during enteric nervous system development and in the pathogenesis of colonic aganglionosis. Human Molecular Genetics 22, 1206-1217.

Barlow, A.J., Dixon, J., Dixon, M.J., Trainor, P.A., 2012. Balancing neural crest cell intrinsic processes with those of the microenvironment in Tcof1 haploinsufficient mice enables complete enteric nervous system formation. Human Molecular Genetics 21, 1782-1793.

Baynash, A.G., Hosoda, K., Giaid, A., Richardson, J.A., Emoto, N., Hammer, R.E., Yanagisawa, M., 1994. Interaction of endothelin-3 with endothelin-B receptor is essential for development of epidermal melanocytes and enteric neurons. Cell 79, 1277-1285.

Bendich, A., Langseth, L., 1989. Safety of vitamin A. The American journal of clinical nutrition 49, 358-371.

Billings, S.E., Pierzchalski, K., Butler Tjaden, N.E., Pang, X.-Y., Trainor, P.A., Kane, M.A., Moise, A.R., 2013. The retinaldehyde reductase DHRS3 is essential for preventing the formation of excess retinoic acid during embryonic development. The FASEB Journal.

Bodian, M., Carter, O.O., 1963. A family study of Hirschsprung's disease. Annals of Human Genetics 26, 261-277.

Boesmans, W., Lasrado, R., Vanden Berghe, P., Pachnis, V., 2015. Heterogeneity and phenotypic plasticity of glial cells in the mammalian enteric nervous system. Glia 63, 229-241.

Bogni, S., Trainor, P., Natarajan, D., Krumlauf, R., Pachnis, V., 2008. Non-cell-autonomous effects of Ret deletion in early enteric neurogenesis. Development 135, 3007-3011.

Bolk, S., Pelet, A., Hofstra, R.M.W., Angrist, M., Salomon, R., Croaker, D., Buys, C.H.C.M., Lyonnet, S., Chakravarti, A., 2000. A human model for multigenic inheritance: Phenotypic expression in Hirschsprung disease requires both the RET gene and a new 9q31 locus. Proceedings of the National Academy of Sciences 97, 268-273.

Bondurand, N., Natarajan, D., Barlow, A., Thapar, N., Pachnis, V., 2006. Maintenance of mammalian enteric nervous system progenitors by SOX10 and endothelin 3 signalling. Development 133, 2075-2086.

Bondurand, N., Natarajan, D., Thapar, N., Atkins, C., Pachnis, V., 2003. Neuron and glia generating progenitors of the mammalian enteric nervous system isolated from foetal and postnatal gut cultures. Development 130, 6387-6400.

Breau, M.A., Dahmani, A., Broders-Bondon, F., Thiery, J.P., Dufour, S., 2009. Beta1 integrins are required for the invasion of the caecum and proximal hindgut by enteric neural crest cells. Development 136, 2791-2801.

Breau, M.A., Pietri, T., Eder, O., Blanche, M., Brakebusch, C., Fassler, R., Thiery, J.P., Dufour, S., 2006. Lack of beta1 integrins in enteric neural crest cells leads to a Hirschsprung-like phenotype. Development 133, 1725-1734.

Britsch, S., Goerich, D.E., Riethmacher, D., Peirano, R.I., Rossner, M., Nave, K.-A., Birchmeier, C., Wegner, M., 2001. The transcription factor Sox10 is a key regulator of peripheral glial development. Genes & Development 15, 66-78.

Brooks, A.S., Oostra, B.A., Hofstra, R.M.W., 2005. Studying the genetics of Hirschsprung's disease: unraveling an oligogenic disorder. Clinical Genetics 67, 6-14.

Burns, A.J., Champeval, D., Le Douarin, N.M., 2000. Sacral Neural Crest Cells Colonise Aganglionic Hindgut in Vivo but Fail to Compensate for Lack of Enteric Ganglia. Developmental Biology 219, 30-43.

Burns, A.J., Le Douarin, N.M., 1998. The sacral neural crest contributes neurons and glia to the post-umbilical gut: spatiotemporal analysis of the development of the enteric nervous system. Development 125, 4335-4347.

Butler Tjaden, N.E., Sandell, L.L., Aoto, K., Trainor, P.A., [in preparation]. RDH10 is necessary for initial vagal neural crest cell contribution to embryonic gastrointestinal tract development.

Butler Tjaden, N.E., Trainor, P.A., 2013. The developmental etiology and pathogenesis of Hirschsprung disease. Transl Res 162, 1-15.

Cacalano, G., Fariñas, I., Wang, L.-C., Hagler, K., Forgie, A., Moore, M., Armanini, M., Phillips, H., Ryan, A.M., Reichardt, L.F., Hynes, M., Davies, A., Rosenthal, A., 1998. GFRα1 Is an Essential Receptor Component for GDNF in the Developing Nervous System and Kidney. Neuron 21, 53-62.

Cammas, L., Romand, R., Fraulob, V., Mura, C., Dollé, P., 2007. Expression of the murine retinol dehydrogenase 10 (Rdh10) gene correlates with many sites of retinoid

signalling during embryogenesis and organ differentiation. Developmental Dynamics 236, 2899-2908.

Cantrell, V.A., Owens, S.E., Chandler, R.L., Airey, D.C., Bradley, K.M., Smith, J.R., Southard-Smith, E.M., 2004. Interactions between Sox10 and EdnrB modulate penetrance and severity of aganglionosis in the Sox10Dom mouse model of Hirschsprung disease. Human Molecular Genetics 13, 2289-2301.

Carniti, C., Belluco, S., Riccardi, E., Cranston, A.N., Mondellini, P., Ponder, B.A.J., Scanziani, E., Pierotti, M.A., Bongarzone, I., 2006. The RetC620R Mutation Affects Renal and Enteric Development in a Mouse Model of Hirschsprung's Disease. The American Journal of Pathology 168, 1262-1275.

Carrasquillo, M.M., McCallion, A.S., Puffenberger, E.G., Kashuk, C.S., Nouri, N., Chakravarti, A., 2002. Genome-wide association study and mouse model identify interaction between RET and EDNRB pathways in Hirschsprung disease. Nature Genetics 32, 237-244.

Carter, M.T., 2001. Conservation of RET proto-oncogene splicing variants and implications for RET isoform function. Cytogenetics and cell genetics 95, 169-176.

Chambers, D., Wilson, L., Maden, M., Lumsden, A., 2007. RALDH-independent generation of retinoic acid during vertebrate embryogenesis by CYP1B1. Development 134, 1369-1383.

Cheung, M., Chaboissier, M.C., Mynett, A., Hirst, E., Schedl, A., Briscoe, J., 2005. The transcriptional control of trunk neural crest induction, survival, and delamination. Developmental cell 8, 179-192.

Clavel, C., 1988. [Distribution of fibronectin and laminin during development of the human myenteric plexus and Hirschsprung's disease]. Gastroentérologie clinique et biologique 12, 193-197.

Clay, M.R., Halloran, M.C., 2014. Cadherin 6 promotes neural crest cell detachment via F-actin regulation and influences active Rho distribution during epithelial-to-mesenchymal transition. Development 141, 2506-2515.

Clugston, R.D., Blaner, W.S., 2012. The adverse effects of alcohol on vitamin A metabolism. Nutrients 4, 356-371.

Coelho-Aguiar, J.M., Bon-Frauches, A.C., Gomes, A.L., Verissimo, C.P., Aguiar, D.P., Matias, D., Thomasi, B.B., Gomes, A.S., Brito, G.A., Moura-Neto, V., 2015. The Enteric Glia: Identity and Functions. Glia.

Corpening, J.C., Cantrell, V.A., Deal, K.K., Southard-Smith, E.M., 2008. A Histone2BCerulean BAC transgene identifies differential expression of Phox2b in migrating enteric neural crest derivatives and enteric glia. Developmental Dynamics 237, 1119-1132.

Coventry, S., Yost, C., Palmiter, R.D., Kapur, R.P., 1994. Migration of ganglion cell precursors in the ileoceca of normal and lethal spotted embryos, a murine model for Hirschsprung disease. Lab Invest 71, 82-93.

Cunningham, T.J., Chatzi, C., Sandell, L.L., Trainor, P.A., Duester, G., 2011. Rdh10 mutants deficient in limb field retinoic acid signaling exhibit normal limb patterning but display interdigital webbing. Developmental Dynamics 240, 1142-1150.

Cunningham, T.J., Duester, G., 2015. Mechanisms of retinoic acid signalling and its roles in organ and limb development. Nat Rev Mol Cell Biol 16, 110-123.

de Graaff, E., Srinivas, S., Kilkenny, C., D'Agati, V., Mankoo, B.S., Costantini, F., Pachnis, V., 2001. Differential activities of the RET tyrosine kinase receptor isoforms during mammalian embryogenesis. Genes & Development 15, 2433-2444.

De la Torre-Mondragón, L., Ortega-Salgado, J.A., 1998. Transanal endorectal pull-through for Hirschsprung's disease. Journal of Pediatric Surgery 33, 1283-1286.

De la Torre, L., Ortega, A., 2000. Transanal versus open endorectal pull-through for Hirschsprung's disease. Journal of Pediatric Surgery 35, 1630-1632.

de Pee, S., Dary, O., 2002. Biochemical Indicators of Vitamin A Deficiency: Serum Retinol and Serum Retinol Binding Protein. The Journal of Nutrition 132, 2895S-2901S.

De Val, S., Chi, N.C., Meadows, S.M., Minovitsky, S., Anderson, J.P., Harris, I.S., Ehlers, M.L., Agarwal, P., Visel, A., Xu, S.-M., Pennacchio, L.A., Dubchak, I., Krieg, P.A., Stainier, D.Y.R., Black, B.L., 2008. Combinatorial Regulation of Endothelial Gene Expression by Ets and Forkhead Transcription Factors. Cell 135, 1053-1064.

Doray, B., 1998. Mutation of the RET ligand, neurturin, supports multigenic inheritance in Hirschsprung disease. Human Molecular Genetics 7, 1449-1452.

Druckenbrod, N.R., Epstein, M.L., 2005. The pattern of neural crest advance in the cecum and colon. Developmental Biology 287, 125-133.

Druckenbrod, N.R., Epstein, M.L., 2007. Behavior of enteric neural crest-derived cells varies with respect to the migratory wavefront. Developmental Dynamics 236, 84-92.

Druckenbrod, N.R., Epstein, M.L., 2009. Age-dependent changes in the gut environment restrict the invasion of the hindgut by enteric neural progenitors. Development 136, 3195-3203.

Duband, J.L., Thiery, J.P., 1982. Distribution of fibronectin in the early phase of avian cephalic neural crest cell migration. Dev Biol 93, 308-323.

Duester, G., 2008. Retinoic Acid Synthesis and Signaling during Early Organogenesis. Cell 134, 921-931.

Durbec, P.L., Larsson-Blomberg, L.B., Schuchardt, A., Costantini, F., Pachnis, V., 1996. Common origin and developmental dependence on c-ret of subsets of enteric and sympathetic neuroblasts. Development 122, 349-358.

Edery, P., Lyonnet, S., Mulligan, L.M., Pelet, A., Dow, E., Abel, L., Holder, S., Nihoul-Fekete, C., Ponder, B.A.J., Munnich, A., 1994. Mutations of the RET proto-oncogene in Hirschsprung's disease. Nature 367, 378-380.

Eketjäll, S., Ibáñez, C.F., 2002. Functional characterization of mutations in the GDNF gene of patients with Hirschsprung disease. Human Molecular Genetics 11, 325-329.

Elworthy, S., Pinto, J.P., Pettifer, A., Cancela, M.L., Kelsh, R.N., 2005. Phox2b function in the enteric nervous system is conserved in zebrafish and is sox10-dependent. Mechanisms of Development 122, 659-669.

Emir, H., Akman, M., Sarimurat, N., Kilic, N., Erdogan, E., Soylet, Y., 1999. Anorectal manometry during the neonatal period: its specificity in the diagnosis of Hirschsprung's disease. Eur J Pediatr Surg 9, 101-103.

Emison, E.S., McCallion, A.S., Kashuk, C.S., Bush, R.T., Grice, E., Lin, S., Portnoy, M.E., Cutler, D.J., Green, E.D., Chakravarti, A., 2005. A common sex-dependent mutation in a RET enhancer underlies Hirschsprung disease risk. Nature 434, 857-863.

Eng, C., 1999. RET Proto-Oncogene in the Development of Human Cancer. Journal of Clinical Oncology 17, 380.

Erickson, C.A., Perris, R., 1993. The role of cell-cell and cell-matrix interactions in the morphogenesis of the neural crest. Dev Biol 159, 60-74.

Esteban-Pretel, G., Marin, M.P., Renau-Piqueras, J., Sado, Y., Barber, T., Timoneda, J., 2013. Vitamin A deficiency disturbs collagen IV and laminin composition and decreases matrix metalloproteinase concentrations in rat lung. Partial reversibility by retinoic acid. The Journal of nutritional biochemistry 24, 137-145.

Farjo, K.M., Moiseyev, G., Nikolaeva, O., Sandell, L.L., Trainor, P.A., Ma, J.-x., 2011. RDH10 is the primary enzyme responsible for the first step of embryonic Vitamin A metabolism and retinoic acid synthesis. Developmental Biology 357, 347-355.

Faure, C., Chalazonitis, A., Rhéaume, C., Bouchard, G., Sampathkumar, S.G., Yarema, K.J., Gershon, M.D., 2007. Gangliogenesis in the enteric nervous system: Roles of the polysialylation of the neural cell adhesion molecule and its regulation by bone morphogenetic protein-4. Developmental Dynamics 236, 44-59.

Frantz, C., Stewart, K.M., Weaver, V.M., 2010. The extracellular matrix at a glance. Journal of cell science 123, 4195-4200.

Friedrich, G., Soriano, P., 1991. Promoter traps in embryonic stem cells: a genetic screen to identify and mutate developmental genes in mice. Genes Dev 5, 1513-1523.

Fu, M., Chi Hang Lui, V., Har Sham, M., Nga Yin Cheung, A., Kwong Hang Tam, P., 2003. HOXB5 expression is spatially and temporarily regulated in human embryonic gut during neural crest cell colonization and differentiation of enteric neuroblasts. Developmental Dynamics 228, 1-10.

Fu, M., Lui, V.C.H., Sham, M.H., Pachnis, V., Tam, P.K.H., 2004. Sonic hedgehog regulates the proliferation, differentiation, and migration of enteric neural crest cells in gut. The Journal of Cell Biology 166, 673-684.

Fu, M., Sato, Y., Lyons-Warren, A., Zhang, B., Kane, M.A., Napoli, J.L., Heuckeroth, R.O., 2010. Vitamin A facilitates enteric nervous system precursor migration by reducing Pten accumulation. Development 137, 631-640.

Fu, M., Vohra, B.P.S., Wind, D., Heuckeroth, R.O., 2006. BMP signaling regulates murine enteric nervous system precursor migration, neurite fasciculation, and patterning via altered Ncam1 polysialic acid addition. Developmental Biology 299, 137-150.

Fujiwara, N., Kaneyama, K., Okazaki, T., Lane, G.J., Kato, Y., Kobayashi, H., Yamataka, A., 2007. A comparative study of laparoscopy-assisted pull-through and open pull-through for Hirschsprung's disease with special reference to postoperative fecal continence. Journal of Pediatric Surgery 42, 2071-2074.

Gaillard, D., 1982. [Colonic nerve network demonstrated by quinacrine]. Bulletin de l'Association des anatomistes 66, 63-70.

Geerts, A., 2001. History, heterogeneity, developmental biology, and functions of quiescent hepatic stellate cells. Seminars in liver disease 21, 311-335.

Georgeson, K.E., 1999. Primary laparoscopic-assisted endorectal colon pull-through for Hirschsprung's disease: a new gold standard. Annals of surgery 229, 678-682; discussion 682-673.

Georgeson, K.E., Fuenfer, M.M., Hardin, W.D., 1995. Primary laparoscopic pull-through for Hirschsprung's disease in infants and children. Journal of Pediatric Surgery 30, 1017-1022.

Gershon, M.D., 1997. Genes and lineages in the formation of the enteric nervous system. Current Opinion in Neurobiology 7, 101-109.

Gianino, S., Grider, J.R., Cresswell, J., Enomoto, H., Heuckeroth, R.O., 2003. GDNF availability determines enteric neuron number by controlling precursor proliferation. Development 130, 2187-2198.

Goldstein, A.M., Brewer, K.C., Doyle, A.M., Nagy, N., Roberts, D.J., 2005. BMP signaling is necessary for neural crest cell migration and ganglion formation in the enteric nervous system. Mechanisms of Development 122, 821-833.

Greenberg, D.A., 2003. Linking acquired neurodevelopmental disorders to defects in cell adhesion. Proceedings of the National Academy of Sciences 100, 8043-8044.

Griseri, P., Lantieri, F., Puppo, F., Bachetti, T., Di Duca, M., Ravazzolo, R., Ceccherini, I., 2007. A common variant located in the 3′UTR of the RET gene is associated with protection from Hirschsprung disease. Human Mutation 28, 168-176.

Hama, H., Kurokawa, H., Kawano, H., Ando, R., Shimogori, T., Noda, H., Fukami, K., Sakaue-Sawano, A., Miyawaki, A., 2011. Scale: a chemical approach for fluorescence imaging and reconstruction of transparent mouse brain. Nat Neurosci.

Haskell, G.T., LaMantia, A.-S., 2005. Retinoic Acid Signaling Identifies a Distinct Precursor Population in the Developing and Adult Forebrain. The Journal of Neuroscience 25, 7636-7647.

Hayashi, S., McMahon, A.P., 2002. Efficient Recombination in Diverse Tissues by a Tamoxifen-Inducible Form of Cre: A Tool for Temporally Regulated Gene Activation/Inactivation in the Mouse. Developmental Biology 244, 305-318.

Heanue, T.A., Pachnis, V., 2007. Enteric nervous system development and Hirschsprung's disease: advances in genetic and stem cell studies. Nat Rev Neurosci 8, 466-479.

Hearn, C.J., Murphy, M., Newgreen, D., 1998. GDNF and ET-3 Differentially Modulate the Numbers of Avian Enteric Neural Crest Cells and Enteric Neurons in Vitro. Developmental Biology 197, 93-105.

Heuckeroth, R.O., Enomoto, H., Grider, J.R., Golden, J.P., Hanke, J.A., Jackman, A., Molliver, D.C., Bardgett, M.E., Snider, W.D., Johnson Jr, E.M., Milbrandt, J., 1999. Gene Targeting Reveals a Critical Role for Neurturin in the Development and Maintenance of Enteric, Sensory, and Parasympathetic Neurons. Neuron 22, 253-263.

Heuckeroth, R.O., Lampe, P.A., Johnson Jr, E.M., Milbrandt, J., 1998. Neurturin and GDNF Promote Proliferation and Survival of Enteric Neuron and Glial Progenitors in Vitro. Developmental Biology 200, 116-129.

Hoehner, J.C., Wester, T., Påhlman, S., Olsen, L., 1996. Alterations in neurotrophin and neurotrophin-receptor localization in Hirschsprung's disease. Journal of Pediatric Surgery 31, 1524-1529.

Hofstra, R., Elfferich, P., Osinga, J., Verlind, E., Fransen, E., Lopez, P., de Die-Smulders, C.E.M., Stolte-Dijkstra, I., Buys, C., 2002. Hirschsprung disease and L1CAM: is the disturbed sex ratio caused by L1CAM mutations? Journal of Medical Genetics 39, e11-e11.

Hofstra, R.M.W., Osinga, J., Tan-Sindhunata, G., Wu, Y., Kamsteeg, E.-J., Stulp, R.P., Ravenswaaij-Arts, C.v., Majoor-Krakauer, D., Angrist, M., Chakravarti, A., Meijers, C., Buys, C.H.C.M., 1996. A homozygous mutation in the endothelin-3 gene associated with a combined Waardenburg type 2 and Hirschsprung phenotype (Shah-Waardenburg syndrome). Nature Genetics 12, 445-447.

Hofstra, R.M.W., Valdenaire, O., Arch, E., Osinga, J., Kroes, H., Löffler, B.-M., Hamosh, A., Meijers, C., Buys, C.H.C.M., 1999. A Loss-of-Function Mutation in the Endothelin-Converting Enzyme 1 (ECE-1) Associated with Hirschsprung Disease, Cardiac Defects, and Autonomic Dysfunction. The American Journal of Human Genetics 64, 304-307.

Hosoda, K., Hammer, R.E., Richardson, J.A., Baynash, A.G., Cheung, J.C., Giaid, A., Yanagisawa, M., 1994. Targeted and natural (piebald-lethal) mutations of endothelin-B receptor gene produce megacolon associated with spotted coat color in mice. Cell 79, 1267-1276.

Hotta, R., Stamp, L.A., Foong, J.P., McConnell, S.N., Bergner, A.J., Anderson, R.B., Enomoto, H., Newgreen, D.F., Obermayr, F., Furness, J.B., Young, H.M., 2013. Transplanted progenitors generate functional enteric neurons in the postnatal colon. The Journal of Clinical Investigation 123, 1182-1191.

Inoue, K., Tanabe, Y., Lupski, J.R., 1999. Myelin deficiencies in both the central and the peripheral nervous systems associated with a SOX10 mutation. Annals of Neurology 46, 313-318.

Ivanchuk, S.M., Myers, S.M., Eng, C., Mulligan, L.M., 1996. De Novo Mutation of GDNF, Ligand for the RET/GDNFR-α Receptor Complex, in Hirschsprung Disease. Human Molecular Genetics 5, 2023-2026.

J A Badner, W.K.S., K L Garver, A Chakravarti, 1990. A genetic study of Hirschsprung disease. Am J Hum Genet 46, 568-580.

Jona, J.Z., 1998. Laparoscopic pull-through procedure for Hirschsprung's disease. Seminars in Pediatric Surgery 7, 228-231.

Justice, M.J., Carpenter, D.A., Favor, J., Neuhauser-Klaus, A., Hrabe de Angelis, M., Soewarto, D., Moser, A., Cordes, S., Miller, D., Chapman, V., Weber, J.S., Rinchik, E.M., Hunsicker, P.R., Russell, W.L., Bode, V.C., 2000. Effects of ENU dosage on mouse strains. Mammalian genome : official journal of the International Mammalian Genome Society 11, 484-488.

Kapur, R.P., 1999. Early death of neural crest cells is responsible for total enteric aganglionosis in Sox10(Dom)/Sox10(Dom) mouse embryos. Pediatric and Developmental Pathology 2, 559-569.

Kapur, R.P., 2000. Colonization of the Murine Hindgut by Sacral Crest-Derived Neural Precursors: Experimental Support for an Evolutionarily Conserved Model. Developmental Biology 227, 146-155.

Kapur, R.P., 2006. Can We Stop Looking?: Immunohistochemistry and the Diagnosis of Hirschsprung Disease. American Journal of Clinical Pathology 126, 9-12.

Kapur, R.P., 2009. Practical pathology and genetics of Hirschsprung's disease. Seminars in Pediatric Surgery 18, 212-223.

Karaosmanoglu, T., 1996. Regional differences in the number of neurons in the myenteric plexus of the guinea pig small intestine and colon: an evaluation of markers used to count neurons. The Anatomical Record 244, 470-480.

Kelsh, R.N., 2006. Sorting out Sox10 functions in neural crest development. BioEssays 28, 788-798.

Kerosuo, L., Bronner-Fraser, M., 2012. What is bad in cancer is good in the embryo: importance of EMT in neural crest development. Seminars in cell & developmental biology 23, 320-332.

Kerstjens-Frederikse, W.S., Hofstra, R.M.W., van Essen, A.J., Meijers, J.H.C., Buys, C.H.C.M., 1999. A Hirschsprung disease locus at 22q11? Journal of Medical Genetics 36, 221-224.

Kruger, G.M., Mosher, J.T., Tsai, Y.-H., Yeager, K.J., Iwashita, T., Gariepy, C.E., Morrison, S.J., 2003. Temporally Distinct Requirements for Endothelin Receptor B in the Generation and Migration of Gut Neural Crest Stem Cells. Neuron 40, 917-929.

Kumar, S., Sandell, L.L., Trainor, P.A., Koentgen, F., Duester, G., 2011. Alcohol and aldehyde dehydrogenases: Retinoid metabolic effects in mouse knockout models. Biochimica et Biophysica Acta (BBA) - Molecular and Cell Biology of Lipids.

Kurer, M.H., Lawson, J.O., Pambakian, H., 1986. Suction biopsy in Hirschsprung's disease. Archives of Disease in Childhood 61, 83-84.

Kuwajima, T., Sitko, A.A., Bhansali, P., Jurgens, C., Guido, W., Mason, C., 2013. ClearT: a detergent- and solvent-free clearing method for neuronal and non-neuronal tissue. Development 140, 1364-1368.

Lake, J.I., Heuckeroth, R.O., 2013. Enteric nervous system development: migration, differentiation, and disease. American Journal of Physiology - Gastrointestinal and Liver Physiology 305, G1-G24.

Lang, D., Chen, F., Milewski, R., Li, J., Lu, M.M., Epstein, J.A., 2000. Pax3 is required for enteric ganglia formation and functions with Sox10 to modulate expression of c-ret. The Journal of Clinical Investigation 106, 963-971.

Lang, D., Epstein, J.A., 2003. Sox10 and Pax3 physically interact to mediate activation of a conserved c-RET enhancer. Human Molecular Genetics 12, 937-945.

Langer, J.C., 1994. Smooth muscle from aganglionic bowel in Hirschsprung's disease impairs neuronal development in vitro. Cell and Tissue Research 276, 181-186.

Langer, J.C., 1999. Repeat pull-through surgery for complicated Hirschsprung's disease: Indications, techniques, and results. Journal of Pediatric Surgery 34, 1136-1141.

Langer, J.C., Minkes, R.K., Mazziotti, M.V., Skinner, M.A., Winthrop, A.L., 1999. Transanal one-stage soave procedure for infants with Hirschsprung's disease. Journal of Pediatric Surgery 34, 148-152.

Laranjeira, C., Pachnis, V., 2009. Enteric nervous system development: Recent progress and future challenges. Autonomic Neuroscience 151, 61-69.

Leckband, D., Prakasam, A., 2006. Mechanism and dynamics of cadherin adhesion. Annual review of biomedical engineering 8, 259-287.

Lee, H.-O., Levorse, J.M., Shin, M.K., 2003. The endothelin receptor-B is required for the migration of neural crest-derived melanocyte and enteric neuron precursors. Developmental Biology 259, 162-175.

Lee, Y.S., Jeong, W.I., 2012. Retinoic acids and hepatic stellate cells in liver disease. Journal of gastroenterology and hepatology 27 Suppl 2, 75-79.

Leibl, M.A., Ota, T., Woodward, M.N., Kenny, S.E., Lloyd, D.A., Vaillant, C.R., Edgar, D.H., 1999. Expression of endothelin 3 by mesenchymal cells of embryonic mouse caecum. Gut 44, 246-252.

Lenti, E., Farinello, D., Yokoyama, K.K., Penkov, D., Castagnaro, L., Lavorgna, G., Wuputra, K., Sandell, L.L., Butler Tjaden, N.E., Bernassola, F., Pasini, D., Wagner, M., Niederreither, K., Hamada, H., Blasi, F., Tonon, G., Trainor, P.A., Brendolan, A., [in preparation]. The Oncogenic Transcription Factor Tlx1 Regulates Cyp26b1 Expression and Retinoic Acid Signaling to Ensure Spleen Development.

Leone, D.P., Genoud, S.t., Atanasoski, S., Grausenburger, R., Berger, P., Metzger, D., Macklin, W.B., Chambon, P., Suter, U., 2003. Tamoxifen-inducible glia-specific Cre mice for somatic mutagenesis in oligodendrocytes and Schwann cells. Molecular and Cellular Neuroscience 22, 430-440.

Lim, J., Thiery, J.P., 2012. Epithelial-mesenchymal transitions: insights from development. Development 139, 3471-3486.

Lindley, R.M., Hawcutt, D.B., Connell, M.G., Almond, S.L., Vannucchi, M.G., Faussone-Pellegrini, M.S., Edgar, D.H., Kenny, S.E., 2008. Human and mouse enteric nervous system neurosphere transplants regulate the function of aganglionic embryonic distal colon. Gastroenterology 135, 205-216.e206.

Lopez Alonso, M., 1992. [Manometric study in the newborn]. Cir Pediatr 5, 66-71.

Maka, M., Claus Stolt, C., Wegner, M., 2005. Identification of Sox8 as a modifier gene in a mouse model of Hirschsprung disease reveals underlying molecular defect. Developmental Biology 277, 155-169.

Marin, M.P., Esteban-Pretel, G., Alonso, R., Sado, Y., Barber, T., Renau-Piqueras, J., Timoneda, J., 2005. Vitamin A deficiency alters the structure and collagen IV composition of rat renal basement membranes. J Nutr 135, 695-701.

Matsui, T., 1996. Differential activation of the murine laminin B1 gene promoter by RAR alpha, ROR alpha, and AP-1. Biochem Biophys Res Commun 220, 405-410.

May, P.A., Gossage, J.P., Kalberg, W.O., Robinson, L.K., Buckley, D., Manning, M., Hoyme, H.E., 2009. Prevalence and epidemiologic characteristics of FASD from various research methods with an emphasis on recent in-school studies. Developmental disabilities research reviews 15, 176-192.

McCarthy, R.A., Hay, E.D., 1991. Collagen I, laminin, and tenascin: ultrastructure and correlation with avian neural crest formation. Int J Dev Biol 35, 437-452.

Menezes, M., Corbally, M., Puri, P., 2006. Long-term results of bowel function after treatment for Hirschsprung's disease: a 29-year review. Pediatric Surgery International 22, 987-990.

Mic, F.A., Haselbeck, R.J., Cuenca, A.E., Duester, G., 2002. Novel retinoic acid generating activities in the neural tube and heart identified by conditional rescue of Raldh2 null mutant mice. Development 129, 2271-2282.

Mic, F.A., Sirbu, I.O., Duester, G., 2004. Retinoic Acid Synthesis Controlled by Raldh2 Is Required Early for Limb Bud Initiation and Then Later as a Proximodistal Signal during Apical Ectodermal Ridge Formation. Journal of Biological Chemistry 279, 26698-26706.

Minkes, R.K., Langer, J.C., 2000. A prospective study of botulinum toxin for internal anal sphincter hypertonicity in children with Hirschsprung's disease. Journal of Pediatric Surgery 35, 1733-1736.

Molotkov, A., Fan, X., Deltour, L., Foglio, M.H., Martras, S., Farrés, J., Parés, X., Duester, G., 2002. Stimulation of Retinoic Acid Production and Growth by Ubiquitously Expressed Alcohol Dehydrogenase Adh3. Proceedings of the National Academy of Sciences of the United States of America 99, 5337-5342.

Monier-Gavelle, F., Duband, J.L., 1997. Cross talk between adhesion molecules: control of N-cadherin activity by intracellular signals elicited by beta1 and beta3 integrins in migrating neural crest cells. J Cell Biol 137, 1663-1681.

Monsonego-Ornan, E., Kosonovsky, J., Bar, A., Roth, L., Fraggi-Rankis, V., Simsa, S., Kohl, A., Sela-Donenfeld, D., 2012. Matrix metalloproteinase 9/gelatinase B is required for neural crest cell migration. Dev Biol 364, 162-177.

Moore, M.W., Klein, R.D., Farinas, I., Sauer, H., Armanini, M., Phillips, H., Reichardt, L.F., Ryan, A.M., Carver-Moore, K., Rosenthal, A., 1996. Renal and neuronal abnormalities in mice lacking GDNF. Nature 382, 76-79.

Moreau, E., Vilar, J., Lelievre-Pegorier, M., Merlet-Benichou, C., Gilbert, T., 1998. Regulation of c-ret expression by retinoic acid in rat metanephros: implication in nephron mass control. The American journal of physiology 275, F938-945.

Mosher, J.T., Yeager, K.J., Kruger, G.M., Joseph, N.M., Hutchin, M.E., Dlugosz, A.A., Morrison, S.J., 2007. Intrinsic differences among spatially distinct neural crest stem cells in terms of migratory properties, fate determination, and ability to colonize the enteric nervous system. Dev Biol 303, 1-15.

Mulligan, L.M., 2014. RET revisited: expanding the oncogenic portfolio. Nat Rev Cancer 14, 173-186.

Mulligan, L.M., Kwok, J.B.J., Healey, C.S., Elsdon, M.J., Eng, C., Gardner, E., Love, D.R., Mole, S.E., Moore, J.K., Papi, L., Ponder, M.A., Telenius, H., Tunnacliffe, A., Ponder, B.A.J., 1993. Germ-line mutations of the RET proto-oncogene in multiple endocrine neoplasia type 2A. Nature 363, 458-460.

N-Fékété, C., 1986. Total colonic aganglionosis (with or without ileal involvement): a review of 27 cases. Journal of Pediatric Surgery 21, 251-254.

Nagashimada, M., Ohta, H., Li, C., Nakao, K., Uesaka, T., Brunet, J.-F., Amiel, J., Trochet, D., Wakayama, T., Enomoto, H., 2012. Autonomic neurocristopathy-associated mutations in PHOX2B dysregulate Sox10 expression. The Journal of Clinical Investigation 122, 3145-3158.

Nagy A, G.M., Vintersten K, Behringer RR 2003. Manipulating the mouse embryo. Cold Spring Harbor: Cold Spring Harbor Laboratory.

Nagy, N., Goldstein, A.M., 2006. Endothelin-3 regulates neural crest cell proliferation and differentiation in the hindgut enteric nervous system. Developmental Biology 293, 203-217.

Nakagawa, S., Takeichi, M., 1995. Neural crest cell-cell adhesion controlled by sequential and subpopulation-specific expression of novel cadherins. Development 121, 1321-1332.

NAP, 2001. Dietary Reference Intakes for Vitamin A, Vitamin K, Arsenic, Boron, Chromium, Copper, Iodine, Iron, Manganese, Molybdenum, Nickel, Silicon, Vanadium, and Zinc. The National Academies Press, Washington, DC.

Nataf, V., Amemiya, A., Yanagisawa, M., Le Douarin, N.M., 1998. The expression pattern of endothelin 3 in the avian embryo. Mechanisms of Development 73, 217-220.

Natarajan, D., Grigoriou, M., Marcos-Gutierrez, C.V., Atkins, C., Pachnis, V., 1999. Multipotential progenitors of the mammalian enteric nervous system capable of colonising aganglionic bowel in organ culture. Development 126, 157-168.

Natarajan, D., Marcos-Gutierrez, C., Pachnis, V., de Graaff, E., 2002. Requirement of signalling by receptor tyrosine kinase RET for the directed migration of enteric nervous system progenitor cells during mammalian embryogenesis. Development 129, 5151-5160.

Neilson, I.R., Yazbeck, S., 1990. Ultrashort Hirschsprung's disease: Myth or reality. Journal of Pediatric Surgery 25, 1135-1138.

Newgreen, D., Gibbins, I., 1982. Factors controlling the time of onset of the migration of neural crest cells in the fowl embryo. Cell Tissue Res 224, 145-160.

Newgreen, D., Young, H.M., 2002. Enteric Nervous System: Development and Developmental Disturbances—Part 2. Pediatric and Developmental Pathology 5, 329-349.

Newton, D.L., Henderson, W.R., Sporn, M.B., 1980. Structure-Activity Relationships of Retinoids in Hamster Tracheal Organ Culture. Cancer Research 40, 3413-3425.

Niederreither, K., Dolle, P., 2008. Retinoic acid in development: towards an integrated view. Nat Rev Genet 9, 541-553.

Niederreither, K., Vermot, J., Messaddeq, N., Schuhbaur, B., Chambon, P., Dolle, P., 2001. Embryonic retinoic acid synthesis is essential for heart morphogenesis in the mouse. Development 128, 1019-1031.

Niederreither, K., Vermot, J., Roux, I.L., Schuhbaur, B., Chambon, P., Dollé, P., 2003. The regional pattern of retinoic acid synthesis by RALDH2 is essential for the development of posterior pharyngeal arches and the enteric nervous system. Development 130, 2525-2534.

Niederreither, K., Vermot, J., Schuhbaur, B., Chambon, P., Dolle, P., 2000. Retinoic acid synthesis and hindbrain patterning in the mouse embryo. Development 127, 75-85.

Niederreither, K., Vermot, J., Schuhbaur, B., Chambon, P., Dollé, P., 2002. Embryonic retinoic acid synthesis is required for forelimb growth and anteroposterior patterning in the mouse. Development 129, 3563-3574.

Nishiyama, C., Uesaka, T., Manabe, T., Yonekura, Y., Nagasawa, T., Newgreen, D.F., Young, H.M., Enomoto, H., 2012. Trans-mesenteric neural crest cells are the principal source of the colonic enteric nervous system. Nat Neurosci 15, 1211-1218.

Okamoto, N., Wada, Y., Goto, M., 1997. Hydrocephalus and Hirschsprung's disease in a patient with a mutation of L1CAM. Journal of Medical Genetics 34, 670-671.

Paratore, C., Eichenberger, C., Suter, U., Sommer, L., 2002. Sox10 haploinsufficiency affects maintenance of progenitor cells in a mouse model of Hirschsprung disease. Human Molecular Genetics 11, 3075-3085.

Parc, R., 1984. [Megacolon in adults. Apropos of 76 cases]. Annales de gastroentérologie et d'hépatologie 20, 133-141.

Parikh, D.H., Tam, P.K.H., Lloyd, D.A., Van Velzen, D., Edgar, D.H., 1992. Quantitative and qualitative analysis of the extracellular matrix protein, laminin, in Hirschsprung's disease. Journal of Pediatric Surgery 27, 991-996.

Parisi, M.A., 2006. Hirschsprung Disease Overview. GeneReviews.

Parisi, M.A., Kapur, R.P., 2000. Genetics of Hirschsprung disease. Current Opinion in Pediatrics 12, 610-617.

Park, K.S., Gumbiner, B.M., 2010. Cadherin 6B induces BMP signaling and de-epithelialization during the epithelial mesenchymal transition of the neural crest. Development 137, 2691-2701.

Passarge, E., 1967. The Genetics of Hirschsprung's Disease. New England Journal of Medicine 276, 138-143.

Patrus, B., Nasr, A., Langer, J.C., Gerstle, J.T., 2011. Intrasphincteric botulinum toxin decreases the rate of hospitalization for postoperative obstructive symptoms in children with Hirschsprung disease. Journal of Pediatric Surgery 46, 184-187.

Pattyn, A., Morin, X., Cremer, H., Goridis, C., Brunet, J.-F., 1999. The homeobox gene Phox2b is essential for the development of autonomic neural crest derivatives. Nature 399, 366-370.

Perris, R., 1997. The extracellular matrix in neural crest-cell migration. Trends Neurosci 20, 23-31.

Perris, R., Perissinotto, D., 2000. Role of the extracellular matrix during neural crest cell migration. Mechanisms of Development 95, 3-21.

Pichel, J.G., Shen, L., Sheng, H.Z., Granholm, A.-C., Drago, J., Grinberg, A., Lee, E.J., Huang, S.P., Saarma, M., Hoffer, B.J., Sariola, H., Westphal, H., 1996. Defects in enteric innervation and kidney development in mice lacking GDNF. Nature 382, 73-76.

Pingault, V., Bondurand, N., Kuhlbrodt, K., Goerich, D.E., Prehu, M.-O., Puliti, A., Herbarth, B., Hermans-Borgmeyer, I., Legius, E., Matthijs, G., Amiel, J., Lyonnet, S., Ceccherini, I., Romeo, G., Smith, J.C., Read, A.P., Wegner, M., Goossens, M., 1998. SOX10 mutations in patients with Waardenburg-Hirschsprung disease. Nature Genetics 18, 171-173.

Pitera, J.E., Smith, V.V., Woolf, A.S., Milla, P.J., 2001. Embryonic Gut Anomalies in a Mouse Model of Retinoic Acid-induced caudal Regression Syndrome. American Journal of Pathology 159, 2321-2329.

Pitkin, R.M., 2007. Folate and neural tube defects. The American journal of clinical nutrition 85, 285s-288s.

Puffenberger, E.G., Hosoda, K., Washington, S.S., Nakao, K., deWit, D., Yanagisawa, M., Chakravarti, A., 1994. A missense mutation of the endothelin-B receptor gene in multigenic hirschsprung's disease. Cell 79, 1257-1266.

Quemelo, P.R.V., Lourenço, C.M., Peres, L.C., 2007. Teratogenic effect of retinoic acid in swiss mice. Acta Cirurgica Brasileira 22, 451-456.

R J Andrassy, H.I., and J J Weitzman, 1981. Rectal suction biopsy for the diagnosis of Hirschsprung's disease. Annals of Surgery 193, 419-424.

Ramalho-Santos, M., Melton, D.A., McMahon, A.P., 2000. Hedgehog signals regulate multiple aspects of gastrointestinal development. Development 127, 2763-2772.

Ribes, V., Wang, Z., Dollé, P., Niederreither, K., 2006. Retinaldehyde dehydrogenase 2 (RALDH2)-mediated retinoic acid synthesis regulates early mouse embryonic forebrain development by controlling FGF and sonic hedgehog signaling. Development 133, 351-361.

Ro, S., Hwang, S.J., Muto, M., Jewett, W.K., Spencer, N.J., 2006. Anatomic modifications in the enteric nervous system of piebald mice and physiological consequences to colonic motor activity. American Journal of Physiology - Gastrointestinal and Liver Physiology 290, G710-G718.

Robinson, M.D., McCarthy, D.J., Smyth, G.K., 2010. edgeR: a Bioconductor package for differential expression analysis of digital gene expression data. Bioinformatics (Oxford, England) 26, 139-140.

Romeo, G., Ronchetto, P., Luo, Y., Barone, V., Seri, M., Ceccherini, I., Pasini, B., Bocciardi, R., Lerone, M., Kaariainen, H., Martucciello, G., 1994. Point mutations affecting the tyrosine kinase domain of the RET proto-oncogene in Hirschsprung's disease. Nature 367, 377-378.

Rosenfield, N.S., 1984. Hirschsprung disease: accuracy of the barium enema examination. Radiology 150, 393-400.

Ross, S.A., McCaffery, P.J., Drager, U.C., De Luca, L.M., 2000. Retinoids in Embryonal Development. Physiological Reviews 80, 1021-1054.

Rossant, J., Zirngibl, R., Cado, D., Shago, M., Giguère, V., 1991. Expression of a retinoic acid response element-hsplacZ transgene defines specific domains of transcriptional activity during mouse embryogenesis. Genes & Development 5, 1333-1344.

Rossi, J., Herzig, K.-H., Võikar, V., Hiltunen, P.H., Segerstråle, M., Airaksinen, M.S., 2003. Alimentary tract innervation deficits and dysfunction in mice lacking GDNF family receptor α2. The Journal of Clinical Investigation 112, 707-716.

Ryan, E.T., Ecker, J.L., Christakis, N.A., Folkman, J., 1992. Hirschsprung's disease: Associated abnormalities and demography. Journal of Pediatric Surgery 27, 76-81.

Salomon, R., Attie, T., Pelet, A., Bidaud, C., Eng, C., Amiel, J., Sarnacki, S., Goulet, O., Ricour, C., Nihoul-Fekete, C., Munnich, A., Lyonnet, S., 1996. Germline mutations of the RET ligand GDNF are not sufficient to cause Hirschsprung disease. Nature Genetics 14, 345-347.

SAMHSA, 2012. National Survey on Drug Use and Health (NSDUH), in: (SAMHSA), S.A.a.M.H.S.A. (Ed.).

Sanchez, M.P., Silos-Santiago, I., Frisen, J., He, B., Lira, S.A., Barbacid, M., 1996. Renal agenesis and the absence of enteric neurons in mice lacking GDNF. Nature 382, 70-73.

Sandell, L.L., Butler Tjaden, N.E., Barlow, A.J., Trainor, P.A., 2014. Cochleovestibular nerve development is integrated with migratory neural crest cells. Dev Biol 385, 200-210.

Sandell, L.L., Iulianella, A., Melton, K.R., Lynn, M., Walker, M., Inman, K.E., Bhatt, S., Leroux-Berger, M., Crawford, M., Jones, N.C., Dennis, J.F., Trainor, P.A., 2011. A phenotype-driven ENU mutagenesis screen identifies novel alleles with functional roles in early mouse craniofacial development. genesis 49, 342-359.

Sandell, L.L., Lynn, M.L., Inman, K.E., McDowell, W., Trainor, P.A., 2012. RDH10 Oxidation of Vitamin A Is a Critical Control Step in Synthesis of Retinoic Acid during Mouse Embryogenesis. PLoS ONE 7, e30698.

Sandell, L.L., Sanderson, B.W., Moiseyev, G., Johnson, T., Mushegian, A., Young, K., Rey, J.P., Ma, J.x., Staehling-Hampton, K., Trainor, P.A., 2007. RDH10 is essential for synthesis of embryonic retinoic acid and is required for limb, craniofacial, and organ development. Genes & Development 21, 1113-1124.

Sarioglu, A., 1997. Hirschsprung-associated congenital anomalies. European journal of pediatric surgery 7, 331-337.

Sato, Y., Heuckeroth, R.O., 2008. Retinoic acid regulates murine enteric nervous system precursor proliferation, enhances neuronal precursor differentiation, and reduces neurite growth in vitro. Developmental Biology 320, 185-198.

Savagner, P., 2015. Epithelial-mesenchymal transitions: from cell plasticity to concept elasticity. Current topics in developmental biology 112, 273-300.

Schuchardt, A., D'Agati, V., Larsson-Blomberg, L., Costantini, F., Pachnis, V., 1994. Defects in the kidney and enteric nervous system of mice lacking the tyrosine kinase receptor Ret. Nature 367, 380-383.

Shen, L., Pichel, J.G., Mayeli, T., Sariola, H., Lu, B., Westphal, H., 2002. Gdnf Haploinsufficiency Causes Hirschsprung-Like Intestinal Obstruction and Early-Onset Lethality in Mice. The American Journal of Human Genetics 70, 435-447.

Shepherd, I.T., Pietsch, J., Elworthy, S., Kelsh, R.N., Raible, D.W., 2004. Roles for GFRα1 receptors in zebrafish enteric nervous system development. Development 131, 241-249.

Shin, M.K., Levorse, J.M., Ingram, R.S., Tilghman, S.M., 1999. The temporal requirement for endothelin receptor-B signalling during neural crest development. Nature 402, 496-501.

Simkin, J.E., Zhang, D., Rollo, B.N., Newgreen, D.F., 2013. Retinoic Acid Upregulates Ret and Induces Chain Migration and Population Expansion in Vagal Neural Crest Cells to Colonise the Embryonic Gut. PLoS ONE 8, e64077.

Singh, S.J., Croaker, G.D.H., Manglick, P., Wong, C.L., Athanasakos, H., Elliott, E., Cass, D., 2003. Hirschsprung's disease: the Australian Paediatric Surveillance Unit's experience. Pediatric Surgery International 19, 247-250.

Sirbu, I.O., Duester, G., 2006. Retinoic-acid signalling in node ectoderm and posterior neural plate directs left-right patterning of somitic mesoderm. Nat Cell Biol 8, 271-277.

Smith, G.H.H., Cass, D., 1991. Infantile Hirschsprung's disease — is a barium enema useful? Pediatric Surgery International 6, 318-321.

Soriano, P., 1999. Generalized lacZ expression with the ROSA26 Cre reporter strain. Nature Genetics 21, 70-71.

Sotoodehnejadnematalahi, F., Burke, B., 2013. Structure, function and regulation of versican: the most abundant type of proteoglycan in the extracellular matrix. Acta medica Iranica 51, 740-750.

Southard-Smith, E.M., Angrist, M., Ellison, J.S., Agarwala, R., Baxevanis, A.D., Chakravarti, A., Pavan, W.J., 1999. The Sox10Dom Mouse: Modeling the Genetic Variation of Waardenburg-Shah (WS4) Syndrome. Genome Research 9, 215-225.

Southard-Smith, E.M., Kos, L., Pavan, W., 1998. Sox10 mutation disrupts neural crest development in Dom Hirschsprung mouse model. Nature Genetics 18, 60-64.

Spouge, D., 1985. Hirschsprung disease in a large birth cohort. Teratology (Philadelphia) 32, 171-177.

Stanchina, L., Baral, V., Robert, F., Pingault, V., Lemort, N., Pachnis, V., Goossens, M., Bondurand, N., 2006. Interactions between Sox10, Edn3 and Ednrb during enteric nervous system and melanocyte development. Developmental Biology 295, 232-249.

Sternberg, J., Kimber, S.J., 1986. Distribution of fibronectin, laminin and entactin in the environment of migrating neural crest cells in early mouse embryos. J Embryol Exp Morphol 91, 267-282.

Stratton, K.H., Cynthia; Battaglia, Frederick C., 1996. Fetal Alcohol Syndrome: Diagnosis, Epidemiology, Prevention, and Treatment. The National Academies Press, Washington, DC.

Swartz-Basile, D.A., Wang, L., Tang, Y., Pitt, H.A., Rubin, D.C., Levin, M.S., 2003. Vitamin A deficiency inhibits intestinal adaptation by modulating apoptosis, proliferation, and enterocyte migration. Am J Physiol Gastrointest Liver Physiol 285, G424-432.

Tachibana, K., Hirota, S., Iizasa, H., Yoshida, H., Kawabata, K., Kataoka, Y., Kitamura, Y., Matsushima, K., Yoshida, N., Nishikawa, S.-i., Kishimoto, T., Nagasawa, T., 1998. The chemokine receptor CXCR4 is essential for vascularization of the gastrointestinal tract. Nature 393, 591-594.

Takahashi, N., Takasu, S., 2011. A close relationship between type 1 diabetes and vitamin A-deficiency and matrix metalloproteinase and hyaluronidase activities in skin tissues. Experimental dermatology 20, 899-904.

Taneyhill, L.A., 2008. To adhere or not to adhere: the role of Cadherins in neural crest development. Cell adhesion & migration 2, 223-230.

Taneyhill, L.A., Padmanabhan, R., 2014. Chapter 3 - The Cell Biology of Neural Crest Cell Delamination and EMT, in: Trainor, P.A. (Ed.), Neural Crest Cells. Academic Press, Boston, pp. 51-72.

Tansey, M.G., Baloh, R.H., Milbrandt, J., Johnson Jr, E.M., 2000. GFRα-Mediated Localization of RET to Lipid Rafts Is Required for Effective Downstream Signaling, Differentiation, and Neuronal Survival. Neuron 25, 611-623.

Taraviras, S., Marcos-Gutierrez, C.V., Durbec, P., Jani, H., Grigoriou, M., Sukumaran, M., Wang, L.C., Hynes, M., Raisman, G., Pachnis, V., 1999. Signalling by the RET receptor tyrosine kinase and its role in the development of the mammalian enteric nervous system. Development 126, 2785-2797.

Taraviras, S., Pachnis, V., 1999. Development of the mammalian enteric nervous system. Current Opinion in Genetics & Development 9, 321-327.

Tarca, A.L., Draghici, S., Khatri, P., Hassan, S.S., Mittal, P., Kim, J.S., Kim, C.J., Kusanovic, J.P., Romero, R., 2009. A novel signaling pathway impact analysis. Bioinformatics (Oxford, England) 25, 75-82.

Teitelbaum, D.H., Coran, A.G., 2003. Reoperative Surgery for Hirschsprung's Disease. Seminars in Pediatric Surgery 12, 124-131.

Theveneau, E., Mayor, R., 2012. Neural crest delamination and migration: From epithelium-to-mesenchyme transition to collective cell migration. Developmental Biology 366, 34-54.

Theveneau, E., Mayor, R., 2014. Chapter 4 - Neural Crest Cell Migration: Guidance, Pathways, and Cell–Cell Interactions, in: Trainor, P.A. (Ed.), Neural Crest Cells. Academic Press, Boston, pp. 73-88.

Tobon, F., Reid, N.C.R.W., Talbert, J.L., Schuster, M.M., 1968. Nonsurgical Test for the Diagnosis of Hirschsprung's Disease. New England Journal of Medicine 278, 188-194.

Tomac, A.C., Grinberg, A., Huang, S.P., Nosrat, C., Wang, Y., Borlongan, C., Lin, S.Z., Chiang, Y.H., Olson, L., Westphal, H., Hoffer, B.J., 1999. Glial cell line-derived neurotrophic factor receptor α1 availability regulates glial cell line-derived neurotrophic factor signaling: evidence from mice carrying one or two mutated alleles. Neuroscience 95, 1011-1023.

Tosney, K.W., Watanabe, M., Landmesser, L., Rutishauser, U., 1986. The distribution of NCAM in the chick hindlimb during axon outgrowth and synaptogenesis. Developmental Biology 114, 437-452.

Touraine, R.L., Attié-Bitach, T., Manceau, E., Korsch, E., Sarda, P., Pingault, V., Encha-Razavi, F., Pelet, A., Augé, J., Nivelon-Chevallier, A., Holschneider, A.M., Munnes, M., Doerfler, W., Goossens, M., Munnich, A., Vekemans, M., Lyonnet, S., 2000. Neurological Phenotype in Waardenburg Syndrome Type 4 Correlates with Novel SOX10 Truncating Mutations and Expression in Developing Brain. The American Journal of Human Genetics 66, 1496-1503.

Trochet, D., O'Brien, L.M., Gozal, D., Trang, H., Nordenskjöld, A., Laudier, B., Svensson, P.-J., Uhrig, S., Cole, T., Munnich, A., Gaultier, C., Lyonnet, S., Amiel, J., 2005. PHOX2B Genotype Allows for Prediction of Tumor Risk in Congenital Central Hypoventilation Syndrome. The American Journal of Human Genetics 76, 421-426.

Tsang, K.Y., Cheung, M.C., Chan, D., Cheah, K.S., 2010. The developmental roles of the extracellular matrix: beyond structure to regulation. Cell Tissue Res 339, 93-110.

Uesaka, T., Enomoto, H., 2010. Neural Precursor Death Is Central to the Pathogenesis of Intestinal Aganglionosis in Ret Hypomorphic Mice. The Journal of Neuroscience 30, 5211-5218.

Uesaka, T., Jain, S., Yonemura, S., Uchiyama, Y., Milbrandt, J., Enomoto, H., 2007. Conditional ablation of GFRα1 in postmigratory enteric neurons triggers unconventional neuronal death in the colon and causes a Hirschsprung's disease phenotype. Development 134, 2171-2181.

Uesaka, T., Nagashimada, M., Yonemura, S., Enomoto, H., 2008. Diminished Ret expression compromises neuronal survival in the colon and causes intestinal aganglionosis in mice. The Journal of Clinical Investigation 118, 1890-1898.

Underwood, B.A., 1985. VItamin a intoxication. JAMA 254, 232-233.

Van de Putte, T., Francis, A., Nelles, L., van Grunsven, L.A., Huylebroeck, D., 2007. Neural crest-specific removal of Zfhx1b in mouse leads to a wide range of neurocristopathies reminiscent of Mowat-Wilson syndrome. Hum Mol Genet 16, 1423-1436.

Van de Putte, T., Maruhashi, M., Francis, A., Nelles, L., Kondoh, H., Huylebroeck, D., Higashi, Y., 2003. Mice Lacking Zfhx1b, the Gene That Codes for Smad-Interacting Protein-1, Reveal a Role for Multiple Neural Crest Cell Defects in the Etiology of Hirschsprung Disease–Mental Retardation Syndrome. The American Journal of Human Genetics 72, 465-470.

Ventura, A., Kirsch, D.G., McLaughlin, M.E., Tuveson, D.A., Grimm, J., Lintault, L., Newman, J., Reczek, E.E., Weissleder, R., Jacks, T., 2007. Restoration of p53 function leads to tumour regression in vivo. Nature 445, 661-665.

Vermot, J., Pourquie, O., 2005. Retinoic acid coordinates somitogenesis and left-right patterning in vertebrate embryos. Nature 435, 215-220.

Wallace, A.S., Anderson, R.B., 2011. Genetic interactions and modifier genes in Hirschsprung's disease. World J Gastroenterol. 2011 Dec 7;17(45):4937-44.

Wallace, A.S., Burns, A.J., 2005. Development of the enteric nervous system, smooth muscle and interstitial cells of Cajal in the human gastrointestinal tract. Cell and Tissue Research 319, 367-382.

Wallace, A.S., Schmidt, C., Schachner, M., Wegner, M., Anderson, R.B., 2010. L1cam acts as a modifier gene during enteric nervous system development. Neurobiology of disease 40, 622-633.

Wallace, A.S., Tan, M.X., Schachner, M., Anderson, R.B., 2011. L1cam acts as a modifier gene for members of the endothelin signalling pathway during enteric nervous system development. Neurogastroenterology & Motility 23, e510-e522.

Webster, W., 1973. Embryogenesis of the enteric ganglia in normal mice and in mice that develop congenital aganglionic megacolon. Journal of Embryology and Experimental Morphology 30, 573-585.

WHO, 2009. Global prevalence of vitamin A deficiency in populations at risk 1995–2005. WHO Global Database on Vitamin A Deficiency Geneva, World Health Organization.

WHO, 2015. Micronutrient deficiencies: Vitamin A deficiency. Geneva, World Health Organization.

Wildhaber, B.E., Pakarinen, M., Rintala, R.J., Coran, A.G., Teitelbaum, D.H., 2004. Posterior myotomy/myectomy for persistent stooling problems in Hirschsprung's disease. Journal of Pediatric Surgery 39, 920-926.

Wright-Jin, E.C., Grider, J.R., Duester, G., Heuckeroth, R.O., 2013. Retinaldehyde dehydrogenase enzymes regulate colon enteric nervous system structure and function. Dev Biol 381, 28-37.

Wu, J.J., Chen, J.X., Rothman, T.P., Gershon, M.D., 1999. Inhibition of in vitro enteric neuronal development by endothelin-3: mediation by endothelin B receptors. Development 126, 1161-1173.

Xu, D., Emoto, N., Giaid, A., Slaughter, C., Kaw, S., deWit, D., Yanagisawa, M., 1994. ECE-1: A membrane-bound metalloprotease that catalyzes the proteolytic activation of big endothelin-1. Cell 78, 473-485.

Yamada, K., Yamada, Y., Nomura, N., Miura, K., Wakako, R., Hayakawa, C., Matsumoto, A., Kumagai, T., Yoshimura, I., Miyazaki, S., Kato, K., Sonta, S.-i., Ono, H., Yamanaka, T., Nagaya, M., Wakamatsu, N., 2001. Nonsense and Frameshift Mutations in ZFHX1B, Encoding Smad-Interacting Protein 1, Cause a Complex Developmental Disorder with a Great Variety of Clinical Features. The American Journal of Human Genetics 69, 1178-1185.

Yanagisawa, H., Yanagisawa, M., Kapur, R.P., Richardson, J.A., Williams, S.C., Clouthier, D.E., de Wit, D., Emoto, N., Hammer, R.E., 1998. Dual genetic pathways of endothelin-mediated intercellular signaling revealed by targeted disruption of endothelin converting enzyme-1 gene. Development 125, 825-836.

Young, H.M., Bergner, A.J., Anderson, R.B., Enomoto, H., Milbrandt, J., Newgreen, D.F., Whitington, P.M., 2004. Dynamics of neural crest-derived cell migration in the embryonic mouse gut. Developmental Biology 270, 455-473.

Young, H.M., Bergner, A.J., Müller, T., 2003. Acquisition of neuronal and glial markers by neural crest–derived cells in the mouse intestine. The Journal of Comparative Neurology 456, 1-11.

Young, H.M., Hearn, C.J., Ciampoli, D., Southwell, B.R., Brunet, J.F., Newgreen, D.F., 1998. A Single Rostrocaudal Colonization of the Rodent Intestine by Enteric Neuron Precursors Is Revealed by the Expression of Phox2b, Ret, and p75 and by Explants Grown under the Kidney Capsule or in Organ Culture. Developmental Biology 202, 67-84.

Young, H.M., Hearn, C.J., Farlie, P.G., Canty, A.J., Thomas, P.Q., Newgreen, D.F., 2001. GDNF Is a Chemoattractant for Enteric Neural Cells. Developmental Biology 229, 503-516.

Young, H.M., Newgreen, D., 2001. Enteric neural crest-derived cells: Origin, identification, migration, and differentiation. The Anatomical Record 262, 1-15.

Young, H.M., Turner, K.N., Bergner, A.J., 2005. The location and phenotype of proliferating neural-crest-derived cells in the developing mouse gut. Cell and Tissue Research 320, 1-9.

Zhou, T.B., Drummen, G.P., Qin, Y.H., 2012. The controversial role of retinoic Acid in fibrotic diseases: analysis of involved signaling pathways. International journal of molecular sciences 14, 226-243.

Zhu, L., Lee, H.-O., Jordan, C.S., Cantrell, V.A., Southard-Smith, E.M., Shin, M.K., 2004. Spatiotemporal regulation of endothelin receptor-B by SOX10 in neural crest-derived enteric neuron precursors. Nature Genetics 36, 732-737.

Zile, M.H., 1998. Vitamin A and Embryonic Development: An Overview. The Journal of Nutrition 128, 455S-458S.

VII. APPENDIX

This section includes qPCR and RNA sequencing data. Additionally, this section includes the references and contributions for six papers of which I am an author that have been published and/or submitted during my time in the Trainor Laboratory (Aoto et al., 2015; Billings et al., 2013; Butler Tjaden et al., [in preparation]; Butler Tjaden and Trainor, 2013; Lenti et al., [in preparation]; Sandell et al., 2014).

qPCR Data

Nine target genes of interest and three endogenous controls were run on three plates using the same portion of the embryo used in RNA Seq2, from posterior to the otic vesicle to the 7th somite, just anterior to the forelimb bud (Figure II-13 B). Figure VII-1 is a histogram of the relative expression of the nine target genes of interest after being normalized using the three endogenous controls (Figure VII-2). Relative expression (of all genes) results are graphed with 95% confidence intervals.

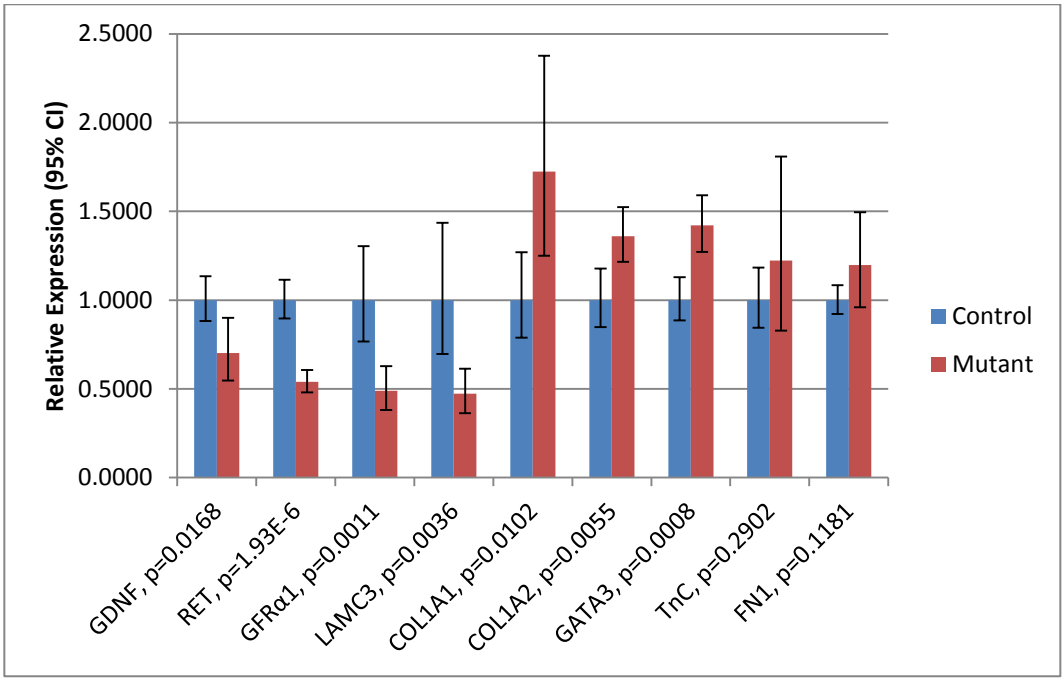

Figure VII-1: Histogram of nine genes of interest after normalization to three endogenous controls. GDNF, RET, GFRα1, LAMC3, COL1A1, COL1A2 and GATA3 have significant p-values ($p<0.05$).

Three appropriate endogenous controls (Figure VII-2) for each sample set were selected from a panel of five primer sets using geNorm in qBase plus. Results are graphed with standard error bars.

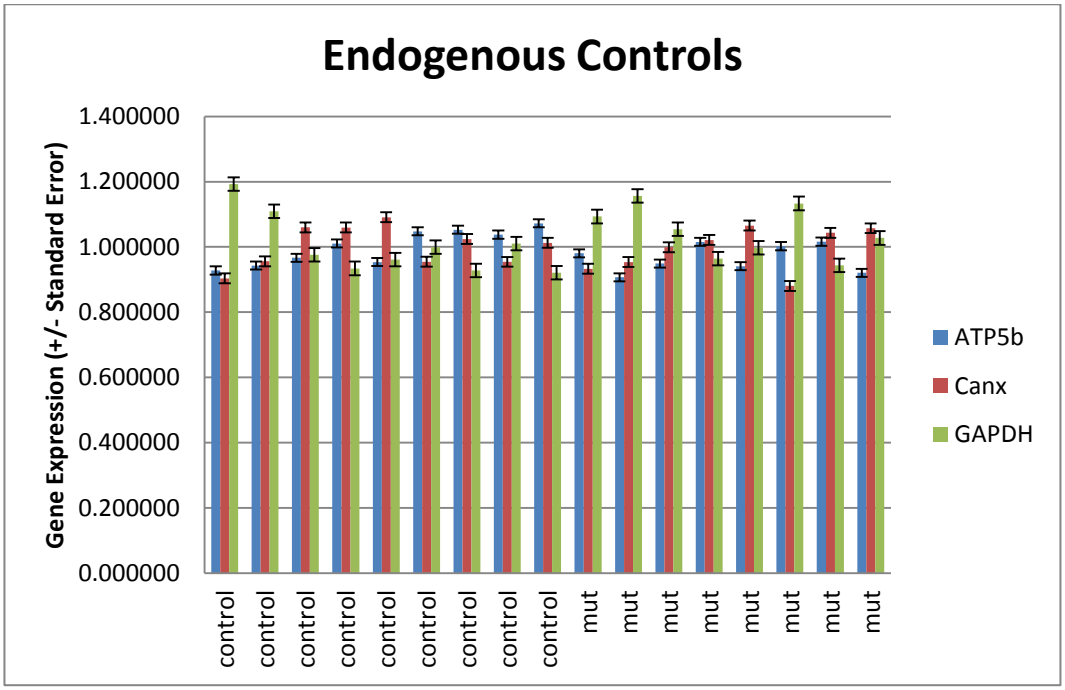

Figure VII-2: Histogram of endogenous controls. Results are graphed with standard error bars.

All primer sets used were experimentally determined to be within 10% of ideal efficiency. Relative quantities (of each gene) are graphed with 95% confidence intervals. For these genes, pooled mutants have statistically significant lower expression of GDNF (Figure VII-3), GFRα1 (Figure VII-4), RET (Figure VII-5) and LAMC3 (Figure VII-6). These same mutants have statistically significant higher expression of COL1A1 (Figure VII-7), COL1A2 (Figure VII-8), and GATA3 (Figure VII-9). There is no statistically significant difference between wild-type and mutant embryos with regards to TNC (Figure VII-10) and FN1 (Figure VII-11).

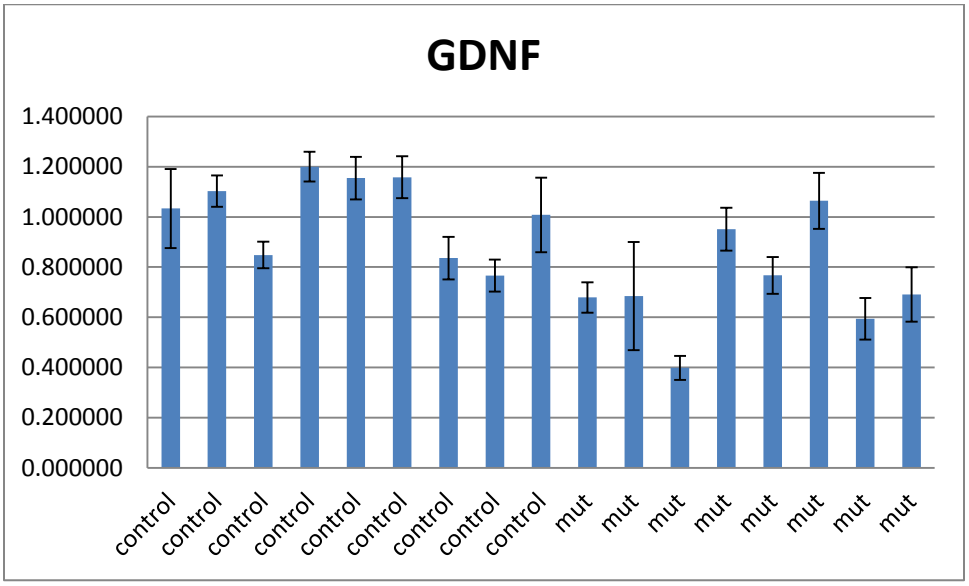

Figure VII-3: Histogram of relative expression levels (+/- 95% Confidence Intervals) of GDNF for all control and mutant embryos.

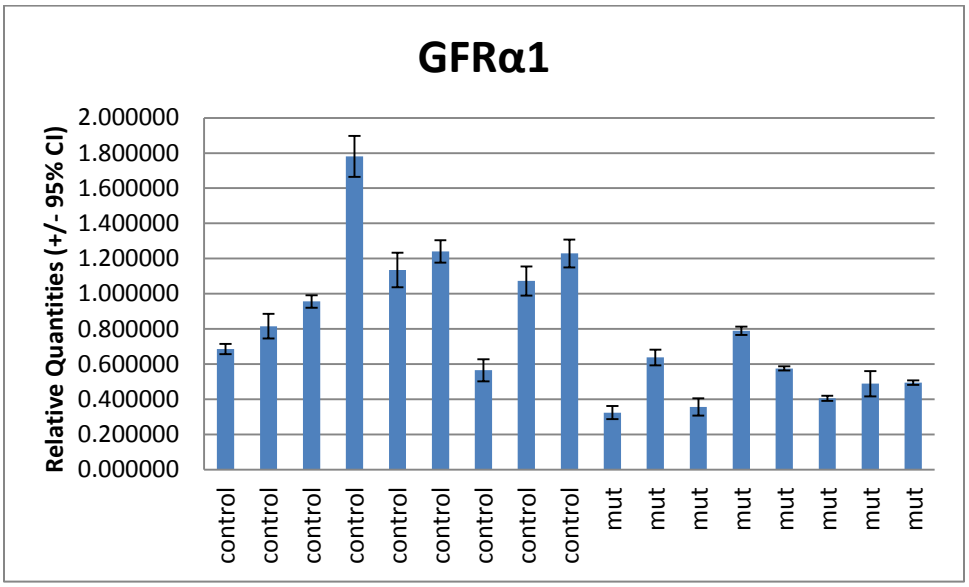

Figure VII-4: Histogram of relative expression levels (+/- 95% Confidence Intervals) of GFRα1 for all control and mutant embryos.

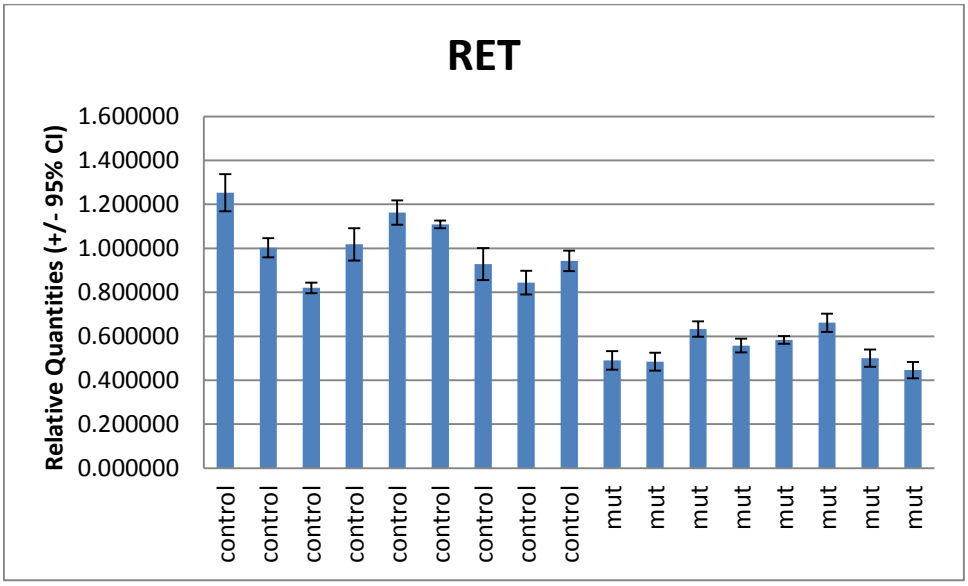

Figure VII-5: Histogram of relative expression levels (+/- 95% Confidence Intervals) of RET for all control and mutant embryos.

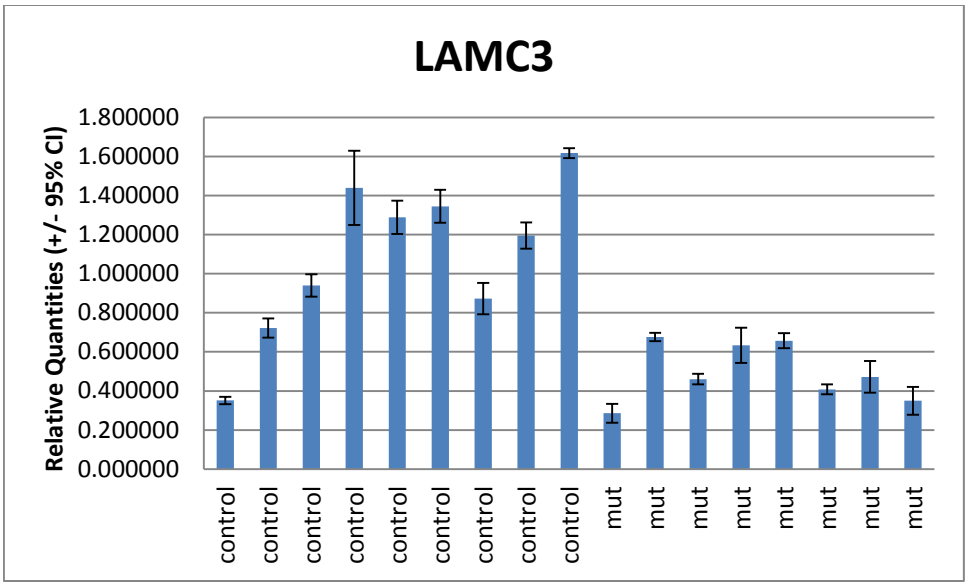

Figure VII-6: Histogram of relative expression levels (+/- 95% Confidence Intervals) of LAMC3 for all control and mutant embryos.

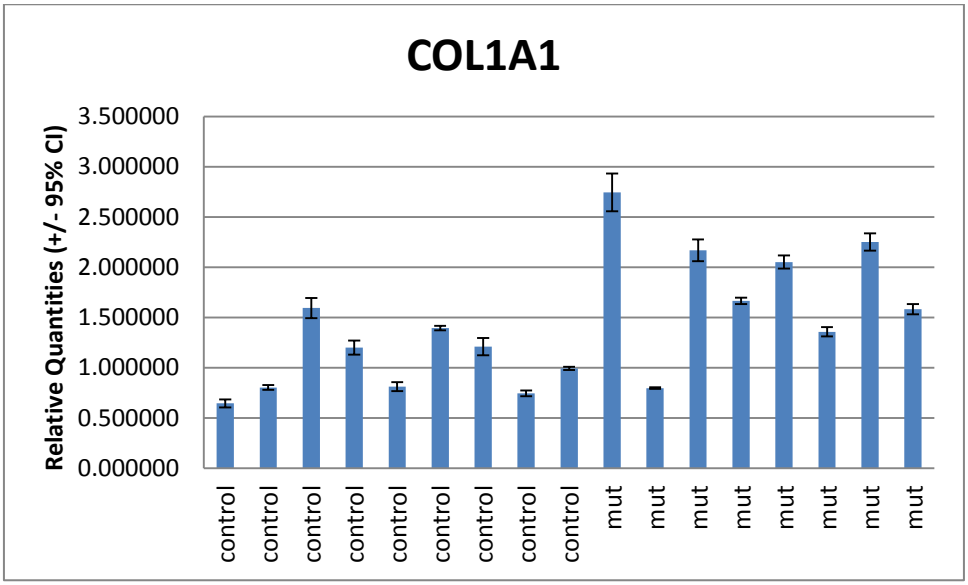

Figure VII-7: Histogram of relative expression levels (+/- 95% Confidence Intervals) of COL1A1 for all control and mutant embryos.

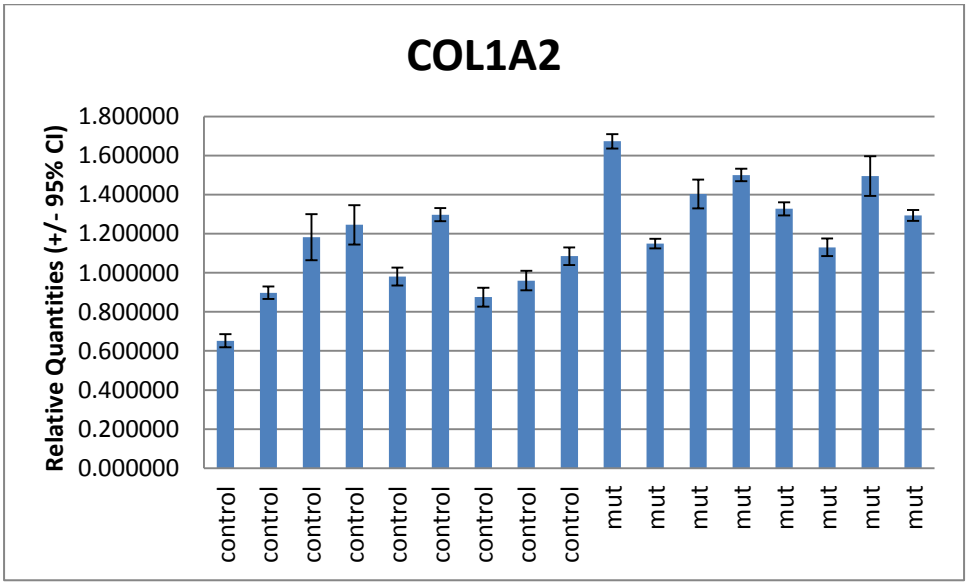

Figure VII-8: Histogram of relative expression levels (+/- 95% Confidence Intervals) of COL1A2 for all control and mutant embryos.

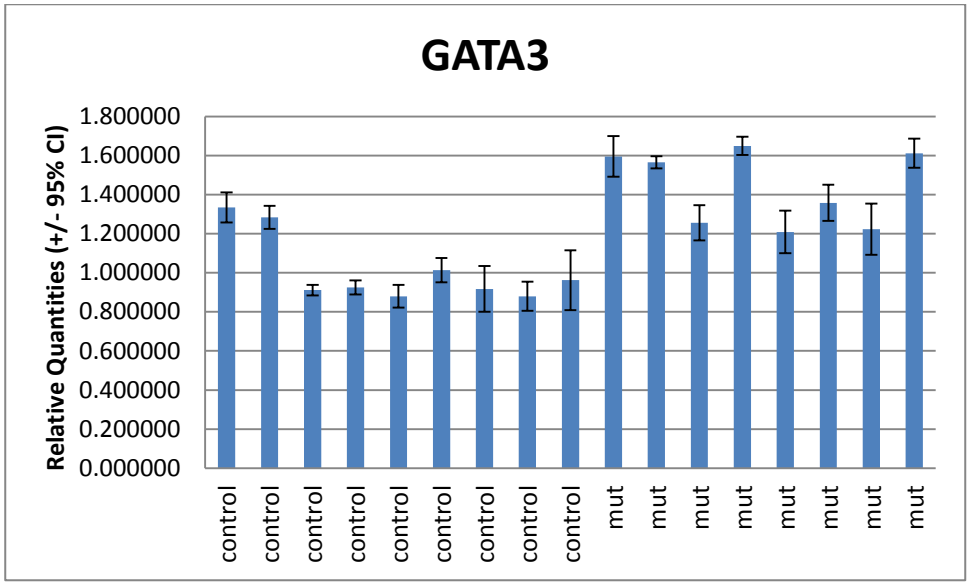

Figure VII-9: Histogram of relative expression levels (+/- 95% Confidence Intervals) of GATA3 for all control and mutant embryos.

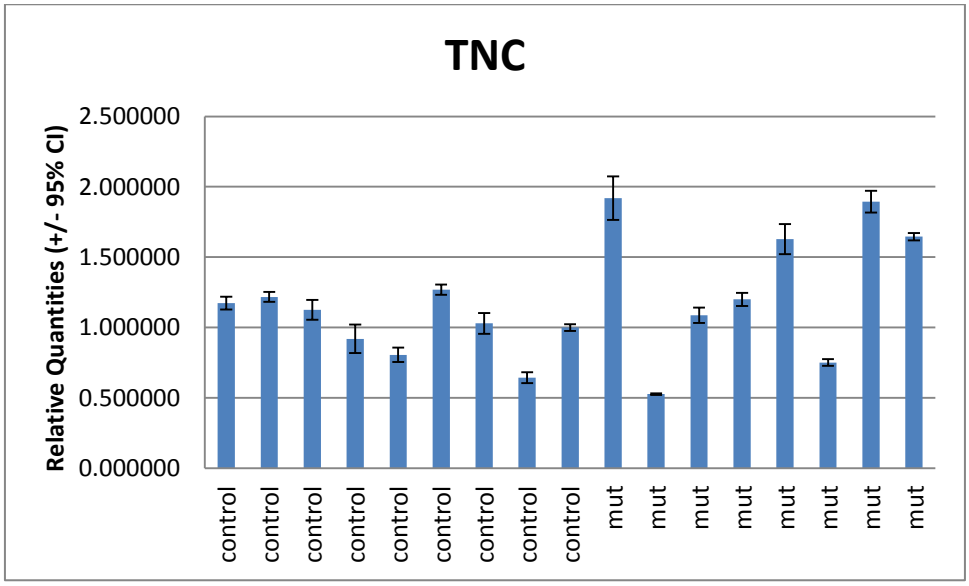

Figure VII-10: Histogram of relative expression levels (+/- 95% Confidence Intervals) of TNC for all control and mutant embryos.

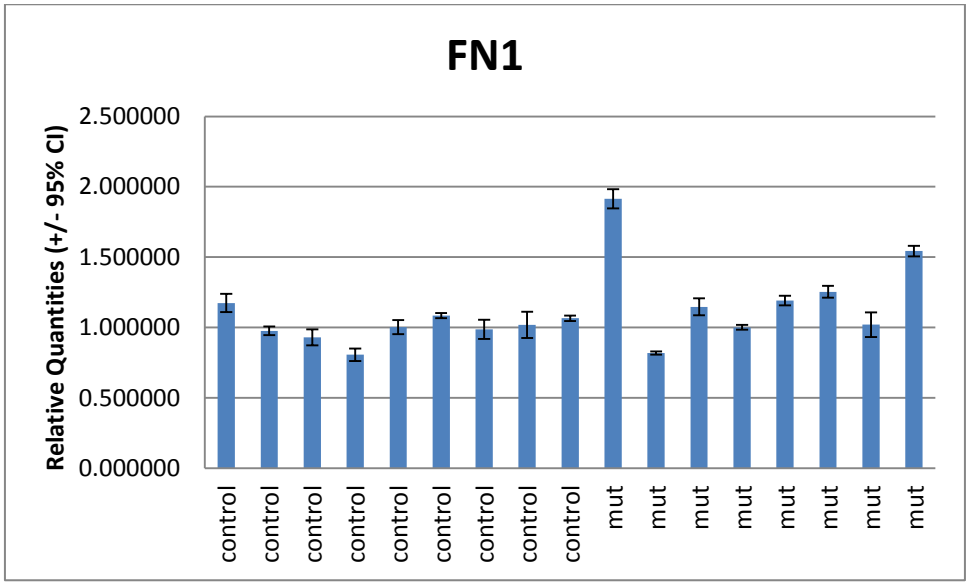

Figure VII-11: Histogram of relative expression levels (+/- 95% Confidence Intervals) of FN1 for all control and mutant embryos.

RNA Sequencing

Two rounds of RNA Sequencing (RNA Seq) were performed on *Rdh10*^{trex} embryos at E9.5. In RNA Seq1, we used a portion of the embryo from below the otic vesicle to the base of the tail. In the RNA Seq2, we used only the portion of the embryo from just below the otic vesicle to just above the forelimb, and excluded the heart (Figure II-13). The RNA sequencing analysis was done by Chris Seidel, PhD (CWS) a genomics specialist at the Stowers Institute. The figures and DE summary tables in this section were created by CWS.

CWS Analysis for RNA Seq1 and RNA Seq2

RNA Seq1 analysis was performed on tissue taken from the torso region of mouse embryos at developmental time E9.5. Total RNA was collected and used to create polyA strand-specific libraries. The experiment was performed in triplicate on 3 mutants and 3

wild-type littermates. Data was collected by counting read mappings to 39017 genes. However after filtering for genes with a sum total of at least 1 count per million (cpm) across all six samples, the final analyzed data set contains 19205 genes.

RNA Seq2 analysis was performed on tissue taken from the area of the first seven somites of mouse embryos at developmental time E9.5. Total RNA was collected and used to create polyA strand-specific libraries. The experiment was performed in triplicate on 4 mutants and 4 wild-type littermates. Data was collected by counting read mappings to 39017 genes. However after filtering for genes with a sum total of at least 1 count per million (cpm) across all eight samples, the final analyzed data set contains 22674 genes.

MA Plot

By plotting the ratio of gene expression (M; log base 2 of trex/wt) against the combined signal from both types of sample (A; average log2 of cpm) we can evaluate the relationship between ratios and the signal strength in the experiment. Genes with low p-values and a fold change of two are highlighted in color. In the MA plots for RNA Seq2 (Figure VII-13), genes considered differentially expressed with a p-value of 0.01 or less are highlighted in color. This experiment shows more evidence of differential expression than RNA Seq1 (Figure VII-12). However, as Figure VII-13 A illustrates, many of genes considered DE based simply on p-value have very low ratios (log2 = 0.2, or 1.15 fold). Figure VII-13 B zooms in to get a better view of this, and Figure VII-13 C illustrates only the genes from the last two columns of the DE Summary Table, with a p-value of less than 0.01 AND at least 2-fold change.

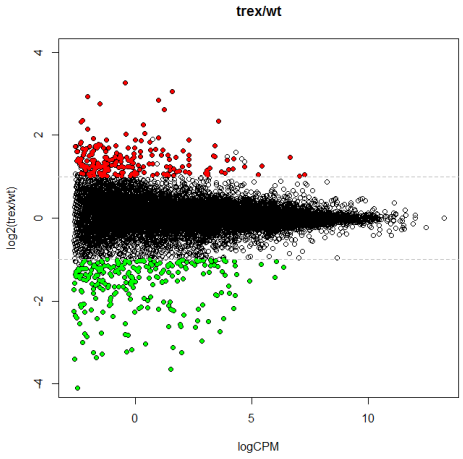

Figure VII-12: MA plot for RNA Seq1

A B C

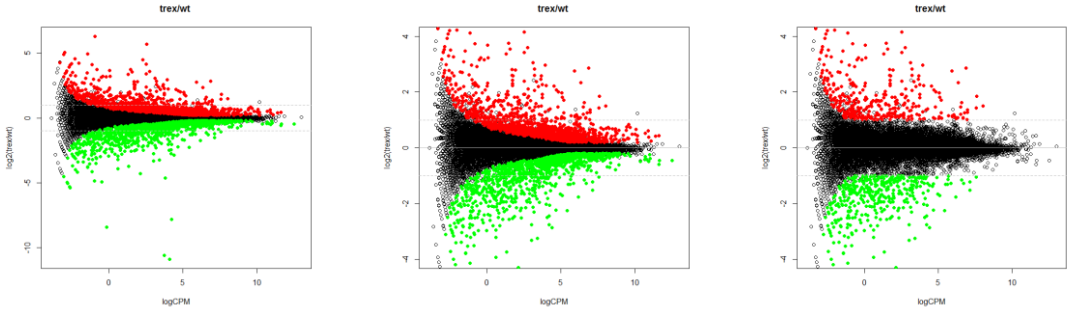

Figure VII-13: MA plot for RNA Seq2. (A) All the data with DE genes highlighted (B) Data plotted on symmetric scale with DE genes highlighted (C) Data points with 2-fold change plotted

Differentially expressed (DE) Summary table

The DE summary table for RNA Seq1 (Table VII-1) shows the number of genes changed up or down by an adjusted p-value of less than 0.05. It also shows how many genes change with an un-adjusted p-value of 0.05 and the minimum expression ratio of the resulting up or down gene sets. The last two columns show the number of genes that change by at least two-fold with a p-value of less than 0.05.

Table VII-1: DE summary table for RNA Seq1

	0.05	0.05	min ratio		fc > 2 and p < 0.05	
ratio	**p.adj**	**p-value**	**up**	**down**	**up**	**Down**
trex/wt	836	2235	0.164	-0.156	220	258

The DE summary table for RNA Seq2 (Table VII-2) shows the number of genes changed up or down by an adjusted p-value of less than 0.01. It also shows how many genes change with an un-adjusted p-value of 0.01 and the minimum expression ratio of the resulting up or down gene sets. The last two columns show the number of genes that change by at least two-fold with a p-value of less than 0.01.

Sample trex_1 had a low correlation when compared to the other samples (see Data Characteristics). So the data was processed two ways – once with all samples (trex all) and once with trex_1 omitted (trex oo, outlier omitted). The majority of the analysis makes use of the data with the outlier omitted, but the DE characteristics for both are shown above, and the significantly flagged genes from both analyses are marked in the final excel table.

Table VII-2: DE summary table for RNA Seq 2

	0.01	0.01			p < 0.01 & FC 2	
data set	**padj**	**pval**	**min.up**	**min.dn**	**up**	**dn**
trex oo	1417	2700	0.192	-0.188	355	408
trex all	1311	2788	0.235	-0.235	493	466

Gene Ontology (GO) Analysis

To get a sense of the biological themes enriched in the mutant, or in wild-type relative to mutant, the up and down gene sets were examined for enrichment of GO terms for the biological process ontology. The top 10 terms by p-value are shown in the bar

plots (Figure VII-14 A, B). The jitter plots represent the gene expression values for all genes mapped to the given GO term (Figure VII-14 C, D), and allow us to gauge the relative enrichment for the term. Because the gene sets for RNA Seq1 (Figure VII-14) are relatively small (220 genes up and 258 genes down), a larger set of genes was defined by taking any gene with a p-value of less than 0.01 (regardless of fold change), leading to up and down sets of 603 and 618 genes respectively (Figure VII-15). These larger sets were examined for GO term enrichment. The number of genes in each set which map to a GO term is shown in the plot title.

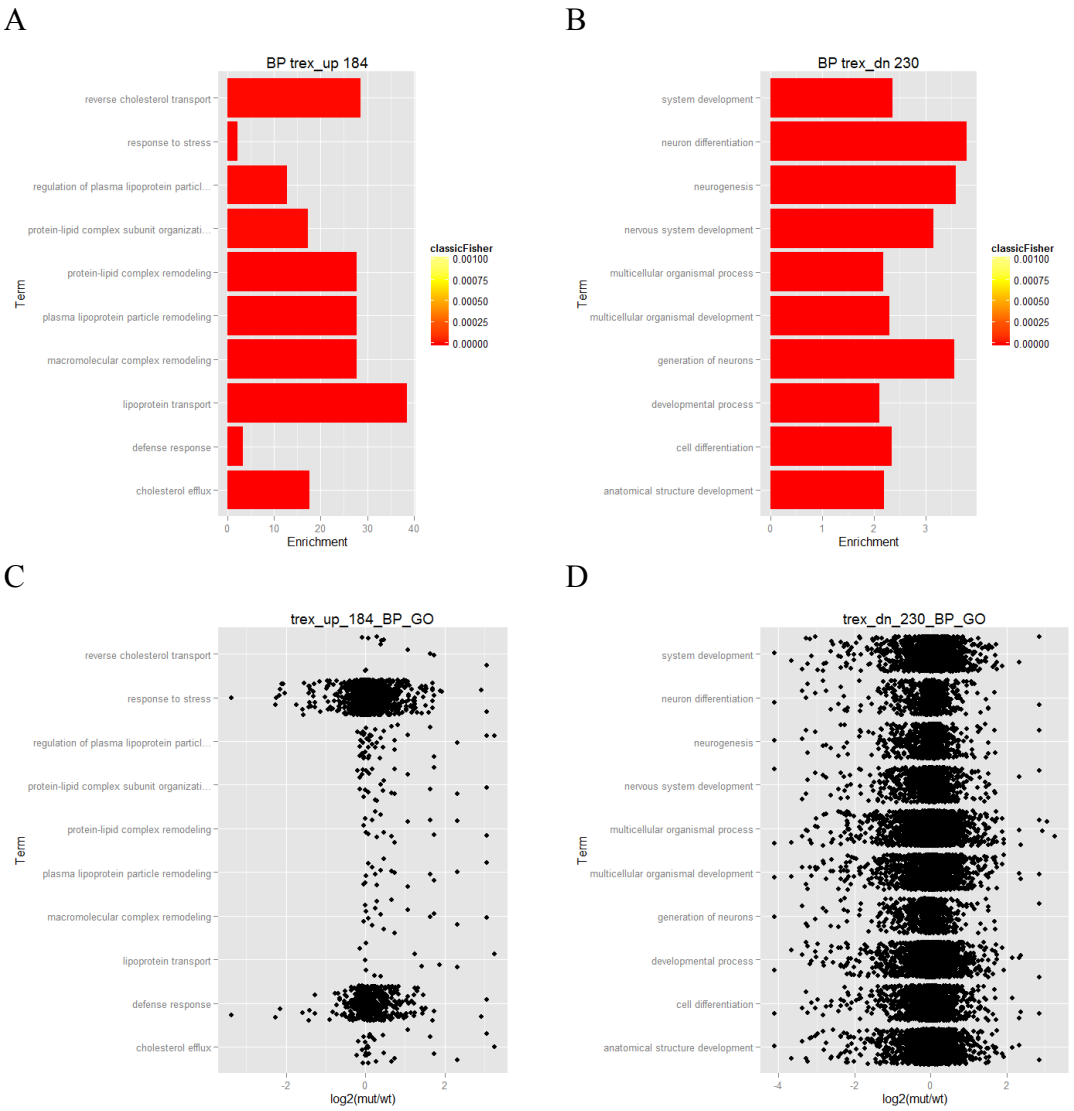

Figure VII-14: Top 10 GO Terms for gene sets for RNA Seq1 with at least two-fold change and p-value less than 0.05. Here there were 220 genes up and 258 genes down.

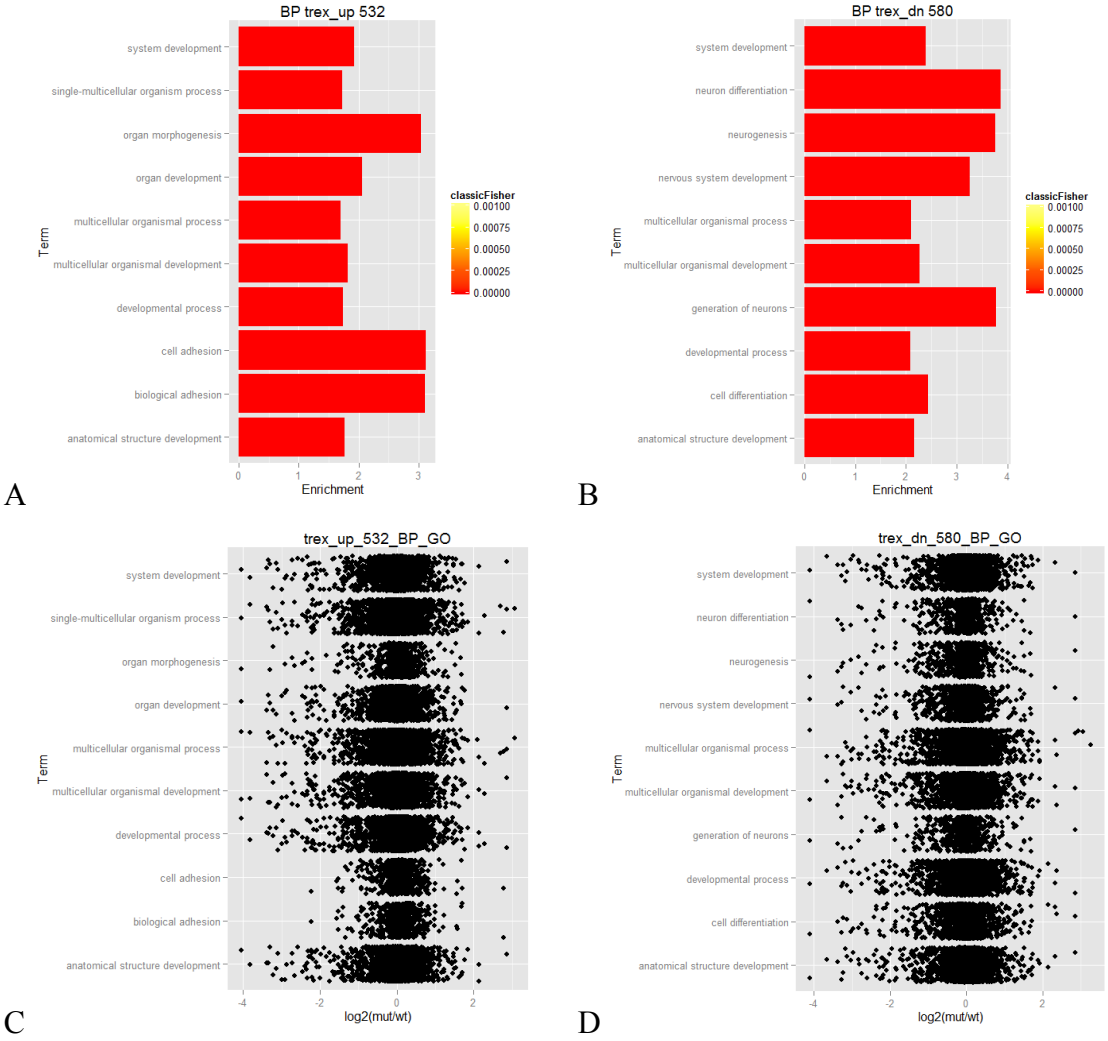

Figure VII-15: Top 10 GO Terms for gene sets for RNA Seq1 with p-value less than 0.01, regardless of fold-change. Here there were 603 genes up and 618 genes down.

In RNA Seq2, the top up or down gene sets according to the last two columns of the DE table were examined for enrichment of GO terms from the Biological Process Ontology. The top 10 terms are shown in the bar plots.

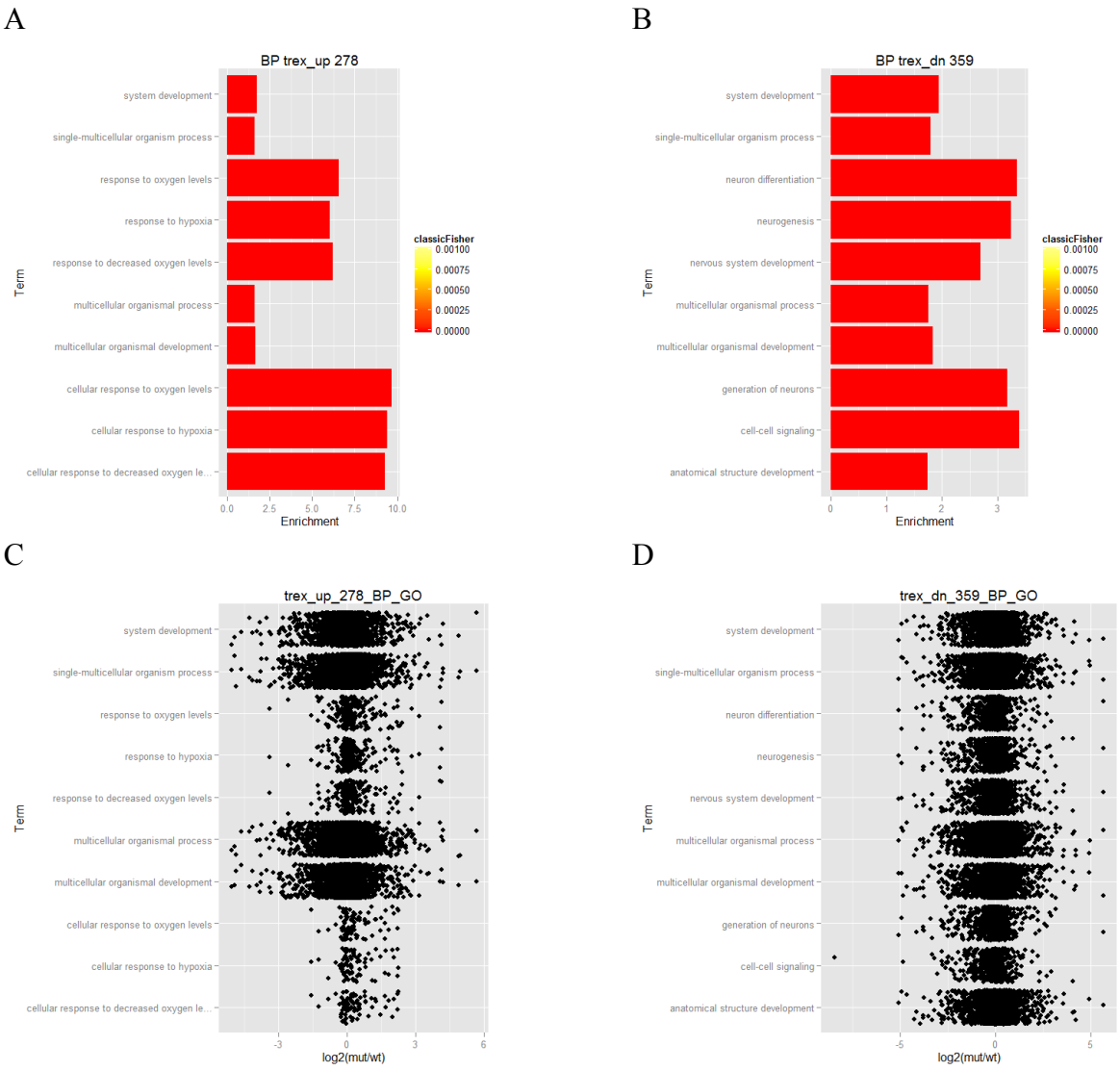

Figure VII-16: Top 10 GO Terms for gene sets for RNA Seq2 with at least two-fold change and p-value less than 0.01. Here there were 278 genes up and 359 genes down.

To examine the overlap between RNA Seq1 (called here “nbu1”) and RNA Seq2 (called here “nbu2”), genes changed in either experiment up or down by a given p-value cutoff were compared (Figure VII-17). For RNA Seq1, the p-value cutoff was 0.05, whereas for RNA Seq2 the p-value cutoff was 0.01.These experiments were performed

about a year apart. During this time the edgeR packaged used for calculating p-values has changed. For the overlap comparison, the data for RNA Seq1 was re-analyzed using the latest version of edgeR.

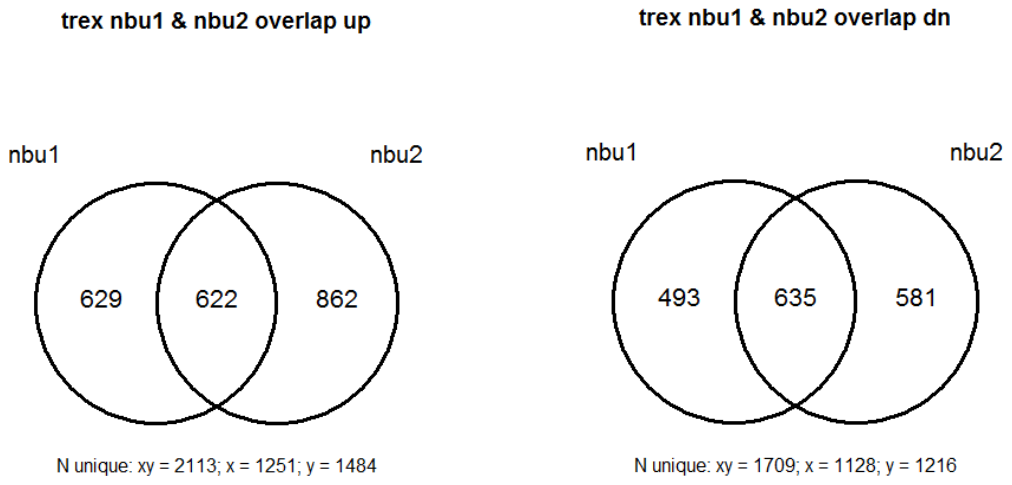

Figure VII-17: Overlap of differentially expressed genes from RNA Seq1 (nbu1) and RNA Seq2 (nbu2) experiments.

Signaling Pathway Impact Analysis (SPIA) algorithm

Signaling Pathway Impact Analysis (SPIA) algorithm (Tarca et al., 2009) was used to assess Kyoto Encyclopedia of Genes and Genomes (KEGG) pathway perturbations. For RNA Seq1, a set of 1357 differentially expressed genes were selected with a p-value of less than 0.01. The top 10 pathways for RNA Seq 1 (Table VII-3) and RNA Seq 2 (Table VII-4) are shown KEGG pathways are mapped to entrez gene ids, whereas the DE genes are based on ensembl identifiers, and thus have to be mapped to entrez ids. RNA Seq1 began with a set of 1357 ensembl ids, and 1200 were successfully mapped to entrez ids. RNASeq2 began with a set of 2700 ensemble ids, and 2424 were successfully mapped to entrez ids.

Table VII-3: SPIA Summary Table for RNA Seq1

Name	pSize	NDE	pNDE	pG	pGFdr	pGFWER	Status
ECM-receptor interaction	86	21	1.71E-08	4.03E-08	4.84E-06	4.84E-06	Inhibited
Focal adhesion	201	33	7.60E-08	2.71E-07	1.63E-05	3.25E-05	Inhibited
Basal cell carcinoma	55	14	2.40E-06	7.30E-06	0.000292	0.0008761	Inhibited
Hedgehog signaling pathway	54	12	5.45E-05	0.0004958	0.0125349	0.0594968	Activated
Melanogenesis	97	15	0.0005128	0.0005223	0.0125349	0.0626746	Inhibited
Maturity onset diabetes of the young	26	7	0.000578	0.0009084	0.018168	0.1090078	Activated
Complement and coagulation cascades	76	11	0.0046533	0.0039642	0.0679573	0.4757012	Inhibited
Transcriptional misregulation in cancer	163	21	0.0005805	0.0049064	0.0688454	0.5887665	Inhibited
Neuroactive ligand-receptor interaction	278	28	0.0038209	0.0051634	0.0688454	0.6196086	Inhibited
Cholinergic synapse	111	10	0.1167815	0.0143377	0.1720526	1	Activated

Table VII-4: SPIA Summary Table for RNA Seq2

Name	pSize	NDE	pNDE	pG	pGFdr	pGFWER	Status
ECM-receptor interaction	85	30	6.36E-07	7.78E-08	7.30E-06	9.18E-06	Activated
Focal adhesion	198	56	1.04E-07	1.24E-07	7.30E-06	1.46E-05	Activated
Axon guidance	128	35	5.24E-05	0.000209	0.00821	0.02463	Activated
Basal cell carcinoma	55	18	0.000322	0.002462	0.072615	0.290459	Inhibited
Cholinergic synapse	108	23	0.024222	0.003622	0.085469	0.427343	Inhibited
TGF-beta signaling pathway	80	20	0.006063	0.010163	0.19987	1	Inhibited
Bladder cancer	40	13	0.002276	0.012629	0.212882	1	Activated
Serotonergic synapse	111	24	0.018216	0.017234	0.254197	1	Inhibited
Retrograde endocannabinoid signaling	96	23	0.005972	0.036247	0.422168	1	Activated
Amoebiasis	91	22	0.006318	0.036349	0.422168	1	Inhibited

Data Characteristics

Total gene counts for RNA Seq 1 (Figure VII-18 A) and RNA Seq 2 (Figure VII-18 B). RNA Seq1 MDS plots are shown in Figure VII-19. MDS Plots with all versus select data are shown in Figure VII-20. CPM correlation and MDS plots for RNA Seq2 are reported in Figure VII-21.

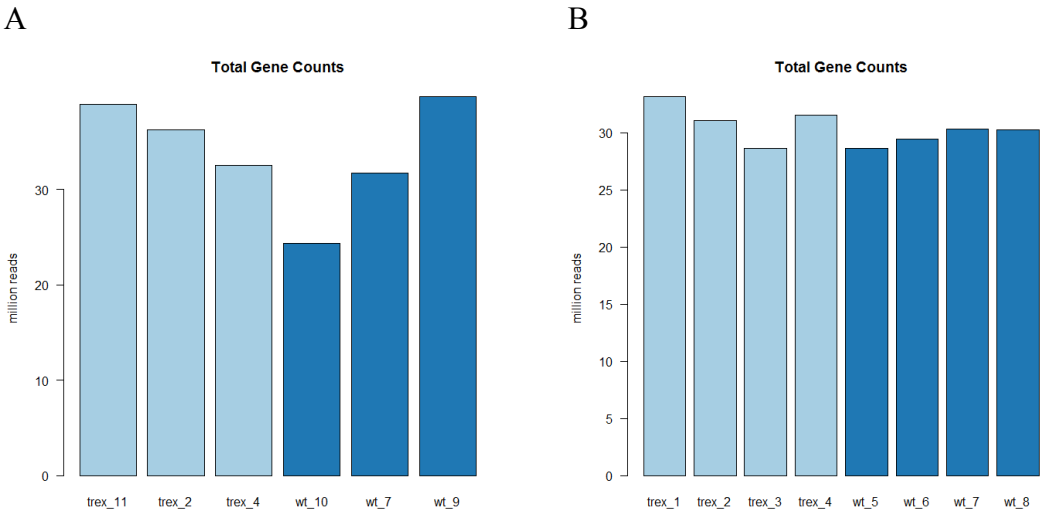

Figure VII-18: Total gene counts for both RNA Seq experiments.

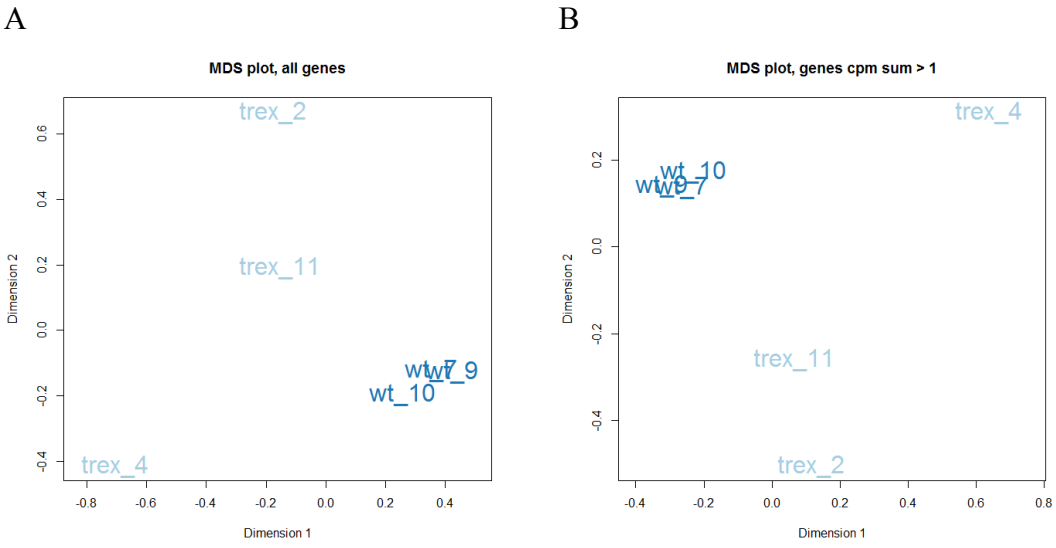

Figure VII-19: RNA Seq1 MDS plots

A B

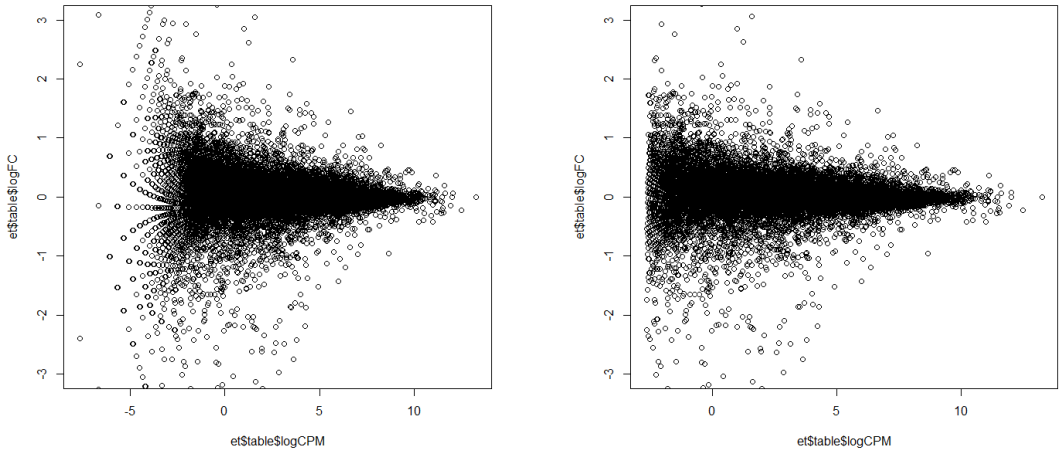

Figure VII-20: RNA Seq1 MDS Plots with all versus select data

A B

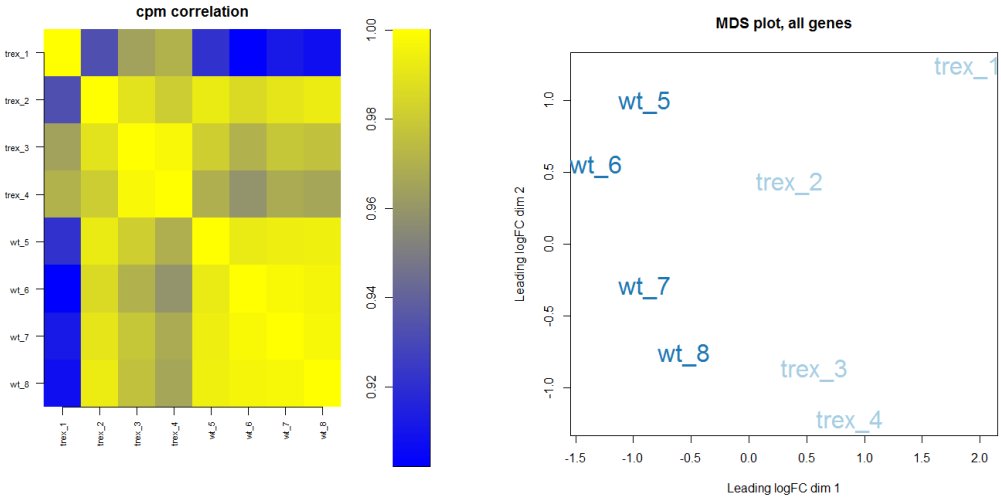

Figure VII-21: CPM correlation and MDS plot for RNA Seq 2

RNA SEQUENCING DATA TABLES

The following tables have been modified from all genes analyzed by CWS. For the following RNA Seq data tables, m=log2 (trex/wt), flag of 1=$p<0.01$, and flag of 2=$p<0.01$ and a fold change of >2. Positive flag values indicate up-regulation and negative flag values indicate down-regulation. In the interest of space, only genes with flag of 2 are included in the tables below of upregulated genes (Table VII-5 and Table VII-7), and flag of -2 of downregulated genes (Table VII-6 VI-6 and Table VI-8). Also included are tables where genes had a flag of 2 (or -2) in both RNA Seq1 and RNA Seq 2 (Table VII-9 and Table VII-10).

Table VII-5: RNA Seq1 Upregulated genes

gene	m	p-value	description
Apoc2	3.262737	0.000403	apolipoprotein C-II
Apoa4	3.054253	0.003068	apolipoprotein A-IV
Kng1	2.928748	0.003715	kininogen 1
Egr2	2.849418	4.18E-08	early growth response 2
Npbwr1	2.758083	7.46E-08	neuropeptides B/W receptor 1
2610528A11Rik	2.622459	3.81E-19	RIKEN cDNA 2610528A11 gene
Slco4c1	2.356697	0.001588	solute carrier organic anion transporter family, member 4C1
Apob	2.327529	0.00062	apolipoprotein B
8030451A03Rik	2.316358	0.00019	RIKEN cDNA 8030451A03 gene
4933402E13Rik	2.253192	0.003181	RIKEN cDNA 4933402E13 gene
Ehf	2.141605	6.71E-05	ets homologous factor
Pdzk1	2.046233	0.001239	PDZ domain containing 1
Fga	1.927084	0.006879	fibrinogen alpha chain
Dppa3	1.919458	0.001136	developmental pluripotency-associated 3
Fxyd2	1.884388	0.007618	FXYD domain-containing ion transport regulator 2
Cubn	1.87574	0.004079	cubilin (intrinsic factor-cobalamin receptor)
Slc2a2	1.871248	0.0018	solute carrier family 2 (facilitated glucose transporter), member 2
Kcna1	1.835507	7.76E-09	potassium voltage-gated channel, shaker-related subfamily, member 1
Kcnv2	1.830699	0.005659	potassium channel, subfamily V, member 2
Mfi2	1.786665	0.009315	antigen p97 (melanoma associated) identified by monoclonal antibodies 133.2 and 96.5
Chdh	1.773377	0.006604	choline dehydrogenase
Tbx22	1.745098	5.40E-06	T-box 22
BC025446	1.741658	0.006696	cDNA sequence BC025446
Tmem40	1.741658	0.000531	transmembrane protein 40
Apoa1	1.737104	0.008686	apolipoprotein A-I
AC108833.1	1.73055	0.007654	
Trim14	1.727948	0.001124	tripartite motif-containing 14
Acan	1.712667	0.000851	aggrecan
Slc39a5	1.697535	0.009476	solute carrier family 39 (metal ion transporter), member 5
Ascl2	1.692857	0.000572	achaete-scute complex homolog 2 (Drosophila)
Cfi	1.692501	0.004585	complement component factor i
Creb3l3	1.69225	0.001874	cAMP responsive element binding protein 3-like 3
A730049H05Rik	1.68436	1.02E-06	RIKEN cDNA A730049H05 gene
Luzp2	1.68081	0.001872	leucine zipper protein 2
Gm4876	1.665338	0.004728	predicted gene 4876
Cldn2	1.655651	0.00035	claudin 2
AC093341.1	1.641567	0.001638	

Apom	1.640644	0.009292	apolipoprotein M
Fgf3	1.63726	1.94E-08	fibroblast growth factor 3
Tdo2	1.627928	6.37E-16	tryptophan 2,3-dioxygenase
Adm2	1.622027	0.001472	adrenomedullin 2
Nxf7	1.607706	0.004585	nuclear RNA export factor 7
Otog	1.600939	0.001025	otogelin
Serpina3m	1.590503	0.009272	serine (or cysteine) peptidase inhibitor, clade A, member 3M
Serpina3e-ps	1.561	0.000109	serine (or cysteine) peptidase inhibitor, clade A, member 3E, pseudogene
WI1-2736D10.2	1.559727	0.007021	
Slc39a4	1.548374	0.00255	solute carrier family 39 (zinc transporter), member 4
Otx1	1.525308	0.001845	orthodenticle homolog 1 (Drosophila)
Nr4a3	1.519571	4.48E-08	nuclear receptor subfamily 4, group A, member 3
Oas1a	1.516998	0.005471	2'-5' oligoadenylate synthetase 1A
Igfbp1	1.516853	0.008216	insulin-like growth factor binding protein 1
Gfra3	1.516324	7.40E-12	glial cell line derived neurotrophic factor family receptor alpha 3
Spink3	1.51467	0.000223	serine peptidase inhibitor, Kazal type 3
Mrc1	1.514218	4.74E-11	mannose receptor, C type 1
Ttr	1.499947	0.000128	transthyretin
Xlr4a	1.498707	0.003468	X-linked lymphocyte-regulated 4A
Hbb-b2	1.480548	0.007766	hemoglobin, beta adult minor chain
RP23-183E20.1	1.479715	8.54E-05	
Ier3	1.464769	1.31E-06	immediate early response 3
Slc26a9	1.462893	0.001126	solute carrier family 26, member 9
Slc44a4	1.460978	0.00559	solute carrier family 44, member 4
CT030259.2	1.458222	0.000468	
Ddit4	1.457286	1.64E-09	DNA-damage-inducible transcript 4
Wnt8a	1.456862	5.32E-06	wingless-related MMTV integration site 8A
Anxa8	1.440242	8.99E-05	annexin A8
Gmnc	1.440242	0.003958	geminin coiled-coil domain containing
F2	1.437928	0.001674	coagulation factor II
Asb10	1.436285	0.000991	ankyrin repeat and SOCS box-containing 10
Gm20483	1.427544	0.007744	predicted gene 20483
Hbb-b1	1.424149	0.006227	hemoglobin, beta adult major chain
Pitx1	1.411706	0.000487	paired-like homeodomain transcription factor 1
Tac2	1.406616	9.96E-09	tachykinin 2
Gm17231	1.396203	1.19E-05	predicted gene 17231
Gpr50	1.39504	3.02E-14	G-protein-coupled receptor 50
Adrb3	1.392615	0.002324	adrenergic receptor, beta 3
March1	1.387459	0.003612	membrane-associated ring finger (C3HC4) 1
Lrrc23	1.386481	0.003778	leucine rich repeat containing 23
Gadl1	1.366664	5.92E-05	glutamate decarboxylase-like 1
3830417A13Rik	1.365108	4.28E-05	RIKEN cDNA 3830417A13 gene

Vstm5	1.362018	0.000504	V-set and transmembrane domain containing 5
Cfc1	1.34504	0.004565	cripto, FRL-1, cryptic family 1
Epyc	1.328295	1.96E-05	epiphycan
Marc1	1.326412	0.003468	mitochondrial amidoxime reducing component 1
9030617O03Rik	1.322264	0.007851	RIKEN cDNA 9030617O03 gene
Folr1	1.308083	0.003349	folate receptor 1 (adult)
Rab17	1.307699	0.008857	RAB17, member RAS oncogene family
C1qc	1.306424	0.002874	complement component 1, q subcomponent, C chain
Slc7a8	1.300695	0.001643	solute carrier family 7 (cationic amino acid transporter, y+ system), member 8
AC107641.1	1.279279	0.003573	
Caln1	1.278649	0.002966	calneuron 1
Rgs11	1.270199	3.68E-05	regulator of G-protein signaling 11
Eno2	1.265891	4.31E-08	enolase 2, gamma neuronal
Gp9	1.263624	0.003472	glycoprotein 9 (platelet)
Hand1	1.262596	2.25E-21	heart and neural crest derivatives expressed transcript 1
Serpina10	1.255682	0.005427	serine (or cysteine) peptidase inhibitor, clade A (alpha-1 antiproteinase, antitrypsin), member 10
Fst	1.244594	2.63E-18	follistatin
Rarres2	1.242338	1.68E-09	retinoic acid receptor responder (tazarotene induced) 2
Scn7a	1.235142	0.000359	sodium channel, voltage-gated, type VII, alpha
Iigp1	1.234903	0.000111	interferon inducible GTPase 1
Neat1	1.232566	1.39E-06	nuclear paraspeckle assembly transcript 1 (non-protein coding)
Actg2	1.231184	8.00E-05	actin, gamma 2, smooth muscle, enteric
BC006965	1.231013	0.004431	cDNA sequence BC006965
Stab2	1.22901	1.54E-07	stabilin 2
Hsd17b14	1.226426	0.001018	hydroxysteroid (17-beta) dehydrogenase 14
Gpx6	1.220721	0.000113	glutathione peroxidase 6
Ccbp2	1.220704	0.006495	chemokine binding protein 2
Hpcal4	1.215086	0.000494	hippocalcin-like 4
Ccdc79	1.212762	0.006638	coiled-coil domain containing 79
Stac	1.209231	0.007195	src homology three (SH3) and cysteine rich domain
Gm129	1.203724	2.40E-07	predicted gene 129
Stc2	1.188874	5.31E-11	stanniocalcin 2
Wdr38	1.180093	3.02E-08	WD repeat domain 38
BC021785	1.177742	0.006219	cDNA sequence BC021785
Lcp2	1.174784	2.55E-05	lymphocyte cytosolic protein 2
Egln3	1.168236	6.50E-11	EGL nine homolog 3 (C. elegans)
Mas1	1.167297	0.008193	MAS1 oncogene
Phlda2	1.158091	9.81E-06	pleckstrin homology-like domain, family A, member 2
Dmrt3	1.154384	0.006563	doublesex and mab-3 related transcription factor 3
Chl1	1.150635	1.60E-11	cell adhesion molecule with homology to L1CAM

Nkx2-3	1.127007	2.09E-07	NK2 transcription factor related, locus 3 (Drosophila)
Trf	1.122882	0.001754	transferrin
AL589650.1	1.119805	0.000213	
Cxcl14	1.109104	0.000179	chemokine (C-X-C motif) ligand 14
Car7	1.107214	4.94E-05	carbonic anhydrase 7
Ang	1.106502	0.006833	angiogenin, ribonuclease, RNase A family, 5
Mr1	1.09826	0.001186	major histocompatibility complex, class I-related
Fmo1	1.096127	5.48E-05	flavin containing monooxygenase 1
Gm12829	1.089854	0.001341	predicted gene 12829
Gm12688	1.08962	0.000294	predicted gene 12688
Bhlhe40	1.084691	1.34E-05	basic helix-loop-helix family, member e40
Proca1	1.083799	0.002105	protein interacting with cyclin A1
Rora	1.083525	1.09E-06	RAR-related orphan receptor alpha
Ndrg1	1.082031	7.48E-11	N-myc downstream regulated gene 1
Gm16439	1.081224	1.68E-08	predicted pseudogene 16439
Mcmdc2	1.074651	0.000181	minichromosome maintenance domain containing 2
AC163637.1	1.070576	0.000132	
Akr1c19	1.070375	0.005073	aldo-keto reductase family 1, member C19
Prss35	1.064669	2.92E-08	protease, serine, 35
Nkx2-9	1.059247	7.74E-06	NK2 transcription factor related, locus 9 (Drosophila)
Cyp26b1	1.048927	3.16E-05	cytochrome P450, family 26, subfamily b, polypeptide 1
Bnip3	1.039486	1.39E-15	BCL2/adenovirus E1B interacting protein 3
Ly96	1.03394	0.00652	lymphocyte antigen 96
Stc1	1.033301	6.08E-06	stanniocalcin 1
Slc13a4	1.026625	0.0034	solute carrier family 13 (sodium/sulfate symporters), member 4
Abi3bp	1.022992	0.000404	ABI gene family, member 3 (NESH) binding protein
Bmp3	1.019009	5.92E-07	bone morphogenetic protein 3
Afp	1.01761	0.001843	alpha fetoprotein
5330426P16Rik	1.015939	0.001389	RIKEN cDNA 5330426P16 gene

Table VII-6: RNA Seq1 Downregulated genes

gene	m	pval	description
Gcg	-8.29156	5.66E-56	glucagon
Hk3	-4.81943	1.45E-51	hexokinase 3
Ptf1a	-4.10094	1.50E-08	pancreas specific transcription factor, 1a
Hoxa10	-3.65309	2.26E-17	homeobox A10
Inmt	-3.39429	8.07E-07	indolethylamine N-methyltransferase
Ghrl	-3.37494	2.80E-10	ghrelin
Gsx1	-3.28215	1.05E-07	GS homeobox 1
Sln	-3.24306	1.66E-09	sarcolipin
Hoxd10	-3.24189	5.95E-34	homeobox D10
Hoxa11as	-3.22849	3.51E-14	HOXA11 antisense RNA (non-protein coding)
Csn3	-3.17569	1.01E-17	casein kappa
Hoxd11	-3.12848	2.95E-21	homeobox D11
Robo3	-3.03242	9.35E-17	roundabout homolog 3 (Drosophila)
Gabrg2	-3.00554	6.68E-07	gamma-aminobutyric acid (GABA) A receptor, subunit gamma 2
Barx1	-2.9671	3.18E-35	BarH-like homeobox 1
2310002L09Rik	-2.86649	1.68E-06	RIKEN cDNA 2310002L09 gene
Lhx5	-2.83101	1.80E-12	LIM homeobox protein 5
Hoxd13	-2.80119	1.69E-09	homeobox D13
Skor1	-2.79293	1.15E-06	SKI family transcriptional corepressor 1
Myom3	-2.78351	1.40E-08	myomesin family, member 3
Unc5a	-2.74687	4.06E-59	unc-5 homolog A (C. elegans)
Rspo4	-2.63469	8.79E-36	R-spondin family, member 4
Chrna3	-2.61797	2.85E-23	cholinergic receptor, nicotinic, alpha polypeptide 3
Hoxa11	-2.61392	1.77E-13	homeobox A11
Tbx15	-2.56279	4.84E-15	T-box 15
Nxf3	-2.55129	4.50E-11	nuclear RNA export factor 3
NA	-2.54666	5.73E-05	NA
Myh3	-2.49175	2.29E-26	myosin, heavy polypeptide 3, skeletal muscle, embryonic
C130071C03Rik	-2.47039	9.02E-23	RIKEN cDNA C130071C03 gene
Lhx9	-2.42406	3.54E-46	LIM homeobox protein 9
Hs3st2	-2.42405	1.31E-06	heparan sulfate (glucosamine) 3-O-sulfotransferase 2
Vwde	-2.40572	6.94E-05	von Willebrand factor D and EGF domains
Bhlhe23	-2.37168	2.65E-08	basic helix-loop-helix family, member e23
Nrg3	-2.35551	0.000167	neuregulin 3
Musk	-2.35551	0.000145	muscle, skeletal, receptor tyrosine kinase
D930028M14Rik	-2.34475	1.23E-16	RIKEN cDNA D930028M14 gene
Chat	-2.27539	0.000134	choline acetyltransferase
Gm13652	-2.26979	1.38E-12	predicted gene 13652
Crp	-2.26167	1.13E-06	C-reactive protein, pentraxin-related
Tenm1	-2.24951	0.000971	teneurin transmembrane protein 1

Stk32a	-2.23385	2.42E-24	serine/threonine kinase 32A
Calb1	-2.22421	6.11E-05	calbindin 1
Cdx1	-2.21435	4.11E-23	caudal type homeobox 1
Alx3	-2.19948	5.95E-34	aristaless-like homeobox 3
En1	-2.19389	2.17E-14	engrailed 1
Chrnb4	-2.19372	4.83E-19	cholinergic receptor, nicotinic, beta polypeptide 4
Cntn2	-2.18273	1.73E-23	contactin 2
Msc	-2.17689	7.59E-11	musculin
Hic1	-2.17209	7.33E-13	hypermethylated in cancer 1
Ankrd2	-2.15414	6.03E-12	ankyrin repeat domain 2 (stretch responsive muscle)
Gpx2	-2.14701	0.000121	glutathione peroxidase 2
Pdx1	-2.11013	1.65E-07	pancreatic and duodenal homeobox 1
Tnnc2	-2.10478	1.51E-16	troponin C2, fast
Actl6b	-2.10154	0.000275	actin-like 6B
Tmem132e	-2.09686	8.01E-28	transmembrane protein 132E
Nr0b1	-2.07599	3.36E-07	nuclear receptor subfamily 0, group B, member 1
Sgcg	-2.06909	0.00032	sarcoglycan, gamma (dystrophin-associated glycoprotein)
AC154412.1	-2.06909	0.00016	
Lin7a	-2.02641	1.52E-17	lin-7 homolog A (C. elegans)
Mstn	-2.02626	2.29E-09	myostatin
Scrt1	-1.99641	1.30E-08	scratch homolog 1, zinc finger protein (Drosophila)
Pyy	-1.9872	3.84E-07	peptide YY
Pou2f2	-1.96167	5.34E-08	POU domain, class 2, transcription factor 2
1110059M19Rik	-1.94114	4.89E-05	RIKEN cDNA 1110059M19 gene
Ecel1	-1.93551	1.21E-10	endothelin converting enzyme-like 1
1700128E19Rik	-1.92091	1.08E-06	RIKEN cDNA 1700128E19 gene
Ppp2r2c	-1.90115	3.55E-13	protein phosphatase 2 (formerly 2A), regulatory subunit B (PR 52), gamma isoform
Nhlh2	-1.86466	7.27E-21	nescient helix loop helix 2
Dcx	-1.86449	2.42E-19	doublecortin
Lhx2	-1.85329	5.93E-25	LIM homeobox protein 2
Sim2	-1.83517	0.000123	single-minded homolog 2 (Drosophila)
Gsx2	-1.83371	5.76E-08	GS homeobox 2
Fam19a1	-1.81625	0.000237	family with sequence similarity 19, member A1
A730090H04Rik	-1.81625	0.000241	RIKEN cDNA A730090H04 gene
C130021I20Rik	-1.81319	1.64E-27	Riken cDNA C130021I20 gene
Nepn	-1.79565	2.18E-26	nephrocan
Slc17a7	-1.79374	3.23E-06	solute carrier family 17 (sodium-dependent inorganic phosphate cotransporter), member 7
Grifin	-1.78892	0.001774	galectin-related inter-fiber protein
Kcnh5	-1.74198	0.001422	potassium voltage-gated channel, subfamily H (eag-related), member 5
Nxph1	-1.73546	0.003329	neurexophilin 1
Gjd4	-1.72906	4.28E-05	gap junction protein, delta 4

Crlf1	-1.72313	7.35E-07	cytokine receptor-like factor 1
Gpr179	-1.71851	0.002578	G protein-coupled receptor 179
Gm7325	-1.67161	0.000179	predicted gene 7325
Chrna1	-1.67107	0.000155	cholinergic receptor, nicotinic, alpha polypeptide 1 (muscle)
Neb	-1.67004	9.19E-07	nebulin
Ephx1	-1.65365	1.63E-06	epoxide hydrolase 1, microsomal
Mylk4	-1.6524	1.24E-05	myosin light chain kinase family, member 4
Syt4	-1.65125	2.69E-06	synaptotagmin IV
Rhbdl3	-1.64246	1.17E-23	rhomboid, veinlet-like 3 (Drosophila)
Nyap2	-1.63231	8.15E-05	neuronal tyrosine-phophorylated phosphoinositide 3-kinase adaptor 2
3110047P20Rik	-1.63231	4.25E-05	RIKEN cDNA 3110047P20 gene
Gm16140	-1.62697	0.00046	predicted gene 16140
Svop	-1.61227	4.39E-05	SV2 related protein
Insc	-1.59986	7.65E-08	inscuteable homolog (Drosophila)
9430024E24Rik	-1.59704	7.30E-07	RIKEN cDNA 9430024E24 gene
Myot	-1.59525	8.65E-05	myotilin
Ppfia2	-1.58456	0.000303	protein tyrosine phosphatase, receptor type, f polypeptide (PTPRF), interacting protein (liprin), alpha 2
Il17b	-1.58177	0.000613	interleukin 17B
Fstl5	-1.58177	0.000652	follistatin-like 5
Lingo4	-1.5707	0.007381	leucine rich repeat and Ig domain containing 4
Rfx6	-1.55712	1.46E-05	regulatory factor X, 6
Nkx2-1	-1.55352	2.73E-05	NK2 homeobox 1
Sst	-1.55351	1.42E-05	somatostatin
Mybph	-1.54288	2.33E-11	myosin binding protein H
Kirrel2	-1.5411	4.32E-06	kin of IRRE like 2 (Drosophila)
Myf6	-1.53729	1.29E-06	myogenic factor 6
Klhl40	-1.53432	0.000265	kelch-like 40
Amica1	-1.52212	1.91E-11	adhesion molecule, interacts with CXADR antigen 1
Rarb	-1.51686	4.66E-37	retinoic acid receptor, beta
Dhrs3	-1.51169	2.22E-13	dehydrogenase/reductase (SDR family) member 3
Chrna5	-1.51163	2.95E-07	cholinergic receptor, nicotinic, alpha polypeptide 5
Gm14343	-1.5086	0.004264	predicted gene 14343
RP23-207N5.1	-1.50767	0.000908	
BC030500	-1.49438	0.00048	cDNA sequence BC030500
Gsc	-1.48519	0.006426	goosecoid homeobox
Scrt2	-1.47379	8.19E-10	scratch homolog 2, zinc finger protein (Drosophila)
Edar	-1.45769	1.80E-06	ectodysplasin-A receptor
Fbll1	-1.45711	0.00987	fibrillarin-like 1
Wfdc1	-1.45339	3.03E-05	WAP four-disulfide core domain 1
Rgs7	-1.44653	0.006035	regulator of G protein signaling 7
3110035E14Rik	-1.43727	8.62E-06	RIKEN cDNA 3110035E14 gene

Sncg	-1.42944	1.55E-06	synuclein, gamma
Arg1	-1.42876	1.33E-46	arginase, liver
Il1rn	-1.42668	0.001805	interleukin 1 receptor antagonist
Foxq1	-1.42424	1.17E-05	forkhead box Q1
Mmp24	-1.417	0.001074	matrix metallopeptidase 24
Cxcl13	-1.40946	7.02E-09	chemokine (C-X-C motif) ligand 13
Grm2	-1.40937	1.55E-05	glutamate receptor, metabotropic 2
Tmem8c	-1.40493	0.000181	transmembrane protein 8C
Atp2a1	-1.40008	1.68E-10	ATPase, Ca++ transporting, cardiac muscle, fast twitch 1
Cps1	-1.39032	0.006936	carbamoyl-phosphate synthetase 1
Srms	-1.38277	0.001792	src-related kinase lacking C-terminal regulatory tyrosine and N-terminal myristylation sites
Barhl2	-1.38277	0.005251	BarH-like 2 (Drosophila)
Ina	-1.37857	1.63E-09	internexin neuronal intermediate filament protein, alpha
Lmx1b	-1.36869	4.89E-23	LIM homeobox transcription factor 1 beta
Islr2	-1.34874	0.000203	immunoglobulin superfamily containing leucine-rich repeat 2
Myog	-1.34069	1.64E-11	myogenin
Gm16010	-1.34007	0.000513	predicted gene 16010
Bhlhe22	-1.32914	5.23E-07	basic helix-loop-helix family, member e22
Pcsk2	-1.32201	0.000227	proprotein convertase subtilisin/kexin type 2
Ntrk1	-1.31822	2.93E-07	neurotrophic tyrosine kinase, receptor, type 1
March4	-1.31708	0.003705	membrane-associated ring finger (C3HC4) 4
Fam163a	-1.3141	0.00075	family with sequence similarity 163, member A
Lhx4	-1.31341	1.11E-06	LIM homeobox protein 4
Mnx1	-1.31188	4.64E-07	motor neuron and pancreas homeobox 1
Fndc5	-1.30622	2.21E-13	fibronectin type III domain containing 5
Nppc	-1.30066	1.75E-05	natriuretic peptide type C
Tecta	-1.29897	0.00049	tectorin alpha
Hoxa4	-1.28821	1.52E-14	homeobox A4
Kcnj10	-1.27811	3.19E-07	potassium inwardly-rectifying channel, subfamily J, member 10
Scml4	-1.2728	2.74E-05	sex comb on midleg-like 4 (Drosophila)
Slc10a4	-1.26966	4.22E-05	solute carrier family 10 (sodium/bile acid cotransporter family), member 4
Scn9a	-1.26865	0.005063	sodium channel, voltage-gated, type IX, alpha
Glra1	-1.25302	9.61E-07	glycine receptor, alpha 1 subunit
Ugt8a	-1.25182	0.000381	UDP galactosyltransferase 8A
Foxn4	-1.23014	0.000909	forkhead box N4
Stmn3	-1.22941	1.93E-07	stathmin-like 3
Trim67	-1.22609	0.000373	tripartite motif-containing 67
Ctxn3	-1.22341	0.00062	cortexin 3
Gm16582	-1.21832	1.84E-06	predicted gene 16582

Cdk5r2	-1.21832	1.84E-06	cyclin-dependent kinase 5, regulatory subunit 2 (p39)
Dlx4	-1.20729	0.009829	distal-less homeobox 4
C78197	-1.20527	0.004576	expressed sequence C78197
Scg2	-1.20439	0.004912	secretogranin II
Srrm3	-1.2001	4.01E-05	serine/arginine repetitive matrix 3
2700069I18Rik	-1.19928	0.001117	RIKEN cDNA 2700069I18 gene
Rasgef1c	-1.19177	8.50E-05	RasGEF domain family, member 1C
Tshz1	-1.18932	9.65E-37	teashirt zinc finger family member 1
Slc38a5	-1.18784	1.98E-07	solute carrier family 38, member 5
Tmem59l	-1.18147	1.88E-05	transmembrane protein 59-like
Pcdh20	-1.17756	0.000977	protocadherin 20
Gfra1	-1.1759	5.36E-11	glial cell line derived neurotrophic factor family receptor alpha 1
Atcay	-1.17337	1.03E-05	ataxia, cerebellar, Cayman type homolog (human)
Nanos3	-1.17303	0.008216	nanos homolog 3 (Drosophila)
Dock10	-1.16576	3.47E-07	dedicator of cytokinesis 10
Pou3f4	-1.16083	5.37E-09	POU domain, class 3, transcription factor 4
Ano5	-1.1524	0.003455	anoctamin 5
Fgf4	-1.14891	0.004583	fibroblast growth factor 4
Elavl3	-1.14779	1.82E-09	ELAV (embryonic lethal, abnormal vision, Drosophila)-like 3 (Hu antigen C)
Pax7	-1.14745	6.02E-12	paired box gene 7
Syndig1	-1.14657	0.000441	synapse differentiation inducing 1
Rgs9	-1.14627	6.23E-08	regulator of G-protein signaling 9
Neurog1	-1.14364	1.56E-07	neurogenin 1
Klhl14	-1.14299	8.04E-06	kelch-like 14
Plk3	-1.13558	4.34E-12	polo-like kinase 3
Stmn4	-1.13302	4.18E-07	stathmin-like 4
Ap3b2	-1.1317	1.15E-08	adaptor-related protein complex 3, beta 2 subunit
Gnat3	-1.12483	0.00414	guanine nucleotide binding protein, alpha transducing 3
Nefm	-1.11882	4.29E-06	neurofilament, medium polypeptide
1700109F18Rik	-1.1139	2.68E-06	RIKEN cDNA 1700109F18 gene
Adcy8	-1.10402	6.84E-07	adenylate cyclase 8
Ttbk1	-1.1001	2.22E-05	tau tubulin kinase 1
C1ql3	-1.09221	0.001522	C1q-like 3
Gm13781	-1.09036	0.000816	predicted gene 13781
Kcnk10	-1.09029	0.002251	potassium channel, subfamily K, member 10
Prdm13	-1.09027	8.44E-08	PR domain containing 13
Asic2	-1.08914	8.39E-06	acid-sensing (proton-gated) ion channel 2
Zfp536	-1.08571	1.03E-05	zinc finger protein 536
Arhgap36	-1.07916	7.86E-06	Rho GTPase activating protein 36
Nkx2-6	-1.06592	0.000319	NK2 transcription factor related, locus 6 (Drosophila)
Galnt9	-1.05442	0.002538	UDP-N-acetyl-alpha-D-galactosamine:polypeptide N-acetylgalactosaminyltransferase 9

Gm15055	-1.0534	0.009146	predicted gene 15055
Rec8	-1.05254	0.001933	REC8 homolog (yeast)
Gm12892	-1.05188	1.17E-14	predicted gene 12892
Tubb3	-1.05104	1.25E-08	tubulin, beta 3 class III
Eva1a	-1.05018	0.000964	eva-1 homolog A (C. elegans)
Mylpf	-1.04946	1.64E-06	myosin light chain, phosphorylatable, fast skeletal muscle
Scg3	-1.04879	1.77E-07	secretogranin III
Rundc3a	-1.04651	5.76E-07	RUN domain containing 3A
Disp2	-1.04641	0.001046	dispatched homolog 2 (Drosophila)
Nkx1-2	-1.0463	0.000739	NK1 transcription factor related, locus 2 (Drosophila)
Stmn2	-1.03964	7.39E-06	stathmin-like 2
Hoxd9	-1.03771	5.49E-10	homeobox D9
E330013P04Rik	-1.037	0.001731	RIKEN cDNA E330013P04 gene
Gm16551	-1.03607	1.62E-08	predicted gene 16551
Myt1	-1.0356	1.07E-06	myelin transcription factor 1
Pnmal1	-1.02742	0.00012	PNMA-like 1
Onecut3	-1.02579	0.000432	one cut domain, family member 3
Onecut2	-1.0257	1.36E-08	one cut domain, family member 2
Arpp21	-1.02504	0.001053	cyclic AMP-regulated phosphoprotein, 21
Ascl1	-1.02091	2.85E-06	achaete-scute complex homolog 1 (Drosophila)
Cabp7	-1.01555	0.005897	calcium binding protein 7
Rab3c	-1.01555	0.000244	RAB3C, member RAS oncogene family
Lamc3	-1.01243	1.99E-06	laminin gamma 3
Emx2	-1.0091	1.26E-06	empty spiracles homeobox 2
Krt5	-1.00886	5.01E-07	keratin 5
Chst8	-1.00395	8.66E-05	carbohydrate (N-acetylgalactosamine 4-0) sulfotransferase 8
Hoxa1	-1.00204	3.36E-11	homeobox A1

Table VII-7: RNA Seq2 Upregulated genes

gene	m	pval	description
S100g	6.3116	1.51E-06	S100 calcium binding protein G
Hoxc8	5.6762	3.78E-69	homeobox C8
Oc90	5.0688	0.002635	otoconin 90
Apoa4	4.9514	6.08E-05	apolipoprotein A-IV
Krt13	4.9056	0.000361	keratin 13
Trappc3l	4.5625	3.40E-07	trafficking protein particle complex 3 like
Gpr50	4.4919	2.61E-38	G-protein-coupled receptor 50
Gm15634	4.2751	0.006069	predicted gene 15634
NA	4.2688	0.008368	NA
Tdgf1	4.2153	2.74E-07	teratocarcinoma-derived growth factor 1
Ms4a2	4.2067	4.93E-06	membrane-spanning 4-domains, subfamily A, member 2
Nppb	4.1482	0.000117	natriuretic peptide type B
4933402E13Rik	4.1186	9.85E-07	RIKEN cDNA 4933402E13 gene
Ccl2	4.0760	0.000298	chemokine (C-C motif) ligand 2
Cldn14	3.9145	4.12E-05	claudin 14
Gm15283	3.7415	7.21E-11	predicted gene 15283
Epyc	3.7284	3.03E-09	epiphycan
2610528A11Rik	3.6810	5.84E-09	RIKEN cDNA 2610528A11 gene
Phf11b	3.6338	0.000394	PHD finger protein 11B
Apob	3.5982	1.81E-07	apolipoprotein B
Chac1	3.5382	1.63E-06	ChaC, cation transport regulator 1
NA	3.5301	0.002692	NA
Clec18a	3.4706	4.22E-06	C-type lectin domain family 18, member A
Chst13	3.4295	0.001138	carbohydrate (chondroitin 4) sulfotransferase 13
Gm11734	3.4244	0.000817	predicted gene 11734
Ier3	3.4155	8.42E-11	immediate early response 3
Tdo2	3.3696	4.54E-11	tryptophan 2,3-dioxygenase
Gmnc	3.2955	0.003174	geminin coiled-coil domain containing
Tac2	3.2249	2.52E-11	tachykinin 2
Pitx1	3.2222	1.88E-08	paired-like homeodomain transcription factor 1
5031434C07Rik	3.1690	0.003766	RIKEN cDNA 5031434C07 gene
Ascl2	3.1602	1.55E-06	achaete-scute complex homolog 2 (Drosophila)
Spp2	3.1559	0.00023	secreted phosphoprotein 2
Abcc2	3.0814	1.02E-05	ATP-binding cassette, sub-family C (CFTR/MRP), member 2
Eno2	3.0518	5.77E-09	enolase 2, gamma neuronal
Scnn1g	2.9885	0.001638	sodium channel, nonvoltage-gated 1 gamma
Aire	2.9717	6.34E-08	autoimmune regulator (autoimmune polyendocrinopathy candidiasis ectodermal dystrophy)
Hand1	2.9643	1.03E-24	heart and neural crest derivatives expressed transcript 1
Egr2	2.9135	0.000452	early growth response 2
Ddit4	2.8577	3.04E-13	DNA-damage-inducible transcript 4

Hoxc6	2.8239	6.76E-10	homeobox C6
Cubn	2.8002	7.40E-06	cubilin (intrinsic factor-cobalamin receptor)
Hoxa9	2.7910	8.50E-05	homeobox A9
Gm22661	2.7695	0.000237	predicted gene, 22661
Gm27505	2.7664	0.000927	predicted gene, 27505
Postn	2.7624	3.31E-23	periostin, osteoblast specific factor
Gm12746	2.7229	8.56E-06	predicted gene 12746
Trap1a	2.7038	0.000209	tumor rejection antigen P1A
Inhbb	2.6890	0.000169	inhibin beta-B
Vax1	2.6850	0.004055	ventral anterior homeobox 1
Muc13	2.6152	1.60E-05	mucin 13, epithelial transmembrane
Hoxa7	2.5947	0.000394	homeobox A7
Card14	2.5809	0.00059	caspase recruitment domain family, member 14
Prss35	2.5807	7.19E-16	protease, serine 35
Bhlhe40	2.5717	1.70E-07	basic helix-loop-helix family, member e40
Gm27533	2.5154	0.00452	predicted gene, 27533
Ppp1r3c	2.4615	2.90E-06	protein phosphatase 1, regulatory (inhibitor) subunit 3C
Adm2	2.4377	9.67E-06	adrenomedullin 2
Rarres2	2.4159	6.12E-17	retinoic acid receptor responder (tazarotene induced) 2
Xlr5c	2.4155	0.002879	X-linked lymphocyte-regulated 5C
5730403I07Rik	2.4112	0.001647	RIKEN cDNA 5730403I07 gene
Mab21l2	2.3708	1.44E-17	mab-21-like 2 (C. elegans)
Hoxb9	2.3384	8.42E-06	homeobox B9
Oxtr	2.3344	4.88E-06	oxytocin receptor
Muc2	2.3090	7.92E-07	mucin 2
Car7	2.2961	3.72E-26	carbonic anhydrase 7
9330159N05Rik	2.2957	6.47E-05	RIKEN cDNA 9330159N05 gene
Stc1	2.2617	1.18E-12	stanniocalcin 1
Gm20467	2.2583	5.38E-10	predicted gene 20467
Gm14685	2.2466	0.000326	predicted gene 14685
Ndrg1	2.2381	3.25E-09	N-myc downstream regulated gene 1
Gfra3	2.2332	5.24E-13	glial cell line derived neurotrophic factor family receptor alpha 3
Otx2	2.2231	5.08E-07	orthodenticle homolog 2
Ptgs2	2.2133	1.35E-09	prostaglandin-endoperoxide synthase 2
Egln3	2.2053	9.01E-13	egl-9 family hypoxia-inducible factor 3
mt-Th	2.2024	0.002926	mitochondrially encoded tRNA histidine
Ciart	2.1966	5.30E-16	circadian associated repressor of transcription
Gm12022	2.1949	0.000438	predicted gene 12022
Cdrt4	2.1518	0.006047	CMT1A duplicated region transcript 4
Gm11027	2.1456	0.007256	predicted gene 11027
S1pr5	2.1240	0.000732	sphingosine-1-phosphate receptor 5
Kcne3	2.1106	4.56E-14	potassium voltage-gated channel, Isk-related subfamily, gene 3
Gm28006	2.1080	0.00509	predicted gene, 28006

Gm17202	2.0993	0.00032	predicted gene 17202
Stc2	2.0729	3.23E-13	stanniocalcin 2
Wnt8a	2.0659	7.46E-13	wingless-type MMTV integration site family, member 8A
Gm16439	2.0629	5.18E-11	predicted pseudogene 16439
Trib3	2.0300	4.02E-05	tribbles homolog 3 (Drosophila)
Serpina3f	1.9971	0.003113	serine (or cysteine) peptidase inhibitor, clade A, member 3F
Slc22a3	1.9707	2.36E-07	solute carrier family 22 (organic cation transporter), member 3
P4ha2	1.9672	3.35E-14	procollagen-proline, 2-oxoglutarate 4-dioxygenase (proline 4-hydroxylase), alpha II polypeptide
Hmx2	1.9522	0.007064	H6 homeobox 2
Bhlhe41	1.9245	2.49E-05	basic helix-loop-helix family, member e41
Neat1	1.9199	1.61E-09	nuclear paraspeckle assembly transcript 1 (non-protein coding)
Ankrd37	1.9152	1.92E-07	ankyrin repeat domain 37
Adm	1.9099	0.000358	adrenomedullin
Nkx2-3	1.8991	2.68E-15	NK2 homeobox 3
Avpr1b	1.8909	2.14E-05	arginine vasopressin receptor 1B
Tmem211	1.8877	0.002634	transmembrane protein 211
Rgs11	1.8856	8.75E-07	regulator of G-protein signaling 11
Dio3os	1.8852	4.19E-05	deiodinase, iodothyronine type III, opposite strand
Lrrc15	1.8456	0.000149	leucine rich repeat containing 15
Chl1	1.8436	4.67E-16	cell adhesion molecule with homology to L1CAM
Bnip3	1.8414	1.01E-13	BCL2/adenovirus E1B interacting protein 3
Nxf7	1.8316	0.000185	nuclear RNA export factor 7
Vldlr	1.8170	5.13E-12	very low density lipoprotein receptor
Pla1a	1.8167	0.005513	phospholipase A1 member A
Kcnh7	1.8160	2.64E-08	potassium voltage-gated channel, subfamily H (eag-related), member 7
5033428I22Rik	1.8159	5.01E-09	RIKEN cDNA 5033428I22 gene
Tsix	1.8061	0.008786	X (inactive)-specific transcript, opposite strand
Ndufa4l2	1.8008	0.000129	NADH dehydrogenase (ubiquinone) 1 alpha subcomplex, 4-like 2
1110018N20Rik	1.7993	0.003328	RIKEN cDNA 1110018N20 gene
Syndig1l	1.7993	0.004407	synapse differentiation inducing 1 like
Prdm6	1.7960	2.84E-12	PR domain containing 6
Krt19	1.7883	1.80E-09	keratin 19
Hoxc9	1.7637	0.00019	homeobox C9
Vstm5	1.7598	8.22E-06	V-set and transmembrane domain containing 5
NA	1.7528	0.000395	NA
Rhox5	1.7197	7.25E-06	reproductive homeobox 5
Hoxd8	1.7032	0.004158	homeobox D8
Gm26992	1.7030	0.007749	predicted gene, 26992
Il19	1.7027	0.001991	interleukin 19

Pfkp	1.7024	1.34E-10	phosphofructokinase, platelet
1700001L05Rik	1.6988	3.17E-07	RIKEN cDNA 1700001L05 gene
Kcnk3	1.6926	7.28E-07	potassium channel, subfamily K, member 3
Rxfp1	1.6917	1.29E-08	relaxin/insulin-like family peptide receptor 1
Pparg	1.6856	0.000889	peroxisome proliferator activated receptor gamma
Gm14506	1.6832	1.26E-06	predicted gene 14506
Mgarp	1.6821	1.37E-08	mitochondria localized glutamic acid rich protein
Fam184b	1.6811	9.50E-08	family with sequence similarity 184, member B
Upk1b	1.6593	0.000615	uroplakin 1B
Abi3bp	1.6585	5.07E-11	ABI gene family, member 3 (NESH) binding protein
Gm11536	1.6534	0.001737	predicted gene 11536
Cox4i2	1.6471	6.33E-08	cytochrome c oxidase subunit IV isoform 2
Gm6277	1.6350	8.25E-06	predicted gene 6277
Pfkfb3	1.6140	3.93E-13	6-phosphofructo-2-kinase/fructose-2,6-biphosphatase 3
Gm16754	1.6090	2.12E-10	predicted gene, 16754
Pla2g5	1.6052	0.000239	phospholipase A2, group V
Adamts2	1.6021	2.09E-11	a disintegrin-like and metallopeptidase (reprolysin type) with thrombospondin type 1 motif, 2
Mir483	1.5994	0.00293	microRNA 483
Pof1b	1.5968	7.91E-05	premature ovarian failure 1B
Kcna1	1.5941	4.65E-05	potassium voltage-gated channel, shaker-related subfamily, member 1
Efna3	1.5928	7.24E-10	ephrin A3
Gjb5	1.5813	2.36E-09	gap junction protein, beta 5
Fam65c	1.5721	5.17E-11	family with sequence similarity 65, member C
Gdf10	1.5500	3.43E-09	growth differentiation factor 10
Hoxa6	1.5482	2.18E-05	homeobox A6
Phlda2	1.5360	9.66E-07	pleckstrin homology-like domain, family A, member 2
Tnfaip3	1.5306	1.07E-06	tumor necrosis factor, alpha-induced protein 3
Ppp1r3g	1.5266	3.84E-06	protein phosphatase 1, regulatory (inhibitor) subunit 3G
Bmp3	1.5179	1.00E-08	bone morphogenetic protein 3
H2-Ab1	1.5146	0.006489	histocompatibility 2, class II antigen A, beta 1
Gm15850	1.5143	0.002541	predicted gene 15850
Fas	1.5127	4.17E-07	Fas (TNF receptor superfamily member 6)
Hoxb5os	1.4983	1.92E-09	homeobox B5 and homeobox B6, opposite strand
Fam71f2	1.4946	0.000342	family with sequence similarity 71, member F2
A730049H05Rik	1.4938	1.51E-06	RIKEN cDNA A730049H05 gene
Slc2a3	1.4910	3.31E-12	solute carrier family 2 (facilitated glucose transporter), member 3
Fat2	1.4787	2.15E-06	FAT tumor suppressor homolog 2 (Drosophila)
Rora	1.4781	9.40E-08	RAR-related orphan receptor alpha
Cbln3	1.4743	1.72E-06	cerebellin 3 precursor protein
Fst	1.4674	1.50E-29	follistatin
Col1a1	1.4652	8.60E-15	collagen, type I, alpha 1
Plcxd1	1.4581	2.31E-05	phosphatidylinositol-specific phospholipase C, X domain

			containing 1
Adamts18	1.4562	3.55E-11	a disintegrin-like and metallopeptidase (reprolysin type) with thrombospondin type 1 motif, 18
Pi15	1.4481	4.53E-05	peptidase inhibitor 15
Stac	1.4473	6.03E-05	src homology three (SH3) and cysteine rich domain
Hrct1	1.4416	0.009552	histidine rich carboxyl terminus 1
Gm26670	1.4394	0.004075	predicted gene, 26670
Notumos	1.4375	0.003677	notum pectinacetylesterase homolog (Drosophila), opposite strand
Slc16a3	1.4339	2.70E-19	solute carrier family 16 (monocarboxylic acid transporters), member 3
Dkk2	1.4248	6.04E-09	dickkopf homolog 2 (Xenopus laevis)
2500002B13Rik	1.4220	7.32E-09	RIKEN cDNA 2500002B13 gene
5330426P16Rik	1.4199	4.42E-05	RIKEN cDNA 5330426P16 gene
Ptprv	1.4099	1.50E-07	protein tyrosine phosphatase, receptor type, V
Lyve1	1.4095	2.07E-05	lymphatic vessel endothelial hyaluronan receptor 1
NA	1.4077	0.000193	NA
Tmem45a	1.4055	3.14E-07	transmembrane protein 45a
Nr4a3	1.3927	3.79E-09	nuclear receptor subfamily 4, group A, member 3
Apln	1.3880	6.26E-16	apelin
Gpx6	1.3869	0.005065	glutathione peroxidase 6
Grhl3	1.3820	8.06E-09	grainyhead-like 3 (Drosophila)
Fgf3	1.3676	2.50E-08	fibroblast growth factor 3
Smoc2	1.3654	3.79E-08	SPARC related modular calcium binding 2
Hk2	1.3586	2.27E-13	hexokinase 2
Cdk15	1.3445	0.00631	cyclin-dependent kinase 15
Sp7	1.3443	0.000246	Sp7 transcription factor 7
Gm26826	1.3429	0.000509	predicted gene, 26826
Wisp1	1.3363	5.75E-08	WNT1 inducible signaling pathway protein 1
Hpcal4	1.3350	0.000762	hippocalcin-like 4
Col14a1	1.3273	1.12E-14	collagen, type XIV, alpha 1
Klk13	1.3058	0.000591	kallikrein related-peptidase 13
Aldoc	1.3029	4.18E-06	aldolase C, fructose-bisphosphate
Zan	1.2993	3.21E-07	zonadhesin
Gm15179	1.2978	0.001406	predicted gene 15179
Appbp2os	1.2963	5.53E-05	amyloid beta precursor protein (cytoplasmic tail) binding protein 2, opposite strand
3110057O12Rik	1.2848	2.30E-07	RIKEN cDNA 3110057O12 gene
3830417A13Rik	1.2792	0.001321	RIKEN cDNA 3830417A13 gene
Pdk1	1.2668	2.93E-16	pyruvate dehydrogenase kinase, isoenzyme 1
Ero1l	1.2570	2.47E-10	ERO1-like (S. cerevisiae)
Cyp26b1	1.2569	8.30E-06	cytochrome P450, family 26, subfamily b, polypeptide 1
Rgcc	1.2568	4.64E-07	regulator of cell cycle
Kdm4d	1.2567	0.003917	lysine (K)-specific demethylase 4D
Ovol1	1.2544	0.004006	OVO homolog-like 1 (Drosophila)

Gdap10	1.2510	1.36E-06	ganglioside-induced differentiation-associated-protein 10
Tlr12	1.2493	0.001699	toll-like receptor 12
Slc39a4	1.2493	0.002273	solute carrier family 39 (zinc transporter), member 4
G430049J08Rik	1.2469	5.84E-05	RIKEN cDNA G430049J08 gene
Gm12758	1.2459	6.38E-06	predicted gene 12758
Hoxb7	1.2403	1.31E-09	homeobox B7
Cabp1	1.2311	4.45E-09	calcium binding protein 1
9530026P05Rik	1.2310	1.35E-08	RIKEN cDNA 9530026P05 gene
March10	1.2294	0.000374	membrane-associated ring finger (C3HC4) 10
Oas3	1.2195	0.000477	2'-5' oligoadenylate synthetase 3
Cyp2s1	1.2179	0.00131	cytochrome P450, family 2, subfamily s, polypeptide 1
Stab2	1.2069	5.27E-07	stabilin 2
Hgfac	1.2064	0.006643	hepatocyte growth factor activator
Fgf15	1.2062	1.56E-11	fibroblast growth factor 15
F7	1.2039	0.002034	coagulation factor VII
Calml4	1.1981	0.000716	calmodulin-like 4
Arrdc3	1.1973	3.59E-10	arrestin domain containing 3
Gm11454	1.1911	0.002667	predicted gene 11454
Serpine1	1.1881	0.001276	serine (or cysteine) peptidase inhibitor, clade E, member 1
C1qtnf7	1.1863	1.78E-06	C1q and tumor necrosis factor related protein 7
0610040F04Rik	1.1775	0.004962	RIKEN cDNA 0610040F04 gene
Pgm2	1.1772	1.71E-07	phosphoglucomutase 2
Gm17382	1.1737	0.001136	predicted gene, 17382
Gm2117	1.1726	9.29E-06	predicted gene 2117
Arhgef4	1.1718	0.000135	Rho guanine nucleotide exchange factor (GEF) 4
Bmp2	1.1640	4.03E-05	bone morphogenetic protein 2
Cfap70	1.1630	0.00134	cilia and flagella associated protein 70
Gm12688	1.1622	2.42E-08	predicted gene 12688
Fosl2	1.1609	7.40E-06	fos-like antigen 2
Pde4b	1.1586	1.47E-06	phosphodiesterase 4B, cAMP specific
Nfatc2	1.1549	2.94E-06	nuclear factor of activated T cells, cytoplasmic, calcineurin dependent 2
4833403I15Rik	1.1543	0.006369	RIKEN cDNA 4833403I15 gene
Adamts9	1.1528	6.83E-17	a disintegrin-like and metallopeptidase (reprolysin type) with thrombospondin type 1 motif, 9
Iigp1	1.1511	0.000884	interferon inducible GTPase 1
Ahnak	1.1475	6.33E-20	AHNAK nucleoprotein (desmoyokin)
Hes7	1.1473	0.002624	hairy and enhancer of split 7 (Drosophila)
Mtus2	1.1463	9.00E-07	microtubule associated tumor suppressor candidate 2
Mt1	1.1454	7.55E-05	metallothionein 1
Adra2c	1.1454	0.002593	adrenergic receptor, alpha 2c
Proser2	1.1424	0.000175	proline and serine rich 2
Gm2061	1.1411	0.003243	predicted gene 2061

Prima1	1.1409	0.001729	proline rich membrane anchor 1
2310002F09Rik	1.1403	3.50E-07	RIKEN cDNA 2310002F09 gene
Apold1	1.1389	2.54E-05	apolipoprotein L domain containing 1
Sowahb	1.1376	2.07E-09	sosondowah ankyrin repeat domain family member B
Gm17501	1.1273	0.003506	predicted gene, 17501
NA	1.1254	0.001118	NA
Kbtbd11	1.1231	1.03E-14	kelch repeat and BTB (POZ) domain containing 11
B230323A14Rik	1.1211	4.93E-06	RIKEN cDNA B230323A14 gene
Abcc8	1.1189	4.52E-06	ATP-binding cassette, sub-family C (CFTR/MRP), member 8
Col6a3	1.1188	6.58E-08	collagen, type VI, alpha 3
Lamb3	1.1152	0.004279	laminin, beta 3
Plekha2	1.1151	1.97E-05	pleckstrin homology domain-containing, family A (phosphoinositide binding specific) member 2
Notum	1.1137	2.66E-08	notum pectinacetylesterase homolog (Drosophila)
BC006965	1.1135	0.003903	cDNA sequence BC006965
Cysltr1	1.1107	2.94E-06	cysteinyl leukotriene receptor 1
1810010H24Rik	1.1103	0.002492	RIKEN cDNA 1810010H24 gene
Pmaip1	1.1039	3.00E-07	phorbol-12-myristate-13-acetate-induced protein 1
Gm26600	1.0945	0.000311	predicted gene, 26600
Il16	1.0930	7.46E-05	interleukin 16
Gabre	1.0923	5.89E-07	gamma-aminobutyric acid (GABA) A receptor, subunit epsilon
Gm16046	1.0913	0.000598	predicted gene 16046
Gm26721	1.0890	0.00122	predicted gene, 26721
Krt8	1.0859	4.64E-08	keratin 8
Gm16201	1.0845	0.008769	predicted gene 16201
P4ha1	1.0825	2.68E-14	procollagen-proline, 2-oxoglutarate 4-dioxygenase (proline 4-hydroxylase), alpha 1 polypeptide
Tmprss13	1.0750	0.007021	transmembrane protease, serine 13
F630040K05Rik	1.0674	0.000453	RIKEN cDNA F630040K05 gene
Fam162a	1.0668	3.89E-12	family with sequence similarity 162, member A
Gm19705	1.0636	0.007092	predicted gene, 19705
Ccdc80	1.0511	8.59E-11	coiled-coil domain containing 80
Smtnl2	1.0484	0.00026	smoothelin-like 2
Gm26908	1.0343	0.001184	predicted gene, 26908
Gm17399	1.0258	4.40E-05	predicted gene, 17399
Zfp804a	1.0223	0.001958	zinc finger protein 804A
Prelid2	1.0222	1.05E-07	PRELI domain containing 2
Plod2	1.0144	1.31E-09	procollagen lysine, 2-oxoglutarate 5-dioxygenase 2
D930048N14Rik	1.0138	1.08E-05	RIKEN cDNA D930048N14 gene
Adamts16	1.0092	2.66E-06	a disintegrin-like and metallopeptidase (reprolysin type) with thrombospondin type 1 motif, 16
Ndrg2	1.0008	0.009803	N-myc downstream regulated gene 2
Ntrk2	0.9997	1.20E-09	neurotrophic tyrosine kinase, receptor, type 2

Ikbke	0.9991	1.69E-05	inhibitor of kappaB kinase epsilon
Ticam2	0.9955	0.00057	toll-like receptor adaptor molecule 2
Gpr146	0.9946	0.00095	G protein-coupled receptor 146
Dlx5	0.9903	5.24E-06	distal-less homeobox 5
Tacstd2	0.9902	0.000278	tumor-associated calcium signal transducer 2
Gm15834	0.9901	0.001606	predicted gene 15834
Fam196b	0.9892	7.10E-07	family with sequence similarity 196, member B
Car12	0.9800	2.95E-07	carbonic anyhydrase 12
Maff	0.9779	4.60E-05	v-maf musculoaponeurotic fibrosarcoma oncogene family, protein F (avian)
Pygl	0.9761	7.71E-06	liver glycogen phosphorylase
Tchh	0.9722	0.005754	trichohyalin
Lrp2	0.9721	3.13E-11	low density lipoprotein receptor-related protein 2
C920006O11Rik	0.9720	0.008273	RIKEN cDNA C920006O11 gene
C1ql2	0.9617	0.0045	complement component 1, q subcomponent-like 2
Slc7a3	0.9598	0.000426	solute carrier family 7 (cationic amino acid transporter, y+ system), member 3
Cav1	0.9593	0.001112	caveolin 1, caveolae protein
Hmox1	0.9561	2.38E-05	heme oxygenase (decycling) 1
Lbx1	0.9521	0.000329	ladybird homeobox homolog 1 (Drosophila)
A530016L24Rik	0.9484	0.002008	RIKEN cDNA A530016L24 gene
Slc26a10	0.9466	0.000216	solute carrier family 26, member 10
4632428C04Rik	0.9440	0.001396	RIKEN cDNA 4632428C04 gene
Cd300a	0.9411	0.002866	CD300A antigen
Ccser1	0.9410	3.35E-05	coiled-coil serine rich 1
Hmha1	0.9385	3.17E-12	histocompatibility (minor) HA-1
Nabp1	0.9345	7.30E-07	nucleic acid binding protein 1
Fstl3	0.9341	0.000171	follistatin-like 3
Ccng2	0.9238	5.93E-06	cyclin G2
Cnnm1	0.9223	1.53E-06	cyclin M1
Snx31	0.9204	0.00872	sorting nexin 31
Aldoart1	0.8944	1.88E-05	aldolase 1 A, retrogene 1
Pik3ip1	0.8907	0.000714	phosphoinositide-3-kinase interacting protein 1
Gm16091	0.8903	0.006066	predicted gene 16091
Jpx	0.8867	0.000147	Jpx transcript, Xist activator (non-protein coding)
Mir6950	0.8817	1.79E-05	microRNA 6950
Mt2	0.8812	0.000525	metallothionein 2
Upp1	0.8724	0.001325	uridine phosphorylase 1
Cftr	0.8720	0.004048	cystic fibrosis transmembrane conductance regulator
Ppargc1b	0.8681	0.000362	peroxisome proliferative activated receptor, gamma, coactivator 1 beta
Egln1	0.8674	1.74E-06	egl-9 family hypoxia-inducible factor 1
Gm14321	0.8630	1.40E-05	predicted gene 14321
Gng8	0.8621	0.000139	guanine nucleotide binding protein (G protein), gamma 8

Mpp2	0.8590	6.33E-05	membrane protein, palmitoylated 2 (MAGUK p55 subfamily member 2)
Gm16008	0.8567	3.67E-05	predicted gene 16008
Lingo3	0.8548	0.002815	leucine rich repeat and Ig domain containing 3
A930033H14Rik	0.8492	0.005468	RIKEN cDNA A930033H14 gene
Proca1	0.8427	0.005133	protein interacting with cyclin A1
Klf15	0.8309	1.39E-05	Kruppel-like factor 15
Aldoa	0.8308	3.01E-14	aldolase A, fructose-bisphosphate
Sdc4	0.8292	0.001106	syndecan 4
NA	0.8259	0.002611	NA
Clcn3	0.8221	3.10E-08	chloride channel 3
Gys1	0.8188	1.41E-08	glycogen synthase 1, muscle
Stab1	0.8173	3.11E-18	stabilin 1
Ccdc68	0.8173	0.000106	coiled-coil domain containing 68
NA	0.8160	0.002043	NA
Neil2	0.8085	0.000869	nei like 2 (E. coli)
NA	0.8041	0.004386	NA
Lama5	0.7993	6.77E-13	laminin, alpha 5
Vegfa	0.7974	2.25E-07	vascular endothelial growth factor A
Jade2	0.7962	0.002028	jade family PHD finger 2
Gm12905	0.7888	0.00039	predicted gene 12905
Idua	0.7680	0.001104	iduronidase, alpha-L-
Leprel1	0.7622	2.94E-08	leprecan-like 1
Sez6l	0.7570	0.000952	seizure related 6 homolog like
Pgk1	0.7519	6.17E-12	phosphoglycerate kinase 1
Galnt14	0.7490	0.005704	UDP-N-acetyl-alpha-D-galactosamine:polypeptide N-acetylgalactosaminyltransferase 14
Ppil6	0.7463	0.009482	peptidylprolyl isomerase (cyclophilin)-like 6
Gm16759	0.7413	0.009797	predicted gene, 16759
Loxl2	0.7385	4.86E-09	lysyl oxidase-like 2
Irx4	0.7335	0.00056	Iroquois related homeobox 4 (Drosophila)
Gm27247	0.7331	0.008319	predicted gene 27247
Gm21451	0.7308	1.61E-08	predicted gene, 21451
Adamts17	0.7294	0.001537	a disintegrin-like and metallopeptidase (reprolysin type) with thrombospondin type 1 motif, 17
9130020K20Rik	0.7288	0.007371	RIKEN cDNA 9130020K20 gene
Nrxn3	0.7240	0.003173	neurexin III
Gm5537	0.7237	1.12E-09	predicted gene 5537
Slc38a3	0.7166	0.009121	solute carrier family 38, member 3
Grem1	0.7114	3.72E-06	gremlin 1
Pgk1-rs7	0.7013	1.20E-09	phosphoglycerate kinase-1, related sequence-7
Gm11457	0.6901	0.005323	predicted gene 11457
4930581F22Rik	0.6836	0.000914	RIKEN cDNA 4930581F22 gene
Pappa	0.6659	3.17E-07	pregnancy-associated plasma protein A
Crebrf	0.6648	0.000849	CREB3 regulatory factor

Dbp	0.6410	0.000435	D site albumin promoter binding protein
Sesn2	0.6400	0.002055	sestrin 2
Renbp	0.5822	0.004922	renin binding protein
Zfr2	0.5820	0.004232	zinc finger RNA binding protein 2
Pls1	0.5628	0.008874	plastin 1 (I-isoform)
Pck2	0.5394	0.001264	phosphoenolpyruvate carboxykinase 2 (mitochondrial)
Lmx1a	0.5220	0.00727	LIM homeobox transcription factor 1 alpha
Snora19	4.2910	0.010113	small nucleolar RNA, H/ACA box 19
Gm20519	3.8206	0.031506	predicted gene 20519
Slc28a1	3.5223	0.07143	solute carrier family 28 (sodium-coupled nucleoside transporter), member 1
Mir126a	2.8644	0.01557	microRNA 126a
Gm14488	2.8627	0.014594	predicted gene 14488
Fut1	2.8595	0.016065	fucosyltransferase 1
1700001C19Rik	2.6795	0.031216	RIKEN cDNA 1700001C19 gene
Gm6214	2.4686	0.061049	predicted gene 6214
Serpina3e-ps	2.4556	0.012386	serine (or cysteine) peptidase inhibitor, clade A, member 3E, pseudogene
Gm22858	2.4340	0.013852	predicted gene, 22858
Wnt8b	2.2977	0.037083	wingless-type MMTV integration site family, member 8B
Gpr132	2.2230	0.118686	G protein-coupled receptor 132
Gm18199	2.2015	0.011976	predicted gene, 18199
Gm6471	2.2005	0.010632	predicted gene 6471
Gm13594	2.1256	0.048411	predicted gene 13594
AI747448	2.0847	0.024155	expressed sequence AI747448
Gm11549	2.0824	0.023002	predicted gene 11549
Mir3100	2.0738	0.021297	microRNA 3100
Spink13	1.9461	0.033918	serine peptidase inhibitor, Kazal type 13
4833427G06Rik	1.9454	0.035172	RIKEN cDNA 4833427G06 gene
Arhgef38	1.9434	0.096119	Rho guanine nucleotide exchange factor (GEF) 38
Gm9869	1.9421	0.02172	predicted gene 9869
Mir335	1.7607	0.018899	microRNA 335
AU018091	1.5919	0.010629	expressed sequence AU018091
Gm13735	1.5883	0.027831	predicted gene 13735
Gm16126	1.5862	0.023326	predicted gene 16126
D6Ertd527e	1.5437	0.048866	DNA segment, Chr 6, ERATO Doi 527, expressed
Slc26a9	1.4921	0.019569	solute carrier family 26, member 9
Gm26984	1.4642	0.011527	predicted gene, 26984
Gm12981	1.4604	0.011418	predicted gene 12981
Nkpd1	1.4126	0.037624	NTPase, KAP family P-loop domain containing 1
Nrn1	1.3397	0.042069	neuritin 1
Gm53	1.3340	0.017683	predicted gene 53
Slc22a30	1.3313	0.036909	solute carrier family 22, member 30
Amdhd1	1.3272	0.033479	amidohydrolase domain containing 1
Il17f	1.3145	0.078024	interleukin 17F

Prss33	1.2922	0.12203	protease, serine 33
Cct6b	1.2922	0.025637	chaperonin containing Tcp1, subunit 6b (zeta)
mt-Tg	1.2682	0.013559	mitochondrially encoded tRNA glycine
NA	1.2649	0.015202	NA
Gm26665	1.2595	0.032755	predicted gene, 26665
Gipr	1.2396	0.022775	gastric inhibitory polypeptide receptor
9630001P10Rik	1.2132	0.014674	RIKEN cDNA 9630001P10 gene
4930509E16Rik	1.1698	0.020072	RIKEN cDNA 4930509E16 gene
Gm15482	1.1547	0.049394	predicted gene 15482
Them7	1.1289	0.021342	thioesterase superfamily member 7
Gm15327	1.1285	0.095969	predicted gene 15327
Lgals3	1.1172	0.015271	lectin, galactose binding, soluble 3
Hmx3	1.0847	0.324376	H6 homeobox 3
Zfp296	1.0795	0.044361	zinc finger protein 296
Gm10037	1.0716	0.0544	predicted gene 10037
Gm960	1.0615	0.010942	predicted gene 960
4930547M16Rik	1.0583	0.019667	RIKEN cDNA 4930547M16 gene
4933405D12Rik	1.0255	0.022324	RIKEN cDNA 4933405D12 gene
Wfdc3	1.0167	0.028827	WAP four-disulfide core domain 3
Dmrt3	1.0017	0.017948	doublesex and mab-3 related transcription factor 3
Tmem221	0.9856	0.019006	transmembrane protein 221
Tppp	0.9646	0.011359	tubulin polymerization promoting protein
4933433G15Rik	0.9625	0.058176	RIKEN cDNA 4933433G15 gene
Gm17509	0.9434	0.012218	predicted gene, 17509
Runx3	0.9285	0.029809	runt related transcription factor 3
Car9	0.9013	0.031226	carbonic anhydrase 9
Gabrg1	0.8880	0.011267	gamma-aminobutyric acid (GABA) A receptor, subunit gamma 1
Unc5cl	0.8760	0.040075	unc-5 homolog C (C. elegans)-like
Gm17249	0.8759	0.045134	predicted gene, 17249
Acan	0.8712	0.032858	aggrecan
Mir363	0.8685	0.03347	microRNA 363
Ackr2	0.8675	0.016523	atypical chemokine receptor 2
Gm13710	0.8621	0.056722	predicted gene 13710
Otog	0.8550	0.102197	otogelin
Lrfn2	0.8528	0.071106	leucine rich repeat and fibronectin type III domain containing 2
Rasgrp1	0.8489	0.02024	RAS guanyl releasing protein 1
Gm16251	0.8487	0.057285	predicted gene 16251
Insl3	0.8343	0.072218	insulin-like 3
Apol7d	0.8281	0.01423	apolipoprotein L 7d
Adgb	0.8258	0.02522	androglobin
Creg2	0.8183	0.014344	cellular repressor of E1A-stimulated genes 2
Npas2	0.8019	0.053954	neuronal PAS domain protein 2
5730405O15Rik	0.7919	0.035313	RIKEN cDNA 5730405O15 gene

Gm21905	0.7894	0.093381	predicted gene, 21905
Catsperd	0.7785	0.011706	catsper channel auxiliary subunit delta
C230037L18Rik	0.7769	0.010725	RIKEN cDNA C230037L18 gene
A730020E08Rik	0.7681	0.030041	RIKEN cDNA A730020E08 gene
Cyb5r2	0.7642	0.02078	cytochrome b5 reductase 2
Gm13830	0.7636	0.010082	predicted gene 13830
Gm12762	0.7563	0.044293	predicted gene 12762
Fgf11	0.7496	0.013861	fibroblast growth factor 11
Tmem74b	0.7473	0.017437	transmembrane protein 74B
Gm9929	0.7416	0.033198	predicted gene 9929
Vstm2l	0.7291	0.066502	V-set and transmembrane domain containing 2-like
Hk1os	0.7289	0.043254	hexokinase 1, opposite strand
Cfap44	0.7191	0.056252	cilia and flagella associated protein 44
Cblc	0.7094	0.058288	Casitas B-lineage lymphoma c
Gm6297	0.7044	0.032469	predicted gene 6297
Extl1	0.7025	0.032671	exostoses (multiple)-like 1
4933406C10Rik	0.7011	0.038591	RIKEN cDNA 4933406C10 gene
Tnfsf13os	0.6887	0.048634	tumor necrosis factor (ligand) superfamily, member 13, opposite strand
Grip1os3	0.6865	0.019209	glutamate receptor interacting protein 1, opposite strand 3
BB218582	0.6751	0.010453	expressed sequence BB218582
Ttll10	0.6650	0.021826	tubulin tyrosine ligase-like family, member 10
Zfp133-ps	0.6543	0.013436	zinc finger protein 133, pseudogene
Gm12454	0.6479	0.061544	predicted gene 12454
A2m	0.6430	0.019693	alpha-2-macroglobulin
Catsperg2	0.6385	0.122745	catsper channel auxiliary subunit gamma 2
Zc3h6	0.6019	0.020286	zinc finger CCCH type containing 6
1700029J07Rik	0.5914	0.013494	RIKEN cDNA 1700029J07 gene
Chrna6	0.5839	0.159565	cholinergic receptor, nicotinic, alpha polypeptide 6
Ace	0.5744	0.057498	angiotensin I converting enzyme (peptidyl-dipeptidase A) 1
Catsperg1	0.5616	0.023239	catsper channel auxiliary subunit gamma 1
Sncb	0.5593	0.102107	synuclein, beta
Trim66	0.5560	0.264916	tripartite motif-containing 66
Mef2b	0.5011	0.21463	myocyte enhancer factor 2B
Fhad1	0.4944	0.210794	forkhead-associated (FHA) phosphopeptide binding domain 1
Gad1os	0.4938	0.09448	glutamate decarboxylase 1, opposite strand
BC107364	0.4936	0.209646	cDNA sequence BC107364
Stag3	0.4831	0.015149	stromal antigen 3
Aldh1l2	0.0175	0.956757	aldehyde dehydrogenase 1 family, member L2
Gm853	0.0000	1	predicted gene 853

Table VII-8: RNA Seq2 Downregulated genes

gene	m	pval	description
Eif2s3y	-10.919	9.33E-10	eukaryotic translation initiation factor 2, subunit 3, structural gene Y-linked
Kdm5d	-10.596	2.23E-09	lysine (K)-specific demethylase 5D
Gcg	-8.426	9.44E-08	glucagon
Ddx3y	-7.820	1.93E-07	DEAD (Asp-Glu-Ala-Asp) box polypeptide 3, Y-linked
Insm2	-5.375	8.77E-05	insulinoma-associated 2
Rgs13	-5.307	0.001073	regulator of G-protein signaling 13
Vsx2	-5.061	0.000711	visual system homeobox 2
Otp	-4.926	5.52E-10	orthopedia homolog (Drosophila)
Gabrg2	-4.860	9.39E-13	gamma-aminobutyric acid (GABA) A receptor, subunit gamma 2
Uty	-4.629	0.000212	ubiquitously transcribed tetratricopeptide repeat gene, Y chromosome
Cox8b	-4.542	0.007044	cytochrome c oxidase subunit VIIIb
Gm5590	-4.541	0.004983	predicted gene 5590
Hk3	-4.288	4.44E-47	hexokinase 3
Dhrs7c	-4.183	4.14E-06	dehydrogenase/reductase (SDR family) member 7C
Ptf1a	-4.130	2.13E-11	pancreas specific transcription factor, 1a
Gm27199	-3.999	0.000358	predicted gene 27199
Msc	-3.934	1.94E-26	musculin
Gsx1	-3.794	1.02E-06	GS homeobox 1
Tlx3	-3.767	3.00E-07	T cell leukemia, homeobox 3
Robo3	-3.736	1.70E-11	roundabout homolog 3 (Drosophila)
Fmo2	-3.714	0.000117	flavin containing monooxygenase 2
Scg2	-3.529	3.53E-09	secretogranin II
2310002L09Rik	-3.511	4.75E-12	RIKEN cDNA 2310002L09 gene
Cxcl11	-3.399	2.32E-05	chemokine (C-X-C motif) ligand 11
Crp	-3.379	6.06E-07	C-reactive protein, pentraxin-related
Chrna3	-3.321	1.39E-42	cholinergic receptor, nicotinic, alpha polypeptide 3
C130071C03Rik	-3.248	5.09E-22	RIKEN cDNA C130071C03 gene
AI854517	-3.211	5.40E-11	expressed sequence AI854517
Il1rn	-3.207	5.43E-10	interleukin 1 receptor antagonist
Hes2	-3.166	5.51E-07	hairy and enhancer of split 2 (Drosophila)
Folr4	-3.152	0.000305	folate receptor 4 (delta)
Prr32	-3.115	5.06E-09	proline rich 32
Skor1	-3.107	6.01E-09	SKI family transcriptional corepressor 1
NA	-3.060	4.09E-11	NA
Lrrc75aos2	-3.046	0.000657	leucine rich repeat containing 75A, opposite strand 2
Slc6a5	-3.038	9.16E-05	solute carrier family 6 (neurotransmitter transporter, glycine), member 5
Olfr315	-2.985	0.00054	olfactory receptor 315
1700128E19Rik	-2.959	2.03E-15	RIKEN cDNA 1700128E19 gene

Csn3	-2.946	5.03E-22	casein kappa
Chrna9	-2.928	0.00144	cholinergic receptor, nicotinic, alpha polypeptide 9
Hoxa10	-2.870	0.008068	homeobox A10
Unc5a	-2.862	1.40E-87	unc-5 homolog A (C. elegans)
Slc6a20a	-2.846	0.000616	solute carrier family 6 (neurotransmitter transporter), member 20A
Gm12082	-2.834	8.23E-05	predicted gene 12082
Lhx5	-2.800	5.71E-11	LIM homeobox protein 5
Gm12224	-2.800	0.001533	predicted gene 12224
Ttc9b	-2.798	2.19E-06	tetratricopeptide repeat domain 9B
Nkx2-1	-2.793	6.87E-17	NK2 homeobox 1
Ppp1r3a	-2.772	3.52E-08	protein phosphatase 1, regulatory (inhibitor) subunit 3A
Barx1	-2.760	1.33E-07	BarH-like homeobox 1
Myh3	-2.758	1.32E-61	myosin, heavy polypeptide 3, skeletal muscle, embryonic
1810010K12Rik	-2.739	5.08E-08	RIKEN cDNA 1810010K12 gene
Fbll1	-2.704	0.000429	fibrillarin-like 1
A730046J19Rik	-2.686	0.00016	RIKEN cDNA A730046J19 gene
Bhlhe23	-2.685	5.34E-08	basic helix-loop-helix family, member e23
Tlx2	-2.679	7.97E-08	T cell leukemia, homeobox 2
Lamp5	-2.609	0.000793	lysosomal-associated membrane protein family, member 5
Kirrel2	-2.602	8.53E-14	kin of IRRE like 2 (Drosophila)
Adcyap1	-2.591	2.45E-09	adenylate cyclase activating polypeptide 1
Gm24105	-2.585	0.004302	predicted gene, 24105
Klhl14	-2.562	6.87E-18	kelch-like 14
Nppc	-2.557	8.48E-13	natriuretic peptide type C
Grifin	-2.552	7.96E-06	galectin-related inter-fiber protein
Tnnc2	-2.522	7.07E-26	troponin C2, fast
NA	-2.518	4.27E-05	NA
Musk	-2.513	1.40E-07	muscle, skeletal, receptor tyrosine kinase
Chrnb4	-2.507	2.04E-25	cholinergic receptor, nicotinic, beta polypeptide 4
Myot	-2.505	9.70E-08	myotilin
Pitx3	-2.504	0.008777	paired-like homeodomain transcription factor 3
Mstn	-2.504	2.68E-24	myostatin
Nhlh2	-2.503	5.26E-19	nescient helix loop helix 2
Klhl35	-2.494	6.52E-06	kelch-like 35
Grm2	-2.489	6.24E-10	glutamate receptor, metabotropic 2
Bhlhe22	-2.466	1.66E-19	basic helix-loop-helix family, member e22
Klhl40	-2.449	1.22E-07	kelch-like 40
Barhl1	-2.449	6.35E-05	BarH-like 1 (Drosophila)
Cntn2	-2.444	7.40E-23	contactin 2
Sln	-2.428	4.35E-07	sarcolipin
Gnat3	-2.420	2.21E-09	guanine nucleotide binding protein, alpha transducing

			3
Mylk4	-2.413	1.29E-08	myosin light chain kinase family, member 4
Scml4	-2.389	2.04E-12	sex comb on midleg-like 4 (Drosophila)
Hist2h4	-2.376	0.002318	histone cluster 2, H4
Nwd2	-2.372	2.49E-07	NACHT and WD repeat domain containing 2
Scrt1	-2.345	5.08E-08	scratch homolog 1, zinc finger protein (Drosophila)
Kctd8	-2.308	0.000795	potassium channel tetramerisation domain containing 8
Tmem132e	-2.301	8.19E-22	transmembrane protein 132E
Gm12408	-2.297	0.005693	predicted gene 12408
Gm16140	-2.289	8.15E-07	predicted gene 16140
3110039M20Rik	-2.279	3.87E-14	RIKEN cDNA 3110039M20 gene
St8sia3os	-2.278	8.85E-07	ST8 alpha-N-acetyl-neuraminide alpha-2,8-sialyltransferase 3, opposite strand
Sgcg	-2.278	1.36E-05	sarcoglycan, gamma (dystrophin-associated glycoprotein)
Cabp7	-2.261	4.46E-08	calcium binding protein 7
Nefm	-2.260	1.21E-23	neurofilament, medium polypeptide
Tmem182	-2.249	1.89E-07	transmembrane protein 182
Stk32a	-2.247	1.68E-25	serine/threonine kinase 32A
Dcx	-2.242	1.66E-22	doublecortin
Nacad	-2.234	3.60E-11	NAC alpha domain containing
B3galt2	-2.224	0.003333	UDP-Gal:betaGlcNAc beta 1,3-galactosyltransferase, polypeptide 2
Oit1	-2.223	0.00388	oncoprotein induced transcript 1
Foxg1	-2.222	7.73E-14	forkhead box G1
D930028M14Rik	-2.173	8.32E-16	RIKEN cDNA D930028M14 gene
Il7	-2.165	0.003468	interleukin 7
Ecel1	-2.162	2.13E-09	endothelin converting enzyme-like 1
Phox2a	-2.155	7.09E-17	paired-like homeobox 2a
Alx3	-2.154	4.76E-18	aristaless-like homeobox 3
Gm14133	-2.154	0.009814	predicted gene 14133
Mypn	-2.136	0.000108	myopalladin
Mylpf	-2.133	3.74E-28	myosin light chain, phosphorylatable, fast skeletal muscle
Inmt	-2.118	0.000328	indolethylamine N-methyltransferase
Gsx2	-2.116	6.72E-14	GS homeobox 2
Ankrd2	-2.104	2.98E-11	ankyrin repeat domain 2 (stretch responsive muscle)
Cdhr1	-2.103	4.02E-08	cadherin-related family member 1
Neb	-2.090	2.07E-15	nebulin
C1ql3	-2.087	6.50E-09	C1q-like 3
Gjd4	-2.069	3.16E-06	gap junction protein, delta 4
Stmn2	-2.063	1.09E-17	stathmin-like 2
Dbh	-2.060	0.000712	dopamine beta hydroxylase
Resp18	-2.058	0.004709	regulated endocrine-specific protein 18

Myh13	-2.057	0.000177	myosin, heavy polypeptide 13, skeletal muscle
Oasl2	-2.051	0.000133	2'-5' oligoadenylate synthetase-like 2
Htr2a	-2.049	0.008644	5-hydroxytryptamine (serotonin) receptor 2A
Ina	-2.032	1.43E-15	internexin neuronal intermediate filament protein, alpha
Cps1	-2.019	0.000189	carbamoyl-phosphate synthetase 1
3110035E14Rik	-2.013	4.84E-09	RIKEN cDNA 3110035E14 gene
Myh2	-2.009	0.000586	myosin, heavy polypeptide 2, skeletal muscle, adult
Myoz2	-2.005	0.002367	myozenin 2
4930469K13Rik	-1.998	3.08E-06	RIKEN cDNA 4930469K13 gene
Ctxn3	-1.997	1.47E-10	cortexin 3
Sstr3	-1.987	0.009493	somatostatin receptor 3
Hs3st2	-1.987	2.40E-05	heparan sulfate (glucosamine) 3-O-sulfotransferase 2
Kcnh5	-1.976	0.007434	potassium voltage-gated channel, subfamily H (eag-related), member 5
Phox2b	-1.955	9.87E-26	paired-like homeobox 2b
Gm16582	-1.954	1.38E-10	predicted gene 16582
Stmn3	-1.949	2.19E-14	stathmin-like 3
1700011H14Rik	-1.949	2.36E-07	RIKEN cDNA 1700011H14 gene
Sst	-1.946	2.29E-09	somatostatin
Stmn4	-1.945	3.52E-12	stathmin-like 4
Neurod1	-1.942	2.28E-10	neurogenic differentiation 1
Chat	-1.939	9.76E-13	choline acetyltransferase
Aldh1a7	-1.937	5.08E-13	aldehyde dehydrogenase family 1, subfamily A7
Myom3	-1.923	7.00E-07	myomesin family, member 3
Cdk5r2	-1.917	6.41E-10	cyclin-dependent kinase 5, regulatory subunit 2 (p39)
Chrng	-1.914	1.49E-08	cholinergic receptor, nicotinic, gamma polypeptide
Fgf6	-1.909	0.000204	fibroblast growth factor 6
Ppp1r17	-1.905	4.53E-12	protein phosphatase 1, regulatory subunit 17
BC048679	-1.900	0.000504	cDNA sequence BC048679
B3gat2	-1.891	0.000413	beta-1,3-glucuronyltransferase 2 (glucuronosyltransferase S)
Insc	-1.888	9.17E-09	inscuteable homolog (Drosophila)
Pou2f2	-1.886	1.77E-07	POU domain, class 2, transcription factor 2
Syt4	-1.868	3.62E-08	synaptotagmin IV
Cerkl	-1.841	9.68E-10	ceramide kinase-like
Prdm13	-1.839	6.09E-17	PR domain containing 13
Lin7a	-1.831	3.68E-11	lin-7 homolog A (C. elegans)
Casq2	-1.825	3.59E-09	calsequestrin 2
Rhbdl3	-1.813	4.63E-20	rhomboid, veinlet-like 3 (Drosophila)
Hic1	-1.812	2.94E-12	hypermethylated in cancer 1
Mybph	-1.810	1.62E-14	myosin binding protein H
Scn9a	-1.810	1.19E-06	sodium channel, voltage-gated, type IX, alpha
Gabrq	-1.807	0.001399	gamma-aminobutyric acid (GABA) A receptor, subunit theta

Chrna5	-1.803	5.45E-10	cholinergic receptor, nicotinic, alpha polypeptide 5
Gm2990	-1.802	1.73E-05	predicted gene 2990
Myf6	-1.802	5.89E-09	myogenic factor 6
4930426D05Rik	-1.792	2.84E-13	RIKEN cDNA 4930426D05 gene
Ttbk1	-1.790	2.53E-12	tau tubulin kinase 1
Atcay	-1.778	4.02E-11	ataxia, cerebellar, Cayman type homolog (human)
6030408B16Rik	-1.765	0.000313	RIKEN cDNA 6030408B16 gene
Tubb3	-1.761	2.15E-27	tubulin, beta 3 class III
Thsd7b	-1.760	1.10E-06	thrombospondin, type I, domain containing 7B
NA	-1.759	2.21E-06	NA
Cck	-1.745	8.67E-08	cholecystokinin
Wfdc1	-1.745	1.28E-09	WAP four-disulfide core domain 1
Xkr7	-1.740	3.52E-09	X Kell blood group precursor related family member 7 homolog
Ablim3	-1.735	2.15E-10	actin binding LIM protein family, member 3
Ano5	-1.727	4.13E-07	anoctamin 5
Dhrs3	-1.725	1.53E-11	dehydrogenase/reductase (SDR family) member 3
Insm1	-1.722	1.09E-17	insulinoma-associated 1
Kcnj8	-1.718	0.005016	potassium inwardly-rectifying channel, subfamily J, member 8
Nefl	-1.717	2.17E-17	neurofilament, light polypeptide
Unc79	-1.714	3.09E-06	unc-79 homolog (C. elegans)
Ppfia2	-1.711	0.000137	protein tyrosine phosphatase, receptor type, f polypeptide (PTPRF), interacting protein (liprin), alpha 2
Filip1	-1.709	8.97E-17	filamin A interacting protein 1
En1	-1.690	3.61E-09	engrailed 1
Il17b	-1.679	0.001633	interleukin 17B
Pah	-1.678	7.49E-06	phenylalanine hydroxylase
Fam163a	-1.671	6.50E-06	family with sequence similarity 163, member A
Sncg	-1.671	1.40E-09	synuclein, gamma
Elavl3	-1.665	3.77E-15	ELAV (embryonic lethal, abnormal vision, Drosophila)-like 3 (Hu antigen C)
Scrt2	-1.660	1.86E-09	scratch homolog 2, zinc finger protein (Drosophila)
Hs3st5	-1.654	0.000693	heparan sulfate (glucosamine) 3-O-sulfotransferase 5
Ap3b2	-1.648	1.53E-09	adaptor-related protein complex 3, beta 2 subunit
Pou3f4	-1.646	1.88E-08	POU domain, class 3, transcription factor 4
Gm14343	-1.646	0.000172	predicted gene 14343
Nrg3	-1.645	1.09E-06	neuregulin 3
Gm12239	-1.644	0.000147	predicted gene 12239
Ntrk1	-1.643	2.54E-12	neurotrophic tyrosine kinase, receptor, type 1
Tmem8c	-1.639	4.70E-06	transmembrane protein 8C
Gfra1	-1.625	2.72E-18	glial cell line derived neurotrophic factor family receptor alpha 1
Vsx1	-1.613	4.41E-05	visual system homeobox 1 homolog (zebrafish)

Htr3a	-1.608	0.001446	5-hydroxytryptamine (serotonin) receptor 3A
Neurog1	-1.607	5.82E-12	neurogenin 1
Galnt9	-1.601	1.33E-07	UDP-N-acetyl-alpha-D-galactosamine:polypeptide N-acetylgalactosaminyltransferase 9
Rundc3a	-1.598	9.44E-10	RUN domain containing 3A
Lhx1	-1.593	5.19E-06	LIM homeobox protein 1
Iqsec3	-1.591	0.00014	IQ motif and Sec7 domain 3
Mmp24	-1.591	5.88E-07	matrix metallopeptidase 24
Halr1	-1.590	4.62E-09	Hoxa adjacent long noncoding RNA 1
Slc17a7	-1.584	7.04E-07	solute carrier family 17 (sodium-dependent inorganic phosphate cotransporter), member 7
Fstl5	-1.583	0.000294	follistatin-like 5
Gm26871	-1.582	0.001957	predicted gene, 26871
Gabra1	-1.578	0.006439	gamma-aminobutyric acid (GABA) A receptor, subunit alpha 1
Cacna1s	-1.575	0.000303	calcium channel, voltage-dependent, L type, alpha 1S subunit
Pnmal1	-1.565	2.68E-09	PNMA-like 1
Abcb4	-1.547	0.00387	ATP-binding cassette, sub-family B (MDR/TAP), member 4
Svop	-1.547	2.00E-05	SV2 related protein
Arpp21	-1.547	6.30E-10	cyclic AMP-regulated phosphoprotein, 21
Gcnt4	-1.545	3.68E-14	glucosaminyl (N-acetyl) transferase 4, core 2 (beta-1,6-N-acetylglucosaminyltransferase)
Otor	-1.542	0.000404	otoraplin
Gm12892	-1.540	1.86E-18	predicted gene 12892
Syt2	-1.526	2.78E-06	synaptotagmin II
Fndc5	-1.525	8.93E-15	fibronectin type III domain containing 5
Kcnj10	-1.522	1.59E-06	potassium inwardly-rectifying channel, subfamily J, member 10
Ckb	-1.517	9.34E-33	creatine kinase, brain
Nr0b1	-1.515	0.000179	nuclear receptor subfamily 0, group B, member 1
Chrna1	-1.513	6.52E-06	cholinergic receptor, nicotinic, alpha polypeptide 1 (muscle)
Lrrtm3	-1.513	3.44E-10	leucine rich repeat transmembrane neuronal 3
Glra1	-1.510	1.01E-05	glycine receptor, alpha 1 subunit
Foxn4	-1.505	1.86E-05	forkhead box N4
Myt1	-1.501	5.10E-11	myelin transcription factor 1
Onecut3	-1.486	5.75E-05	one cut domain, family member 3
Trim67	-1.481	9.95E-06	tripartite motif-containing 67
2310015B20Rik	-1.480	5.24E-05	RIKEN cDNA 2310015B20 gene
Ptpn5	-1.476	6.79E-10	protein tyrosine phosphatase, non-receptor type 5
Gabrb2	-1.461	1.34E-07	gamma-aminobutyric acid (GABA) A receptor, subunit beta 2
Hmx1	-1.461	0.003807	H6 homeobox 1

Hpca	-1.460	1.71E-07	hippocalcin
Lamc3	-1.459	1.90E-11	laminin gamma 3
St18	-1.459	5.67E-08	suppression of tumorigenicity 18
Tecta	-1.457	4.50E-06	tectorin alpha
Cacng2	-1.453	0.002181	calcium channel, voltage-dependent, gamma subunit 2
Myog	-1.453	4.69E-11	myogenin
Prrxl1	-1.440	0.002036	paired related homeobox protein-like 1
Cxcl13	-1.440	5.24E-11	chemokine (C-X-C motif) ligand 13
Mast1	-1.435	0.000183	microtubule associated serine/threonine kinase 1
Scg3	-1.429	2.01E-10	secretogranin III
1700106J16Rik	-1.424	1.50E-05	RIKEN cDNA 1700106J16 gene
Pax7	-1.421	6.09E-18	paired box 7
Gm7325	-1.414	5.81E-05	predicted gene 7325
Gm20501	-1.413	0.005398	predicted gene 20501
Rab9b	-1.411	0.00293	RAB9B, member RAS oncogene family
Nyap2	-1.408	4.14E-05	neuronal tyrosine-phophorylated phosphoinositide 3-kinase adaptor 2
Wnt2b	-1.396	1.32E-08	wingless-type MMTV integration site family, member 2B
mt-Tt	-1.393	1.71E-10	mitochondrially encoded tRNA threonine
Art1	-1.381	3.14E-05	ADP-ribosyltransferase 1
Aldh1a1	-1.381	0.004949	aldehyde dehydrogenase family 1, subfamily A1
Ascl1	-1.380	6.14E-11	achaete-scute complex homolog 1 (Drosophila)
Apc2	-1.380	3.81E-11	adenomatosis polyposis coli 2
Rgs18	-1.378	0.002921	regulator of G-protein signaling 18
Dmrtb1	-1.376	4.91E-06	DMRT-like family B with proline-rich C-terminal, 1
Cacng6	-1.374	0.000806	calcium channel, voltage-dependent, gamma subunit 6
Srrm3	-1.372	4.91E-06	serine/arginine repetitive matrix 3
Fabp7	-1.371	2.09E-10	fatty acid binding protein 7, brain
Sez6	-1.365	0.000183	seizure related gene 6
Clvs1	-1.363	2.51E-11	clavesin 1
Cdh9	-1.351	0.008476	cadherin 9
Gm16551	-1.346	2.13E-11	predicted gene 16551
Dusp15	-1.345	0.000914	dual specificity phosphatase-like 15
Atp1a3	-1.344	5.22E-06	ATPase, Na+/K+ transporting, alpha 3 polypeptide
Msx3	-1.336	4.88E-24	msh homeobox 3
Chgb	-1.332	1.11E-06	chromogranin B
Snord50b	-1.330	0.004671	small nucleolar RNA, C/D box 50B
Adcy8	-1.326	3.87E-09	adenylate cyclase 8
Ripply3	-1.320	1.83E-17	ripply3 homolog (zebrafish)
Nccrp1	-1.319	0.000779	non-specific cytotoxic cell receptor protein 1 homolog (zebrafish)
Apba2	-1.310	2.77E-32	amyloid beta (A4) precursor protein-binding, family A,

			member 2
Rarb	-1.308	1.83E-28	retinoic acid receptor, beta
Syt1	-1.306	4.24E-06	synaptotagmin I
C2cd4a	-1.299	0.006393	C2 calcium-dependent domain containing 4A
Gm15680	-1.295	0.002992	predicted gene 15680
Ugt8a	-1.294	5.78E-05	UDP galactosyltransferase 8A
Sox3	-1.294	8.77E-19	SRY (sex determining region Y)-box 3
Slitrk6	-1.292	2.00E-09	SLIT and NTRK-like family, member 6
mt-Tl1	-1.282	0.004199	mitochondrially encoded tRNA leucine 1
Chrnb2	-1.282	7.31E-07	cholinergic receptor, nicotinic, beta polypeptide 2 (neuronal)
Dbx1	-1.282	3.83E-16	developing brain homeobox 1
Chga	-1.281	1.39E-08	chromogranin A
Arg1	-1.278	5.65E-37	arginase, liver
Celf3	-1.277	5.75E-07	CUGBP, Elav-like family member 3
Onecut2	-1.276	1.29E-17	one cut domain, family member 2
Itgb8	-1.274	2.51E-18	integrin beta 8
BC030500	-1.270	0.00037	cDNA sequence BC030500
Cdx1	-1.258	2.30E-05	caudal type homeobox 1
Gng3	-1.255	3.28E-05	guanine nucleotide binding protein (G protein), gamma 3
Tmem178b	-1.250	1.55E-05	transmembrane protein 178B
Ncan	-1.248	6.14E-08	neurocan
Rgs9	-1.237	3.85E-15	regulator of G-protein signaling 9
Dner	-1.234	7.09E-06	delta/notch-like EGF-related receptor
Plk3	-1.224	3.23E-12	polo-like kinase 3
Cd83	-1.223	4.31E-08	CD83 antigen
Gm16010	-1.222	7.83E-05	predicted gene 16010
Dtx4	-1.219	1.65E-26	deltex 4 homolog (Drosophila)
Klhl41	-1.219	6.34E-09	kelch-like 41
C130060K24Rik	-1.217	6.69E-05	RIKEN cDNA C130060K24 gene
Kcnn1	-1.216	8.59E-07	potassium intermediate/small conductance calcium-activated channel, subfamily N, member 1
Atp2b2	-1.213	0.002805	ATPase, Ca++ transporting, plasma membrane 2
Slc10a4	-1.212	0.000346	solute carrier family 10 (sodium/bile acid cotransporter family), member 4
Nhlh1	-1.212	1.61E-08	nescient helix loop helix 1
Doc2b	-1.208	9.66E-06	double C2, beta
Arhgap36	-1.208	8.92E-07	Rho GTPase activating protein 36
1810041L15Rik	-1.203	5.14E-10	RIKEN cDNA 1810041L15 gene
Abhd15	-1.201	1.94E-05	abhydrolase domain containing 15
Ass1	-1.190	9.00E-09	argininosuccinate synthetase 1
Drd2	-1.188	0.000413	dopamine receptor D2
Has3	-1.185	0.001334	hyaluronan synthase 3
Akap6	-1.180	5.30E-08	A kinase (PRKA) anchor protein 6

Disp2	-1.179	0.00059	dispatched homolog 2 (Drosophila)
Clec1b	-1.166	9.28E-10	C-type lectin domain family 1, member b
Slc6a7	-1.163	0.000361	solute carrier family 6 (neurotransmitter transporter, L-proline), member 7
Dusp14	-1.161	1.75E-08	dual specificity phosphatase 14
Tshz1	-1.159	5.37E-36	teashirt zinc finger family member 1
Srpk3	-1.157	0.003842	serine/arginine-rich protein specific kinase 3
mt-Tk	-1.155	6.07E-06	mitochondrially encoded tRNA lysine
Arhgap20	-1.152	3.49E-08	Rho GTPase activating protein 20
Grm3	-1.148	0.001033	glutamate receptor, metabotropic 3
Hfe2	-1.147	1.56E-05	hemochromatosis type 2 (juvenile) (human homolog)
Clec1a	-1.143	7.07E-05	C-type lectin domain family 1, member a
Lzts1	-1.143	1.68E-05	leucine zipper, putative tumor suppressor 1
Lrtm1	-1.143	0.000757	leucine-rich repeats and transmembrane domains 1
Nlrp5-ps	-1.141	0.004423	NLR family, pyrin domain containing 5, pseudogene
Foxq1	-1.139	0.00151	forkhead box Q1
Stk33	-1.138	2.73E-05	serine/threonine kinase 33
Syt11	-1.138	3.90E-21	synaptotagmin XI
Atp2a1	-1.129	2.87E-08	ATPase, Ca++ transporting, cardiac muscle, fast twitch 1
Gm807	-1.125	0.007918	predicted gene 807
Ksr2	-1.125	2.63E-05	kinase suppressor of ras 2
Sez6l2	-1.125	0.000484	seizure related 6 homolog like 2
Gdap1	-1.122	1.11E-06	ganglioside-induced differentiation-associated-protein 1
Ttyh1	-1.109	3.06E-06	tweety homolog 1 (Drosophila)
Slc45a1	-1.108	0.006267	solute carrier family 45, member 1
Gm20649	-1.106	9.25E-16	predicted gene 20649
Tmem35	-1.105	5.79E-06	transmembrane protein 35
Moxd1	-1.104	1.59E-08	monooxygenase, DBH-like 1
Trh	-1.103	0.001386	thyrotropin releasing hormone
Prdm12	-1.098	1.55E-07	PR domain containing 12
Lrrc4	-1.094	5.57E-09	leucine rich repeat containing 4
Gpr179	-1.088	0.003242	G protein-coupled receptor 179
Lhfpl4	-1.083	1.34E-09	lipoma HMGIC fusion partner-like protein 4
Mapk8ip2	-1.079	3.26E-08	mitogen-activated protein kinase 8 interacting protein 2
Islr2	-1.073	0.006343	immunoglobulin superfamily containing leucine-rich repeat 2
Fam57b	-1.070	8.97E-05	family with sequence similarity 57, member B
Rgs8	-1.065	3.76E-10	regulator of G-protein signaling 8
Syp	-1.063	1.35E-08	synaptophysin
Rem2	-1.062	3.77E-07	rad and gem related GTP binding protein 2
Pou3f3	-1.059	2.26E-11	POU domain, class 3, transcription factor 3
Myom2	-1.059	0.004424	myomesin 2

Tppp3	-1.056	4.89E-14	tubulin polymerization-promoting protein family member 3
Metrn	-1.054	3.11E-37	meteorin, glial cell differentiation regulator
Chst8	-1.044	6.99E-08	carbohydrate (N-acetylgalactosamine 4-0) sulfotransferase 8
Celsr3	-1.042	4.60E-06	cadherin, EGF LAG seven-pass G-type receptor 3 (flamingo homolog, Drosophila)
Trim9	-1.040	7.73E-07	tripartite motif-containing 9
Slco4a1	-1.039	0.000112	solute carrier organic anion transporter family, member 4a1
Rfx6	-1.035	0.001282	regulatory factor X, 6
Zic4	-1.034	5.46E-08	zinc finger protein of the cerebellum 4
Slc16a12	-1.033	0.005662	solute carrier family 16 (monocarboxylic acid transporters), member 12
Tox	-1.032	3.20E-09	thymocyte selection-associated high mobility group box
Fcgrt	-1.031	2.58E-06	Fc receptor, IgG, alpha chain transporter
Hecw1	-1.031	0.000617	HECT, C2 and WW domain containing E3 ubiquitin protein ligase 1
Gm715	-1.029	6.35E-05	predicted gene 715
Syndig1	-1.022	0.001017	synapse differentiation inducing 1
Syn1	-1.022	0.000103	synapsin I
Gm20646	-1.020	5.33E-11	predicted gene 20646
Lhx4	-1.015	1.43E-05	LIM homeobox protein 4
Gm15385	-1.012	0.00536	predicted gene 15385
Tspan17	-1.012	0.000226	tetraspanin 17
Gprin1	-1.009	6.55E-13	G protein-regulated inducer of neurite outgrowth 1
Gucy2f	-1.007	0.006457	guanylate cyclase 2f
Pdzrn4	-1.005	0.000132	PDZ domain containing RING finger 4
Ptpro	-1.005	7.09E-05	protein tyrosine phosphatase, receptor type, O
Hpdl	-1.002	4.02E-05	4-hydroxyphenylpyruvate dioxygenase-like
Gdap1l1	-1.002	4.11E-06	ganglioside-induced differentiation-associated protein 1-like 1
Smpd3	-0.995	5.96E-08	sphingomyelin phosphodiesterase 3, neutral
Slc1a2	-0.986	2.78E-07	solute carrier family 1 (glial high affinity glutamate transporter), member 2
Ccdc177	-0.965	8.16E-05	coiled-coil domain containing 177
Rgs4	-0.965	0.000647	regulator of G-protein signaling 4
Gm26786	-0.963	2.18E-07	predicted gene, 26786
Rab3c	-0.963	0.000908	RAB3C, member RAS oncogene family
Elavl4	-0.952	1.47E-10	ELAV (embryonic lethal, abnormal vision, Drosophila)-like 4 (Hu antigen D)
Klf2	-0.947	3.98E-06	Kruppel-like factor 2 (lung)
Tnnt1	-0.944	6.14E-05	troponin T1, skeletal, slow
Add2	-0.941	6.50E-07	adducin 2 (beta)

Gm20594	-0.940	0.001526	predicted gene, 20594
Dll3	-0.939	2.20E-06	delta-like 3 (Drosophila)
Ntn4	-0.934	1.57E-05	netrin 4
Jakmip2	-0.933	1.13E-08	janus kinase and microtubule interacting protein 2
Pmepa1	-0.925	0.000145	prostate transmembrane protein, androgen induced 1
C1qtnf3	-0.920	5.31E-05	C1q and tumor necrosis factor related protein 3
Tagln3	-0.918	4.99E-08	transgelin 3
Neurod4	-0.918	3.68E-07	neurogenic differentiation 4
Hoxa4	-0.917	9.18E-09	homeobox A4
BC064078	-0.899	0.000378	cDNA sequence BC064078
mt-Tw	-0.897	0.000545	mitochondrially encoded tRNA tryptophan
Wnt16	-0.895	1.83E-06	wingless-type MMTV integration site family, member 16
Sarm1	-0.895	0.000145	sterile alpha and HEAT/Armadillo motif containing 1
Tmem74	-0.893	0.003084	transmembrane protein 74
Maneal	-0.891	1.70E-06	mannosidase, endo-alpha-like
Dpysl4	-0.891	2.94E-13	dihydropyrimidinase-like 4
Mab21l1	-0.888	0.009815	mab-21-like 1 (C. elegans)
1500004A13Rik	-0.887	0.001374	RIKEN cDNA 1500004A13 gene
Eva1a	-0.887	0.003189	eva-1 homolog A (C. elegans)
Dpysl3	-0.885	1.50E-19	dihydropyrimidinase-like 3
Hist1h4j	-0.885	0.005509	histone cluster 1, H4j
Pantr1	-0.872	9.23E-07	POU domain, class 3, transcription factor 3 adjacent noncoding transcript 1
Slc25a48	-0.866	0.001275	solute carrier family 25, member 48
Pcdh10	-0.834	0.000144	protocadherin 10
Mgat5b	-0.832	2.97E-05	mannoside acetylglucosaminyltransferase 5, isoenzyme B
Miat	-0.830	0.000766	myocardial infarction associated transcript (non-protein coding)
Srrm4	-0.825	2.55E-05	serine/arginine repetitive matrix 4
Onecut1	-0.814	6.84E-06	one cut domain, family member 1
Nfasc	-0.792	0.000101	neurofascin
Dio2	-0.787	0.002909	deiodinase, iodothyronine, type II
Cplx1	-0.784	0.00714	complexin 1
C5ar1	-4.265	0.014909	complement component 5a receptor 1
1700024G13Rik	-2.917	0.015107	RIKEN cDNA 1700024G13 gene
Duox2	-2.804	0.022449	dual oxidase 2
Nkx1-1	-2.499	0.012863	NK1 transcription factor related, locus 1 (Drosophila)
Gm2449	-2.419	0.012221	predicted gene 2449
Gm14302	-2.231	0.026194	predicted gene 14302
Crct1	-2.229	0.026248	cysteine-rich C-terminal 1
A930017M01Rik	-2.128	0.03656	RIKEN cDNA A930017M01 gene
NA	-2.079	0.019347	NA
Ear1	-1.999	0.026975	eosinophil-associated, ribonuclease A family, member

			1
Gm14273	-1.990	0.011877	predicted gene 14273
Actl6b	-1.722	0.02109	actin-like 6B
6330409D20Rik	-1.672	0.013378	RIKEN cDNA 6330409D20 gene
Siah3	-1.583	0.025657	seven in absentia homolog 3 (Drosophila)
Btn1a1	-1.554	0.04385	butyrophilin, subfamily 1, member A1
Gm26191	-1.510	0.01362	predicted gene, 26191
Gm16796	-1.496	0.044201	predicted gene, 16796
Birc7	-1.487	0.010907	baculoviral IAP repeat-containing 7 (livin)
Impg1	-1.442	0.045222	interphotoreceptor matrix proteoglycan 1
Lingo4	-1.401	0.011204	leucine rich repeat and Ig domain containing 4
Ptprq	-1.351	0.019085	protein tyrosine phosphatase, receptor type, Q
Cpne6	-1.321	0.016862	copine VI
Olfm3	-1.306	0.018957	olfactomedin 3
Slc22a6	-1.299	0.012658	solute carrier family 22 (organic anion transporter), member 6
A530084C06Rik	-1.294	0.022763	RIKEN cDNA A530084C06 gene
Spn	-1.141	0.014094	sialophorin
Gm15218	-1.106	0.012899	predicted gene 15218
Pyy	-1.104	0.011684	peptide YY
Aspdh	-1.074	0.021587	aspartate dehydrogenase domain containing
Hcrtr2	-1.073	0.01019	hypocretin (orexin) receptor 2
Gm9951	-1.058	0.033985	predicted gene 9951
Tbx15	-1.052	0.017731	T-box 15
Col28a1	-1.044	0.052163	collagen, type XXVIII, alpha 1
Tmem196	-1.037	0.011855	transmembrane protein 196
Slco1c1	-1.036	0.019351	solute carrier organic anion transporter family, member 1c1
Myt1l	-1.006	0.020269	myelin transcription factor 1-like
Hrh3	-0.974	0.026719	histamine receptor H3
Padi4	-0.950	0.023123	peptidyl arginine deiminase, type IV
Galntl6	-0.948	0.012321	UDP-N-acetyl-alpha-D-galactosamine:polypeptide N-acetylgalactosaminyltransferase-like 6
Pantr2	-0.908	0.019866	POU domain, class 3, transcription factor 3 adjacent noncoding transcript 2
Nckap1l	-0.892	0.019571	NCK associated protein 1 like
Rims4	-0.845	0.018411	regulating synaptic membrane exocytosis 4
Olfm4	-0.839	0.018012	olfactomedin 4
Cckar	-0.815	0.030533	cholecystokinin A receptor
Kcnh4	-0.795	0.030118	potassium voltage-gated channel, subfamily H (eag-related), member 4
Aldh1b1	-0.766	0.019483	aldehyde dehydrogenase 1 family, member B1

Table VII-9: Flag 2 for both RNA Seq1 and RNA Seq2: Upregulated genes

gene	m	pval	description
S100g	6.312	1.51E-06	S100 calcium binding protein G
Hoxc8	5.676	3.78E-69	homeobox C8
Oc90	5.069	0.002635	otoconin 90
Apoa4	4.951	6.08E-05	apolipoprotein A-IV
Krt13	4.906	0.000361	keratin 13
Trappc3l	4.562	3.40E-07	trafficking protein particle complex 3 like
Gpr50	4.492	2.61E-38	G-protein-coupled receptor 50
Gm15634	4.275	0.006069	predicted gene 15634
NA	4.269	0.008368	NA
Tdgf1	4.215	2.74E-07	teratocarcinoma-derived growth factor 1
Ms4a2	4.207	4.93E-06	membrane-spanning 4-domains, subfamily A, member 2
Nppb	4.148	0.000117	natriuretic peptide type B
4933402E13Rik	4.119	9.85E-07	RIKEN cDNA 4933402E13 gene
Ccl2	4.076	0.000298	chemokine (C-C motif) ligand 2
Cldn14	3.915	4.12E-05	claudin 14
Gm15283	3.741	7.21E-11	predicted gene 15283
Epyc	3.728	3.03E-09	epiphycan
2610528A11Rik	3.681	5.84E-09	RIKEN cDNA 2610528A11 gene
Phf11b	3.634	0.000394	PHD finger protein 11B
Apob	3.598	1.81E-07	apolipoprotein B
Chac1	3.538	1.63E-06	ChaC, cation transport regulator 1
NA	3.530	0.002692	NA
Clec18a	3.471	4.22E-06	C-type lectin domain family 18, member A
Chst13	3.430	0.001138	carbohydrate (chondroitin 4) sulfotransferase 13
Gm11734	3.424	0.000817	predicted gene 11734
Ier3	3.416	8.42E-11	immediate early response 3
Tdo2	3.370	4.54E-11	tryptophan 2,3-dioxygenase
Gmnc	3.295	0.003174	geminin coiled-coil domain containing
Tac2	3.225	2.52E-11	tachykinin 2
Pitx1	3.222	1.88E-08	paired-like homeodomain transcription factor 1
5031434C07Rik	3.169	0.003766	RIKEN cDNA 5031434C07 gene
Ascl2	3.160	1.55E-06	achaete-scute complex homolog 2 (Drosophila)
Spp2	3.156	0.00023	secreted phosphoprotein 2
Abcc2	3.081	1.02E-05	ATP-binding cassette, sub-family C (CFTR/MRP), member 2
Eno2	3.052	5.77E-09	enolase 2, gamma neuronal
Scnn1g	2.989	0.001638	sodium channel, nonvoltage-gated 1 gamma
Aire	2.972	6.34E-08	autoimmune regulator (autoimmune polyendocrinopathy candidiasis ectodermal dystrophy)
Hand1	2.964	1.03E-24	heart and neural crest derivatives expressed

			transcript 1
Egr2	2.913	0.000452	early growth response 2
Ddit4	2.858	3.04E-13	DNA-damage-inducible transcript 4
Hoxc6	2.824	6.76E-10	homeobox C6
Cubn	2.800	7.40E-06	cubilin (intrinsic factor-cobalamin receptor)
Hoxa9	2.791	8.50E-05	homeobox A9
Gm22661	2.770	0.000237	predicted gene, 22661
Gm27505	2.766	0.000927	predicted gene, 27505
Postn	2.762	3.31E-23	periostin, osteoblast specific factor
Gm12746	2.723	8.56E-06	predicted gene 12746
Trap1a	2.704	0.000209	tumor rejection antigen P1A
Inhbb	2.689	0.000169	inhibin beta-B
Vax1	2.685	0.004055	ventral anterior homeobox 1
Muc13	2.615	1.60E-05	mucin 13, epithelial transmembrane
Hoxa7	2.595	0.000394	homeobox A7
Card14	2.581	0.00059	caspase recruitment domain family, member 14
Prss35	2.581	7.19E-16	protease, serine 35
Bhlhe40	2.572	1.70E-07	basic helix-loop-helix family, member e40
Gm27533	2.515	0.00452	predicted gene, 27533
Ppp1r3c	2.462	2.90E-06	protein phosphatase 1, regulatory (inhibitor) subunit 3C
Adm2	2.438	9.67E-06	adrenomedullin 2
Rarres2	2.416	6.12E-17	retinoic acid receptor responder (tazarotene induced) 2
Xlr5c	2.415	0.002879	X-linked lymphocyte-regulated 5C
5730403I07Rik	2.411	0.001647	RIKEN cDNA 5730403I07 gene
Mab21l2	2.371	1.44E-17	mab-21-like 2 (C. elegans)
Hoxb9	2.338	8.42E-06	homeobox B9
Oxtr	2.334	4.88E-06	oxytocin receptor
Muc2	2.309	7.92E-07	mucin 2
Car7	2.296	3.72E-26	carbonic anhydrase 7
9330159N05Rik	2.296	6.47E-05	RIKEN cDNA 9330159N05 gene
Stc1	2.262	1.18E-12	stanniocalcin 1
Gm20467	2.258	5.38E-10	predicted gene 20467
Gm14685	2.247	0.000326	predicted gene 14685
Ndrg1	2.238	3.25E-09	N-myc downstream regulated gene 1
Gfra3	2.233	5.24E-13	glial cell line derived neurotrophic factor family receptor alpha 3
Otx2	2.223	5.08E-07	orthodenticle homolog 2
Ptgs2	2.213	1.35E-09	prostaglandin-endoperoxide synthase 2
Egln3	2.205	9.01E-13	egl-9 family hypoxia-inducible factor 3
mt-Th	2.202	0.002926	mitochondrially encoded tRNA histidine
Ciart	2.197	5.30E-16	circadian associated repressor of transcription
Gm12022	2.195	0.000438	predicted gene 12022

Cdrt4	2.152	0.006047	CMT1A duplicated region transcript 4
Gm11027	2.146	0.007256	predicted gene 11027
S1pr5	2.124	0.000732	sphingosine-1-phosphate receptor 5
Kcne3	2.111	4.56E-14	potassium voltage-gated channel, Isk-related subfamily, gene 3
Gm28006	2.108	0.00509	predicted gene, 28006
Gm17202	2.099	0.00032	predicted gene 17202
Stc2	2.073	3.23E-13	stanniocalcin 2
Wnt8a	2.066	7.46E-13	wingless-type MMTV integration site family, member 8A
Gm16439	2.063	5.18E-11	predicted pseudogene 16439
Trib3	2.030	4.02E-05	tribbles homolog 3 (Drosophila)
Serpina3f	1.997	0.003113	serine (or cysteine) peptidase inhibitor, clade A, member 3F
Slc22a3	1.971	2.36E-07	solute carrier family 22 (organic cation transporter), member 3
P4ha2	1.967	3.35E-14	procollagen-proline, 2-oxoglutarate 4-dioxygenase (proline 4-hydroxylase), alpha II polypeptide
Hmx2	1.952	0.007064	H6 homeobox 2
Bhlhe41	1.925	2.49E-05	basic helix-loop-helix family, member e41
Neat1	1.920	1.61E-09	nuclear paraspeckle assembly transcript 1 (non-protein coding)
Ankrd37	1.915	1.92E-07	ankyrin repeat domain 37
Adm	1.910	0.000358	adrenomedullin
Nkx2-3	1.899	2.68E-15	NK2 homeobox 3
Avpr1b	1.891	2.14E-05	arginine vasopressin receptor 1B
Tmem211	1.888	0.002634	transmembrane protein 211
Rgs11	1.886	8.75E-07	regulator of G-protein signaling 11
Dio3os	1.885	4.19E-05	deiodinase, iodothyronine type III, opposite strand
Lrrc15	1.846	0.000149	leucine rich repeat containing 15
Chl1	1.844	4.67E-16	cell adhesion molecule with homology to L1CAM
Bnip3	1.841	1.01E-13	BCL2/adenovirus E1B interacting protein 3
Nxf7	1.832	0.000185	nuclear RNA export factor 7
Vldlr	1.817	5.13E-12	very low density lipoprotein receptor
Pla1a	1.817	0.005513	phospholipase A1 member A
Kcnh7	1.816	2.64E-08	potassium voltage-gated channel, subfamily H (eag-related), member 7
5033428I22Rik	1.816	5.01E-09	RIKEN cDNA 5033428I22 gene
Tsix	1.806	0.008786	X (inactive)-specific transcript, opposite strand
Ndufa4l2	1.801	0.000129	NADH dehydrogenase (ubiquinone) 1 alpha subcomplex, 4-like 2
1110018N20Rik	1.799	0.003328	RIKEN cDNA 1110018N20 gene
Syndig1l	1.799	0.004407	synapse differentiation inducing 1 like
Prdm6	1.796	2.84E-12	PR domain containing 6

Krt19	1.788	1.80E-09	keratin 19
Hoxc9	1.764	0.00019	homeobox C9
Vstm5	1.760	8.22E-06	V-set and transmembrane domain containing 5
NA	1.753	0.000395	NA
Rhox5	1.720	7.25E-06	reproductive homeobox 5
Hoxd8	1.703	0.004158	homeobox D8
Gm26992	1.703	0.007749	predicted gene, 26992
Il19	1.703	0.001991	interleukin 19
Pfkp	1.702	1.34E-10	phosphofructokinase, platelet
1700001L05Rik	1.699	3.17E-07	RIKEN cDNA 1700001L05 gene
Kcnk3	1.693	7.28E-07	potassium channel, subfamily K, member 3
Rxfp1	1.692	1.29E-08	relaxin/insulin-like family peptide receptor 1
Pparg	1.686	0.000889	peroxisome proliferator activated receptor gamma
Gm14506	1.683	1.26E-06	predicted gene 14506
Mgarp	1.682	1.37E-08	mitochondria localized glutamic acid rich protein
Fam184b	1.681	9.50E-08	family with sequence similarity 184, member B
Upk1b	1.659	0.000615	uroplakin 1B
Abi3bp	1.659	5.07E-11	ABI gene family, member 3 (NESH) binding protein
Gm11536	1.653	0.001737	predicted gene 11536
Cox4i2	1.647	6.33E-08	cytochrome c oxidase subunit IV isoform 2
Gm6277	1.635	8.25E-06	predicted gene 6277
Pfkfb3	1.614	3.93E-13	6-phosphofructo-2-kinase/fructose-2,6-biphosphatase 3
Gm16754	1.609	2.12E-10	predicted gene, 16754
Pla2g5	1.605	0.000239	phospholipase A2, group V
Adamts2	1.602	2.09E-11	a disintegrin-like and metallopeptidase (reprolysin type) with thrombospondin type 1 motif, 2
Mir483	1.599	0.00293	microRNA 483
Pof1b	1.597	7.91E-05	premature ovarian failure 1B
Kcna1	1.594	4.65E-05	potassium voltage-gated channel, shaker-related subfamily, member 1
Efna3	1.593	7.24E-10	ephrin A3
Gjb5	1.581	2.36E-09	gap junction protein, beta 5
Fam65c	1.572	5.17E-11	family with sequence similarity 65, member C
Gdf10	1.550	3.43E-09	growth differentiation factor 10
Hoxa6	1.548	2.18E-05	homeobox A6
Phlda2	1.536	9.66E-07	pleckstrin homology-like domain, family A, member 2
Tnfaip3	1.531	1.07E-06	tumor necrosis factor, alpha-induced protein 3
Ppp1r3g	1.527	3.84E-06	protein phosphatase 1, regulatory (inhibitor) subunit 3G
Bmp3	1.518	1.00E-08	bone morphogenetic protein 3
H2-Ab1	1.515	0.006489	histocompatibility 2, class II antigen A, beta 1
Gm15850	1.514	0.002541	predicted gene 15850
Fas	1.513	4.17E-07	Fas (TNF receptor superfamily member 6)
Hoxb5os	1.498	1.92E-09	homeobox B5 and homeobox B6, opposite strand

Fam71f2	1.495	0.000342	family with sequence similarity 71, member F2
A730049H05Rik	1.494	1.51E-06	RIKEN cDNA A730049H05 gene
Slc2a3	1.491	3.31E-12	solute carrier family 2 (facilitated glucose transporter), member 3
Fat2	1.479	2.15E-06	FAT tumor suppressor homolog 2 (Drosophila)
Rora	1.478	9.40E-08	RAR-related orphan receptor alpha
Cbln3	1.474	1.72E-06	cerebellin 3 precursor protein
Fst	1.467	1.50E-29	follistatin
Col1a1	1.465	8.60E-15	collagen, type I, alpha 1
Plcxd1	1.458	2.31E-05	phosphatidylinositol-specific phospholipase C, X domain containing 1
Adamts18	1.456	3.55E-11	a disintegrin-like and metallopeptidase (reprolysin type) with thrombospondin type 1 motif, 18
Pi15	1.448	4.53E-05	peptidase inhibitor 15
Stac	1.447	6.03E-05	src homology three (SH3) and cysteine rich domain
Hrct1	1.442	0.009552	histidine rich carboxyl terminus 1
Gm26670	1.439	0.004075	predicted gene, 26670
Notumos	1.438	0.003677	notum pectinacetylesterase homolog (Drosophila), opposite strand
Slc16a3	1.434	2.70E-19	solute carrier family 16 (monocarboxylic acid transporters), member 3
Dkk2	1.425	6.04E-09	dickkopf homolog 2 (Xenopus laevis)
2500002B13Rik	1.422	7.32E-09	RIKEN cDNA 2500002B13 gene
5330426P16Rik	1.420	4.42E-05	RIKEN cDNA 5330426P16 gene
Ptprv	1.410	1.50E-07	protein tyrosine phosphatase, receptor type, V
Lyve1	1.410	2.07E-05	lymphatic vessel endothelial hyaluronan receptor 1
NA	1.408	0.000193	NA
Tmem45a	1.405	3.14E-07	transmembrane protein 45a
Nr4a3	1.393	3.79E-09	nuclear receptor subfamily 4, group A, member 3
Apln	1.388	6.26E-16	apelin
Gpx6	1.387	0.005065	glutathione peroxidase 6
Grhl3	1.382	8.06E-09	grainyhead-like 3 (Drosophila)
Fgf3	1.368	2.50E-08	fibroblast growth factor 3
Smoc2	1.365	3.79E-08	SPARC related modular calcium binding 2
Hk2	1.359	2.27E-13	hexokinase 2
Cdk15	1.344	0.00631	cyclin-dependent kinase 15
Sp7	1.344	0.000246	Sp7 transcription factor 7
Gm26826	1.343	0.000509	predicted gene, 26826
Wisp1	1.336	5.75E-08	WNT1 inducible signaling pathway protein 1
Hpcal4	1.335	0.000762	hippocalcin-like 4
Col14a1	1.327	1.12E-14	collagen, type XIV, alpha 1
Klk13	1.306	0.000591	kallikrein related-peptidase 13
Aldoc	1.303	4.18E-06	aldolase C, fructose-bisphosphate
Zan	1.299	3.21E-07	zonadhesin

Gm15179	1.298	0.001406	predicted gene 15179
Appbp2os	1.296	5.53E-05	amyloid beta precursor protein (cytoplasmic tail) binding protein 2, opposite strand
3110057O12Rik	1.285	2.30E-07	RIKEN cDNA 3110057O12 gene
3830417A13Rik	1.279	0.001321	RIKEN cDNA 3830417A13 gene
Pdk1	1.267	2.93E-16	pyruvate dehydrogenase kinase, isoenzyme 1
Ero1l	1.257	2.47E-10	ERO1-like (S. cerevisiae)
Cyp26b1	1.257	8.30E-06	cytochrome P450, family 26, subfamily b, polypeptide 1
Rgcc	1.257	4.64E-07	regulator of cell cycle
Kdm4d	1.257	0.003917	lysine (K)-specific demethylase 4D
Ovol1	1.254	0.004006	OVO homolog-like 1 (Drosophila)
Gdap10	1.251	1.36E-06	ganglioside-induced differentiation-associated-protein 10
Tlr12	1.249	0.001699	toll-like receptor 12
Slc39a4	1.249	0.002273	solute carrier family 39 (zinc transporter), member 4
G430049J08Rik	1.247	5.84E-05	RIKEN cDNA G430049J08 gene
Gm12758	1.246	6.38E-06	predicted gene 12758
Hoxb7	1.240	1.31E-09	homeobox B7
Cabp1	1.231	4.45E-09	calcium binding protein 1
9530026P05Rik	1.231	1.35E-08	RIKEN cDNA 9530026P05 gene
March10	1.229	0.000374	membrane-associated ring finger (C3HC4) 10
Oas3	1.220	0.000477	2'-5' oligoadenylate synthetase 3
Cyp2s1	1.218	0.00131	cytochrome P450, family 2, subfamily s, polypeptide 1
Stab2	1.207	5.27E-07	stabilin 2
Hgfac	1.206	0.006643	hepatocyte growth factor activator
Fgf15	1.206	1.56E-11	fibroblast growth factor 15
F7	1.204	0.002034	coagulation factor VII
Calml4	1.198	0.000716	calmodulin-like 4
Arrdc3	1.197	3.59E-10	arrestin domain containing 3
Gm11454	1.191	0.002667	predicted gene 11454
Serpine1	1.188	0.001276	serine (or cysteine) peptidase inhibitor, clade E, member 1
C1qtnf7	1.186	1.78E-06	C1q and tumor necrosis factor related protein 7
0610040F04Rik	1.177	0.004962	RIKEN cDNA 0610040F04 gene
Pgm2	1.177	1.71E-07	phosphoglucomutase 2
Gm17382	1.174	0.001136	predicted gene, 17382
Gm2117	1.173	9.29E-06	predicted gene 2117
Arhgef4	1.172	0.000135	Rho guanine nucleotide exchange factor (GEF) 4
Bmp2	1.164	4.03E-05	bone morphogenetic protein 2
Cfap70	1.163	0.00134	cilia and flagella associated protein 70
Gm12688	1.162	2.42E-08	predicted gene 12688
Fosl2	1.161	7.40E-06	fos-like antigen 2
Pde4b	1.159	1.47E-06	phosphodiesterase 4B, cAMP specific

Nfatc2	1.155	2.94E-06	nuclear factor of activated T cells, cytoplasmic, calcineurin dependent 2
4833403I15Rik	1.154	0.006369	RIKEN cDNA 4833403I15 gene
Adamts9	1.153	6.83E-17	a disintegrin-like and metallopeptidase (reprolysin type) with thrombospondin type 1 motif, 9
Iigp1	1.151	0.000884	interferon inducible GTPase 1
Ahnak	1.147	6.33E-20	AHNAK nucleoprotein (desmoyokin)
Hes7	1.147	0.002624	hairy and enhancer of split 7 (Drosophila)
Mtus2	1.146	9.00E-07	microtubule associated tumor suppressor candidate 2
Mt1	1.145	7.55E-05	metallothionein 1
Adra2c	1.145	0.002593	adrenergic receptor, alpha 2c
Proser2	1.142	0.000175	proline and serine rich 2
Gm2061	1.141	0.003243	predicted gene 2061
Prima1	1.141	0.001729	proline rich membrane anchor 1
2310002F09Rik	1.140	3.50E-07	RIKEN cDNA 2310002F09 gene
Apold1	1.139	2.54E-05	apolipoprotein L domain containing 1
Sowahb	1.138	2.07E-09	sosondowah ankyrin repeat domain family member B
Gm17501	1.127	0.003506	predicted gene, 17501
NA	1.125	0.001118	NA
Kbtbd11	1.123	1.03E-14	kelch repeat and BTB (POZ) domain containing 11
B230323A14Rik	1.121	4.93E-06	RIKEN cDNA B230323A14 gene
Abcc8	1.119	4.52E-06	ATP-binding cassette, sub-family C (CFTR/MRP), member 8
Col6a3	1.119	6.58E-08	collagen, type VI, alpha 3
Lamb3	1.115	0.004279	laminin, beta 3
Plekha2	1.115	1.97E-05	pleckstrin homology domain-containing, family A (phosphoinositide binding specific) member 2
Notum	1.114	2.66E-08	notum pectinacetylesterase homolog (Drosophila)
BC006965	1.113	0.003903	cDNA sequence BC006965
Cysltr1	1.111	2.94E-06	cysteinyl leukotriene receptor 1
1810010H24Rik	1.110	0.002492	RIKEN cDNA 1810010H24 gene
Pmaip1	1.104	3.00E-07	phorbol-12-myristate-13-acetate-induced protein 1
Gm26600	1.095	0.000311	predicted gene, 26600
Il16	1.093	7.46E-05	interleukin 16
Gabre	1.092	5.89E-07	gamma-aminobutyric acid (GABA) A receptor, subunit epsilon
Gm16046	1.091	0.000598	predicted gene 16046
Gm26721	1.089	0.00122	predicted gene, 26721
Krt8	1.086	4.64E-08	keratin 8
Gm16201	1.085	0.008769	predicted gene 16201
P4ha1	1.083	2.68E-14	procollagen-proline, 2-oxoglutarate 4-dioxygenase (proline 4-hydroxylase), alpha 1 polypeptide
Tmprss13	1.075	0.007021	transmembrane protease, serine 13

F630040K05Rik	1.067	0.000453	RIKEN cDNA F630040K05 gene
Fam162a	1.067	3.89E-12	family with sequence similarity 162, member A
Gm19705	1.064	0.007092	predicted gene, 19705
Ccdc80	1.051	8.59E-11	coiled-coil domain containing 80
Smtnl2	1.048	0.00026	smoothelin-like 2
Gm26908	1.034	0.001184	predicted gene, 26908
Gm17399	1.026	4.40E-05	predicted gene, 17399
Zfp804a	1.022	0.001958	zinc finger protein 804A
Prelid2	1.022	1.05E-07	PRELI domain containing 2
Plod2	1.014	1.31E-09	procollagen lysine, 2-oxoglutarate 5-dioxygenase 2
D930048N14Rik	1.014	1.08E-05	RIKEN cDNA D930048N14 gene
Adamts16	1.009	2.66E-06	a disintegrin-like and metallopeptidase (reprolysin type) with thrombospondin type 1 motif, 16
Ndrg2	1.001	0.009803	N-myc downstream regulated gene 2

Table VII-10: Flag -2 for both RNA Seq1 and RNA Seq2: Downregulated Genes

gene	m	pval	description
Eif2s3y	-10.919	9.33E-10	eukaryotic translation initiation factor 2, subunit 3, structural gene Y-linked
Kdm5d	-10.596	2.23E-09	lysine (K)-specific demethylase 5D
Gcg	-8.426	9.44E-08	glucagon
Ddx3y	-7.820	1.93E-07	DEAD (Asp-Glu-Ala-Asp) box polypeptide 3, Y-linked
Insm2	-5.375	8.77E-05	insulinoma-associated 2
Rgs13	-5.307	0.001073	regulator of G-protein signaling 13
Vsx2	-5.061	0.000711	visual system homeobox 2
Otp	-4.926	5.52E-10	orthopedia homolog (Drosophila)
Gabrg2	-4.860	9.39E-13	gamma-aminobutyric acid (GABA) A receptor, subunit gamma 2
Uty	-4.629	0.000212	ubiquitously transcribed tetratricopeptide repeat gene, Y chromosome
Cox8b	-4.542	0.007044	cytochrome c oxidase subunit VIIIb
Gm5590	-4.541	0.004983	predicted gene 5590
Hk3	-4.288	4.44E-47	hexokinase 3
Dhrs7c	-4.183	4.14E-06	dehydrogenase/reductase (SDR family) member 7C
Ptf1a	-4.130	2.13E-11	pancreas specific transcription factor, 1a
Gm27199	-3.999	0.000358	predicted gene 27199
Msc	-3.934	1.94E-26	musculin
Gsx1	-3.794	1.02E-06	GS homeobox 1
Tlx3	-3.767	3.00E-07	T cell leukemia, homeobox 3
Robo3	-3.736	1.70E-11	roundabout homolog 3 (Drosophila)
Fmo2	-3.714	0.000117	flavin containing monooxygenase 2
Scg2	-3.529	3.53E-09	secretogranin II
2310002L09Rik	-3.511	4.75E-12	RIKEN cDNA 2310002L09 gene
Cxcl11	-3.399	2.32E-05	chemokine (C-X-C motif) ligand 11
Crp	-3.379	6.06E-07	C-reactive protein, pentraxin-related
Chrna3	-3.321	1.39E-42	cholinergic receptor, nicotinic, alpha polypeptide 3
C130071C03Rik	-3.248	5.09E-22	RIKEN cDNA C130071C03 gene
AI854517	-3.211	5.40E-11	expressed sequence AI854517
Il1rn	-3.207	5.43E-10	interleukin 1 receptor antagonist
Hes2	-3.166	5.51E-07	hairy and enhancer of split 2 (Drosophila)
Folr4	-3.152	0.000305	folate receptor 4 (delta)
Prr32	-3.115	5.06E-09	proline rich 32
Skor1	-3.107	6.01E-09	SKI family transcriptional corepressor 1
NA	-3.060	4.09E-11	NA
Lrrc75aos2	-3.046	0.000657	leucine rich repeat containing 75A, opposite strand 2
Slc6a5	-3.038	9.16E-05	solute carrier family 6 (neurotransmitter transporter, glycine), member 5
Olfr315	-2.985	0.00054	olfactory receptor 315
1700128E19Rik	-2.959	2.03E-15	RIKEN cDNA 1700128E19 gene

Csn3	-2.946	5.03E-22	casein kappa
Chrna9	-2.928	0.00144	cholinergic receptor, nicotinic, alpha polypeptide 9
Hoxa10	-2.870	0.008068	homeobox A10
Unc5a	-2.862	1.40E-87	unc-5 homolog A (C. elegans)
Slc6a20a	-2.846	0.000616	solute carrier family 6 (neurotransmitter transporter), member 20A
Gm12082	-2.834	8.23E-05	predicted gene 12082
Lhx5	-2.800	5.71E-11	LIM homeobox protein 5
Gm12224	-2.800	0.001533	predicted gene 12224
Ttc9b	-2.798	2.19E-06	tetratricopeptide repeat domain 9B
Nkx2-1	-2.793	6.87E-17	NK2 homeobox 1
Ppp1r3a	-2.772	3.52E-08	protein phosphatase 1, regulatory (inhibitor) subunit 3A
Barx1	-2.760	1.33E-07	BarH-like homeobox 1
Myh3	-2.758	1.32E-61	myosin, heavy polypeptide 3, skeletal muscle, embryonic
1810010K12Rik	-2.739	5.08E-08	RIKEN cDNA 1810010K12 gene
Fbll1	-2.704	0.000429	fibrillarin-like 1
A730046J19Rik	-2.686	0.00016	RIKEN cDNA A730046J19 gene
Bhlhe23	-2.685	5.34E-08	basic helix-loop-helix family, member e23
Tlx2	-2.679	7.97E-08	T cell leukemia, homeobox 2
Lamp5	-2.609	0.000793	lysosomal-associated membrane protein family, member 5
Kirrel2	-2.602	8.53E-14	kin of IRRE like 2 (Drosophila)
Adcyap1	-2.591	2.45E-09	adenylate cyclase activating polypeptide 1
Gm24105	-2.585	0.004302	predicted gene, 24105
Klhl14	-2.562	6.87E-18	kelch-like 14
Nppc	-2.557	8.48E-13	natriuretic peptide type C
Grifin	-2.552	7.96E-06	galectin-related inter-fiber protein
Tnnc2	-2.522	7.07E-26	troponin C2, fast
NA	-2.518	4.27E-05	NA
Musk	-2.513	1.40E-07	muscle, skeletal, receptor tyrosine kinase
Chrnb4	-2.507	2.04E-25	cholinergic receptor, nicotinic, beta polypeptide 4
Myot	-2.505	9.70E-08	myotilin
Pitx3	-2.504	0.008777	paired-like homeodomain transcription factor 3
Mstn	-2.504	2.68E-24	myostatin
Nhlh2	-2.503	5.26E-19	nescient helix loop helix 2
Klhl35	-2.494	6.52E-06	kelch-like 35
Grm2	-2.489	6.24E-10	glutamate receptor, metabotropic 2
Bhlhe22	-2.466	1.66E-19	basic helix-loop-helix family, member e22
Klhl40	-2.449	1.22E-07	kelch-like 40
Barhl1	-2.449	6.35E-05	BarH-like 1 (Drosophila)
Cntn2	-2.444	7.40E-23	contactin 2
Sln	-2.428	4.35E-07	sarcolipin
Gnat3	-2.420	2.21E-09	guanine nucleotide binding protein, alpha transducing

			3
Mylk4	-2.413	1.29E-08	myosin light chain kinase family, member 4
Scml4	-2.389	2.04E-12	sex comb on midleg-like 4 (Drosophila)
Hist2h4	-2.376	0.002318	histone cluster 2, H4
Nwd2	-2.372	2.49E-07	NACHT and WD repeat domain containing 2
Scrt1	-2.345	5.08E-08	scratch homolog 1, zinc finger protein (Drosophila)
Kctd8	-2.308	0.000795	potassium channel tetramerisation domain containing 8
Tmem132e	-2.301	8.19E-22	transmembrane protein 132E
Gm12408	-2.297	0.005693	predicted gene 12408
Gm16140	-2.289	8.15E-07	predicted gene 16140
3110039M20Rik	-2.279	3.87E-14	RIKEN cDNA 3110039M20 gene
St8sia3os	-2.278	8.85E-07	ST8 alpha-N-acetyl-neuraminide alpha-2,8-sialyltransferase 3, opposite strand
Sgcg	-2.278	1.36E-05	sarcoglycan, gamma (dystrophin-associated glycoprotein)
Cabp7	-2.261	4.46E-08	calcium binding protein 7
Nefm	-2.260	1.21E-23	neurofilament, medium polypeptide
Tmem182	-2.249	1.89E-07	transmembrane protein 182
Stk32a	-2.247	1.68E-25	serine/threonine kinase 32A
Dcx	-2.242	1.66E-22	doublecortin
Nacad	-2.234	3.60E-11	NAC alpha domain containing
B3galt2	-2.224	0.003333	UDP-Gal:betaGlcNAc beta 1,3-galactosyltransferase, polypeptide 2
Oit1	-2.223	0.00388	oncoprotein induced transcript 1
Foxg1	-2.222	7.73E-14	forkhead box G1
D930028M14Rik	-2.173	8.32E-16	RIKEN cDNA D930028M14 gene
Il7	-2.165	0.003468	interleukin 7
Ecel1	-2.162	2.13E-09	endothelin converting enzyme-like 1
Phox2a	-2.155	7.09E-17	paired-like homeobox 2a
Alx3	-2.154	4.76E-18	aristaless-like homeobox 3
Gm14133	-2.154	0.009814	predicted gene 14133
Mypn	-2.136	0.000108	myopalladin
Mylpf	-2.133	3.74E-28	myosin light chain, phosphorylatable, fast skeletal muscle
Inmt	-2.118	0.000328	indolethylamine N-methyltransferase
Gsx2	-2.116	6.72E-14	GS homeobox 2
Ankrd2	-2.104	2.98E-11	ankyrin repeat domain 2 (stretch responsive muscle)
Cdhr1	-2.103	4.02E-08	cadherin-related family member 1
Neb	-2.090	2.07E-15	nebulin
C1ql3	-2.087	6.50E-09	C1q-like 3
Gjd4	-2.069	3.16E-06	gap junction protein, delta 4
Stmn2	-2.063	1.09E-17	stathmin-like 2
Dbh	-2.060	0.000712	dopamine beta hydroxylase
Resp18	-2.058	0.004709	regulated endocrine-specific protein 18

Myh13	-2.057	0.000177	myosin, heavy polypeptide 13, skeletal muscle
Oasl2	-2.051	0.000133	2'-5' oligoadenylate synthetase-like 2
Htr2a	-2.049	0.008644	5-hydroxytryptamine (serotonin) receptor 2A
Ina	-2.032	1.43E-15	internexin neuronal intermediate filament protein, alpha
Cps1	-2.019	0.000189	carbamoyl-phosphate synthetase 1
3110035E14Rik	-2.013	4.84E-09	RIKEN cDNA 3110035E14 gene
Myh2	-2.009	0.000586	myosin, heavy polypeptide 2, skeletal muscle, adult
Myoz2	-2.005	0.002367	myozenin 2
4930469K13Rik	-1.998	3.08E-06	RIKEN cDNA 4930469K13 gene
Ctxn3	-1.997	1.47E-10	cortexin 3
Sstr3	-1.987	0.009493	somatostatin receptor 3
Hs3st2	-1.987	2.40E-05	heparan sulfate (glucosamine) 3-O-sulfotransferase 2
Kcnh5	-1.976	0.007434	potassium voltage-gated channel, subfamily H (eag-related), member 5
Phox2b	-1.955	9.87E-26	paired-like homeobox 2b
Gm16582	-1.954	1.38E-10	predicted gene 16582
Stmn3	-1.949	2.19E-14	stathmin-like 3
1700011H14Rik	-1.949	2.36E-07	RIKEN cDNA 1700011H14 gene
Sst	-1.946	2.29E-09	somatostatin
Stmn4	-1.945	3.52E-12	stathmin-like 4
Neurod1	-1.942	2.28E-10	neurogenic differentiation 1
Chat	-1.939	9.76E-13	choline acetyltransferase
Aldh1a7	-1.937	5.08E-13	aldehyde dehydrogenase family 1, subfamily A7
Myom3	-1.923	7.00E-07	myomesin family, member 3
Cdk5r2	-1.917	6.41E-10	cyclin-dependent kinase 5, regulatory subunit 2 (p39)
Chrng	-1.914	1.49E-08	cholinergic receptor, nicotinic, gamma polypeptide
Fgf6	-1.909	0.000204	fibroblast growth factor 6
Ppp1r17	-1.905	4.53E-12	protein phosphatase 1, regulatory subunit 17
BC048679	-1.900	0.000504	cDNA sequence BC048679
B3gat2	-1.891	0.000413	beta-1,3-glucuronyltransferase 2 (glucuronosyltransferase S)
Insc	-1.888	9.17E-09	inscuteable homolog (Drosophila)
Pou2f2	-1.886	1.77E-07	POU domain, class 2, transcription factor 2
Syt4	-1.868	3.62E-08	synaptotagmin IV
Cerkl	-1.841	9.68E-10	ceramide kinase-like
Prdm13	-1.839	6.09E-17	PR domain containing 13
Lin7a	-1.831	3.68E-11	lin-7 homolog A (C. elegans)
Casq2	-1.825	3.59E-09	calsequestrin 2
Rhbdl3	-1.813	4.63E-20	rhomboid, veinlet-like 3 (Drosophila)
Hic1	-1.812	2.94E-12	hypermethylated in cancer 1
Mybph	-1.810	1.62E-14	myosin binding protein H
Scn9a	-1.810	1.19E-06	sodium channel, voltage-gated, type IX, alpha
Gabrq	-1.807	0.001399	gamma-aminobutyric acid (GABA) A receptor, subunit theta

Chrna5	-1.803	5.45E-10	cholinergic receptor, nicotinic, alpha polypeptide 5
Gm2990	-1.802	1.73E-05	predicted gene 2990
Myf6	-1.802	5.89E-09	myogenic factor 6
4930426D05Rik	-1.792	2.84E-13	RIKEN cDNA 4930426D05 gene
Ttbk1	-1.790	2.53E-12	tau tubulin kinase 1
Atcay	-1.778	4.02E-11	ataxia, cerebellar, Cayman type homolog (human)
6030408B16Rik	-1.765	0.000313	RIKEN cDNA 6030408B16 gene
Tubb3	-1.761	2.15E-27	tubulin, beta 3 class III
Thsd7b	-1.760	1.10E-06	thrombospondin, type I, domain containing 7B
NA	-1.759	2.21E-06	NA
Cck	-1.745	8.67E-08	cholecystokinin
Wfdc1	-1.745	1.28E-09	WAP four-disulfide core domain 1
Xkr7	-1.740	3.52E-09	X Kell blood group precursor related family member 7 homolog
Ablim3	-1.735	2.15E-10	actin binding LIM protein family, member 3
Ano5	-1.727	4.13E-07	anoctamin 5
Dhrs3	-1.725	1.53E-11	dehydrogenase/reductase (SDR family) member 3
Insm1	-1.722	1.09E-17	insulinoma-associated 1
Kcnj8	-1.718	0.005016	potassium inwardly-rectifying channel, subfamily J, member 8
Nefl	-1.717	2.17E-17	neurofilament, light polypeptide
Unc79	-1.714	3.09E-06	unc-79 homolog (C. elegans)
Ppfia2	-1.711	0.000137	protein tyrosine phosphatase, receptor type, f polypeptide (PTPRF), interacting protein (liprin), alpha 2
Filip1	-1.709	8.97E-17	filamin A interacting protein 1
En1	-1.690	3.61E-09	engrailed 1
Il17b	-1.679	0.001633	interleukin 17B
Pah	-1.678	7.49E-06	phenylalanine hydroxylase
Fam163a	-1.671	6.50E-06	family with sequence similarity 163, member A
Sncg	-1.671	1.40E-09	synuclein, gamma
Elavl3	-1.665	3.77E-15	ELAV (embryonic lethal, abnormal vision, Drosophila)-like 3 (Hu antigen C)
Scrt2	-1.660	1.86E-09	scratch homolog 2, zinc finger protein (Drosophila)
Hs3st5	-1.654	0.000693	heparan sulfate (glucosamine) 3-O-sulfotransferase 5
Ap3b2	-1.648	1.53E-09	adaptor-related protein complex 3, beta 2 subunit
Pou3f4	-1.646	1.88E-08	POU domain, class 3, transcription factor 4
Gm14343	-1.646	0.000172	predicted gene 14343
Nrg3	-1.645	1.09E-06	neuregulin 3
Gm12239	-1.644	0.000147	predicted gene 12239
Ntrk1	-1.643	2.54E-12	neurotrophic tyrosine kinase, receptor, type 1
Tmem8c	-1.639	4.70E-06	transmembrane protein 8C
Gfra1	-1.625	2.72E-18	glial cell line derived neurotrophic factor family receptor alpha 1
Vsx1	-1.613	4.41E-05	visual system homeobox 1 homolog (zebrafish)

Htr3a	-1.608	0.001446	5-hydroxytryptamine (serotonin) receptor 3A
Neurog1	-1.607	5.82E-12	neurogenin 1
Galnt9	-1.601	1.33E-07	UDP-N-acetyl-alpha-D-galactosamine:polypeptide N-acetylgalactosaminyltransferase 9
Rundc3a	-1.598	9.44E-10	RUN domain containing 3A
Lhx1	-1.593	5.19E-06	LIM homeobox protein 1
Iqsec3	-1.591	0.00014	IQ motif and Sec7 domain 3
Mmp24	-1.591	5.88E-07	matrix metallopeptidase 24
Halr1	-1.590	4.62E-09	Hoxa adjacent long noncoding RNA 1
Slc17a7	-1.584	7.04E-07	solute carrier family 17 (sodium-dependent inorganic phosphate cotransporter), member 7
Fstl5	-1.583	0.000294	follistatin-like 5
Gm26871	-1.582	0.001957	predicted gene, 26871
Gabra1	-1.578	0.006439	gamma-aminobutyric acid (GABA) A receptor, subunit alpha 1
Cacna1s	-1.575	0.000303	calcium channel, voltage-dependent, L type, alpha 1S subunit
Pnmal1	-1.565	2.68E-09	PNMA-like 1
Abcb4	-1.547	0.00387	ATP-binding cassette, sub-family B (MDR/TAP), member 4
Svop	-1.547	2.00E-05	SV2 related protein
Arpp21	-1.547	6.30E-10	cyclic AMP-regulated phosphoprotein, 21
Gcnt4	-1.545	3.68E-14	glucosaminyl (N-acetyl) transferase 4, core 2 (beta-1,6-N-acetylglucosaminyltransferase)
Otor	-1.542	0.000404	otoraplin
Gm12892	-1.540	1.86E-18	predicted gene 12892
Syt2	-1.526	2.78E-06	synaptotagmin II
Fndc5	-1.525	8.93E-15	fibronectin type III domain containing 5
Kcnj10	-1.522	1.59E-06	potassium inwardly-rectifying channel, subfamily J, member 10
Ckb	-1.517	9.34E-33	creatine kinase, brain
Nr0b1	-1.515	0.000179	nuclear receptor subfamily 0, group B, member 1
Chrna1	-1.513	6.52E-06	cholinergic receptor, nicotinic, alpha polypeptide 1 (muscle)
Lrrtm3	-1.513	3.44E-10	leucine rich repeat transmembrane neuronal 3
Glra1	-1.510	1.01E-05	glycine receptor, alpha 1 subunit
Foxn4	-1.505	1.86E-05	forkhead box N4
Myt1	-1.501	5.10E-11	myelin transcription factor 1
Onecut3	-1.486	5.75E-05	one cut domain, family member 3
Trim67	-1.481	9.95E-06	tripartite motif-containing 67
2310015B20Rik	-1.480	5.24E-05	RIKEN cDNA 2310015B20 gene
Ptpn5	-1.476	6.79E-10	protein tyrosine phosphatase, non-receptor type 5
Gabrb2	-1.461	1.34E-07	gamma-aminobutyric acid (GABA) A receptor, subunit beta 2
Hmx1	-1.461	0.003807	H6 homeobox 1

Hpca	-1.460	1.71E-07	hippocalcin
Lamc3	-1.459	1.90E-11	laminin gamma 3
St18	-1.459	5.67E-08	suppression of tumorigenicity 18
Tecta	-1.457	4.50E-06	tectorin alpha
Cacng2	-1.453	0.002181	calcium channel, voltage-dependent, gamma subunit 2
Myog	-1.453	4.69E-11	myogenin
Prrxl1	-1.440	0.002036	paired related homeobox protein-like 1
Cxcl13	-1.440	5.24E-11	chemokine (C-X-C motif) ligand 13
Mast1	-1.435	0.000183	microtubule associated serine/threonine kinase 1
Scg3	-1.429	2.01E-10	secretogranin III
1700106J16Rik	-1.424	1.50E-05	RIKEN cDNA 1700106J16 gene
Pax7	-1.421	6.09E-18	paired box 7
Gm7325	-1.414	5.81E-05	predicted gene 7325
Gm20501	-1.413	0.005398	predicted gene 20501
Rab9b	-1.411	0.00293	RAB9B, member RAS oncogene family
Nyap2	-1.408	4.14E-05	neuronal tyrosine-phophorylated phosphoinositide 3-kinase adaptor 2
Wnt2b	-1.396	1.32E-08	wingless-type MMTV integration site family, member 2B
mt-Tt	-1.393	1.71E-10	mitochondrially encoded tRNA threonine
Art1	-1.381	3.14E-05	ADP-ribosyltransferase 1
Aldh1a1	-1.381	0.004949	aldehyde dehydrogenase family 1, subfamily A1
Ascl1	-1.380	6.14E-11	achaete-scute complex homolog 1 (Drosophila)
Apc2	-1.380	3.81E-11	adenomatosis polyposis coli 2
Rgs18	-1.378	0.002921	regulator of G-protein signaling 18
Dmrtb1	-1.376	4.91E-06	DMRT-like family B with proline-rich C-terminal, 1
Cacng6	-1.374	0.000806	calcium channel, voltage-dependent, gamma subunit 6
Srrm3	-1.372	4.91E-06	serine/arginine repetitive matrix 3
Fabp7	-1.371	2.09E-10	fatty acid binding protein 7, brain
Sez6	-1.365	0.000183	seizure related gene 6
Clvs1	-1.363	2.51E-11	clavesin 1
Cdh9	-1.351	0.008476	cadherin 9
Gm16551	-1.346	2.13E-11	predicted gene 16551
Dusp15	-1.345	0.000914	dual specificity phosphatase-like 15
Atp1a3	-1.344	5.22E-06	ATPase, Na+/K+ transporting, alpha 3 polypeptide
Msx3	-1.336	4.88E-24	msh homeobox 3
Chgb	-1.332	1.11E-06	chromogranin B
Snord50b	-1.330	0.004671	small nucleolar RNA, C/D box 50B
Adcy8	-1.326	3.87E-09	adenylate cyclase 8
Ripply3	-1.320	1.83E-17	ripply3 homolog (zebrafish)
Nccrp1	-1.319	0.000779	non-specific cytotoxic cell receptor protein 1 homolog (zebrafish)
Apba2	-1.310	2.77E-32	amyloid beta (A4) precursor protein-binding, family A, member 2
Rarb	-1.308	1.83E-28	retinoic acid receptor, beta

Syt1	-1.306	4.24E-06	synaptotagmin I
C2cd4a	-1.299	0.006393	C2 calcium-dependent domain containing 4A
Gm15680	-1.295	0.002992	predicted gene 15680
Ugt8a	-1.294	5.78E-05	UDP galactosyltransferase 8A
Sox3	-1.294	8.77E-19	SRY (sex determining region Y)-box 3
Slitrk6	-1.292	2.00E-09	SLIT and NTRK-like family, member 6
mt-Tl1	-1.282	0.004199	mitochondrially encoded tRNA leucine 1
Chrnb2	-1.282	7.31E-07	cholinergic receptor, nicotinic, beta polypeptide 2 (neuronal)
Dbx1	-1.282	3.83E-16	developing brain homeobox 1
Chga	-1.281	1.39E-08	chromogranin A
Arg1	-1.278	5.65E-37	arginase, liver
Celf3	-1.277	5.75E-07	CUGBP, Elav-like family member 3
Onecut2	-1.276	1.29E-17	one cut domain, family member 2
Itgb8	-1.274	2.51E-18	integrin beta 8
BC030500	-1.270	0.00037	cDNA sequence BC030500
Cdx1	-1.258	2.30E-05	caudal type homeobox 1
Gng3	-1.255	3.28E-05	guanine nucleotide binding protein (G protein), gamma 3
Tmem178b	-1.250	1.55E-05	transmembrane protein 178B
Ncan	-1.248	6.14E-08	neurocan
Rgs9	-1.237	3.85E-15	regulator of G-protein signaling 9
Dner	-1.234	7.09E-06	delta/notch-like EGF-related receptor
Plk3	-1.224	3.23E-12	polo-like kinase 3
Cd83	-1.223	4.31E-08	CD83 antigen
Gm16010	-1.222	7.83E-05	predicted gene 16010
Dtx4	-1.219	1.65E-26	deltex 4 homolog (Drosophila)
Klhl41	-1.219	6.34E-09	kelch-like 41
C130060K24Rik	-1.217	6.69E-05	RIKEN cDNA C130060K24 gene
Kcnn1	-1.216	8.59E-07	potassium intermediate/small conductance calcium-activated channel, subfamily N, member 1
Atp2b2	-1.213	0.002805	ATPase, Ca++ transporting, plasma membrane 2
Slc10a4	-1.212	0.000346	solute carrier family 10 (sodium/bile acid cotransporter family), member 4
Nhlh1	-1.212	1.61E-08	nescient helix loop helix 1
Doc2b	-1.208	9.66E-06	double C2, beta
Arhgap36	-1.208	8.92E-07	Rho GTPase activating protein 36
1810041L15Rik	-1.203	5.14E-10	RIKEN cDNA 1810041L15 gene
Abhd15	-1.201	1.94E-05	abhydrolase domain containing 15
Ass1	-1.190	9.00E-09	argininosuccinate synthetase 1
Drd2	-1.188	0.000413	dopamine receptor D2
Has3	-1.185	0.001334	hyaluronan synthase 3
Akap6	-1.180	5.30E-08	A kinase (PRKA) anchor protein 6
Disp2	-1.179	0.00059	dispatched homolog 2 (Drosophila)
Clec1b	-1.166	9.28E-10	C-type lectin domain family 1, member b

Slc6a7	-1.163	0.000361	solute carrier family 6 (neurotransmitter transporter, L-proline), member 7
Dusp14	-1.161	1.75E-08	dual specificity phosphatase 14
Tshz1	-1.159	5.37E-36	teashirt zinc finger family member 1
Srpk3	-1.157	0.003842	serine/arginine-rich protein specific kinase 3
mt-Tk	-1.155	6.07E-06	mitochondrially encoded tRNA lysine
Arhgap20	-1.152	3.49E-08	Rho GTPase activating protein 20
Grm3	-1.148	0.001033	glutamate receptor, metabotropic 3
Hfe2	-1.147	1.56E-05	hemochromatosis type 2 (juvenile) (human homolog)
Clec1a	-1.143	7.07E-05	C-type lectin domain family 1, member a
Lzts1	-1.143	1.68E-05	leucine zipper, putative tumor suppressor 1
Lrtm1	-1.143	0.000757	leucine-rich repeats and transmembrane domains 1
Nlrp5-ps	-1.141	0.004423	NLR family, pyrin domain containing 5, pseudogene
Foxq1	-1.139	0.00151	forkhead box Q1
Stk33	-1.138	2.73E-05	serine/threonine kinase 33
Syt11	-1.138	3.90E-21	synaptotagmin XI
Atp2a1	-1.129	2.87E-08	ATPase, Ca++ transporting, cardiac muscle, fast twitch 1
Gm807	-1.125	0.007918	predicted gene 807
Ksr2	-1.125	2.63E-05	kinase suppressor of ras 2
Sez6l2	-1.125	0.000484	seizure related 6 homolog like 2
Gdap1	-1.122	1.11E-06	ganglioside-induced differentiation-associated-protein 1
Ttyh1	-1.109	3.06E-06	tweety homolog 1 (Drosophila)
Slc45a1	-1.108	0.006267	solute carrier family 45, member 1
Gm20649	-1.106	9.25E-16	predicted gene 20649
Tmem35	-1.105	5.79E-06	transmembrane protein 35
Moxd1	-1.104	1.59E-08	monooxygenase, DBH-like 1
Trh	-1.103	0.001386	thyrotropin releasing hormone
Prdm12	-1.098	1.55E-07	PR domain containing 12
Lrrc4	-1.094	5.57E-09	leucine rich repeat containing 4
Gpr179	-1.088	0.003242	G protein-coupled receptor 179
Lhfpl4	-1.083	1.34E-09	lipoma HMGIC fusion partner-like protein 4
Mapk8ip2	-1.079	3.26E-08	mitogen-activated protein kinase 8 interacting protein 2
Islr2	-1.073	0.006343	immunoglobulin superfamily containing leucine-rich repeat 2
Fam57b	-1.070	8.97E-05	family with sequence similarity 57, member B
Rgs8	-1.065	3.76E-10	regulator of G-protein signaling 8
Syp	-1.063	1.35E-08	synaptophysin
Rem2	-1.062	3.77E-07	rad and gem related GTP binding protein 2
Pou3f3	-1.059	2.26E-11	POU domain, class 3, transcription factor 3
Myom2	-1.059	0.004424	myomesin 2
Tppp3	-1.056	4.89E-14	tubulin polymerization-promoting protein family member 3

Metrn	-1.054	3.11E-37	meteorin, glial cell differentiation regulator
Chst8	-1.044	6.99E-08	carbohydrate (N-acetylgalactosamine 4-0) sulfotransferase 8
Celsr3	-1.042	4.60E-06	cadherin, EGF LAG seven-pass G-type receptor 3 (flamingo homolog, Drosophila)
Trim9	-1.040	7.73E-07	tripartite motif-containing 9
Slco4a1	-1.039	0.000112	solute carrier organic anion transporter family, member 4a1
Rfx6	-1.035	0.001282	regulatory factor X, 6
Zic4	-1.034	5.46E-08	zinc finger protein of the cerebellum 4
Slc16a12	-1.033	0.005662	solute carrier family 16 (monocarboxylic acid transporters), member 12
Tox	-1.032	3.20E-09	thymocyte selection-associated high mobility group box
Fcgrt	-1.031	2.58E-06	Fc receptor, IgG, alpha chain transporter
Hecw1	-1.031	0.000617	HECT, C2 and WW domain containing E3 ubiquitin protein ligase 1
Gm715	-1.029	6.35E-05	predicted gene 715
Syndig1	-1.022	0.001017	synapse differentiation inducing 1
Syn1	-1.022	0.000103	synapsin I
Gm20646	-1.020	5.33E-11	predicted gene 20646
Lhx4	-1.015	1.43E-05	LIM homeobox protein 4
Gm15385	-1.012	0.00536	predicted gene 15385
Tspan17	-1.012	0.000226	tetraspanin 17
Gprin1	-1.009	6.55E-13	G protein-regulated inducer of neurite outgrowth 1
Gucy2f	-1.007	0.006457	guanylate cyclase 2f
Pdzrn4	-1.005	0.000132	PDZ domain containing RING finger 4
Ptpro	-1.005	7.09E-05	protein tyrosine phosphatase, receptor type, O
Hpdl	-1.002	4.02E-05	4-hydroxyphenylpyruvate dioxygenase-like
Gdap1l1	-1.002	4.11E-06	ganglioside-induced differentiation-associated protein 1-like 1

Paper 1: The retinaldehyde reductase DHRS3 is essential for preventing the formation of excess retinoic acid during embryonic development

This paper was a collaborative effort with the Alex Moise laboratory at the University of Kansas in Lawrence, Kansas. We performed and analyzed skeletal preparations of the embryos (Figure 7 and Supplemental Figure S2).

Reference: Billings, S.E., Pierzchalski, K., Butler Tjaden, N.E., Pang, X.-Y., Trainor, P.A., Kane, M.A., Moise, A.R., 2013. The retinaldehyde reductase DHRS3 is essential for preventing the formation of excess retinoic acid during embryonic development. The FASEB Journal.

Paper 2: The developmental etiology and pathogenesis of Hirschsprung disease

This paper was an invited review from Translational Research to be included in the "Featured New Investigator" series of the journal. My work was selected due to my attendance of the 2012 Combined Annual Meeting of the Central Society for Clinical Research and Midwestern Section American Federation for Medical Research.

Reference: Butler Tjaden, N.E., Trainor, P.A., 2013. The developmental etiology and pathogenesis of Hirschsprung disease. Transl Res 162, 1-15.

Paper 3: Cochleovestibular nerve development is integrated with migratory neural crest

For this project, I contributed to the methodology development and dissection of numerous ears to be used for skeletal preparations and lacZ staining. Specifically, I contributed to Figure 1 C and D and Figure 5F.

Reference: Sandell, L.L., Butler Tjaden, N.E., Barlow, A.J., Trainor, P.A., 2014. Cochleovestibular nerve development is integrated with migratory neural crest cells. Dev Biol 385, 200-210.

Paper 4: The *Mef2c-F10N* enhancer is active in migrating neural crest cells facilitating analyses of gene function and lineage

For this paper, I completed the initial miniprep and maxiprep of the *Mef2c-F10N* plasmid from Brian Black (De Val et al., 2008), as well as the mouse colony maintenance and initial descriptions and embryo time course of the *Mef2c-F10N* line. Specifically, I contributed to Figure 1: M,N,O; Figure 2 A-D; and provided embryos for sectioning in Figure 2 E-H; and Supplemental Figure 1.

Reference: Aoto, K., Sandell, L.L., Butler Tjaden, N.E., Yuen, K.C., Watt, K.E., Black, B.L., Durnin, M., Trainor, P.A., 2015. Mef2c-F10N enhancer driven beta-galactosidase (LacZ) and Cre recombinase mice facilitate analyses of gene function and lineage fate in neural crest cells. Dev Biol 402, 3-16.

Paper 5: The Oncogenic Transcription Factor Tlx1 Regulates Cyp26b1 Expression and Retinoic Acid Signaling to Ensure Spleen Development

For this paper, I harvested spleens of *Rdh10*$^{flox/flox}$;*ER*^{T2}*Cre* animals after tamoxifen administration at E7.5 and E10.5. The results from these embryos are used in figure 2B and 2C.

Reference: Lenti, E., Farinello, D., Yokoyama, K.K., Penkov, D., Castagnaro, L., Lavorgna, G., Wuputra, K., Sandell, L.L., Butler Tjaden, N.E., Bernassola, F., Pasini, D., Wagner, M., Niederreither, K., Hamada, H., Blasi, F., Tonon, G., Trainor, P.A., Brendolan, A., [in preparation]. The Oncogenic Transcription Factor Tlx1 Regulates Cyp26b1 Expression and Retinoic Acid Signaling to Ensure Spleen Development.

Paper 6: RDH10 is necessary for initial vagal neural crest cell contribution to embryonic gastrointestinal tract development

This paper is the bulk of my PhD Thesis work, and is currently in preparation. It will be submitted to Human Molecular Genetics.

Reference: Butler Tjaden, N.E., Sandell, L.L., Aoto, K., Trainor, P.A., [in preparation]. RDH10 is necessary for initial vagal neural crest cell contribution to embryonic gastrointestinal tract development.